

Investigating Class III Fusion Proteins as Vaccine Candidates Against Rabies Virus and Epstein-Barr Virus

Thesis Submitted for the Degree of Doctor of Philosophy

Hilary Term 2025

Solomon English

Investigating Class III Fusion Proteins as Vaccine Candidates Against Rabies Virus and Epstein-Barr Virus

Thesis submitted for the degree of Doctor of Philosophy, Hilary Term 2025.
Solomon English, Oriel College, University of Oxford.
Main text word count: ~48,000.

Abstract

The fusion proteins of enveloped viruses, responsible for membrane fusion and cell entry, are common targets for subunit vaccines. Fusion proteins undergo major conformational changes from a metastable pre-fusion state to a stable post-fusion one. The pre-fusion conformation may better expose neutralizing epitopes, and thus represent a better vaccine target, than the post-fusion. This phenomenon appears true for some Class I fusion proteins including those of respiratory syncytial virus and possibly SARS-CoV-2.

This thesis explores whether this principle applies to two Class III fusion proteins, where evidence remains limited. Rabies glycoprotein (RabG) and Epstein-Barr virus (EBV) glycoprotein B (gB) are investigated with a focus on understanding induction of neutralising antibody by their pre-fusion conformations.

For RabG, structure-guided mutagenesis strategies successfully stabilised the pre-fusion antigen and/or augmented expression *in vitro*. Promising mutations did not, however, improve the magnitude or quality of the antibody response raised to the wild-type form in mice.

For EBV gB, monoclonal antibodies (mAbs) were isolated from mice immunised with viral-vectored immunogens encoding the full-length antigen to express the membrane-stabilised, pre-fusion conformation of gB *in vivo*. 40 mAbs were successfully isolated against gB and investigated in detail, revealing previously-uncharacterised non-neutralising epitopes and a site of vulnerability on gB targeted by rare neutralising antibodies. Despite use of a screening method designed for discovery of conformationally specific anti-gB mAbs, none of those isolated displayed this phenotype.

Together, these findings do not support pre-fusion stabilisation for vaccines targeting two viruses employing Class III fusogens. Regarding RabG, however, the mutants characterised may still act as steps towards improving RabG immunogenicity in future vaccines. Similarly, whilst the mAbs isolated against EBV gB are not pre-fusion specific, they may represent useful tools for characterising gB as an antigen, including interrogation of whether non-neutralising antibodies can exert a protective effect *in vivo*.

Efforts to develop new vaccines targeting these proteins should not focus exclusively on pre-fusion stabilisation. Comparisons of vaccine platforms for antigen delivery, of protein candidates for subunit vaccines and on understanding the mechanisms by which antibodies to these fusion proteins convey protection remain critical for developing new rabies and EBV vaccines.

Acknowledgements

The work comprising this thesis would not have been possible without the significant support, effort and advice of the many people I have worked with in Oxford, collaborated with elsewhere and that I know personally. Where I have benefitted from others' assistance experimentally, I have gratefully acknowledged their contributions at the beginning of each results chapter in this thesis. I would, however, like to also mention here several people who have been especially generous with their wisdom and support.

I owe the greatest thanks to my primary DPhil supervisor Sandy Douglas who has spent countless hours with me discussing this work, my personal development and much more. Joining his team during the COVID-19 pandemic whilst he worked 20+ hour days on the Oxford/AstraZeneca vaccine project, the last thing he needed was the utterly inexperienced student he received. In over four years I have never once been turned away from a request to meet or from a late-night call for help. He has taught me an enormous amount about what it means to be a science researcher, and I am deeply thankful to have had him as a mentor.

My secondary supervisor Simon Draper proved time and time again to be a level-headed, encouraging advisor throughout my DPhil, often providing wisdom and clarity when neither I nor Sandy could. Members of his team have also been extremely generous with their time, teaching me experimental techniques and providing crucial advice. I would particularly like to thank Kirsty McHugh, Ana Rodrigues, Barney Williams and Mimi Hou for being so willing to help me.

A number of collaborators at the University of Edinburgh have contributed greatly to this work. I would like to especially thank Rennos Fragkoudis and Gaynor Campbell for welcoming me so warmly into their lab and for their tireless efforts. Equally, a great deal of thanks must go to Rob Stass and Thomas Bowden in the Department of Structural Biology for all their work on parts of this DPhil. I could not have asked for more committed collaborators.

Many staff members in the Jenner Institute have played a central role in the completion of this work. I am grateful to Drew Worth for his advice and assistance with flow cytometry, Will Taylor for producing mRNA vaccines on my behalf and Adam Truby for invaluable assistance with animal work throughout my DPhil. Finally, without Hana Osman, Alan Jeffreys and Mariya Mykhaylyk, my greatest friend in the lab, there would be no functional lab to operate in. I can only apologise for how annoying I was to all three of them and to thank them for their patience.

I would like to acknowledge the supreme efforts of all those in Oxford University Biomedical Services for their assistance with animal work during my DPhil. Special mention must go to Douglas Dos Santos Passos and Luke Harris for training me and to Heather Chandler for running such a tight ship!

I am forever grateful to the wider Douglas Group for being such a reliable and friendly support network throughout my time at Oxford, all of whom played major roles in making my DPhil enjoyable and in keeping me on track. I am particularly indebted to Adam Ritchie for all his behind-the-scenes work keeping the Douglas Group ticking (and for providing me with comic relief through his support of Tottenham Hotspur) and Rameswara Segireddy who has taught me a huge amount of lab biology over four years with nothing but good humour and patience.

Without doubt, the greatest privilege of my DPhil has been to supervise two fantastic master's students, Francisco Orliacq and Orthi Onupom. I am immensely proud of all that they have achieved in their research projects and more generally. I cannot thank them enough for their enormous efforts and contributions to the work in this thesis, nor for how much joy they have both brought me.

Finally, this work would not have been possible without the tireless support of friends, family and previous mentors. I owe a huge debt of gratitude to my previous supervisors, Mairi Kilkenny and Daniel Dunkelmann, for encouraging me to pursue a PhD and for rightly telling me how foolish I was for so arbitrarily ruling it out as a possibility. They have continued to support me throughout it. To the many friends who so perfectly showed the right amount of interest that I knew they cared whilst also reminding me that it was far from the only thing of importance in my life. To Mum, Dad, Atti, Rex, George and Izzy – thank you for doing everything else.

Note to the Examiners

The digital version of this thesis is formatted such that chapter headings are navigable using the 'Bookmarks' functionality in any PDF viewing software (Adobe, Chrome, Firefox etc.).

Table of Contents

Abstract 2

Acknowledgements 4

Table of Contents 6

Table of Figures 13

Table of Tables 16

List of Abbreviations 17

1 Introduction 20

1.1 Hypothesis 20

1.2 Viral Fusion Protein Biology 20

1.2.1 Cell Entry 20

1.2.2 Structural Characteristics 24

1.2.3 Pre-fusion Stabilisation for Improved Immunogenicity 26

1.3 Rabies Virus 29

1.3.1 Disease Biology 29

1.3.2 Current Status of Rabies Treatments 30

1.3.3 Pre-fusion Stabilisation of RabG 32

1.3.4 Rabies Virus Objectives 34

1.4 Epstein-Barr Virus 35

1.4.1 Disease Biology 35

1.4.2 Human Herpesvirus Biology 37

1.4.3 Human Herpesvirus Fusion 38

1.4.4 Glycoprotein B Structure 40

1.4.5 Glycoprotein B Immunology 42

1.4.6 Historic gB-based Vaccine Developments 47

1.4.7 EBV Objectives 48
1.5 Appendix I: gB-based HHV Vaccines in Clinical Trials 50
2 General Materials and Methods 55
2.1.1 Molecular Biology 55
2.1.2 Transient Transfection of Expi293F Suspension Cells 55
2.1.3 Transient Transfection of ExpiCHO Suspension Cells 56
2.1.4 Animal Work Statement 56
2.1.5 Enzyme Linked Immunosorbent Assay (ELISA) 57
2.1.6 Flow Cytometry Data Analysis 58
2.1.7 Data Visualisation and Statistical Analysis 58
2.1.8 Schematic Figures 58
2.1.9 Protein Structure Visualisation 58
3 Results I: Targeted Mutations of the Rabies Glycoprotein Improve Antigen Expression and Stability, but not Immunogenicity 59
3.1 Statement of Authorship 59
3.2 Chapter Overview 60
3.3 Introduction 60
3.3.1 RabG Mutagenesis to Improve Pre-fusion Stabilisation and Immunogenicity 60
3.3.2 Considerations for Designing *In Vivo* RabG Mutant Screens 65
3.4 Materials and Methods 67
3.4.1 Production of RabG Mutant-encoding Plasmid DNA 67
3.4.2 96 Deep-well Plate Transfections for RabG Mutant Screening 67
3.4.3 Conjugation of Amine-reactive Fluorophores to Antibodies 67
3.4.4 Flow Cytometry Assay for the Screening of RabG Mutants 67
3.4.5 Production of Adenovirus-vectored RabG Vaccines 68
3.4.6 *In Vitro* Transcription to Produce 5'-capped RabG mRNA 68
3.4.7 Transient Transfection of RabG mRNA 69
3.4.8 Intramuscular Administration of RabG Vaccines 69
3.4.9 Production of Detergent-extracted RabG Protein 69
3.4.10 ELISA for Quantification of Anti-RabG IgG 71

3.4.11 Virus Neutralising Antibody Titrations 71
3.5 Results....72
3.5.1 Establishment of a Whole-panel RabG Mutant Screening Assay 72
3.5.2 Screening of a RabG Single Mutant Panel 76
3.5.3 The H270P Mutant Does Not Improve the Immunogenicity of RabG in an Adenovirus-vectored Vaccine 81
3.5.4 Refinement of the RabG Mutant Screen 82
3.5.5 Stability and Expression Screening of the RabG Mutation Combinations 85
3.5.6 Mutants that Improve Expression and/or Acid Stabilisation Do Not Improve the Immunogenicity of RabG Using an mRNA Vaccine Platform 87
3.6 Discussion....92
3.7 Appendix II: Combinatorial RabG Mutants 97
4 Results II: Development of a Workflow for the Isolation of Monoclonal Antibodies Against an Unstable Membrane Glycoprotein 98
4.1 Statement of authorship....98
4.2 Chapter Overview 99
4.3 Introduction 100
4.4 Materials and Methods....109
4.4.1 Production of Protein and Viral-vectored Immunogens 109
4.4.2 Animal Immunisations 110
4.4.3 Tissue Processing and Freezing 111
4.4.4 B Cell Enzyme-linked ImmunoSpot (ELISpot) Assay 112
4.4.5 Production and Purification of Recombinant Biotinylated gB Ectodomain for Use as a Protein Probe....112
4.4.6 Flow Cytometry-based Screen of Biotinylated gBect as a Probe Antigen 114
4.4.7 Transient transfection of CHO cells to generate a gB-expressing cell probe for Beacon screens 114
4.4.8 Conjugation of Biotinylated Antigen to Streptavidin Coated Beads....115
4.4.9 Isolation of Antibody-secreting Cells by Magnetic-Activated Cell Sorting (MACS) 115
4.4.10 Isolation of Antibody-secreting Cells by Fluorescence-Activated Cell Sorting (FACS) 116

4.4.11 Screening and Export of Plasma Cells on the Beacon 117

4.4.12 Reverse Transcription PCR for Antibody Heavy- and Light-Chain Amplification from Wild-type Mice 117

4.4.13 RT-PCR on OmniMouse-derived Antibody Secreting Cells 118

4.4.14 Sequencing and Synthesis of mAb Heavy- and Light-chains 119

4.4.15 Expression and Purification of mAbs by Small-scale Transient Transfection 120

4.4.16 ELISA-based Screening of Antibody Binding to gBect 121

4.4.17 Flow-cytometry-based Screening of Antibody binding to Membrane-expressed gB 121

4.4.18 Screening of OmniMouse Antibody Responses by ELISpot and ELISA ..122

4.5 Results 123

4.5.1 gB Bead- and Cell-based Probes are Functional on a Beacon Optofluidics Chip 123

4.5.2 Beacon Screens on Fresh Samples Yield Modest Hit Numbers from both FACS- and MACS-enriched Splenocytes 129

4.5.3 FACS and MACS Plasma Cell Enrichment Methods Isolate Subtly Different Cell Populations to Capture IgG-Secreting Cells 133

4.5.4 Beacon Campaigns on Frozen Cell Samples Reveal MACS-Based Enrichment of Plasma Cells Out-Performs FACS Despite RBC Contamination 136

4.5.5 An Added MACS Step Successfully Removes RBC Contaminants from Frozen Samples 139

4.5.6 Bone Marrow Samples Pen More Efficiently than Splenocyte Samples, but Yield Fewer gB-Reactive Hits on the Beacon 142

4.5.7 The 'Live B Cell Penning' Algorithm is Less Efficient than 'Pen Plasma Cells' but can be Supplemented by Performing an Extra Round of Penning 145

4.5.8 Integrating Method Improvements to Screen for Conformationally-specific Anti-gB mAbs Identifies >200 Single Cell Hits 146

4.5.9 A Published RT-PCR Protocol Recovers Paired H/L-Chains from Single-Cell Hits with Greater Efficiency than the Beacon Method 149

4.5.10 A Panel of 40 gB-Specific mAbs Show Diverse V/J Gene Usage with 3 mAbs Showing Preferential Binding to Recombinant gB Ectodomain 154

4.5.11 Human IgG-transgenic Mice Raise Antibody Responses to gB Vaccines, but Amplification of the Heavy-chain Sequences is Challenging 156

4.6 Discussion 160

4.7 Appendix III: RT-PCR Primer Sequences....165

5 Results III: Characterisation of the Binding and Function of a Mouse Monoclonal Antibody Panel Against gB....169

5.1 Statement of Authorship....169

5.2 Chapter Overview....170

5.3 Introduction....170

5.3.1 Antibodies Against EBV gB....170

5.3.2 Methods for the Mapping of Epitopes....172

5.3.3 Glycosylation in the Context of the Anti-gB Response....175

5.3.4 *In Vitro* Neutralisation Assays to Study Anti-gB mAb Functionality....176

5.3.5 Investigating Complement-dependent Anti-gB Antibody Functionality....179

5.4 Materials and Methods....180

5.4.1 Expression and Purification of Recombinant gB Ectodomain....180

5.4.2 Expression and Purification of Anti-gB Antibodies in Fab Format....180

5.4.3 Western Blot Analysis of the Mouse mAb Panel....181

5.4.4 Peptide Mapping ELISA....181

5.4.5 Deglycosylation of gB and ELISA Binding Analysis....182

5.4.6 gB Binding Competition ELISA....183

5.4.7 Competition Analysis Using the LSA Carterra....184

5.4.8 ELISA-based Competition Assay Cluster and Network Analysis....185

5.4.9 LSA-based Competition Assay Cluster and Network Analysis....186

5.4.10 Cell Culture....186

5.4.11 Production of GFP-tagged EBV from Epithelial and B Cell Lines....187

5.4.12 *In Vitro* Neutralisation Assay....188

5.5 Results....190

5.5.1 Beacon-Isolated mAbs Recognise Epitopes in Both Fragments of the Denatured gB Ectodomain as well as Conformational Epitopes....190

5.5.2 mAbs Capable of Binding Denatured gBect Do Not Recognise gB-derived Peptides by ELISA....192

5.5.3 Two mAbs Exhibit Variable Antigen Binding Depending on gB's Glycosylation State....194

5.5.4 An ELISA-based Competition Mapping Method Reveals Five Distinct Clusters of gB-binding mAbs 197

5.5.5 SPR-based Competition Measurements Reveal a Similar Profile to the ELISA-based Method 204

5.5.6 Two New mAbs Efficiently Neutralise *In Vitro* Infection of B Cells and Epithelial Cells by EBV 208

5.5.7 Apparent Infection Enhancement by Some mAbs in Neutralisation Assays is Not Dose-dependent 214

5.6 Discussion 215

5.6.1 Mapping the Antigenic Landscape of gB 215

5.6.2 Desirability of Improved EBV Production Methods 220

5.6.3 The Neutralising Response to gB 222

5.6.4 Anti-gB Enhancement of Infection 222

5.6.5 Implications for Pre-fusion Stabilisation 224

5.7 Appendix IV: Raw Western Blot Images 226

6 Results IV: Structural Characterisation of Neutralising mAb-gB Complexes 230

6.1 Statement of Authorship 230

6.2 Chapter Overview 231

6.3 Introduction 231

6.4 Materials and Methods 234

6.4.1 Generation of gB-Fab Complexes for HPLC-SEC 234

6.4.2 Negative Stain Electron Microscopy (NSEM) 235

6.4.3 Detergent Extraction of FL-gB and Production of FL-gB·Fab_n Complexes 235

6.4.4 Cryo-EM Sample Preparation and Data Collection 236

6.4.5 Cryo-EM Data Processing 237

6.5 Results 238

6.5.1 A HPLC-SEC-based Method for Purifying gB·Fab Complexes Reproduces the Structure of gBect in Complex with 3A3 and 3A5 238

6.5.2 Disperse Complexes of Full-length, Membrane-extracted gB Coordinated by Fabs can be Isolated but Aggregate on Cryo-EM Grids 242

6.5.3 A Doubly Fab-decorated gBect Complex Reveals the Binding Site of the ECO12 Neutralising Antibody 246
6.6 Discussion 254
6.7 Appendix V: Data Collection and Processing for the $gBect_{ECO12\cdot3A5}$ Complex 261
6.8 Appendix VI: Electron Density at the gBect-ECO12 Interface 262
7 Concluding Remarks 263
7.1 Summary of Findings 263
7.1.1 Rabies Virus Glycoprotein 263
7.1.2 Epstein-Barr Virus Glycoprotein B 266
7.1.3 Pre-fusion Stabilisation in the Context of Vaccination 270
7.2 Future Directions 273
7.2.1 Rabies Virus 273
7.2.2 Epstein-Barr Virus 274
7.3 Final Remarks 277
8 Bibliography 278

Table of Figures

Figure 1.2-1: Enveloped virus entry of host cells. 24
Figure 1.2-2: Example structures for Class I, Class II and Class III fusogens. 25
Figure 1.3-1: Antigenic sites on the rabies glycoprotein. 34
Figure 1.4-1: Human Herpesvirus Fusion Machinery. 39
Figure 1.4-2: Human herpesvirus glycoprotein B. 41
Figure 1.4-3: Pre-fusion glycoprotein B structures. 42
Figure 3.3-1: RabG mutagenesis strategies. 64
Figure 3.5-1: In vitro RabG mutant screening assay. 73
Figure 3.5-2: 96-well plate transfection assay optimisation. 75
Figure 3.5-3: RabG transfection reproducibility. 76
Figure 3.5-4: RabG single mutant panel screening. 79
Figure 3.5-5: RabG mutant expression & stability analysis. 80
Figure 3.5-6: in vivo screening of ChAdOx2-vectored H270P. 82
Figure 3.5-7: Refinement of the RabG in vitro expression assay. 84
Figure 3.5-8: RabG double mutant panel screening. 86
Figure 3.5-9: RabG mutant mRNA vaccine production and screening. 90
Figure 3.5-10: Immune responses to WT and mutant RabG mRNA vaccines. 92
Figure 4.2-1: Chapter Summary. 99
Figure 4.3-1: Plasma cell screening using a Beacon (Bruker Cellular Analysis) 106
Figure 4.5-1: Post-fusion gB Beacon probe production. 125
Figure 4.5-2: CHO cell-based gB Beacon probe production. 128
Figure 4.5-3: Beacon runs on fresh mouse splenocytes. 132
Figure 4.5-4: Antibody secreting cell numbers in different B cell populations. 135
Figure 4.5-5: First Beacon screens on frozen splenocyte samples. 138
Figure 4.5-6: Red blood cell removal by an added MACS protocol step. 142
Figure 4.5-7: Beacon screens on spleen and bone marrow tissues. 144
Figure 4.5-8: Comparing antibody secreting cell penning algorithms. 145
Figure 4.5-9: Refinement of the Beacon-based antibody discovery pipeline. 148
Figure 4.5-10: Comparison of reverse transcription PCR methods. 150
Figure 4.5-11: FACS-based generation of dummy Beacon export plates for RT-PCR optimisation. 151

Figure 4.5-12: Comparison of mAb chain recovery rates after RT-PCR by two different methods. 153
Figure 4.5-13: Anti-gB mAb sequence variability and antigen binding behaviour. 156
Figure 4.5-14: Investigating OmniMice as transgenic animals for human-like mAb isolation.....157
Figure 4.5-15: RT-PCR of OmniMouse antibody heavy- and light-chain sequences. ...159
Figure 5.3-1: Glycosylation sites on EBV gB. 176
Figure 5.5-1: Anti-gB mAb recognition of denatured gB by Western Blot. 191
Figure 5.5-2: Anti-gB mAb recognition of linear epitopes in peptide format. 193
Figure 5.5-3: Glycan dependencies of anti-gB mAbs. 196
Figure 5.5-4: Assay development for the screening of mAb-mAb competition for gBect binding. 199
Figure 5.5-5: Unclustered competition heatmap for the full panel of anti-gB mAbs....201
Figure 5.5-6: Cluster analysis of antibody competition by ELISA. 202
Figure 5.5-7: Exploring antibody competition for gB binding using a network analysis. 203
Figure 5.5-8: Cluster analysis of antibody competition by SPR using a Carterra. 205
Figure 5.5-9: SPR-based competition interactions plotted as a network. 206
Figure 5.5-10: Correlation between two different competition assays. 207
Figure 5.5-11: Neutralisation of in vitro Raji B cell infection with EBV-GFP. 209
Figure 5.5-12: Dilution series for antibodies capable of neutralising Raji B cell infection in vitro. 211
Figure 5.5-13: In vitro neutralisation of HEK293T cell infection by EBV-GFP.....213
Figure 5.5-14: Antibodies displaying 'enhancement'-like behaviour. 214
Figure 5.6-1: Proposed antigenic sites on the post-fusion conformation of gB. 219
Figure 5.6-2: Example FACS gating for a mAb that 'enhances' in vitro Raji B cell infection. 223
Figure 5.6-3: The relationship between binding of gBect and membrane-expressed gB. 225
Figure 5.7-1: Raw Western blot images using anti-gB mAbs to stain denatured gBect. 229
Figure 6.5-1: gBect·Fab complex isolation by HPLC-SEC. 239

Figure 6.5-2: Isolation and structural characterisation of gBect coordinated by 3A3 and 3A5 Fabs. 242
Figure 6.5-3: Membrane extraction of full-length gB for the generation of gB·Fab complexes. 243
Figure 6.5-4: Pilot membrane extraction of full-length gB complexed with 3A3 and 3A5. 245
Figure 6.5-5: of gBect coordinated by ECO12 and 3A5 Fabs. 248
Figure 6.5-6: Structural characterisation of the ECO12 epitope. 250
Figure 6.5-7: Electrostatic interactions between gB and ECO12. 251
Figure 6.5-8: Structural comparison of the 3A3 and ECO12 epitopes on post-fusion gB. 253
Figure 6.6-1: Modelling the ECO12 epitope on pre-fusion gB. 257
Figure 6.8-1: Electron density at the gBect-ECO12 interface. 262

Table of Tables

Table 1.4-1: Immunogenic hotspots on glycoprotein B, as described for HCMV and HSV-1/2. 43
Table 1.5-1: Completed and ongoing clinical trials of gB-based/containing vaccines against herpes simplex virus-2 (HSV-2) and human cytomegalovirus (HCMV). 54
Table 3.3-1: Mutation Strategies to improve cell surface expression and/or pre-fusion stabilisation of RabG. 62
Table 3.4-1: ELISA protocol details for determining anti-RabG IgG titres from mouse serum samples. 71
Table 3.7-1: Combinatorial RabG mutants. 97
Table 4.3-1: Common approaches for the isolation of monoclonal antibodies 104
Table 4.4-1: Staining panel for the enrichment of $CD138^{High}$ $B220^{Low}$ mouse plasma B cells from splenocyte samples. 116
Table 4.4-2: ELISA protocol for confirming mAb binding to gB ectodomain. 121
Table 4.4-3: ELISA protocol for determining anti-gB titres in OmniMouse animals. ..122
Table 4.7-1: Primer sequences (5' – 3') for PCR amplifications. 166
Table 4.7-2: Primer sequences (5' – 3') for PCR amplifications of OmniMouse-derived human/rat transgenic IgG heavy and $\varkappa$ light chains. 168
Table 5.3-1: Summary of binding and in vitro neutralisation characteristics for published anti-gB monoclonal antibodies. 172
Table 5.3-2: Common approaches to the characterisation of antigen-antibody binding sites, their advantages and disadvantages. 174
Table 5.4-1: ELISA protocol for determining whether anti-gB antibodies could recognise linear peptide epitopes. 182
Table 5.4-2: ELISA protocol for determining each mAb's ability to bind gBect in its native, glycosylated state, and after N-deglycosylation with PNGase F. 183
Table 5.4-3: Assay parameters for different competition ELISA configurations. 184
Table 5.5-1: EC_{50} values for all mAbs tested by in vitro neutralisation of EBV infection of Raji B cells and HEK293T cells. 212
Table 6.3-1: Studies of the HCMV gB immune responses that have sought to characterise the immunodominance of the antigen's different subdomains. 232
Table 6.7-1: Summary of data acquisition and processing for the $gBect_{ECO12\text{-}3A5}$ complex after imaging on a Titan Krios G31 cryo-TEM. 261

List of Abbreviations

AA	Amino Acid
Ab	Antibody
ACK	Ammonium-Chloride-Potassium
AD	Antigenic Domain
ADCC	Antibody-Dependent Cellular Cytotoxicity
ADCP	Antibody-Dependent Cellular Phagocytosis
Ag	Antigen
AP	Alkaline Phosphatase
APC	Allophycocyanin
ASC	Antibody-Secreting Cell
BSA	Bovine Serum Albumin
CDR	Complementarity Determining Region (of an antibody)
CDS	Amino acid-coding sequence
ChAdOx	Chimpanzee Adenovirus Oxford (engineered from serotype Y25)
CI	Confidence Interval
CNS	Central Nervous System
Cryo-EM	Cryogenic Electron Microscopy
CTD	C-Terminal Domain
CV	Coefficient of Variation
DLS	Dynamic Light Scattering
DMSO	Dimethyl Sulfoxide
DTT	Dithiothreitol
EBV	Epstein-Barr Virus
EC_{50}	50% Effective Concentration
ELISA	Enzyme Linked Immunosorbent Assay
ELISpot	Enzyme Linked Immunosorbent Spot
ER	Endoplasmic Reticulum
Fab	Fragment antigen binding (region of immunoglobulin molecule)
FACS	Fluorescence-Activated Cell Sorting
FBS	Foetal Bovine Serum
Fc	Fragment, crystallisable (non-antigen-binding region of immunoglobulin molecule)
FITC	Fluorescein Isothiocyanate
FL-gB	Full-length Glycoprotein B (including transmembrane and intravirion domains)
FoV	Field of View
FP	Fusion Protein
FR	Functional Region
Fv	Fragment, variable (antigen-binding region of immunoglobulin molecule)
gB	Glycoprotein B
gBect	Recombinant Glycoprotein B Ectodomain
gBmutK	Glycoprotein B with ^{836}RRRR^{839} → KKKK mutation
GFP	Green Fluorescent Protein
gH	Glycoprotein H
gL	Glycoprotein L
gp350	Glycoprotein 350
gp42	Glycoprotein 42
HA	Haemagglutinin

HCMV	Human Cytomegalovirus
HEK293	Human Embryonic Kidney 293 (cell line)
HHV	Human Herpesvirus
HPLC	High-Performance Liquid Chromatography
HRP	Horseradish Peroxidase
HSV	Herpes Simplex Virus
I.M.	Intramuscular
I.P.	Intraperitoneal
I.V.	Intravenous
IM	Infectious Mononucleosis
IU	International Units
mAb	Monoclonal Antibody
MACS	Magnet-Activated Cell Sorting
MERS	Middle Eastern Respiratory Syndrome
MFI	Median Fluorescence Intensity
MHV-68	Murine γ-Herpesvirus 68
MPR	Membrane Proximal Region
MS	Multiple Sclerosis
MVA	Modified Vaccinia Ankara
Mw	Molecular Weight
MWCO	Molecular Weight Cut-Off
nAb	Neutralising Antibody
NAG	N-acetylglucosamine
NCBI	National Centre for Biotechnology Information
NIAID	National Institute for Allergy and Infectious Disease
NMR	Nuclear Magnetic Resonance
NSEM	Negative Stain Electron Microscopy
NTD	N-Terminal Domain
O/N	Overnight
OD	Optical Density
OEP	Optical-Electro Positioning
PAGE	Polyacrylamide Gel Electrophoresis
PBS	Phosphate Buffered Saline
PBS/T	0.05% Tween-20 in Phosphate Buffered Saline
PC	Pentameric Complex
PCR	Polymerase Chain Reaction
PDB	Protein Data Bank
PEP	Post-Exposure Prophylaxis
PFU	Plaque Forming Units
PrEP	Pre-Exposure Prophylaxis
PVDF	Polyvinylidene Difluoride
PVoG	Pasteur Virus optimised Glycoprotein
RabG	Rabies Glycoprotein
RAIN	Resistant to Acid Induced Neutralisation
RBC	Red Blood Cell
Rh	Hydrodynamic Radius
RH5	Reticulocyte Binding Protein Homologue 5
rhLCV	Rhesus Lymphocryptovirus

RIG	Rabies Immune Globulin
RMSD	Root Mean Square Deviation
RSV	Respiratory Syncytial Virus
RT	Room temperature
RT-PCR	Reverse-Transcription Polymerase Chain Reaction
RU	Response Units
S	Spike Protein
S.C.	Subcutaneous
SARS	Severe Acute Respiratory Syndrome
SARS-CoV-2	Severe Acute Respiratory Syndrome Coronavirus 2
SEC	Size Exclusion Chromatography
SFU	Spot Forming Units
SLS	Static Light Scattering
SPR	Surface Plasmon Resonance
TEM	Transmission Electron Microscopy
tIgG	Total Immunoglobulin G
TMB	3,3',5,5'-Tetramethylbenzidine
TMD	Transmembrane Domain
TS-II	TwinStrep Tag II
UTR	Untranslated Region
vH	Variable Heavy (region of immunoglobulin molecule)
vL	Variable Light (κ or λ, region of immunoglobulin molecule)
VNA	Virus Neutralising Antibody
vp	Virus particles
VZV	Varicella Zoster Virus
WB	Western Blot
WT	Wild-type
β-OG	n-octyl-β-glucoside

1 Introduction

1.1 Hypothesis

Viral fusion proteins are frequently targets for protective antibody-inducing vaccines, reflecting their central role in host cell invasion. For some viruses, it is known that the pre-fusion conformation presents epitopes targeted by neutralising antibodies (nAbs) in a conformationally specific manner. It follows that stabilising fusion proteins in their pre-fusion form may therefore improve their ability to raise protective antibody responses.

This thesis seeks to investigate whether this may be true in the cases of two Class III fusion proteins, rabies virus glycoprotein (RabG) and/or Epstein-Barr virus glycoprotein B (gB). Ultimately, this may shed light on the conditions under which pre-fusion stabilisation of fusion proteins is beneficial for designing new fusion protein-based vaccines.

1.2 Viral Fusion Protein Biology

1.2.1 Cell Entry

To successfully enter the cells of their host organism, enveloped viruses must undergo a membrane fusion step. Though fusion of the virion membrane with that of the host cell is thermodynamically favourable, there is a high kinetic barrier associated with the two membranes coming into proximity and fusion being initiated (Harrison, 2015). Viral fusion proteins overcome this barrier, facilitating viral entry.

These proteins are expressed on the virion surface, typically as single-pass membrane proteins (Harrison, 2008). They catalyse membrane fusion by undergoing a series of conformational changes. Fusion proteins start in a relatively high energy pre-fusion form and convert to a thermodynamically stable post-fusion one (Harrison, 2008). Given the thermodynamically favourable nature of this restructuring, sufficient energy is released by the process to overcome the energy barrier described above.

Though fusion proteins may be structurally distinct and/or activated through different mechanisms, they follow a common pathway to catalyse viral entry. This process has

recently been summarised by White and colleagues as consisting of five general steps: priming, triggering, extending, folding back and zippering (White *et al*, 2023), shown graphically (***Figure 1.2-1***).

In brief, priming of the fusion proteins often involves a proteolytic cleavage step from a single polypeptide chain pre-cursor to the mature fusion protein (White *et al*, 2023). Triggering of the mature fusogen is subsequently a response to one or more stimuli including:

1) Signalling from other proteins on the virion surface that interact with the fusogen. This is often preceded by the accessory proteins binding host cell receptors, indicating arrival at the target cell membrane. Herpesviruses make extensive use of this mechanism, with multiple surface glycoproteins contributing to fusion protein activation (Vollmer & Grünewald, 2020).

2) Changes to pH that are detected by the fusion protein. Acidification of endosomes after endocytosis is exploited as a fusion trigger by multiple viruses including influenza and vesicular stomatitis virus amongst others (Yao *et al*, 2003; Bullough *et al*, 1994; Schowalter *et al*, 2008; Mair *et al*, 2014; Glauser *et al*, 2012).

   Most relevant to this thesis, the rabies virus glycoprotein undergoes its pre- to post-fusion transition at low pH (~5.8) (Gaudin *et al*, 1993). Additionally, a drop in pH appears to trigger structural changes in the herpes simplex virus fusogen, gB (Dollery *et al*, 2010; Nicola, 2016; Weed *et al*, 2017), though its exact role in viral entry is unclear.

3) *Trans* protein cleavage steps, catalysed by host cell surface-expressed proteases. This is true of coronaviruses including SARS and SARS-CoV-2. TMPRSS2, a surface protease, cleaves the virus' spike protein (S) after ACE2 receptor binding, leading to fusion (Koch *et al*, 2021; Glowacka *et al*, 2011; White *et al*, 2023).

The subsequent extension, folding back and zippering steps all correspond to conformational changes in the fusogen. Hydrophobic fusion peptides are commonly

inserted into the host cell membrane (extension) before a jackknife movement draws the two membranes together (folding back). This is followed by membrane hemifusion and lastly full fusion (zippering) (White *et al*, 2023).

Which step in fusion is rate determining is not well understood. However, studies of influenza haemagglutinin (HA) and the West Nile virus (WNV) E protein provide evidence that the hemifusion step or one after it has highest energy barrier (Ivanovic *et al*, 2013; Chao *et al*, 2014; Harrison, 2015).

Proposed fusion pathways are regularly depicted as being facilitated by more than one fusion protein molecule on the virion surface. In the cases of influenza HA and WNV E, at least three fusion proteins must adopt the extended intermediate conformation and undergo the folding back step in parallel to provide sufficient energy to trigger membrane fusion (Benhaim & Lee, 2018; Chao *et al*, 2014; Ivanovic *et al*, 2013).

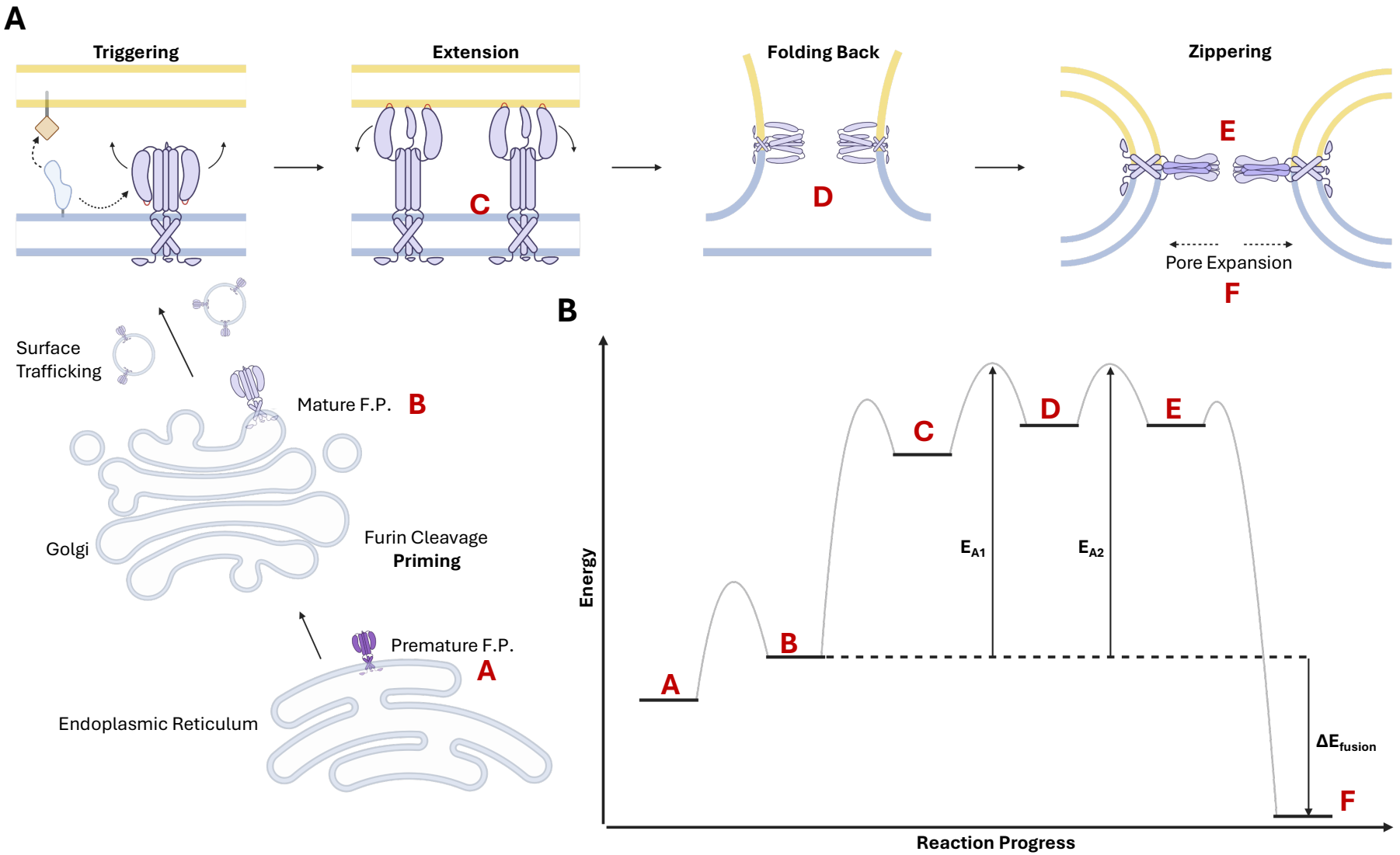

A
Triggering
Extension
Folding Back
Zippering
C
D
E
Pore Expansion
F
Surface
Trafficking
Mature F.P.
B
Golgi
Furin Cleavage
Priming
Premature F.P.
A
Endoplasmic Reticulum
B
Energy
A
B
C
D
E
F
E_{A1}
E_{A2}
ΔE_{fusion}
Reaction Progress

Figure 1.2-1: Enveloped virus entry of host cells.

(A) Cell entry by enveloped viruses, catalysed by a fusion protein (F.P.). The generalised mechanism highlights the five steps of fusion, as outlined by White and colleagues *(White* et al*, 2023)*. **Priming:** the premature fusogen, often expressed on the ER membrane, is proteolytically cleaved into its active form during trafficking to the surface membrane, via the Golgi. **Triggering:** additional surface glycoproteins that recognise host cell surface receptors or changes to pH, amongst others, promote conformational changes in the fusion protein. **Extension:** fusion loops/peptides on the fusion protein are inserted into the host cell membrane. **Folding back:** the fusion protein undergoes a jackknife-style movement, drawing the two membranes together. **Zippering:** hemifusion is proceeded by pore formation. Pores subsequently expand, leading to the final, fused product.

(B) An approximate energy profile of the fusion process. Exact energies of intermediates are unknown. Evidence from influenza HA and West Nile Virus E suggest hemifusion or early pore formation may incur the highest energy penalty. E_{A1} and E_{A2} represent the possible activation energies for fusion. Expansion of the pore is highly energetically favourable, resulting in a negative ΔE for the fusion process as a whole.

Schematic created with BioRender.com.

1.2.2 Structural Characteristics

The fusion proteins of enveloped viruses are almost invariably multimeric in nature. They share structural features such that they can be categorised into three classes, I, II and III; examples of each are shown graphically (***Figure 1.2-2***). Class I fusion proteins, including HA and HIV env, are trimers largely comprised of α-helices. Class II fusogens include those of the flaviviruses and form pre-fusion dimers rich in β-sheets (White *et al*, 2023).

Class III fusion proteins, the focus of this work, are trimers and include the herpesviruses' gB proteins and RabG. These fusion proteins share structural characteristics with one another despite their distant evolutionary relatedness. In addition, the Class III fusogens appear to mix elements of both Class I and II fusion proteins (Baquero *et al*, 2015).

The hydrophobic fusion loops of Class III proteins are contained within a β-rich domain, tucked against the lipid membrane (Baquero *et al*, 2015). They also contain a plekstrin-homology fold, commonly found at protein-protein interaction sites, and a central helical bundle (at least in the post-fusion) forming the core of the trimer (Backovic & Jardetzky, 2011). These ultimately connect to a transmembrane domain and an intravirion C-terminal domain.

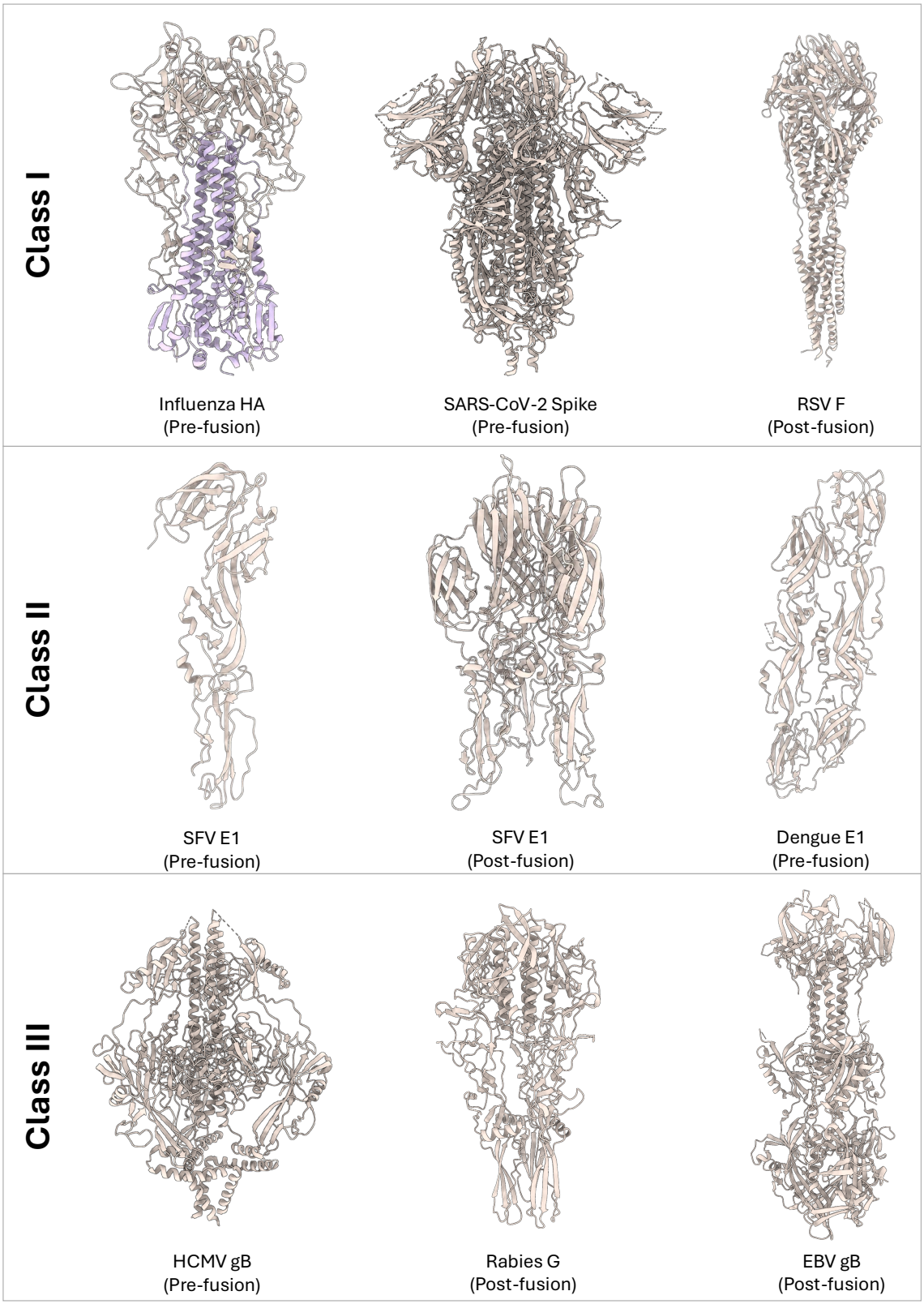


Figure 1.2-2: Example structures for Class I, Class II and Class III fusogens.
Class I: Influenza haemagglutinin (HA, PDB: 1QFU), SARS-CoV-2 Spike (PDB: 6VXX), respiratory syncytial virus F (PDB: 3RRR). **Class II:** Semliki Forest Virus E1 (PDB: 1ALA – prefusion monomer, PDB: 1RER – post-fusion trimer), Dengue virus E1 (PDB: 1TG8). **Class III:** human cytomegalovirus gB (PDB: 7KDP), rabies virus G (PDB: 6LGW), Epstein-Barr virus gB (PDB: 3FVC). The subunits of the influenza haemagglutinin are coloured (HA_1 = pink, HA_2 = beige) to highlight that fusogens are often proteolytically cleaved after expression.

For RabG, structural transitions from the pre- to the post-fusion conformation are reversible upon changing the pH (Baquero *et al*, 2015). For the herpesvirus' gB, however, the metastable nature of the pre-fusion conformation renders the structural transition to the post-fusion irreversible (Vollmer & Grünewald, 2020).

1.2.3 Pre-fusion Stabilisation for Improved Immunogenicity

Multiple viral vaccines have already been developed that target fusion proteins, inducing potent neutralising antibody responses (Ebel *et al*, 2022). Over the past decade, there has been increasing interest in specifically targeting the pre-fusion conformation of these proteins. It is generally thought that antibodies binding this form may disrupt the complex structural transitions to the post-fusion state that are required for cell entry. Such disruption could, in theory, prevent primary cell infection, representing an ideal vaccine strategy.

There is a growing body of evidence suggesting this strategy is a promising one. The most concrete example is that of respiratory syncytial virus (RSV) F protein (Class I). Here, pre-fusion stabilisation exposes conformationally specific neutralising epitopes that play a major role in protection against infection (Ngwuta *et al*, 2015; McLellan, 2015). Recently, a single-dose, protein-in-adjuvant vaccine based on the stabilised F showed >80% efficacy against PCR-positive RSV disease (Papi *et al*, 2023). This result should be compared to an earlier clinical trial of a post-fusion F protein-in-adjuvant vaccine that showed 0% efficacy in adults over 60 (Falloon *et al*, 2017).

Furthermore, this success came decades after previous attempts to immunise against RSV that revealed anti-F antibody-dependent enhancement of disease in children vaccinated with an unstabilised version of the protein (Kim *et al*, 1969). Together, these findings strongly support the pre-fusion stabilisation of fusion proteins for targeting as vaccines.

Additional examples of success using this strategy include parainfluenza virus F protein (Class I). Pre-fusion stabilisation appears to induce greater neutralising antibody titres than the unstable form in animal studies (Stewart-Jones et al., 2018). Similar evidence can be also found for Nipah virus F protein (Class I) (Loomis *et al*, 2020).

In the case of the coronaviruses, there is some evidence that pre-fusion stabilisation of the spike protein (Class I) conveys an immunological benefit. Animal data comparing responses to recombinant protein vaccines of the WT spike and a pre-fusion stabilised version, S2-P, show improved neutralising titres against some strains of MERS virus in a pseudovirus assay (Pallesen *et al*, 2017).

For SARS-CoV-2, pre-fusion stabilisation of the spike protein was successfully deployed in mRNA vaccines developed by Moderna and Pfizer. These both showed strong efficacy data, summarised elsewhere (Patel *et al*, 2022). However, it is important to note that other vaccines with high efficacy did not utilise a pre-fusion stabilised version of spike. Notable examples include the adenovirus vectored vaccine developed by the University of Oxford and AstraZeneca, showing an efficacy of >70% (summarised by Knoll & Wonodi, 2021), and an mRNA vectored vaccine encoding the WT spike sequence (Puthanakit *et al*, 2024).

Whether pre-fusion stabilisation is beneficial for adenoviral vectored SARS-CoV-2 vaccines remains contentious. In mice, an Ad26 vaccine developed by Johnson & Johnson encoding a pre-fusion stabilised spike variant improved the ratio of neutralising to non-neutralising antibody induced (Bos *et al*, 2020). Conversely, immunisation of mice with a chimpanzee adenovirus vaccine platform (ChAdOx1) encoding pre-fusion stabilised spike from the B.1.351 strain did not improve anti-S titres or neutralising titres compared to the unstabilised version (Spencer *et al*, 2022). In this case, a suggested explanation for this lack of improvement is that pre-fusion spike is already well presented *in vivo* after immunisation with the unstabilised antigen using this platform (Watanabe *et al*, 2021).

Taken together, these findings suggest that presenting the pre-fusion conformation of spike to the immune system induces a protective antibody response. For some vaccine platforms (mRNA and some adenovirus), stabilising the pre-fusion antigen conveys a benefit likely through the improved presentation of this conformation. For the ChAdOx1 platform, however, given much of the antigen expressed *in vivo* adopts the pre-fusion conformation *without* adding stabilising mutations, engineering the antigen does not result in improved immunogenicity. On this premise, pre-fusion stabilisation is only

advantageous where this conformation better presents neutralising epitopes to the immune system, and where it is not sufficiently stable in the 'wild-type' form – this appears to be vaccine platform dependent.

Pre-fusion stabilisation has been well studied as a strategy to improve immunogenicity for Class I fusion proteins, but less so for Class II and III. Some relevant data has emerged during the course of the work reported in this thesis. In 2024, mouse studies investigating the Class III fusion proteins human cytomegalovirus (HCMV) gB and RabG yielded mixed results. Stabilisation of a 'pre-fusion like' HCMV gB construct by structure-guided mutagenesis did not improve antibody responses compared to the WT (Sponholtz *et al*, 2024; Karthigeyan *et al*, 2024). For RabG, however, administering a pre-fusion stabilised version of the antigen using an encapsulated mRNA vaccine platform appeared to show modest improvements to neutralising antibody titres (Cao *et al*, 2024). These two cases are discussed in more detail later, on account of their relevance to this thesis.

In summary, pre-fusion stabilisation strategies can convey substantial advantages in the context of antibody inducing vaccine development. However, the benefits do not appear universal across the enveloped viruses and are only well studied for the Class I fusion proteins.

These findings raise two important considerations with respect to the pre-fusion stabilisation strategy:

1) Under what circumstances is pre-fusion stabilisation beneficial to antigen immunogenicity?

2) Given their inherent instability, what strategies might be employed to study fusion proteins that have not successfully been stabilised in their pre-fusion conformation?

This work seeks to contribute to the current knowledge of these outstanding questions in the context of rabies and Epstein-Barr virus. The recent publication of the pre-fusion structure of RabG (Ng *et al*, 2022; Callaway *et al*, 2022) has allowed for study of its

stabilisation and effect on immunogenicity. The same was not true of EBV gB for most of the period of this project: a pre-fusion structure of EBV gB has been elucidated very recently (McCallum & Veesler, 2024), and its antigenicity remains uncharacterised.

1.3 Rabies Virus

1.3.1 Disease Biology

Rabies virus is a small, single-stranded RNA virus of the lyssavirus family, with a genome encoding only five proteins. As is characteristic of this family, rabies is a neurotropic virus that infects a wide range of mammalian hosts. These include bats, cattle, cats and racoons amongst others, though dogs are responsible for >99% of human infections (Kumar *et al*, 2023).

Rabies is spread through the bite of an infected animal. Virus particles in the saliva are typically delivered upon skin puncture, after which they enter the peripheral nervous system (Fooks *et al*, 2017). From here, the virus migrates into the central nervous system (CNS) via retrograde transport in the motor neurons. Symptom onset proceeds after CNS infection at which point disease progression is nearly 100% fatal (Fooks *et al*, 2017).

Rabies disease kills approximately 55,000 people each year, predominantly in Africa and temperate Asia (WHO EXPERT CONSULTATION ON RABIES: THIRD REPORT, 2018). This is despite vaccines against the disease having existed since the 19th Century, and the protective immune response against rabies being well characterised (RABIES VACCINES: WHO POSITION PAPER WEEKLY EPIDEMIOLOGICAL RECORD, 2010).

Eradicating rabies faces major challenges. Perhaps most important, the virus' ability to infect a wide variety of mammalian species greatly hampers the ability to disrupt its reservoirs. Given, however, that dogs are responsible for nearly all transmission to humans, the human disease burden may be greatly reduced through a three-pronged, One Health approach. This may operate by 1) raising awareness of rabies disease and the risk posed by dogs; 2) vaccinating dogs; 3) administering pre- and post-exposure prophylaxis to those at risk of or recently exposed to the virus (Shafaati *et al*, 2023).

1.3.2 Current Status of Rabies Treatments

The prevention of symptomatic rabies disease is achieved by a combination of pre-exposure prophylaxis (PrEP) and post-exposure prophylaxis (PEP), or the latter alone. PrEP comprises administering an approved rabies vaccine commonly using a 3-dose regimen over the course of three weeks. PEP involves the administration of 4 or 5 doses of the same or an equivalent vaccine over one month immediately following exposure (WHO EXPERT CONSULTATION ON RABIES: THIRD REPORT, 2018).

In addition to the PEP vaccine regimen, thorough wound cleaning is performed, and rabies immune globulin (RIG) may be administered for high-risk exposures. Either human- or equine-derived, RIG is administered at doses of up to 20 and 40 International Units (IU)/mL, respectively (WHO EXPERT CONSULTATION ON RABIES: THIRD REPORT, 2018).

Though PEP alone is considered sufficient for protection from disease, there are substantial challenges associated with its use. Firstly, treatment must commence within days of exposure given that symptom onset may begin fewer than 20 days after a bite (Fooks *et al*, 2017). In addition, the effectiveness of PEP depreciates rapidly if commencement of the protocol is delayed: breakthrough infections have been reported in patients administered PEP as little as 2 days post-exposure (Whitehouse *et al*, 2023).

Rabies disproportionately affects those living in rural, underprivileged settings (RABIES VACCINES: WHO POSITION PAPER, 2018). Considering this, access to a clinic capable of administering PEP on the appropriate timescale can be extremely challenging. Additionally, completion of the multi-dose regimen would require repeated trips to the clinic. This may be unfeasible for those living and/or working far from a healthcare provider.

On top of these logistical challenges, the cost associated with a full PEP regimen is non-trivial. Though prices vary widely by geographical region, estimates for the cost of PEP in India, where rabies deaths are most prevalent, is approximately $58 per course (Haradanhalli *et al*, 2019). If passed on to the patient, the cost of PEP may be a

considerable barrier to access, especially when combined with a lack of understanding of the risk of rabies disease (Changalucha *et al*, 2019). Best estimates place the total financial burden of PEP alone at approximately $1.8bn annually (WHO EXPERT CONSULTATION ON RABIES: THIRD REPORT, 2018). This is a substantial contributor to the global financial burden of rabies as a whole, valued at $8.6bn per year (Hampson *et al*, 2015).

Though PEP is a more expensive method of controlling rabies disease than dog vaccination (Brunker & Mollentze, 2018), dog vaccination rates must be maintained at >70% for effective disease mitigation (WHO EXPERT CONSULTATION ON RABIES: THIRD REPORT, 2018). Taken together, these observations warrant further investigation of the cost-effectiveness of PrEP, though few studies have sought to do this (Quiambao *et al*, 2020; Royal *et al*, 2022; Ritchie *et al*, 2025).

Given its reliance on the same vaccine platforms as PEP, administering PrEP may also be costly. However, effective administration of PrEP reduces the number of doses of PEP required for protection and avoids the need for RIG in severe exposure cases (RABIES VACCINES: WHO POSITION PAPER, 2018). Further, PrEP administration extends the window in which effective PEP may be administered, likely due to the anamnestic response that can be induced decades after original vaccination (De Pijper *et al*, 2021). Although it would never be recommended that a previously PrEP-vaccinated individual would not require PEP after an exposure, it is well known that many people are unable to access PEP when needed, and also (primarily from animal data) that PrEP can achieve substantial, albeit imperfect, protection without PEP. It is therefore possible that routine PrEP could save lives that would not be saved by a PEP-only approach.

Despite these factors, consensus thinking is that PrEP largely remains cost ineffective relative to the combination of PEP and dog vaccination. The analyses that support these conclusions, however, are highly dependent on the cost of vaccine (Ritchie *et al*, 2025).

Though there have been varied efforts to develop next-generation rabies vaccines over the past 15 years (Fisher & Schnell, 2018), rabies vaccines in wide circulation are decades

old. These whole-virus inactivated vaccines are produced either in cell culture or using embryonated egg-based culture (RABIES VACCINES: WHO POSITION PAPER, 2018), methods that remain largely unchanged since the 1960s. Furthermore, current vaccines require multiple (up to 5) doses for a full course. It follows that the development of new, cheaper rabies vaccines that rely on modern production and vaccinology techniques may substantially alter the cost-benefit landscape of pre-exposure rabies interventions.

Vaccines that specifically focus on the rabies glycoprotein are a particularly attractive prospect. RabG is well understood to be the target of the virus-neutralising antibody (VNA) response (Shi *et al*, 2022). In addition, VNA titres above a threshold of 0.5 IU/mL are considered a surrogate of clinical protection (WHO EXPERT CONSULTATION ON RABIES: THIRD REPORT, 2018).

Taken together, there are significant grounds for investigating RabG subunit vaccine platforms as possible next-generation rabies prophylactics. Ideally, such vaccines would be cheap to manufacture and require only a single dose to achieve VNA titres above the threshold deemed protective.

1.3.3 Pre-fusion Stabilisation of RabG

Of the five proteins that the rabies virus genome encodes, infection of neuronal host cells is entirely mediated by RabG for all mammals the virus infects (Fisher *et al*, 2018). RabG not only acts as the fusogen but likely binds cell surface receptors to facilitate virion docking. Multiple proteins have been suggested as putative RabG receptors, without firm evidence that any individual receptor is essential in all contexts: RabG may be able to bind nicotinic acetylcholine receptors (nAChR), the neural cell adhesion molecule (NCAM), the neurotrophin receptor $p75^{NTR}$, and the metabotropic glutamate receptor 2 (mGluR2) (Fisher *et al*, 2018; Guo *et al*, 2019b).

It is perhaps receptor redundancy that permits virion entry into such a wide variety of cells in different host species. Despite this possible redundancy, however, the RabG protein itself remains essential for entry to all cell types, making it a robust target for a vaccine-induced protective antibody response.

Neutralising antibodies raised against RabG generally target four well characterised antigenic sites, I-IV, along with a minor fifth (site 'a') on the antigen ectodomain, summarised by Shi and colleagues (Shi *et al*, 2022). Whilst sites I, II, III and 'a' are expressed on the surface of both pre- and post-fusion RabG, their conformations and level of surface exposure differ. Site IV is buried in the post-fusion structure (***Figure 1.3-1***).

This may have important implications with respect to vaccine development should one conformation of RabG better present neutralising epitopes to the immune system. Examples of neutralising monoclonal antibodies, such as RVC20 (Site I), that exhibit conformational specificity exist (Hellert *et al*, 2020). However, it is unclear whether the pre- or post-fusion conformation are more potent in inducing VNA.

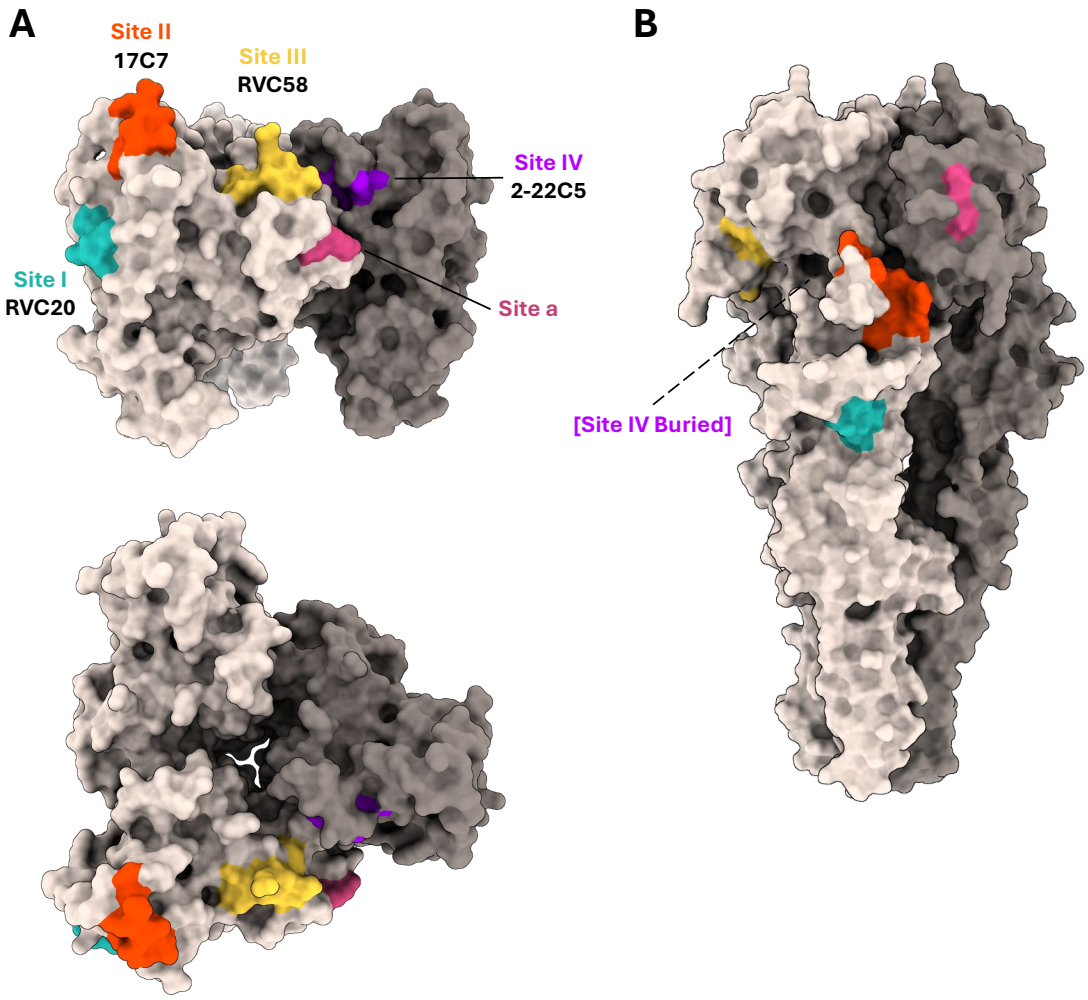


Figure 1.3-1: Antigenic sites on the rabies glycoprotein.
(A) Structure of the pre-fusion RabG trimer (PDB: 8A1E) from a side-on perspective (top) and looking down at the trimer (bottom). Known antigenic sites are highlighted in colour. For clarity, Site IV is displayed on an adjacent monomer to the other sites.
(B) Structure of the post-fusion RabG trimer (PDB: 6LGW) with antigenic sites coloured as per (A). For clarity, Site 'a' is shown on an adjacent monomer to the other sites. In the trimeric model, Site IV appears buried.

1.3.4 Rabies Virus Objectives

The lack of understanding with respect to conformation-specific immunogenicity is due in part to the difficulty of stabilising the pre-fusion conformation of RabG. The work described here therefore seeks to identify mutation strategies for stabilising the pre-fusion conformation. Successful mutants were screened *in vivo* to compare their immunogenicity relative to the wild-type RabG.

In this work, immunogenicity studies are carried out using an adenovirus vectored vaccine platform, ChAdOx2, and lipid nanoparticle-encapsulated mRNA encoding RabG. These platforms were investigated instead of protein-based subunit vaccines on account of the

challenges associated with expressing properly folded, trimeric RabG antigen (Ertl, 2019; Li *et al*, 2023). In addition, the relative expensiveness of protein-in-adjuvant vaccines is likely to hinder their cost-effectiveness (Ertl, 2019), a key consideration in the rabies vaccine space.

Use of vectored delivery of a pre-fusion stabilised antigen is a different approach from the majority of early work on pre-fusion stabilised Class I fusion proteins, which focused on use of soluble recombinant proteins. However, with the success of mRNA and viral vectored COVID-19 vaccines, vectored delivery is now a mainstream approach. Investigation of vectored delivery of stabilised RabG constructs may therefore be informative regarding the use of similar strategies for other stabilised antigens.

This is a particularly pertinent question given that the test-case with which these strategies are generally premised, the RSV F vaccine, was one of those conducted using a protein-based immunogen. It has therefore, at least in part, been assumed that engineering strategies successful in this protein vaccine context may also be applied to the vectored vaccine one. Further investigation of this assumption's validity is warranted.

1.4 Epstein-Barr Virus

1.4.1 Disease Biology

EBV is a γ-herpesvirus that infects over 95% of the world's population (Cesarman, 2014). It is predominantly spread via the saliva with the majority of transmission occurring in two waves: early childhood and early adulthood (Naughton *et al*, 2021). Though childhood transmission is largely asymptomatic, infection with EBV as a young adult produces acute symptoms in many cases, known as infectious mononucleosis (IM) (Naughton *et al*, 2021).

After primary infection of epithelial cells in the nasopharynx, EBV infects B cells in the tonsillar lymphoid tissue (Münz, 2019). The virus is subsequently able to establish life-long latency in the memory B cell compartment. At this point virus antigen expression is almost entirely suppressed, hampering the immune system's detection of infected cells (Münz, 2019).

Re-entry into the lytic phase may occur decades after primary infection. This may result in viraemic disease, particularly in immunocompromised individuals who can develop chronic symptoms (Kerr, 2019). The lytic replication pathway, which occurs in EBV-infected plasma cells, can also drive the development of cancers such as primary effusion lymphoma (Münz, 2019). Furthermore, this process ultimately leads to reinfection of epithelial cells. Alongside viral shedding into the saliva, EBV may drive uncontrolled epithelial cell growth, leading to cancers including nasopharyngeal carcinoma (Münz, 2019).

Latent EBV is also able to contribute to disease. The virus-driven proliferation of B cells to maintain a stable pool of infected cells not only facilitates viral persistence but is fundamental to the development of B cell cancers (Münz, 2019). These include Burkitt, Hodgkin and non-Hodgkin lymphomas (Indari *et al*, 2024). Cumulatively, EBV contributes to the development of nearly 2% of cancers globally (Young *et al*, 2016).

More recently, solid epidemiological data has implicated EBV infection in the development of multiple sclerosis (MS) (Bjornevik *et al*, 2022). Though current mechanistic understanding is incomplete, high titres of antibodies against the EBV nuclear antigen (EBNA1) have been associated with increased MS risk (Bjornevik *et al*, 2023). These antibodies may cross react with self-antigen, leading to MS disease. Anti-EBNA1 antibodies have recently been identified that are also capable of binding the glial cell adhesion molecule (GlialCAM) (Lanz *et al*, 2022).

The considerable disease burden of the EBV-associated cancers as well as that of MS has sparked renewed interest in the development of vaccines against the virus. Given their related architecture and proteome, many of the vaccine strategies being investigated for EBV are relevant to other herpesviruses and vice versa. It is therefore important to outline the current status of human herpesvirus vaccine research more broadly.

1.4.2 Human Herpesvirus Biology

The human herpesviruses (HHVs) are double stranded DNA viruses (~130 - 250 kb) of considerably greater complexity than rabies. To date, eight HHVs have been identified (Cohen, 2020), all with near-obligate human tropism, as well as a simian herpesvirus that can also infect humans (Hu *et al*, 2022).

Like for EBV, most HHV infection is asymptomatic or causes mild symptoms, but the viruses establish life-long infection and can remain latent for decades before reactivating (Cohen, 2020). In a minority of cases reactivation can result in significant or even life-threatening disease (Damania *et al*, 2022; Gugliesi *et al*, 2020; Kennedy & Gershon, 2018).

There is particular interest in the development of vaccines and therapeutics against the five HHVs that cause the greatest burden of disease: Epstein-Barr virus (EBV), discussed earlier, human cytomegalovirus (HCMV), herpes simplex virus (HSV) 1 and 2 and varicella zoster virus (VZV).

HCMV infection represents the leading cause of congenital disability (Leung *et al*, 2003). HSV-1 and HSV-2 are common causes of oral, ocular and sexually transmitted infections (Johnston *et al*, 2024). HSV-2 is particularly important as a co-factor in the acquisition of HIV (Desai & Kulkarni, 2015; Schiffer & Gottlieb, 2019; Thurman & Doncel, 2012). Along with EBV, no vaccines for these viruses exist. VZV, the cause of chicken pox in children and shingles in adults, remains the only HHV for which vaccines have been licensed (Andrei & Snoeck, 2021).

VZV vaccines have historically made use of a live-attenuated strain of the virus to treat both infant and adult VZV disease (Gabutti *et al*, 2019). More recently, however, an adjuvanted subunit vaccine based on glycoprotein E (gE), VZV's most abundant surface protein, has achieved high efficacy (>90%) against adult shingles (Lal *et al*, 2015; Cunningham *et al*, 2016).

The success of this gE-based VZV vaccine demonstrates the potential of rationally designed subunit vaccines against HHV glycoproteins. In the case of rabies, antigen selection is self-evident – RabG is the only surface expressed antigen and the target of

the neutralising antibody response. HHVs, however, make use of multiple surface-expressed glycoproteins to facilitate cell docking and entry, greatly complicating choice of a target antigen.

1.4.3 Human Herpesvirus Fusion

Each HHV has one or more species-specific glycoproteins that bind to cell surface receptors. These determine viral tropism and initiate the fusion mechanism upon cell surface docking (Connolly *et al*, 2020). Of these, HSV gD and its EBV analogue gp42 are essential, as are gO, UL128, UL130A and UL131 in HCMV (***Figure 1.4-1***) (Backovic & Jardetzky, 2011; Cooper & Heldwein, 2015).

The core fusion machinery, involved in entry to all target cell types, is conserved across the HHVs. Signals from the accessory proteins are fed through the gH/gL heterodimer which acts as the master fusion regulator. It ultimately activates the fusogen itself, gB, triggering its structural rearrangement (Cooper & Heldwein, 2015).

There has been extensive review of these antigens as candidates for vaccines against the major herpesviruses (Johnston *et al*, 2016; Ike *et al*, 2020; Egan *et al*, 2020; Escalante *et al*, 2022; Balfour *et al*, 2020; Nelson *et al*, 2018a; Rühl *et al*, 2020; Van Zyl *et al*, 2019). Despite multiple clinical trials of vaccines targeting them, however, none have made it to the clinic.

The focus of this work is specifically on gB as a vaccine candidate. gB represents a promising target on account of its immunogenicity and its central role in viral infection. Acting as the fusogen, it is involved in the entry of all cell types infected by the HHVs. It follows that a vaccine capable of raising a potent anti-gB response could prevent primary infection entirely, or at least limit infection of the different cell types.

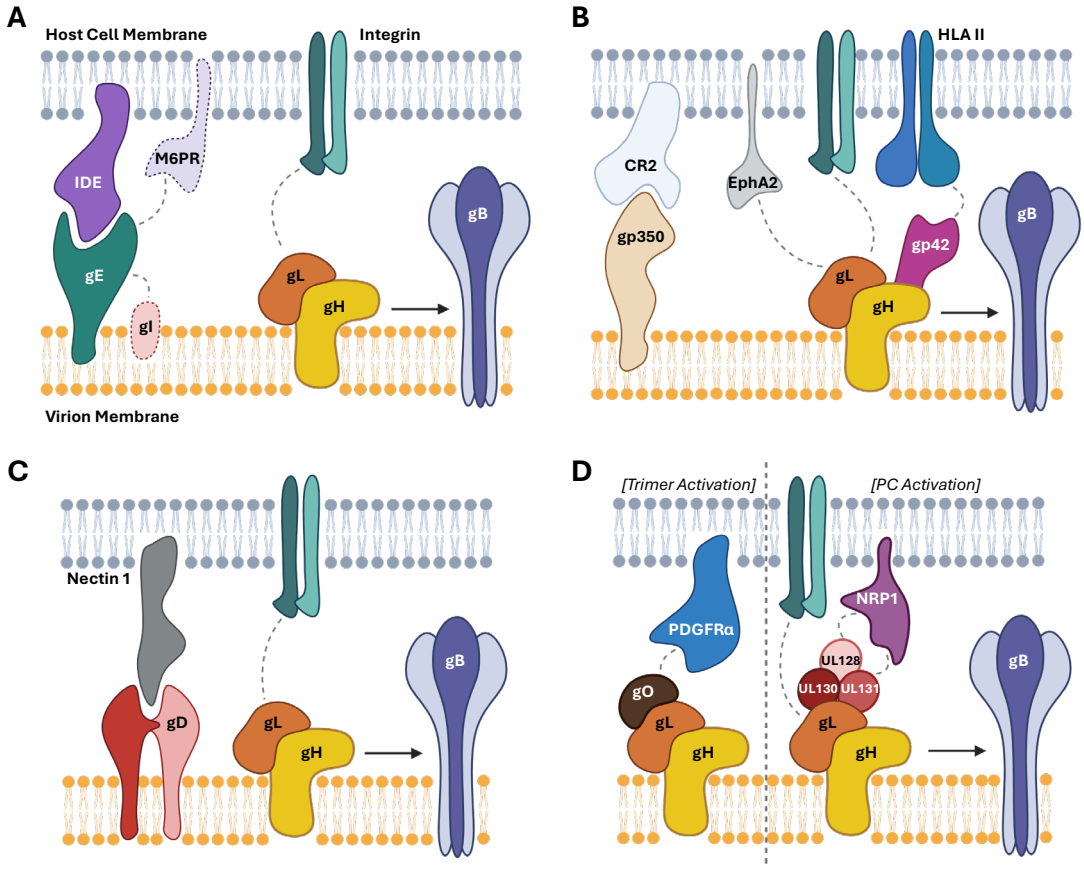


Figure 1.4-1: Human Herpesvirus Fusion Machinery.
Surface glycoproteins involved in the entry of host cells by varicella zoster virus (A), Epstein-Barr virus (B), herpes simplex-1/2 (C) and human cytomegalovirus (D). In all cases, the gH/gL heterodimer acts as the master regulator, ultimately triggering the structural transitions in gB that result in membrane fusion. gB is the fusogen. Species-specific glycoproteins are discussed below.

(A) gE is the major surface protein of VZV. It recognises insulin degrading enzyme (IDE) on host cells, seemingly to promote membrane fusion *(Li* et al*, 2006)* though how essential this is to virion entry is debated *(Oliver* et al*, 2016)*. gI is not essential to the fusion process.

(B) gp350 and gp42 are required for EBV entry into B cells, recognising different receptors on the B cell surface. For epithelial cell entry, only gH/gL and gB are required. The expression pattern of the surface glycoproteins on EBV differ depending on the producing cell type: virion particles produced in B cells express lower levels of gp350 and gp42, resulting in epithelial cell tropism. Virus produced in epithelial cells exhibit higher expression of these antigens, leading to B cell tropism *(Borza & Hutt-Fletcher, 2002)*.

(C) gD's primary host cell receptor is Nectin-1, a Ca^{2+}-independent cell adhesion molecule that is highly expressed on epithelial and neuronal cell membranes. gD binding of Nectin-1 is the initial step of HSV-1/2 entry *(Huang* et al*, 2022)*.

(D) HCMV requires different accessory glycoproteins for entry into different cell types. The pentameric complex's (PC) interaction with neuropillin-1 (NRP-1) is required for entry into epithelial cells and endothelial cells *(Connolly* et al*, 2020)*. For entry into fibroblast cells, gB restricting is triggered by the interaction between the trimeric complex and host-cell PDGFR-α *(Connolly* et al*, 2020)*.

Schematic created with BioRender.com.

1.4.4 Glycoprotein B Structure

As introduced in *Section 1.4.2*, the gB proteins of HHVs are homotrimeric Class III fusion proteins, sharing certain features with Class I proteins and others with Class II.

Although the gB proteins of the different HHVs only share ~30% sequence homology (Burke & Heldwein, 2015; Chandramouli *et al*, 2015), their structures are remarkably well conserved (***Figure 1.4-2A***). As Class III fusion proteins, their homotrimeric structures consist of an α-helical central bundle akin to the Class I fusogens (Backovic & Jardetzky, 2011), and β-rich fusion domains reminiscent of Class II fusogens (White *et al*, 2008).

The gB proteins consist of a large extracellular domain attached to a membrane proximal region (MPR), single-pass transmembrane domain (TMD) and an intravirion C-terminal domain (CTD). The ectodomain can be further subdivided into 5 'domains', DI – DV, encoded as a palindrome in the primary amino acid sequence (***Figure 1.4-2B***).

The topology of the domains in the post-fusion structure have been well characterised in the last 20 years (Burke & Heldwein, 2015; Backovic *et al*, 2009; Oliver *et al*, 2020; Heldwein *et al*, 2006). DI contains the two hydrophobic fusion loops that are inserted into the host cell membrane during fusion. DII has a pleckstrin homology domain and is considered a possible docking site for the gH/gL heterodimer (Burke & Heldwein, 2015; Cairns *et al*, 2014a; Spindler *et al*, 2014; Vennard *et al*, 2018), although this remains uncertain. DIII contains the central helix involved in trimerisation. DIV forms the crown of the post-fusion structure, adjoining DV which runs down the trimeric core to membrane-proximal region (MPR). The MPR sits atop the outer leaflet of the lipid bilayer, stabilising the fusion loops by protecting them from the aqueous environment (Shelly *et al*, 2012)

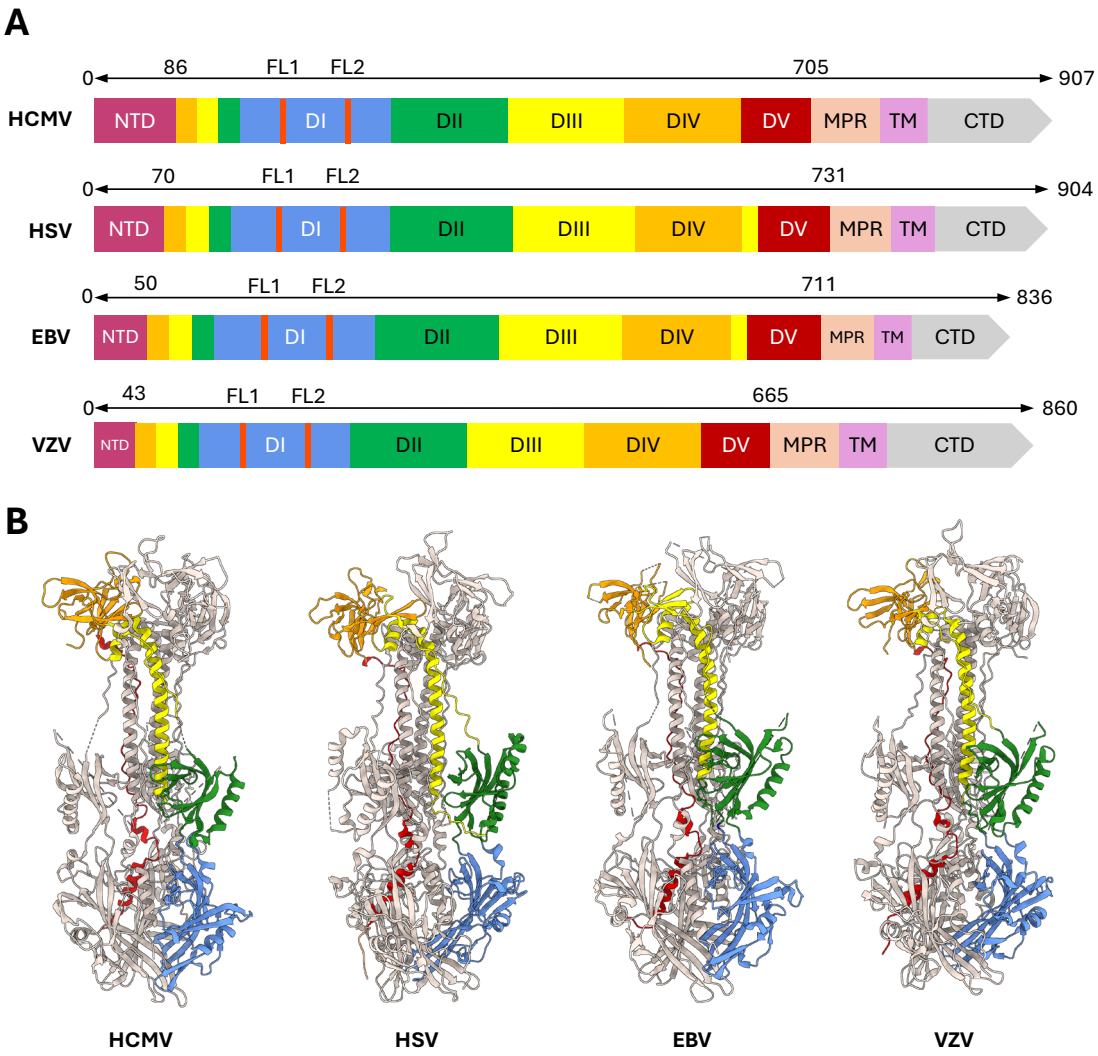


Figure 1.4-2: Human herpesvirus glycoprotein B.

(A) Ribbon diagrams showing domain arrangements in the polypeptide chains of the different HHV gB proteins. The N-terminal domain (NTD, magenta) are largely unstructured. Domain I (DI, blue) contains the fusion loops. DII (green) contains a pleckstrin homology fold. DIII (yellow) is a long helix that forms the core of the trimer. DIV (orange) is the crown of the post-fusion conformation. DV (red) tracks down the ectodomain to the membrane proximal region (MPR). This leads to the transmembrane (TMD) and C-terminal domains (CTD). The respective lengths of the NTD, ectodomain and full gB protein are shown for each virus.

(B) The post-fusion structures of each of the gB protein trimers: HCMV (PDB: 5CXF), HSV-1 (PDB: 5V2S), EBV (PDB: 3FVC) and VZV (PDB: 6VLK). Domains are coloured as per (A) for a single monomer in the trimer.

On the surface of the virion, gB exists predominantly in the pre-fusion form before the series of conformational changes that facilitate membrane fusion. This conformation is generally far less well characterised. A high-resolution structure exists for HCMV gB (Liu *et al*, 2021a) as does a low-resolution one for HSV-2 gB (Vollmer *et al*, 2020). As with the post-fusion, these structures appear well conserved with respect to domain arrangements across the HHVs (***Figure 1.4-3***). Though DI and DII form the flanks of

the pre-fusion trimer, as in the post-fusion, DIV is buried within its centre. This highlights the considerable rearrangement from pre- to post-fusion gB, the details of which are still being elucidated (McCallum & Veesler, 2024).

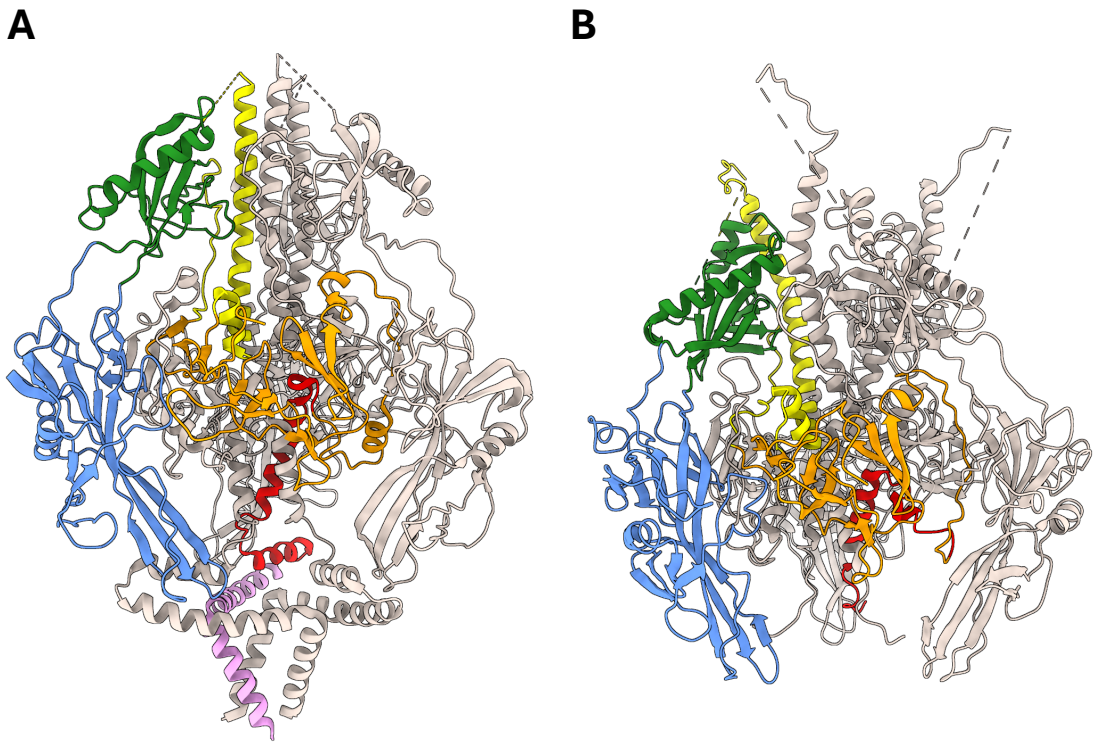


Figure 1.4-3: Pre-fusion glycoprotein B structures.

(A) The high-resolution (3.6 Å) Cryo-EM structure of pre-fusion HCMV gB (PDB: 7KDP). Domains are coloured as per **Figure 1.4-2**. Though the folds of each domain are similar between the pre- and post-fusion conformations, the arrangement of the domains with respect to one another is markedly different. DIV, the crown of the post-fusion structure, is tucked away in the centre of the trimer. DIV no longer runs the length of the trimeric core.

(B) Pseudoatomic model of HSV-1 gB from its low-resolution (9 Å) structure (PDB: 6Z9M). Arrangements of the domains are similar to those of pre-fusion HCMV gB (A) with the exception of DIII. The DIII helix expands outwards from the axis of C_3 rotational symmetry, resembling a more 'open' structure than that in (A). This may be a byproduct of the low-resolution map to which models were fitted, or a reflection that the two structures elucidated present different configurations of the pre-fusion DIII helices, the 'closed' state (A) and the 'open' state. gB fusogens interchangeably adopting 'open' and 'closed' configurations is supported by recent structural analyses of pre-fusion gB constructs and Class III fusion proteins more broadly *(McCallum & Veesler, 2024)*.

1.4.5 Glycoprotein B Immunology

gB is well understood to be the target of a robust antibody response consisting of both neutralising (nAb) and non-neutralising antibodies (non-nAb). In the case of HCMV, efforts to map the antibody response to gB date back over 30 years (Wagner *et al*, 1992). Immunological hotspots for both HCMV, termed 'antigen domains (AD)', and equivalents for HSV-1/2, 'functional regions (FR)', have been characterised over various studies.

Where these regions correspond to on gB and their immunological relevance are a summarised in ***Table 1.4-1***. No analogous system has been described for EBV gB, which remains understudied.

Structural Domain	HCMV Antigenic Domain	HSV Functional Regions	Comments	Ref
Unstructured N-terminus	AD2	FR4	For both HSV-1 and HCMV, this antigenic hotspot can be subdivided into two sites, one that is heterogeneous across laboratory strains, and another that is conserved. The latter is targeted by neutralising antibodies.	(Meyer *et al*, 1992; Cairns *et al*, 2014a; Bender *et al*, 2007)
DI (inc. Fusion Loops)	AD5	FR1 (Encompasses DI as well as the base of DV near the membrane)	Key for site for neutralising antibody. The suggested mechanism of neutralisation is the inhibition of Fusion Loop insertion into host membrane.	(Perotti *et al*, 2020; Cairns *et al*, 2014a; Spindler *et al*, 2014; Wiegers *et al*, 2015)
DII	AD4	FR2	Recognised by neutralising antibody. Antibodies to DII possibly disrupt gH/gL docking on gB.	(Cairns *et al*, 2014a; Spindler *et al*, 2014; Vennard *et al*, 2018)
DIV	AD1	FR3	Recognised by neutralising and non-neutralising antibody. For HCMV, AD1 has been referred to as immunodominant on account of anti-AD1 antibodies being common to human serum samples. This is discussed in more detail in *Results IV*.	(Pötzsch *et al*, 2011; Schoppel *et al*, 1996)
DV / C-terminus of the ectodomain	AD6		Antibody against this domain is non-neutralising, though appears to play a role in limiting cell-to-cell HCMV spread *in vitro*.	(Gomes *et al*, 2023)
Intravirion C-terminal Domain	AD3		Not recognised by any neutralising antibodies.	(Pötzsch *et al*, 2011)

Table 1.4-1: Immunogenic hotspots on glycoprotein B, as described for HCMV and HSV-1/2.

It is unclear to what extent naturally-acquired anti-gB antibody contributes to control of HHV infection (Martinez & Krams, 2017; Cairns *et al*, 2014b). Whilst neutralising antibodies, by definition, can prevent cellular infection, less is known about the potential role(s) of the non-neutralising response.

The term 'non-neutralising' may wrongly imply a lack of functionality or indeed a minor role in protection against viral infection and disease. Instead, the importance of non-nAb has been well described for multiple viruses, notably HIV (Mayr *et al*, 2017) and influenza in animal models (Ko *et al*, 2021; Asthagiri Arunkumar *et al*, 2019).

Non-nAbs largely act through engagement of the antibody Fc region with an Fc-receptor on a host cell (Van Erp *et al*, 2019). Chandler and colleagues have recently reviewed the main mechanisms by which non-nAb, including against HHVs, may disrupt viral replication (Chandler *et al*, 2023). These mechanisms include the destroying of infected cells via:

1) Antibody-dependent cellular cytotoxicity (ADCC). Deposition of antibody on the surface of antigen-presenting infected cells is detected by mononuclear (NK cells, macrophages) and/or polymorphonuclear cells (neutrophils, eosinophils, basophils) via their Fcγ Receptors type I, II and III (FcγRI-III). Cross-linking of these receptors on the effector cell surface triggers downstream expression and release of perforins and granzymes and reactive oxygen species to kill target cells (Gómez Román *et al*, 2014).

2) The clearing of infected cells by antibody-dependent cellular phagocytosis (ADCP) or of extracellular virion. ADCP is facilitated in a similar fashion to ADCC: cell-/virion-expressed antigen is complexed predominantly by IgG type antibody, which in turn is recognised by FcγR on the surface of phagocytic cells (generally macrophages). Given the low affinity nature of the FcγR/IgG interaction, multiple interactions and receptor cross-linking are required to activate the phagocyte (or inhibit it, in the case of FcγRIIb). Once activated,

these cells engulf the antibody-decorated virion or cell and subsequently destroy them in the phagolysosome (Tay *et al*, 2019).

3) The activation of the classical complement pathway to destroy virion or to lyse infected cells. Antibody deposited on the virion/cell surface are coordinated by complement factor C1q which catalyses the deposition of the classical pathway c3 convertase, C4bC2a. The subsequent cleavage and deposition of C3b on the membrane, followed analogously by C5b deposition results in the culminates in the formation of membrane attack complexes that lyse the virion/infected cell (Stoermer & Morrison, 2011).

For the HHVs, clinical trial data investigating gB vaccines would appear to show that anti-gB nAb responses are not a good predictor of efficacy. To provide contrasting examples, a subunit vaccine against HSV-2 comprising of gB and gD was able to induce high nAb titres in participants across two Phase II trials but showed poor efficacy (Corey *et al*, 1999). In almost the inverse case, Phase II trials of the gB-based HCMV protein vaccine administered with a squalene-based adjuvant, MF59 (gB/MF59 hereon, discussed in detail later), show very poor induction of nAb and yet the vaccine achieved ~50% efficacy (Baraniak *et al*, 2018a). Mouse models point toward to a similar conclusion: in the case of murine cytomegalovirus, both nAb and non-nAb against gB can protect against lethal challenge when administered prophylactically (Bootz *et al*, 2017).

There is also some evidence that anti-gB antibodies may protect against HSV-2 infection via ADCC. A mouse challenge study showed that protection against infection is only seen in the case where antibody is co-administered with human mononuclear cells capable of performing ADCC and is not predicted by *in vitro* neutralisation (Kohl *et al*, 1990).

A more recent study has subsequently shown that a new monoclonal non-nAb against HSV-2 gB is protective in a mouse challenge model and is able to activate murine FcγRIV, a biomarker of ADCC (Kuraoka *et al*, 2023). Authors investigating the bivalent gB/gD HSV-2 vaccine that showed poor clinical efficacy suggest the poor induction of ADCC may explain the lack of protection despite high nAb titres (Kohl *et al*, 2000).

Whilst titres of antibody capable of inducing ADCC have been shown to correlate with protection against congenital HCMV infection (Semmes *et al*, 2022), this effector function did not appear to be differentially mediated by anti-gB antibodies when comparing protected participants to infected ones (Semmes *et al*, 2023). Follow-up immunological studies of the gB/MF59 Phase II trials support this notion, showing that immunised patients do not generate strong ADCC responses post-vaccination (Baraniak *et al*, 2018a).

ADCP, on the other hand, was potently induced after vaccination with gB/MF59, so may provide a mechanism by which anti-gB antibody was protective (Nelson *et al*, 2018b). A study of $HCMV^{+}$-donor, $HCMV^{-}$-recipient lung transplant patients has subsequently shown that strong ADCP responses are induced post-transplant, with control of infection correlating with anti-gB IgG3 titres (Eberhard *et al*, 2021).

Non-nAb may also contribute to protection by mediating complement-dependent virion- or infected cell-killing, at least for HCMV. Multiple mouse studies have shown complement-dependent enhancement of neutralisation *in vitro* (Cui *et al*, 2018; Chiuppesi *et al*, 2018; Loomis *et al*, 2013) as well as in gB/MF59 vaccinees (Li *et al*, 2017). This suggests that anti-gB antibody capable of binding to virion, but not necessarily able to prevent cellular invasion directly, could still contribute to protection.

It therefore seems clear that both neutralising and non-neutralising antibody against gB may protect against primary infection with other HHVs. This may occur by binding to extracellular virion and directly preventing cell entry or destroying virus particles via complement activation. Acting via ADCC and/or ADCP, anti-gB antibodies may also limit viral dissemination by facilitating the killing infected cells.

Studies of non-nAb functionality against EBV gB are, however, lacking – this is partly due to the historical focus on gp350 as a prime vaccine candidate (Escalante *et al*, 2022). None could be identified that investigate the possible functions of non-neutralising anti-gB antibodies in protection. This is perhaps surprising given the evidence presented above of their importance in the context of HCMV and HSV-1/2 gB. In addition to their contribution to preventing infection, non-neutralising anti-gB antibodies have also been

implicated in controlling direct cell-to-cell spread of HCMV after gB/MF59 vaccination (Gomes *et al*, 2023). This mechanism of viral propagation is a key aspect of EBV's persistence and immune evasion after infection (Nanbo *et al*, 2016).

1.4.6 Historic gB-based Vaccine Developments

gB-based vaccines have been the subject of multiple clinical trials for HCMV and HSV-1/2, but not EBV. These are summarised in *Appendix I* with descriptions of their outcomes where available.

Perhaps most relevant to this thesis are the clinical trials of the HCMV gB/MF59 vaccine. Across multiple Phase II studies, the vaccine showed ~50% efficacy against HCMV infection (Pass *et al*, 2009; Bernstein *et al*, 2016; Griffiths *et al*, 2011). As mentioned earlier, protection against infection does not appear to be associated with neutralising antibodies against gB, which are not induced in high titres (Baraniak *et al*, 2018a).

Instead, a follow-up immunology study suggested protection is correlated with antibody titres against a cell membrane-expressed, 'native' gB (Jenks *et al*, 2020). That is, antibodies capable of binding gB that is presumably predominantly in its pre-fusion conformation appear to convey protection; those binding the recombinant gB ectodomain, entirely in the post-fusion, do not (Jenks *et al*, 2020). Further investigation of the pre-fusion form of gB is warranted given its potential in improving the protective immune response.

Despite its failure to reach licensure, the gB/MF59 vaccine against HCMV is perhaps the closest candidate to a successful vaccine of all those tried against HCMV, HSV-1/2 or EBV. gB therefore represents a promising antigen to target for the HHVs more generally.

For EBV in particular, gB is poorly understood as a vaccine target – ongoing EBV clinical trials either continue to target gp350 (NIAID, ClinicalTrials.gov: NCT04645147) or combinations of surface antigens that do not include the fusogen (Moderna Tx, ClinicalTrials.gov: NCT05164094). Given the promise of gB from HCMV studies, and its lack of study in the context of EBV, this work seeks to investigate gB and its immunology.

Jenks and colleagues' study of the anti-gB response induced to in gB/MF59 vaccinees suggest antibodies to the pre-fusion conformation are important for protection (Jenks *et al*, 2020). Whether this is true for EBV is entirely unknown given the lack of understanding of its pre-fusion structure, limiting the ability to study it.

1.4.7 EBV Objectives

Our understanding of the pre-fusion conformation of gB lags far behind that of the rabies glycoprotein. Studying the pre-fusion form of RabG is greatly facilitated by two important aspects of our pre-existing knowledge of the protein.

First, a clear physiological trigger to the pre- to post-fusion transition is known: exposing RabG to acidic conditions (Gaudin *et al*, 1993). This characteristic can be exploited as it provides control over protein conformation. In this work, it is used in mutant screening experiments to identify mutants that retain the pre-fusion structure after exposure to low pH conditions.

Second, a pre-fusion-specific anti-RabG antibody has already been discovered (Hellert *et al*, 2020). This greatly facilitates the study of pre-fusion RabG by acting as a method for directly probing antigen conformation. In this capacity, the RVC20 antibody allows for identification of mutants considered 'productive. These can then be tested *in vivo* to study the effect of pre-fusions stabilisation on immunogenicity.

For EBV gB, no clear physiological trigger has been identified for the pre- to post-fusion transition, and no conformationally specific antibody has been characterised. As a result, performing mutagenesis screens for stabilising mutants in the same fashion as for RabG is unfeasible.

Identifying a conformationally specific antibody would therefore facilitate downstream study of pre-fusion gB, as RVC20 did for RabG. This work sought to develop a method for isolating such monoclonal antibodies (mAbs) with the intention of using them as tools for characterising pre-fusion gB.

mAb isolation against pre-fusion gB is, however, greatly challenging given the current inability to stabilise it, raising a chicken-and-egg-style paradox. Such mAbs enable the characterisation of pre-fusion gB, but their isolation is dependent on acquiring B cells that have encountered pre-fusion gB.

Work presented in *Results II* describes the design of a strategy to try and isolate pre-fusion specific antibodies against gB such that the paradox described might be avoided. These antibodies were investigated functionally and structurally to better characterise the anti-gB response, results of which are described in *Results III* and *IV*. Together, this work aims to shed light on whether antibody-inducing vaccines against gB, in the pre- or post-fusion form, present a promising approach for developing EBV therapeutics.

1.5 Appendix I: gB-based HHV Vaccines in Clinical Trials

Virus	Nature of Antigen	Vaccine Platform	Stage	Evidence for Immunogenicity and/or Efficacy	Ref
HSV-2	gB, gD, gC/gE glycoprotein mixture	Alum-adsorbed glycoproteins extracted from HSV-2 infected chick embryo fibroblasts.	Phase II	Anti-gB and gD titres reported as <10% those of naturally infected individuals. Fails to protect against HSV-2 genital infection.	(Mertz *et al*, 1990)
HSV-2	gB & gD	Subunit vaccine administered with MF-59 adjuvant.	Phase II	Otherwise healthy adult men and women from 18-55 years with minimum 1-year HSV-2 infection and >3 genital lesion outbreaks. 10-19% decrease to genital lesion recurrence in vaccine group compared to placebo across 8-month follow-up period. Vaccine failed to meet primary end point efficacy cut-off. Vaccinated cohort showed significant reduction to days until disappearance of lesions as well as to number of days across which new lesions appeared in outbreaks. No significant reduction to viral shedding. Vaccine does boost anti-gD and anti-gB antibody titres, remaining above pre-vaccination levels in 12-month follow-up but no significant correlation between anti-gD or anti-gB titre with improved clinical outcome.	(Straus *et al*, 1997)
HSV-2	gB & gD	Subunit vaccine administered with MF-59 adjuvant.	Phase II	50% lower HSV-2 acquisition rate among vaccine vs placebo in initial 5 months. Overall vaccine efficacy 9% and no influence on duration of first HSV-2 episode or frequency of reactivation.	(Corey *et al*, 1999)

HCMV	gB	Subunit vaccine administered with MF-59 adjuvant.	Phase II	Phase II Clinical trial in HCMV-seronegative women less than 1 year after childbirth showed efficacy of 50% in 42-month follow up. Same vaccine formulation and 3-dose regimen tested in adolescent girls aged 14-17 showed 43% efficacy after 2 years follow up post-third dose. Phase II study of 3-dose regimen in transplant recipients showed anti-gB titres higher in vaccinated cohort compared to placebo. Viremia duration inversely correlated with anti-gB titre and number of required days of ganciclovir treatment significantly reduced in vaccinated cohort compared with placebo. Separate study investigating immune response to vaccine 0-90 days after solid-organ transplant showed faster induction of anti-gB humoral response compared to placebo with proportion of vaccinees raising neutralising anti-gB response.	(Pass *et al*, 2009; Bernstein *et al*, 2016; Griffiths *et al*, 2011; Baraniak *et al*, 2019) NCT00125502 NCT00133497 NCT00815165 NCT00299260

HCMV	gB and phosphoprotein 65	DNA Vaccine with CRL1005 Poloxamer formulation and benzalkonium chloride surfactant to induce nanoparticle formation	Phase II & III	Phase II trial investigated 3-dose regimen in HCMV-positive hematopoietic cell transplant (HCT) recipients aged 18-56 with lymphoma or leukaemia, administered 1-, 3- and 6-months post-transplant. Rate of HCMV-specific initiation of antiviral therapy lower in vaccinated group but not significant (p=0.145). Significant reduction to occurrence of HCMV viremia as measured by PCR amplification of HCMV DNA from patient plasma. Significant reduction to duration of viremia and increase to interval between viraemic episodes. Phase III trial in seropositive HCT transplant recipients with 5-dose regimen showed no significant reduction to composite all-cause mortality and adjudicated HCMV end-organ disease primary endpoint compared with placebo, 1-year post-transplant. Contradictory to Phase II study, pp-65-specific T Cell response higher in placebo group compared to intervention group. Failure to protect attributed to the poor induction of anti-gB antibodies, non-significant when compared to placebo. IFN-gamma-producing T Cells specific to pp65 correlated with protection. In follow-up clinical trial in seronegative kidney transplant recipients receiving HCMV-positive organs, no significant difference in primary endpoint was observed between vaccinated and placebo cohort in a >1 year follow-up. Also attributed to poor induction of a humoral response.	(Wloch *et al*, 2008; Kharfan-Dabaja *et al*, 2012; Smith *et al*, 2013; Vincenti *et al*, 2018; Plotkin *et al*, 2020; Ljungman *et al*, 2021) NCT00285259 NCT02103426 NCT01903928 NCT01974206 NCT01877655

HCMV	gB chimeric protein fused to HSV gD	AS01-E adjuvanted subunit vaccine (GSK)	Phase I non-randomised, open label	No adverse reactions in study of 3 15 µg / dose regimen. Follow-up of a subset of vaccinated participants for 60 months showed elevated anti-gB IgG responses by ELISA compared to naturally infected individuals identified at the initial study screen, however differences were not significant.	NCT00435396 NCT01357915 GSK Study ID: 108890
HCMV	gB, pentameric complex recombinant protein in adjuvant	Phase I/II (Ongoing)		Safety study comparing different doses of gB and pentameric complex in combination. All study arms are administered vaccine at 0, 2 and 6 months, with a minimum follow up to month 18.	NCT05089630
HCMV	gB or pp65/IE1 fusion protein	Alphavirus replicon particle vaccine	Phase I	Seronegative adult participants randomised to vaccine or placebo cohort 4:1 in observer-blinded trial. All participants in vaccine group showed HCMV-specific IFN-gamma production upon T cell stimulation as well as neutralising antibody induction.	(Bernstein *et al*, 2009) NCT00439803
HCMV	gB and pp65	2 non-replicable lymphocytic choriomeningitis virus vectors	Phase I Phase II Terminated	Three doses administered on a 0, 1, 3-month dose regimen to healthy adults. Dose-dependent cell mediated immune response is dominated by pp-65-specific CD8 T cell response. Neutralising anti-gB antibodies induced after two doses, induced in dose-dependent manner. 1 of the 42 participants generated anti-LCMV vector response. Interim Phase II results show no reduction to HCMV viremia, HCMV disease or use of antivirals after two vaccine doses. Reduction in viremia after three doses, however vaccine development halted.	(Kotton *et al*, 2018; Schwendinger *et al*, 2020) NCT02798692 NCT03629080 www.globenewswire.com/news-release/2023/03/15/2627479/0/en/HOOKIPA-Reports-Fourth-Quarter-and-Full-Year-2022-Financial-Results-and-Provides-2023-Outlook.html

HCMV	gB ectodomain fused to VSV-G transmembrane and C-terminal domain .	eVLP derived from murine leukaemia virus gag protein adjuvanted with alum.	Phase I	Three-shot regimen tested in healthy adults with three different doses of gB-G fusion protein. High dose regimen (2 μg) elicited neutralising Abs against fibroblast infection in 100% of patients and against epithelial cell infection in 31% of patients.	NCT02826798
HCMV	gB, pentameric complex, pp65	modified nucleoside mRNA vaccine encoding these antigens in various combinations encapsulated in lipid nanoparticle (LNP).	Phase I - III	Vaccine induces both anti-gB and anti-PC antibody responses in seropositive and seronegative participants, over the 18-month follow-up period. Induction of both neutralising anti-gB antibody and antibody capable of ADCC. Neutralising titres greater than for gB/MF59 vaccinees, however lower overall anti-gB IgG responses and lower ADCP activity. Stronger responses to the PC observed compared to gB. Phase Ib dose-finding study in healthy participants completed 2023. After 3 doses, all dose groups (30, 90, 180, 300 μg mRNA/dose) induce virus neutralising titres comparable to seropositive responses with respect to epithelial cell infection. For fibroblast infection, neutralising titres fall below seropositive controls after 1 year post-follow up. Separate Phase II study in Hematopoietic Cell Transplant patients expected to produce efficacy results in 2025. Phase I/II study in 9-25 year-olds ongoing. Expected results in 2025 to show safety profile in young people as well as immunological response readouts. Phase III study enrolling >6,000 women aged 16-40 expected to finish 2026.	(Hu *et al*, 2024; Fierro *et al*, 2024; Panther *et al*, 2023) NCT03382405 NCT05105048 NCT04232280 NCT04975893 NCT05575492 NCT05085366

Table 1.5-1: Completed and ongoing clinical trials of gB-based/containing vaccines against herpes simplex virus-2 (HSV-2) and human cytomegalovirus (HCMV). At the time of writing, no such trials could be found for EBV or HSV-1.

2 General Materials and Methods

Methods relevant to individual chapters are described in their respective sections. This section includes methods referred to throughout the thesis.

2.1.1 Molecular Biology

For all transformations of plasmid DNA, chemically competent *Escherichia coli* (*E. coli*) were used following the manufacturer's instructions (New England Biolabs, NEB). For newly cloned plasmids, high-efficiency DH5α chemically competent *E. coli* were used (NEB: C2987). Low efficiency *E. coli* were used (NEB C2988) for subcloning. For plasmids encoding constructs for *in vitro* transcription, NEB Stable *E. coli* were used (NEB: C3040). Successfully transformed bacteria were selected for using encoded antibiotic resistance cassettes against carbenicillin or kanamycin (ThermoFisher: 10177012 and 11815024, respectively).

For purification of plasmid DNA, overnight liquid cultures of transformed *E. coli* were grown at 37°C in selective LB media. Bacterial pellets were harvested, lysed and plasmid DNA purified using a QIAGEN Plasmid Plus Midi Kit (QIAGEN: 12945), following the manufacturer's instructions.

2.1.2 Transient Transfection of Expi293F Suspension Cells

Expi293F Cells (ThermoFisher: A14527) were cultured in Expi293 Expression Medium (ThermoFisher: A1435102) in a mammalian cell shaking incubator (SciQuip: SQ-4236) at 37 °C, 8% CO2, 80% humidity, 130 rpm, 25 mm orbital diameter. Cells were transfected at a density of 2.5-3.5 $\times 10^6$/mL using 1 µg plasmid DNA per mL transfection culture. Transfections were performed using the ExpiFectamine transfection kit (ThermoFisher: A14524) as per the manufacturer's instructions. Unless otherwise specified, transfected cultures were incubated for 4 days prior to protein harvest.

To assess the efficiency of each transient transfection, a NanoLuc luciferase (Promega, GenBank ID: JQ513378.1) reporter plasmid was spiked into each transfection at 0.05% of the total plasmid DNA mass. Luciferase readouts were determined by adding 100 µL of the development mix (2 mL PBS, 100 µL NanoGlo assay buffer, 1 µL NanoGlo

substrate, Promega: N1110) to 2 µL of each transfection supernatant and immediately measuring luminescence after excitation at λ_{max} = 460 nm using a ClarioStar Plus Microplate Reader (BMG Labtech). In general, luciferase activity readouts were used simply as a sense-check for successful transfection. For transfections in flasks, scores $>1 \times 10^5$ relative luciferase units (RLU) were considered high efficiency. Scores $<5 \times 10^3$ RLU were considered low efficiency, suggesting erroneous transfection. Luciferase scores in plate-based transfections were generally 10-fold lower than those of flasks.

2.1.3 Transient Transfection of ExpiCHO Suspension Cells

ExpiCHO-S Cells (ThermoFisher: A29127) were cultured in ExpiCHO Expression Medium (ThermoFisher: A2910002) with culture conditions as per *Section 2.1.2*. Cells were transfected at a density of 5.0-6.0 $\times 10^6$/mL using the ExpiFectamine CHO Transfection Kit (ThermoFisher: A29129) using the 'standard protocol' provided by the manufacturer. Unless otherwise specified, transfected cultures were incubated for 9 days prior to protein harvest.

2.1.4 Animal Work Statement

Mice were used in accordance with the UK Animals (Scientific Procedures) Act 1986 under project license numbers P9804B4F1 (October 2020 - January 2022) and PP3331087 (February 2022 onward), granted by the UK Home Office. Content of these licences was approved by the local Animal Welfare and Ethical Review Board at the University of Oxford.

Animals used in experiments were age-matched and randomly assigned to cages upon arrival in the animal housing facility. In all cases, female mice were used. Animals were housed in cage groups using individually ventilated cages under specific-pathogen free conditions. Design of animal experiments was done with attention to the 3Rs principles of Replacement, Reduction and Refinement. All animals were humanely killed at the end of each experiment by an approved Schedule 1 method.

2.1.5 Enzyme Linked Immunosorbent Assay (ELISA)

Multiple ELISA-based experiments are described in this thesis. Details specific to an individual method (e.g. coating antigen or antibody, and detection antibodies) are reported as summary tables in their relevant methods section.

The following elements were, however, common to all ELISA-based experiments described in this thesis, unless stated otherwise:

- ELISA plates (NUNC Maxisorp, ThermoFisher: 442404) were coated at 4 °C overnight in the dark. Coat protein was diluted in phosphate buffered saline (PBS).
- All plate washing steps consisted of 6 washes with PBS + 0.05% Tween-20 (Merck: P9416, PBS/T hereon).
- Washes were performed after every incubation period except that immediately after blocking.
- Coated wells of the ELISA plate were blocked with 200 µL / well blocker casein for (ThermoFisher: 37528).
- All serum samples, proteins and antibodies were diluted in PBS/T.
- For ELISAs that used alkaline phosphatase-conjugated secondary antibodies, the development buffer was formulated as per the manufacturers' instructions using 20 mg 4-nitrophenyl phosphate tablets (Merck: N2765) and diethanolamine buffer (ThermoFisher: 34064). Development buffer was added at 100 µL/well.
- For ELISAs that used horseradish peroxidase (HRP)-conjugated secondary stains, 1-Step TMB ELISA substrate solution (Fisher: 11839260) was added at 100 µL/well. After reaching the development target or incubation time endpoint (specified for each method in thesis), the colorimetric reaction was quenched by the addition of 0.5 M H_2SO_4, 50 µL/well.
- All ELISA plates were read using a CLARIOstar Plus Microplate Reader (BMG Labtech) using absorbance wavelengths of 405 nm and 450 nm for alkaline-phosphatase- and HRP-catalysed detection reactions, respectively.

2.1.6 Flow Cytometry Data Analysis

All flow cytometry data was analysed using FlowJo v10.10.0 (BD Bioscience). Histograms and gating strategy figures were generated using the same software.

2.1.7 Data Visualisation and Statistical Analysis

Graphs and statistical analyses presented in this work were generated using GraphPad Prism v10. Details of statistical analyses are described on a case-by-case basis.

2.1.8 Schematic Figures

Schematic figures that were generated in using BioRender are indicated as such.

2.1.9 Protein Structure Visualisation

Molecular graphics were prepared and analyses performed in UCSF ChimeraX, developed by the Resource for Biocomputing, Visualization, and Informatics at the University of California, San Francisco, with support from National Institutes of Health R01-GM129325 and the Office of Cyber Infrastructure and Computational Biology, National Institute of Allergy and Infectious Diseases (Goddard *et al*, 2018).

3 Results I: Targeted Mutations of the Rabies Glycoprotein Improve Antigen Expression and Stability, but not Immunogenicity.

3.1 Statement of Authorship

All work reported in this chapter was designed and executed by S.E. with the following exceptions:

Dr Sofiya Fedosyuk and Dr Nawsad Alam designed and performed preliminary characterisation of the original set of mutants of the rabies glycoprotein to improve pre-fusion conformational stability of the antigen. Experimental screening of the double mutants was conducted, in part, by Francisco Orliacq as a MSc project directly supervised by S.E.

Animal procedures were conducted with the generous support and training of the Biomedical Services technicians acknowledged earlier.

Adenoviral-vectored RabG vaccines were designed by Assoc Prof Sandy Douglas and Dr Sofiya Fedosyuk and kindly produced by the Viral Vector Core Facility (University of Oxford). mRNA vaccine constructs were designed by S.E. and produced by Dr William Taylor.

VNA Assays were performed by Prof Hildegund Ertl (Wistar Institute) for screening of adenovirus-vectored constructs, and by Biobest Laboratories for screening of mRNA vaccines.

Results from the screening of the original single mutants were submitted as part of a publication on the pre-fusion structure of RabG, on which S.E. is a contributing author:

> Ng, W. M., Fedosyuk, S., English, S., Augusto, G., Berg, A., Thorley, L., Haselon, A.-S., Segireddy, R. R., Bowden, T. A., & Douglas, A. D. (2022). Structure of trimeric pre-fusion rabies virus glycoprotein in complex with two protective antibodies. Cell Host & Microbe, 30(9), 1219-1230.e7.

3.2 Chapter Overview

1) The rabies glycoprotein can be engineered through mutagenesis to improve pre-fusion stability or antigen expression *in vitro*.

2) The effects of productive mutations are additive with respect to pre-fusion stabilisation, but not *in vitro* expression.

3) Selected mutants that best stabilise pre-fusion RabG or that improve expression do not induce greater overall anti-RabG responses or virus neutralising antibody titres than the wild-type.

3.3 Introduction

3.3.1 RabG Mutagenesis to Improve Pre-fusion Stabilisation and Immunogenicity

Two key characteristics of the rabies virus glycoprotein, RabG, make it the most obvious target for rabies vaccines. First, it is the only surface glycoprotein expressed on the virion membrane and the sole player in cellular invasion (Fooks *et al*, 2017; Albertini *et al*, 2012b). Secondly, it is the target of a robust, protective antibody response in vaccinated individuals (Ertl, 2019). Rabies vaccine research is therefore able to focus on improvement of antibody responses against a known antigen target, rather than on antigen discovery, to maximise protection by vaccination.

In general, such efforts seek to improve vaccine responses by a 'quantity-based' approach and/or a 'quality-based' one. Regarding the former, the objective is simply to increase the total antibody titre raised against the target. For the latter, the neutralising antibody response is enhanced without necessarily raising overall titres.

In the case of inactivated whole-virus vaccines and protein subunit vaccines, improving overall antibody quantity is generally achieved through the optimisation of vaccine dose, delivery route, regimen and/or choice of adjuvant (Pollard & Bijker, 2020; Auerswald *et al*, 2023). For viral-vectored vaccines and mRNA vaccine technologies, similar approaches can also be relevant. In addition, there is also scope to enhance antibody quantity by

the improvement of antigen expression on a per-template basis: modifying either the antigen coding sequence (e.g. codon optimisation), untranslated RNA regions, or (in the case of viral vectors) the promoter, may lead to improved protein production *in vivo* which in turn may induce higher antibody titres from an equivalent dose of vaccine.

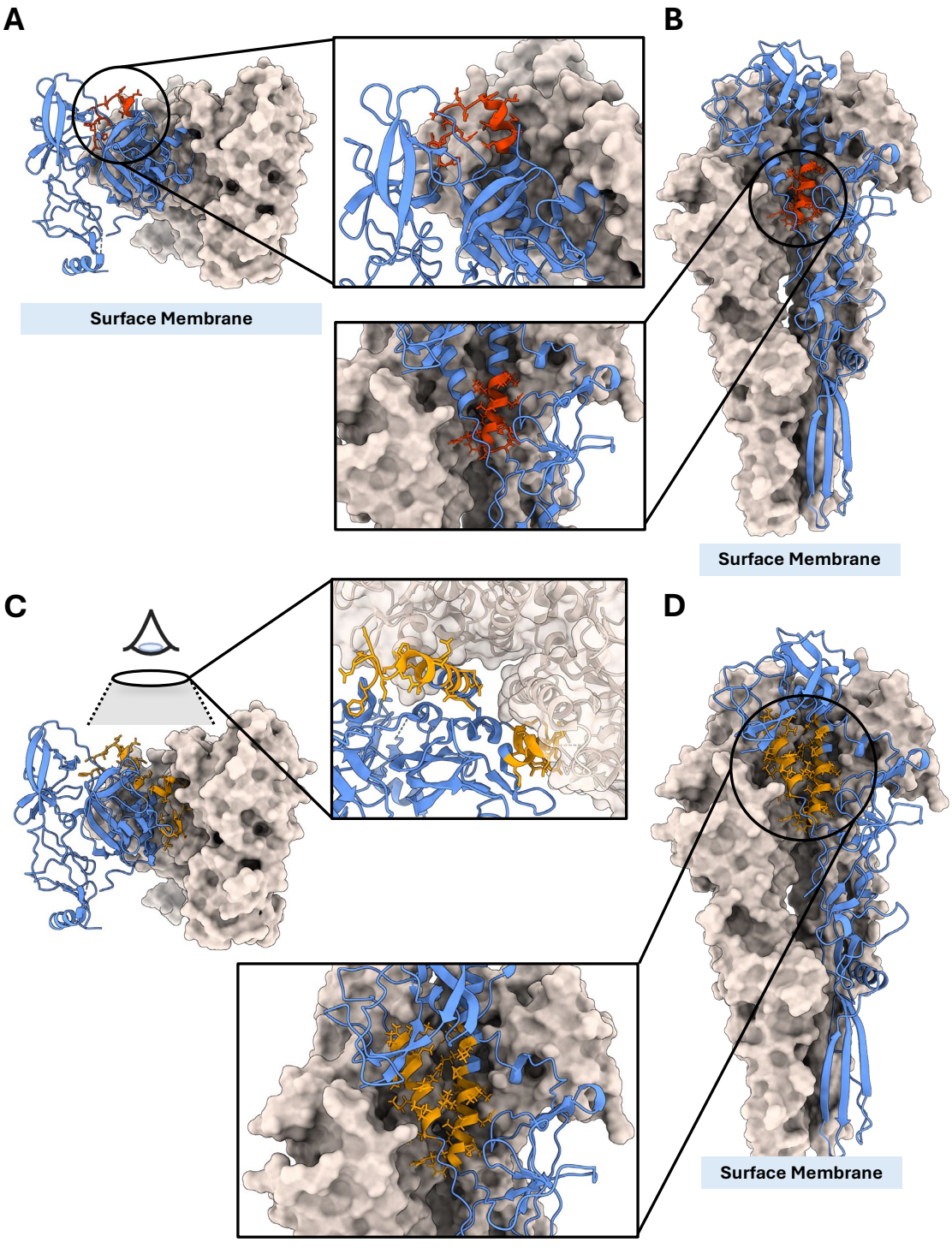
With respect to antibody quality, some inactivated vaccines do induce good-quality responses by preserving both antigen structure and viral architecture to closely mimic real infection. Subunit-, viral-vectored- and mRNA vaccines, however, may all benefit from modifying the antigen itself as discussed in *Section 1.2.3*. For fusion protein targets such as RabG, pre-fusion stabilisation may enhance induction of antibody able to disrupt the cellular invasion pathway, and thus neutralise infection, by presenting the pre-invasion version of the antigen rather than other protein conformations that may be less important targets mechanistically.

Work in this chapter sought to investigate whether mutations to RabG could improve the antibody response raised against the antigen, either quantitatively or qualitatively, by adenovirus- or mRNA-vectored vaccines. The principal strategy used to try and achieve this was to screen a panel of RabG mutants for 1) improved surface expression of the protein relative to the wild-type (WT), and/or 2) improved pre-fusion stability of RabG using a transient transfection model before selecting high-performing mutants for screening *in vivo*.

This work made use of a panel of 73 RabG mutants previously designed by Sofiya Fedosyuk and Nawsad Alam with the intention of stabilising the pre-fusion conformation. These were designed before the availability of a high-resolution pre-fusion structure for RabG. Some mutations (e.g. to position H261) had previously been characterised as inhibiting RabG's function (F. Yang et al., 2020). Others were informed by homology models made using Rosetta (Leman *et al*, 2020) and I-TASSER (Yang *et al*, 2014). A variety of mutagenic strategies were used, summarised in ***Table 3.3-1*** and illustrated structurally in ***Figure 3.3-1***. These include mutants designated 'Rosetta Redesign 1-3' which were informed by assessment of the Rosetta scores of possible combinations of mutations in key parts of the protein (Leman *et al*, 2020).

Mutation Strategy	Rationale
Disulphide bond Introduction (DBD)	Using an online disulphide engineering tool (Craig & Dombkowski, 2013) and a structural model of the pre-fusion RabG designed in Rosetta, disulphide bonds were introduced to positions on the RabG that are proximal in the pre-fusion conformation but separated in the post-fusion form. Covalent linkages in these positions could prevent the rearrangement of RabG to the post-fusion.
Helix-bend-helix proline introduction	A region of the pre-fusion RabG modelled as a flexible loop in the pre-fusion form and unresolved in the basic pH structure of RabG (Yang *et al*, 2020) but that forms part of an extended α-helix in the post-fusion form. Helix disruption by introducing proline residues might therefore prevent formation of the extended post-fusion helix.
Rosetta Redesign 1: Helix-bend-helix	Using the pre-fusion RabG model, the flexible loop that transitions into an extended helix in the post-fusion form was re-designed in Rosetta to stabilise the flexible loop.
Histidine switch deactivation	Acid-dependency of the pre- to post-fusion transition points to an acid sensor in RabG. Based on the pH range that the transition occurs over, ~pH 5.8 - 8 (Irie *et al*, 2006), this may be histidine-controlled. Mutating the pH switch (to amino acids such as leucine which remain hydrophobic at low pH) might prevent rearrangement.
Rosetta Redesign 2: AAs 376-389	Mutations targeting an unstructured region in the Rosetta pre-fusion RabG model that forms into a helix in the post-fusion structure, with the goal of destabilising the helix.
Rosetta Redesign 3: Pre-fusion trimer interface	The mechanism for the pre- to post-fusion transition is still incompletely understood, but it is thought that the RabG trimer may dissociate to allow for rearrangement (Kima *et al*, 2017; Baquero *et al*, 2013; Albertini *et al*, 2012a; Yang *et al*, 2020). Rosetta-guided mutagenesis of the modelled pre-fusion trimer interface aimed to stabilise interactions between monomers to prevent the dissociation of the trimer and therefore the formation of the post-fusion state.
Resistant to Acid-Induced Neutralisation (RAIN)	A set of previously characterised mutants that conveyed resistance to neutralisation by the pre-treatment of virus in acid (Gaudin *et al*, 1996). The resistance is probably the result of stabilising the high pH, pre-fusion structure of RabG (or a transition intermediate) so that some of the surface RabG trimers remain in the pre-fusion conformation and can still trigger fusion.

Table 3.3-1: Mutation Strategies to improve cell surface expression and/or pre-fusion stabilisation of RabG.


A
B
Surface Membrane
Surface Membrane
C
D
Surface Membrane

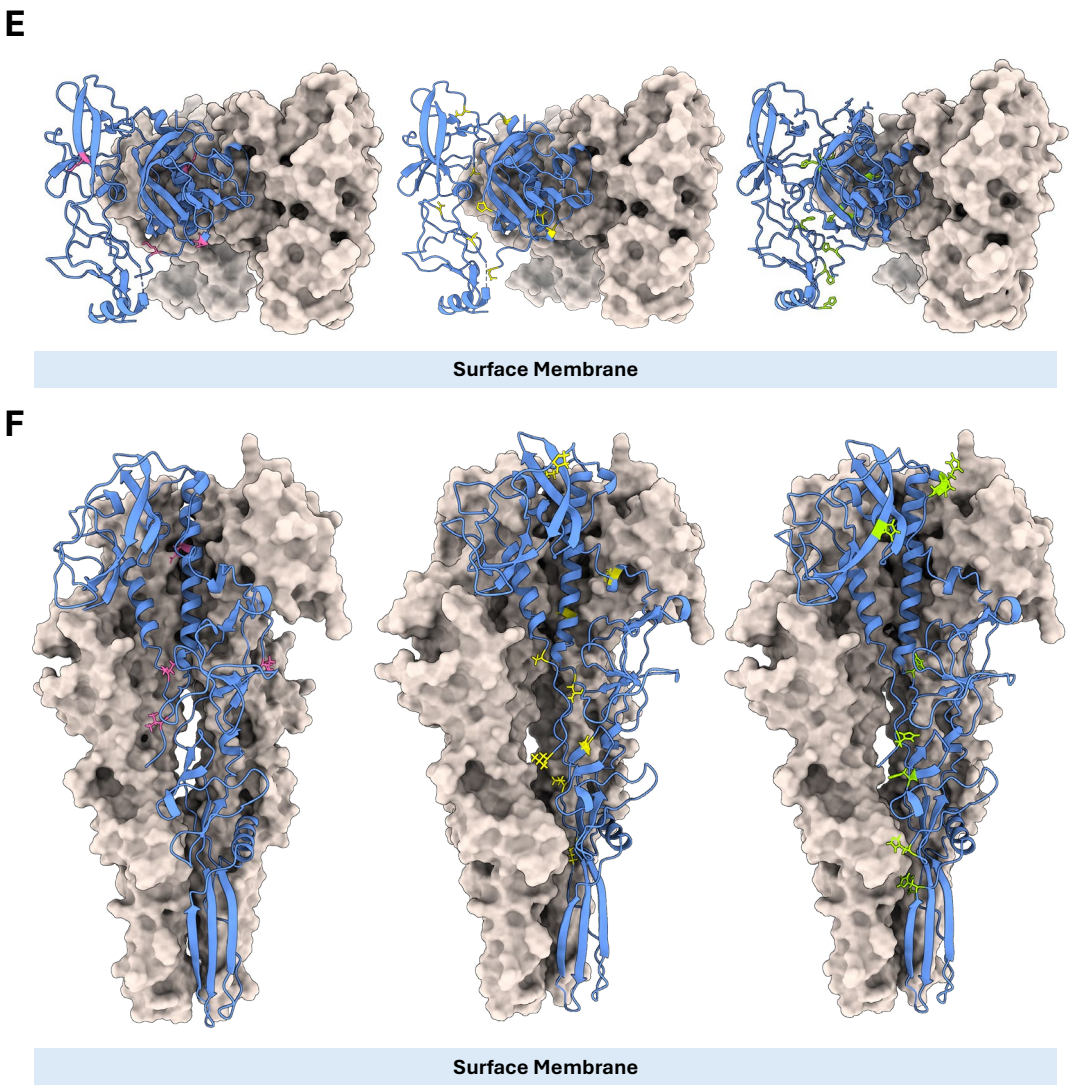


Figure 3.3-1: RabG mutagenesis strategies.
Trimeric RabG ectodomain in the pre-fusion (PDB: 8A1E) and post-fusion conformations (PDB: 6LGW). For all structures, a single monomer is shown in ribbon format (blue), and the remaining monomers as surfaces (grey).

(A) Helix-bend-helix mutations (red) on pre-fusion RabG with the top of the trimer highlighted on the inset.
(B) Helix-bend-helix mutations (red) on post-fusion RabG with the newly formed extended α-helix highlighted on the inset.
(C) Regions of the pre-fusion RabG redesigned computationally using Rosetta (orange). A top-down view of the trimeric interface is highlighted on the inset.
(D) The same Rosetta-redesigned residues highlighted on the post-fusion RabG structure.
(E) Left to right: the pre-fusion RabG structure highlight residues mutated made under the RAIN strategy (pink), disulphide by design strategy (yellow) and histidine-switch strategy (lime), respectively.
(F) The same mutation strategies in (E) displayed on the post-fusion RabG structure.

3.3.2 Considerations for Designing *In Vivo* RabG Mutant Screens

Were a pre-fusion stabilising mutation to influence immunogenicity, it is evident that the underlying mechanism is effective at the protein level. That is to say, it is possible to ascribe the effect of such a mutation to a particular point in the antigen expression pathway after vaccination: a protein-level change had a protein-level effect.

For mutations that might convey greater immunogenicity by simply improving expression of the antigen, understanding where in the protein expression pathway the mutation had an effect is more difficult. Mutations may affect gene transcription rates, mRNA stability, mRNA secondary structure, translation rates and/or efficiency of protein folding (Bailey-Serres, 1999; Gao et al., 2024; Leppek et al., 2022; Liu et al., 2021; Nieuwkoop et al., 2023). Effects at all/any of these stages will contribute to the final amount of protein synthesised.

This greatly complicates the design of *in vivo* experiments that seek to measure whether mutations that improve protein expression influence immunogenicity. In the case of RabG mutants that improve antigen expression, it is unclear if this is the result of improved protein folding efficiency or relevant to mRNA readability, mechanisms for which are described elsewhere (Gao *et al*, 2024; Leppek *et al*, 2022; Nieuwkoop *et al*, 2023).

In the context of RabG, I hypothesise that changes to expression levels of the antigen can be generalised as being the product of how efficiently fully folded antigen is expressed per mRNA template. Given this, expression advantages may not be observable under conditions in which antigen mRNA levels are saturating. Translation is unlikely to be the rate-determining step in protein expression and therefore the effects of mutation would not be detectable.

This problem becomes relevant to the choice of adenovirus or mRNA platforms for delivering RabG *in vivo*. Where mutation stabilises pre-fusion RabG and this improves the antibody response qualitatively, both platforms may be appropriate.

Where mutation conveys an expression advantage, however, adenovirus vaccines may be unsuitable. Given the potency of the intron A-containing CMV immediate early promoter

utilised in the ChAdOx2 platform for transgene expression (Sridhar *et al*, 2008), transcript levels and hence antigen translation may be close to 'saturating' levels after adenovirus transduction. Should the hypothesised mechanism posed here be true, the result of such a scenario would be the negation of any mutation effect and thus no differences in the levels of cell-surface antigen expression or subsequently in total IgG levels.

At the time of conducting the first *in vivo* screen of the H270P pre-fusion stabilising mutant in comparison to the WT, an mRNA vaccine platform was not accessible. Testing this single mutant was therefore performed using the ChAdOx2 platform concurrently with designing the combinatorial RabG mutants for screening *in vitro* and establishing the mRNA vaccine platform. Given the hypothesised limitations of using the ChAdOx2 vector described above, this would appear counterintuitive. However, in the interest of time, *in vivo* data on this mutant with a 'suboptimal' experimental design was still deemed useful for understanding the possible benefits pre-fusion stabilisation might have on RabG's immunogenicity. This is especially true considering that the ChAdOx2 platform is currently being tested in the clinic - identifying if RabG mutagenesis is beneficial for this vaccine platform is therefore directly relevant to future clinical work.

Furthermore, initial screening data of the RabG mutants presented in this chapter showed that H270P's effect on RabG is to stabilise the pre-fusion form with little effect on its *in vitro* expression relative to the WT. Given that I therefore did not expect the H270P mutant to affect expression of the antigen *in vivo*, screening via the ChAdOx2 vector to assess the effects of pre-fusion stabilisation was warranted.

For subsequent *in vivo* screens of H270P alongside combinatorial mutants that *did* influence RabG expression *in vitro*, it was important that such constructs were tested using a vaccine platform that might be best able to convey these expression advantages. These experiments were therefore conducted using mRNA vaccines that were accessible later on in this research project.

3.4 Materials and Methods

3.4.1 Production of RabG Mutant-encoding Plasmid DNA

The WT RabG used in this study (GenBank ID: OR551243.1) is a codon-optimised version of the Pasteur strain RabG (PVoG, Kim et al, 2016), from which all mutants were subsequently derived. RabG sequences were synthesised by Twist Bioscience, pre-cloned into a pTT3 mammalian expression vector backbone described previously (Durocher *et al*, 2002).

3.4.2 96 Deep-well Plate Transfections for RabG Mutant Screening

Small-scale transient transfections of the rabies virus glycoprotein and its mutants were performed in 96-well, deep square well plates using Expi293F cells and the corresponding transfection reagents, as per *Section 2.1.2*, in a transfection volume of 600 µL. Deep well plates were sealed with Breathe-Easy sealing membranes (Merck: Z380059) and incubated at 37 °C, 8% CO_2. Plates were agitated using a microplate shaker (VWR: 444-7094) at 900 rpm, 3 mm orbital diameter.

Transfection efficiencies in each well of the 96-well plate were determined by the luciferase method described in *Section 2.1.2*. Any well transfections in the RabG mutant screens that showed background levels of luciferase activity were considered to have failed during transfection and were removed from the analysis.

3.4.3 Conjugation of Amine-reactive Fluorophores to Antibodies

Direct labelling of antibodies with fluorophore was performed using Alexa Fluor 647 NHS Succinimidyl Ester (ThermoFisher: A37573). Briefly, one vial of Fluor-NHS ester was resuspended in 10 µL dimethyl sulfoxide (DMSO). 2 µL of the resuspended dye was subsequently added to 100 µg of antibody. The reaction mixture was agitated at 1000 rpm using an Eppendorff ThermoMixer for 1 h at room temperature (RT) before storing at -20 °C until use.

3.4.4 Flow Cytometry Assay for the Screening of RabG Mutants

Expi293F cells were transfected with plasmid DNA encoding a full-length version of the RabG protein, either in its WT form or a mutant variant, as described in *Section 3.4.1*.

After 24 h or 48 h (specified in results), 300 µL of transfected cells were centrifuged at 300 ×G for 5 min and resuspended in phosphate buffered saline (PBS). Samples were subsequently divided into two before one half was washed in PBS (pH 7.3), whilst the other was washed in an acidic buffer (50 mM Bis-Tris, 130 mM NaCl, pH 5.8). After two washes in the same buffer, cells were stained with RVC20 IgG conjugated to Alexa Fluor 647 (*Section 3.4.3*). RVC20 stain was diluted to 1 µg/mL in the same buffer cell pellets were washed in and samples left for 20 min to stain at room temperature. Staining solutions were removed by washing in pH-matched buffers (as above) twice followed by a final wash in PBS pH 7.3, before running on a BD LSR II cytometer (BD Bioscience). Analysis of flow cytometry data was performed using FlowJo v10.10.0 (BD Bioscience).

3.4.5 Production of Adenovirus-vectored RabG Vaccines

RabG-encoding adenovirus vectored vaccines were generated by the Viral Vector Core Facility using a ChAdOx2 vector (Morris *et al*, 2016). ChAdOx2 RabG was produced as previously described (Wang *et al*, 2018). Briefly, virus was rescued by transfection of linearised genome into HEK293 Trex cells (ThermoFisher: R71007), followed by growth in the same cells and purification by CsCl density gradient centrifugation, all to ~1 $\times 10^{11}$ vp/mL, and storage at -80 °C.

3.4.6 *In Vitro* Transcription to Produce 5'-capped RabG mRNA

RabG constructs selected for mRNA vaccine production were synthesised by Twist Bioscience. Sequences were pre-cloned into a pUC57 vector, downstream of a T7 RNA polymerase promoter sequence compatible with co-transcriptional 5' capping using the CleanCap AG system (TriLink: N-7113). Each coding sequence was flanked by a 5' untranslated region (UTR) derived from the BNT162b2 Vector (Pfizer BioNTech, GenBank: PP544446.1) and 3' sequences based on partial mtRNR1 and AES 3' UTRs concatenated head-to-tail as per Orlandini von Niessen et al. (Orlandini von Niessen *et al*, 2019).

mRNA constructs were encapsulated using a Nanoassemblr Ignite with the Genvoy ionisable lipid mix, formulated in PNI formulation buffer (all from Precision Nanosystems). All mRNAs were encapsulated with >87% encapsulation efficiency as

measured by a PNI Ribogreen assay, conducted as per Precision Nanosystem's supplied protocol (NIN 1182). Encapsulated mRNA vaccines were stored at -20 °C until use.

3.4.7 Transient Transfection of RabG mRNA

3 $\times 10^5$ HEK293T cells were transfected with 1 µg unencapsulated WT RabG mRNA in a 6-well tissue culture plate using the mRNAfect transfection reagent (Tebubio: 80-40). Complexes were prepared using a 5:1 ratio of mRNAfect : mRNA (µL : µg), using a GFP mRNA transfection condition as a positive control following the same protocol. RabG mRNA-transfected cells were harvested at the 24 h and 48 h timepoints and stained for flow cytometry under neutral conditions, as per *Section 3.4.4*.

3.4.8 Intramuscular Administration of RabG Vaccines

Mice were supplied by Inotive, UK. Mice strains, ages and sexes are described in their relevant results sections. All vaccines described in this chapter were administered by intramuscular (I.M.) injection under general anaesthetic into the hind limb quadriceps muscles with the vaccine dose administered in halves across each hind limb. ChAdOx2 vaccines were administered in a volume of 50 µL/dose, formulated in sterile PBS, whilst mRNA constructs were formulated in a sterile solution of 10% sucrose in PBS and given as 100 µL/dose.

In the design of the mRNA vaccine comparison experiment, a power calculation was performed to determine the size of each experimental group (one-way ANOVA, $\alpha = 0.05$, $\beta = 0.8$). Calculations were performed in GPower 3.1 using the variance observed in the 0.15 µg dose-group from the WT RabG mRNA vaccine pilot experiment (***Figure 3.5-9D***). The predicted effect size (increase in ELISA or VNA response in animals receiving variant vaccines, as compared to the WT comparator) was 0.51 $\log_{10}$-fold. This was in line with effects observed in a similar, recently published study (Cao *et al*, 2024).

3.4.9 Production of Detergent-extracted RabG Protein

Purified RabG protein was required for the coating of ELISA plates for use in the method described in *Section 3.4.10*. WT RabG was expressed by transient transfection of

Expi293F cells as described in *Section 2.1.2*. Plasmid DNA encoded the full-length WT RabG (PVoG, Kim et al, 2016), with a C-terminal C-tag for affinity purification.

After harvesting cell pellets from 100 mL transfections by centrifugation at 1000 ×G for 10 minutes, cells were resuspended in 5 mL freezing buffer (50 mM HEPES pH 7.4, 150 mM NaCl, 5% Glycerol (v/v)) and stored at -80 °C until use. After thawing, pellets were resuspended in 10 mL extraction buffer (50 mM HEPES pH 7.5, 150 mM NaCl, 1% n-octyl-b-d-glucoside (Sigma: 494459), cOmplete Protease Inhibitor cocktail (Roche)) and rocked at 4 °C for 2 h. The cell lysate was clarified by centrifugation for 30 min at 3200 ×G and filtered through a 0.2 µm filter.

C-tagged RabG was purified on an AKTA Pure protein purification system (Cytiva) using a CaptureSelect C-tagXL Pre-packed Column (ThermoFisher: 494307201) as per the manufacturer's instructions with the modification that all buffers prepared for the affinity purification were supplemented with 1% n-octyl-b-d-glucoside. The isolated protein was subsequently buffer exchanged using a PD-10 column (Cytiva: 52130800) into freezing buffer and stored at -80 °C until use.

3.4.10 ELISA for Quantification of Anti-RabG IgG

Total RabG IgG titres were determined using a standardised assay format (Miura *et al*, 2008). ELISAs were performed as summarised in *Section 2.1.5* with protocol-specific steps described in ***Table 3.4-1***.

Protocol step	Description
Coating protein	Detergent-extracted RabG protein produced in *Section 3.4.9*. Concentration: 2 µg/mL, 50 µL/well.
Blocking incubation	1 h at RT in the dark.
Primary stain	50 µL/well serum samples from mice immunised with RabG constructs. Samples run in triplicate wells. Concentration: Unknown serum samples tested at dilutions ranging from 1:300 – 1:30000 such that results fell within the permitted region of the standard curve.
Control conditions	Controls run on each individual plate. Negative control: naïve mouse serum (BioRad: C11SA) diluted 1:300, run in quadruplicate wells, 50 µL/well. Positive control: serum pool from mice immunised with ChAdOx2 RabG was used at a starting dilution of 1:1200 and serially diluted 2-fold to generate a 10-point standard curve. Each standard curve point run in duplicate wells, 50 µL/well.
Primary incubation	2 h at RT in the dark.
Secondary stain	Goat anti-mouse IgG antibody conjugated to alkaline phosphatase (Merck: A3562) at a dilution of 1:5000, 50 µL/well.
Secondary incubation	1 h at RT in the dark.
Development.	Plates were read iteratively until the lowest dilution (1:1200) of the standard curve achieved an $OD_{405\,nm}$ readout between 1.3-1.7, typically 10-12 min.

Table 3.4-1: ELISA protocol details for determining anti-RabG IgG titres from mouse serum samples.

3.4.11 Virus Neutralising Antibody Titrations

Mouse serum samples from experiments testing ChAdOx2-vectored RabG constructs were measured by Rapid Fluorescent Focus Inhibition Test (Yager & Moore, 2015) by the research group of Prof Hildegund Ertl (Wistar Institute, USA), using heat-inactivated serum samples.

Samples from mRNA-vaccinated mice were measured by Fluorescent Antibody Virus Neutralisation assay (Cliquet *et al*, 1998) conducted by BioBest Laboratories UK. Serum samples tested at BioBest were not heat-inactivated prior to testing.

3.5 Results

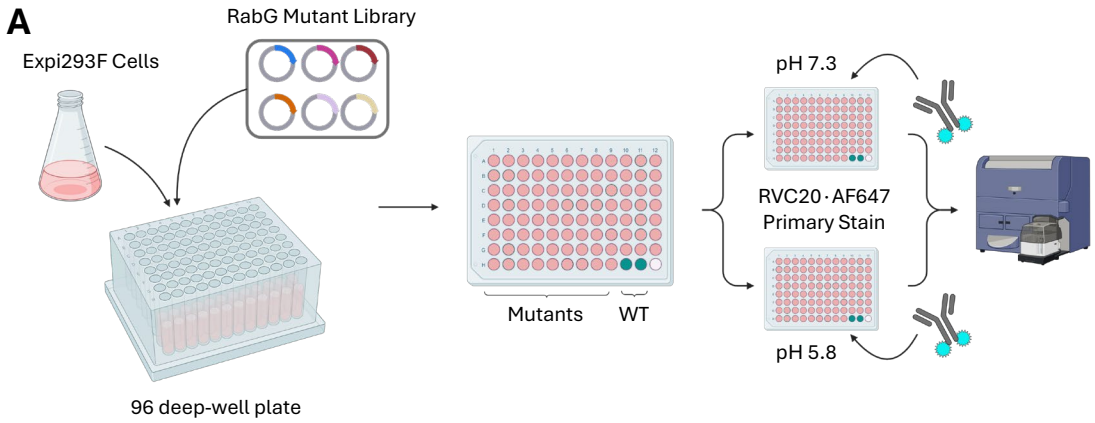
3.5.1 Establishment of a Whole-panel RabG Mutant Screening Assay

As discussed in *Section 3.3.1*, it was hypothesized that two modifications to the RabG protein may improve its immunogenicity and thus, its performance as a vaccine candidate: greater cell-surface expression relative to the WT and improved pre-fusion stability which may lock RabG in a more immunologically-relevant conformation.

To screen a panel of RabG mutants against these two criteria, a medium-throughput transient transfection assay was developed. Expi293F cells (ThermoFisher) were transfected with plasmid DNA encoding either the WT RabG or a mutant version and subsequently stained with a pre-fusion, conformationally specific mAb RVC20 (Hellert *et al*, 2020) conjugated to a fluorophore.

Staining was performed after halves of each transfected cell sample had been pre-incubated at pH 7.3 and pH 5.8. The latter aimed to simulate the acidic conditions that trigger the pre- to post-fusion transition of RabG in the endosome (Irie *et al*, 2006) (***Figure 3.5-1A***). Using a pre-fusion specific antibody under these conditions made it possible to determine expression levels of each RabG variant, by measuring the median fluorescence intensity (MFI) at pH 7.3, and comparing it to the WT. In addition, pre-fusion stabilisation ratios could be calculated for each mutant by dividing the MFI value at pH 5.8 (MFI_{Acid}) by that of the neutral condition (MFI_{Neut}) (***Figure 3.5-1B***). An ideal mutant would therefore exhibit higher expression levels at neutral pH relative to the WT and a MFI_{Acid} : MFI_{Neut} approaching a value of 1. This would suggest that the binding of the pre-fusion specific mAb is not abrogated by staining under conditions that would otherwise trigger a pre- to post-fusion transition in the WT.

The transfection of 73 RabG mutants necessitated adaptation of a suspension Expi293F cell transfection protocol. Performing small-volume transfections in a 96 deep-well plate would allow for all mutants to be manageably screened in duplicate within a single experiment. To test whether such a method was possible, a luciferase reporter plasmid was spiked into each RabG transfection. The luminescence readouts from each transfection supernatant were used as a measure of transfection efficiency.



B

$$Relative\ Expression = \frac{MFI_{Neut}[Mutant]}{MFI_{Neut}[WT]} \qquad Acid\ Stability = \frac{MFI_{Acid}[Mutant]}{MFI_{Neut}[Mutant]}$$

Figure 3.5-1: *In vitro* RabG mutant screening assay.

(A) Development of a plate-based mammalian cell transfection assay for the screening of a RabG mutant library at small scale. RVC20 is a pre-fusion conformation-specific anti-RabG antibody. Schematic created using BioRender.com.

(B) The quantitative readouts used to describe relative expression of each mutant to the WT and the stability ratio of each mutant stained under acidic and neutral conditions.

First, a full 96-well plate was transfected with plasmid DNA encoding the WT RabG (with spiked luciferase) to understand inter-well variation in the transfection efficiency. This could result in artefactual differences to expression/acid stability when comparing mutants to the WT. Using an adapted version of a previously described protocol (Bos *et al*, 2015), transfections were performed at the 1 mL scale, yielding near-background luminescence signals across the plate (μ = 230 RLU, CV = 134%) (Run 1, ***Figure 3.5-2A***).

Randomly sampled wells across the plate showed cell viabilities of approximately 60% at the 48 h timepoint, compared with >90% in standard flask transfections. Cells were also observed settling at the bottom of each well. It was therefore hypothesized that 1 mL transfection volumes were too large for sufficient culture agitation. This would lead to cell settling and might explain low cell viabilities, caused by insufficient oxygenation of the culture.

Shaker speeds >900 rpm resulted in significant splashing and therefore could not be increased to improve agitation and aeration. Instead, smaller transfection volumes were tested. 600 μL and 400 μL shaking transfection cultures were compared across two halves

of the same 96 deep-well plates, one with round wells and another square wells (***Figure 3.5-2A***, Runs 2 and 3, respectively). This arrangement permitted simultaneous testing of an optimal volume and whether square wells may further agitate cell cultures.

On average, square-well conditions showed greater luciferase readouts than round-well (***Figure 3.5-2A***). Luciferase readouts for the 400 µL condition appeared greater than those of the 600 µL condition for the round-well plate (µ = 6760 RLU, µ = 5820 RLU, respectively) and square-well plate (µ =17600 RLU, µ = 7790 RLU, respectively) (***Figure 3.5-2A***). However, cell viability in the 400 µL was ~20% lower across 2 randomly sampled wells compared to sampled 600 µL wells and displayed greater inter-well variation. Visual inspection of plates at the 48 h timepoint showed significant evaporation from the wells and thus highly dense cell suspensions, particularly for the 400 µL wells, which may explain lower cell viability.

To reduce evaporation, a final comparison was made between transfected cell culture plates sealed with a single breathable sealing membrane and with two membranes placed on top of one another (Run 4). Doubly sealing the transfection plate did reduce evaporation on visual inspection without detrimental effects to cell viability or luciferase readouts (***Figure 3.5-2A***). Subsequent screens of RabG mutants were therefore carried out at the 600 µL scale in square-well plates with a double membrane seal. This condition was repeated across a full 96 deep-well plate (Run 5, ***Figure 3.5-2B***), showing the least inter-well variability of all tests conducted.

Over the range observed of luciferase readouts in Runs 4 and 5, there appears to be no correlation between luminescence readout and MFI_{Neut} when staining with RVC20 (***Figure 3.5-2C***), suggesting that luciferase scores in this window should be used more as a yes/no check of transfection success and that the remaining variability in WT RabG expression is not necessarily the result of transfection efficiency. To account for any confounding that may be the result of well position on the deep-well transfection plate, quality of plasmid DNA or plate-based effects, screens of the RabG mutants were performed using two independent plasmid DNA preps per mutant, transfected in separate

96-well plates with randomised well positions, with the entire assay repeated on a different day.

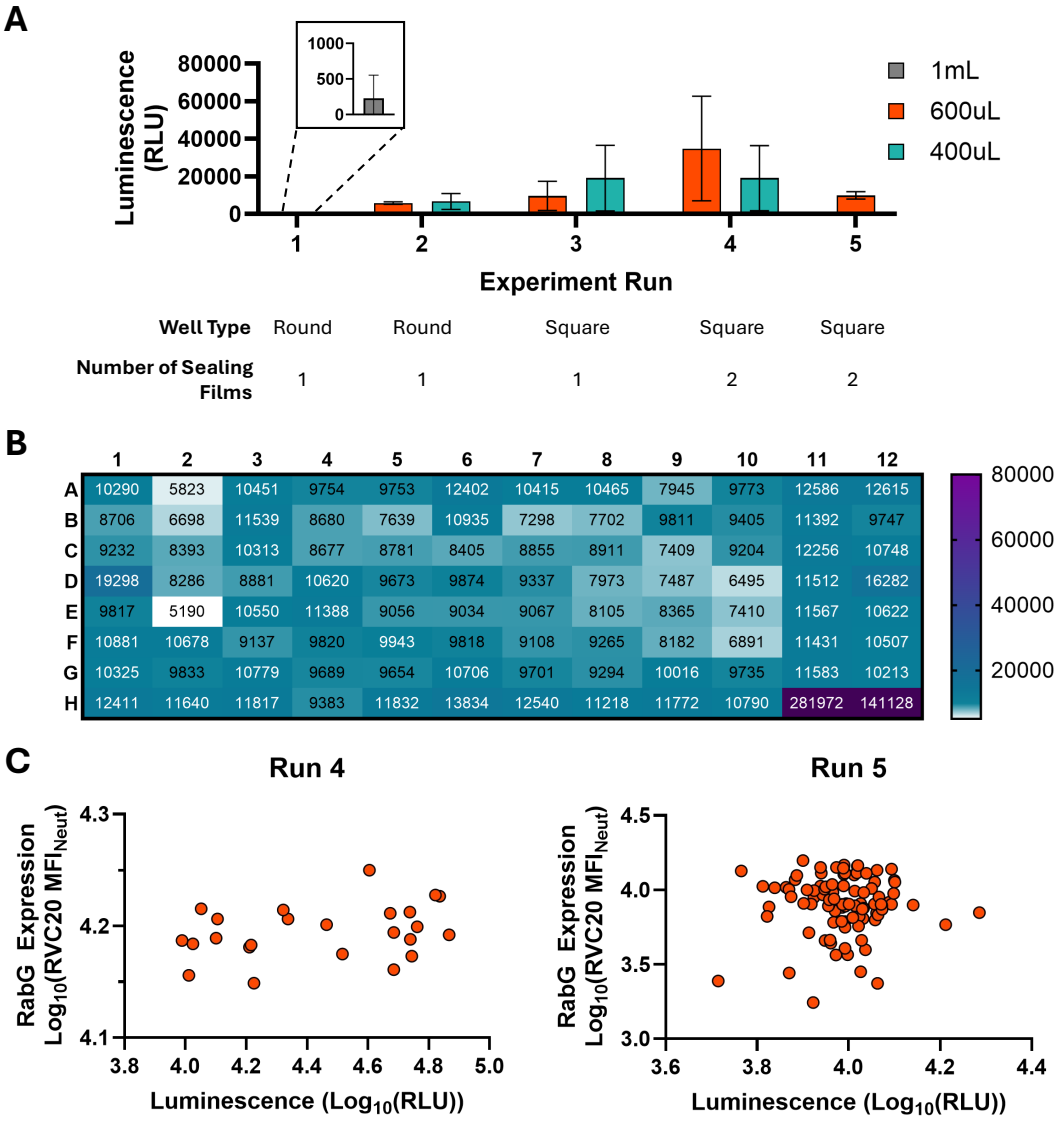


Figure 3.5-2: 96-well plate transfection assay optimisation.

(A) **Top:** NanoGlo luciferase readouts reported for each round of assay optimisation for the 96 deep-well plate transient transfection using WT RabG plasmid DNA as a model transfection condition. Bars represent the mean relative light units across technical replicates (wells of the plate), error bars represent the standard deviation. The legend represents the total culture volume of each well transfected. **Bottom:** The table summarises changes to the plate setup made throughout the optimisation process: switching from round-bottom to square-bottom deep-well plates and sealing each transfection plate with an additional Breathe-Easy film.

(B) NanoGlo luciferase readouts across the 96 deep-well plate of Experiment Run 5. Values represent the raw relative light units of supernatant samples taken from the corresponding well position of the transfection plate. Wells H11 and H12 are positive control supernatant samples from an unrelated high-efficiency transfection.

(C) XY plots representing the 600 µL transfection conditions conducted in Experiment Run 4 (left, plate rows A and B sampled, n = 24) and 5 (right, whole plate sampled, n = 94). Plots show each well's median fluorescence intensity after staining with RVC20 at pH 7.3 against its corresponding NanoGlo relative light unit readout.

3.5.2 Screening of a RabG Single Mutant Panel

73 RabG mutants were screened using the assay in *Section 3.5.1* to determine their expression and pre-fusion acid stability. A subset of the mutants were originally designed as fusion constructs to GFP on the premise that GFP tags could assist in downstream protein purification by fluorescence-detection size exclusion chromatography. 22 mutants were constructed with a GFP tag, 47 were untagged, and 4 made both with and without. Previous work in the group, however, showed that the GFP fusion constructs expressed poorly compared to their untagged equivalents. As a result, panel screens included both the WT RabG and a WT RabG-GFP fusion protein to be able to compare tagged and untagged mutants to their appropriate WT equivalent.

The consistency of the MFI_{Neut} readouts was first investigated across the replicate plasmid DNA preps for each mutant (***Figure 3.5-3A***), as well as across the experimental repeats, performed on different days (***Figure 3.5-3B***). Inter-replicate agreement was good (Pearson's R^2=0.9546, 0.9730, respectively), suggesting the transfection method developed should enable robust comparisons between constructs.

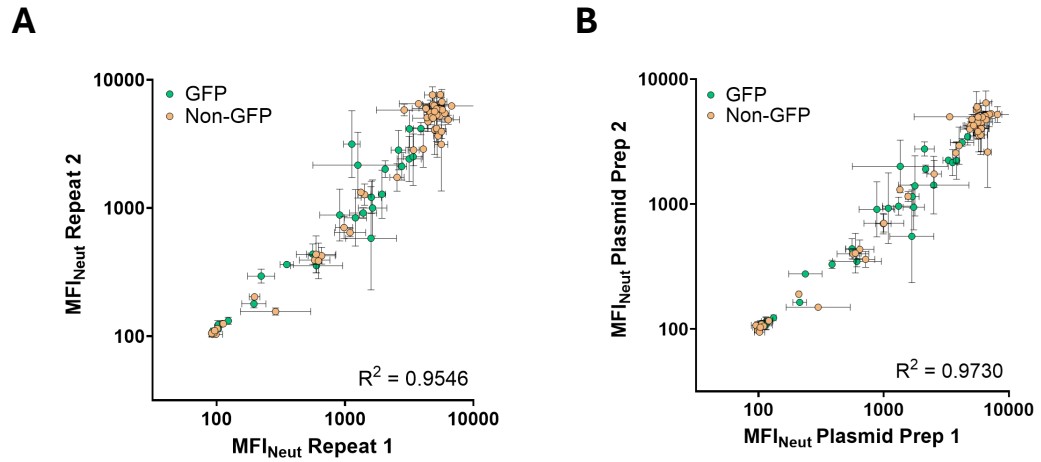


Figure 3.5-3: RabG transfection reproducibility.

(A) XY plot displaying the correlation between independent plasmid DNA preps of the same RabG variant with respect to its cell surface expression after transient transfection. Mutants were constructed with a GFP-tag (green) or without (yellow). Data points represent the geometric means of the median fluorescence intensity (MFI_{Neut}) readouts across duplicate transfections carried out of different days after staining with the RVC20 anti-RabG mAb conjugated to AlexFluor 647, stained at pH 7.3.

(B) XY plot determined by the same method as in (A) to determine the correlation between mutant RabG expression across experiments repeated on different days. Data points represent the average of the MFI_{Neut} readouts across duplicate transfections on a single day, conducted using independent plasmid preps.

In (A) and (B) error bars represent half of the range for log-transformed values across duplicates. Reported R^2 values were calculated using a Pearson correlation test on the combined tagged and untagged variants after log-transformation, calculated in GraphPad Prism.

Expression values, expressed as a fold-change score compared to a WT expression of 1, revealed that a number of mutants essentially abrogated expression (***Figure 3.5-4A***). This was common for mutants that targeted the monomer interface via redesign in Rosetta (termed 'RR Interface...' in ***Figure 3.5-4***), as well as mutations to introduce pre-fusion-locking disulphide bonds (termed 'DB Mutant...' in ***Figure 3.5-4***). Mutants that modified the hinge region between L261 and E274 were generally well-tolerated, as were modifications of histidine to leucine (but usually not to alanine) (***Figure 3.5-4A***).

Mutants that were not detrimental to expression were subsequently tested for their ability to stabilise the pre-fusion conformation under acidic conditions (***Figure 3.5-4B***). Overall, 33 mutants in the panel exhibited expression levels >70% of the WT (matching to GFP-tagged or untagged WT), and 20 showed a >2-fold improvement to the acid stability ratio.

It was identified, however, that use of a ratio between the MFI_{Acid} value and the MFI_{Neut} value for a mutant may identify artificially 'stabilising' variants resulting from poor expression: as MFI_{Neut} values tend to background, stability ratios tend to 1. For example, disulphide bond mutant 4 (D143C + L260C) appeared to convey a 5.6-fold improvement to acid stability relative to the WT, however this value is inflated by its 4-fold reduction to expression. This highlighted the importance of interpreting both expression levels and acid stability readouts for each mutant concurrently. Plotting these values as an XY graph reveals a clear trend that as mutant expression worsens, acid stability scores increase, tracing a reciprocal graph ($y = k/x$) (***Figure 3.5-4E***).

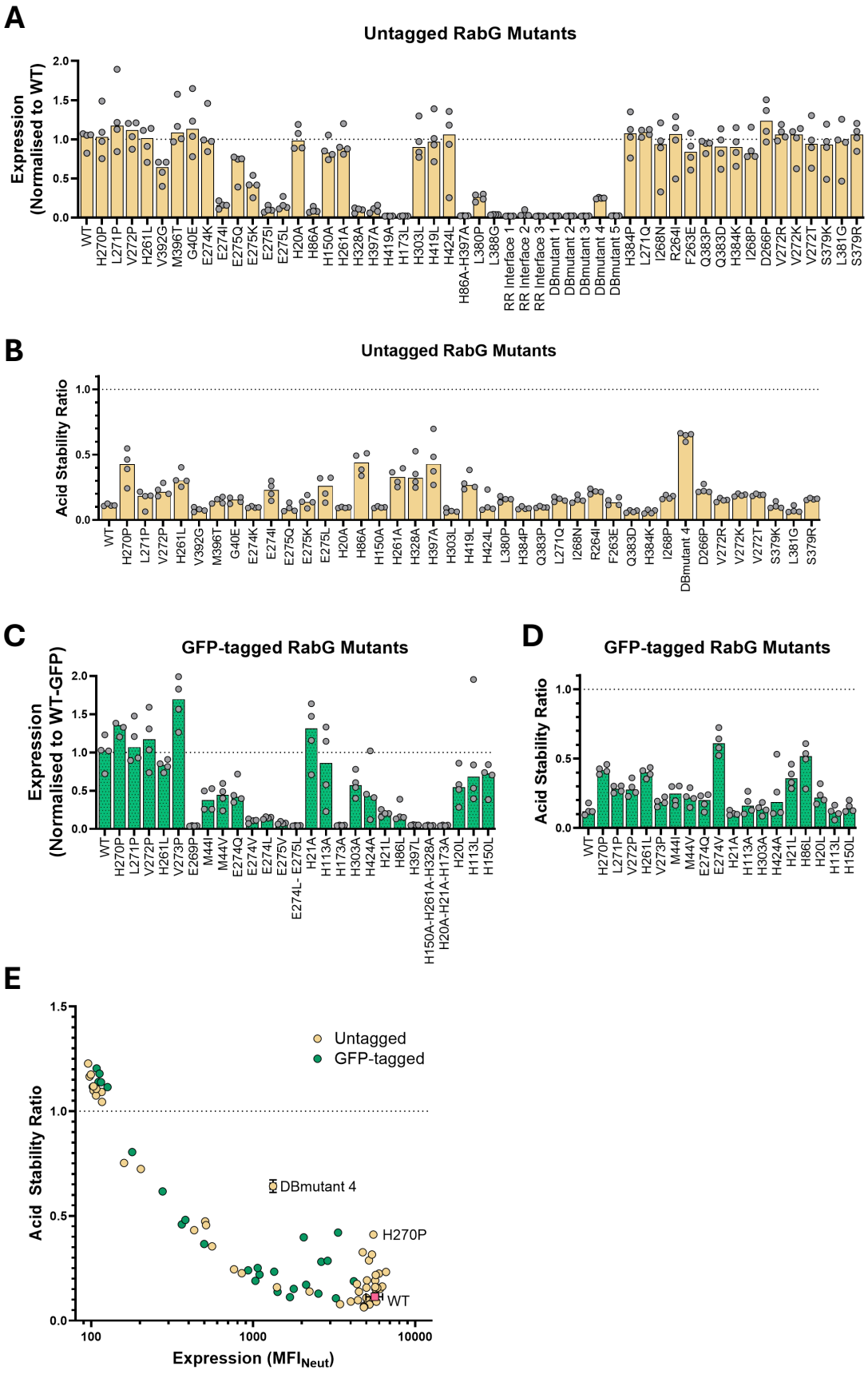

A
Untagged RabG Mutants
Expression (Normalised to WT)
B
Untagged RabG Mutants
Acid Stability Ratio
C
GFP-tagged RabG Mutants
Expression (Normalised to WT-GFP)
D
GFP-tagged RabG Mutants
Acid Stability Ratio
E
Untagged
GFP-tagged
DBmutant 4
H270P
WT
Acid Stability Ratio
Expression (MFI Neut)

Figure 3.5-4: RabG single mutant panel screening.

(A) Expression levels for each RabG variant, determined via their MFI_{Neut} after staining with RVC20 conjugated to AlexaFluor 647. Values are reported as fold-changes relative to the WT RabG, with the average of the WT replicates set to an expression value of 1. Data points represent an individual replicate transfection with data pooled across experiments on different days. Bars display the median of the technical replicates. Mutants labelled 'RR Interface…' correspond to mutants in the Rosetta redesign of the trimeric interface. Mutants labelled 'DB mutant…' correspond to cysteine-incorporating mutants intended to introduce stabilising disulphide bonds.

(B) Acid stability ratios reported for all mutants that did not completely abrogate expression in panel (A). Stability ratios were calculated as per the method in **Figure 3.5-1B**. Data points represent an individual replicate transfection with data pooled across experiments on different days. Bars display the median of the technical replicates.

(C) Expression levels for each GFP-tagged RabG variant, calculated and reported as in (A) with the modification that mutant expression is displayed as relative expression to the GFP-tagged WT RabG. Data points represent an individual replicate transfection with data pooled across experiments on different days. Bars display the median of the technical replicates.

(D) Acid stability ratios reported for all GFP-tagged mutants, calculated and displayed as in panel (B).

(E) XY plot displaying acid stability ratios against MFI_{Neut} (expression) values for each RabG variant including GFP-tagged (green), untagged (yellow) and the WT (pink). Data points represent average values across all technical replicates. For clarity, error bars representing the standard error for each mutant are only displayed for DB mutant 4 and the WT.

Complete data (i.e. including all replicate results) for each panel of mutants (GFP-tagged and untagged) were analysed, with appropriate correction for multiple comparison (i.e. a false-discovery rate approach), to determine which variants had expression or pre-fusion stability statistically significantly different from the WT (***Figure 3.5-5***). Across both expression and acid stability, and indeed in both its GFP-tagged and untagged versions, the H270P helix-breaking mutation appeared to be the best overall single mutant.

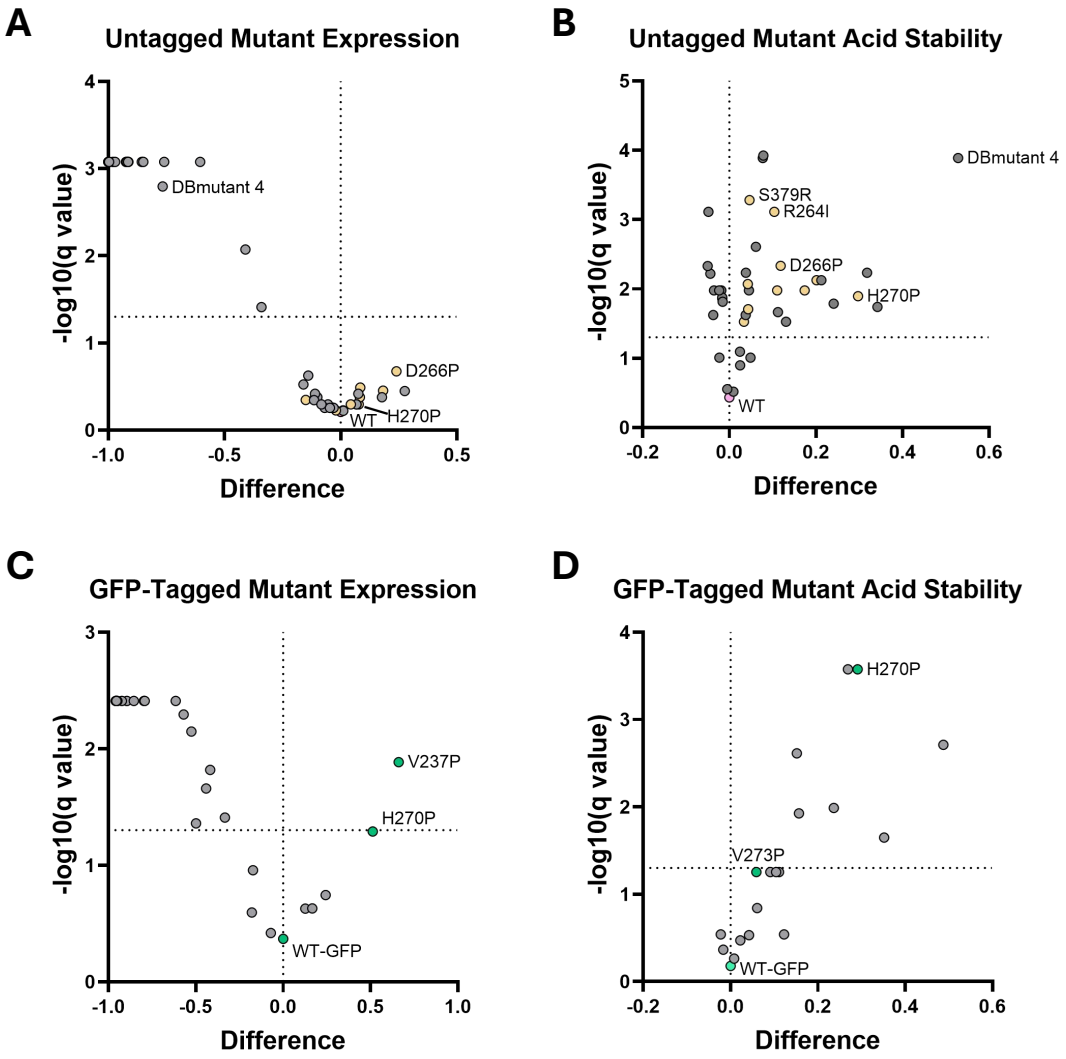


Figure 3.5-5: RabG mutant expression & stability analysis.
Volcano plots displaying each untagged RabG mutant's effect on expression (A) and the pre-fusion stability of RabG under acidic conditions (B) as well as each GFP-tagged mutants effect on the same two readouts (C, D, respectively). Data points represent individual RabG variants.
In all cases, expression and acid stability levels were compared to the WT (or WT-GFP) by multiple unpaired t-tests with Welch's correction, assuming individual variance for each mutant and implementing a false discovery rate of 5% using the two-stage step-up method developed by Benjamini, Krieger and Yekutieli. Differences are plotted such that positive values correspond to greater expression and acid stability in relevant graphs. Horizontal dotted lines represent a significance cut-off of $p<0.05$.
Coloured circles represent mutants that were selected to construct combinatorial mutants, discussed in *Section 3.5.5*.
All graphs and statistical tests were performed using GraphPad Prism.

3.5.3 The H270P Mutant Does Not Improve the Immunogenicity of RabG in an Adenovirus-vectored Vaccine

Given its ability to stabilise the pre-fusion conformation, the H270P mutant of RabG was investigated as a vaccine candidate using the ChAdOx2 adenovirus platform (Morris *et al*, 2016). 6-week-old female CD-1 mice were given two doses of a ChAdOx2 RabG construct encoding the WT antigen derived from the ERA viral strain, currently being investigated in Phase II clinical trials (Jenkin *et al*, 2022), the codon-optimised Pasteur virus WT antigen (PVoG) which was used as the template for mutant design in this study, and the H270P mutant (H270P PVoG). Vaccines were administered intramuscularly, each across 3 dose groups, 1 $\times 10^3$ IU (low), 3 $\times 10^4$ IU (medium) and 1 $\times 10^6$ IU (high) and terminal blood samples taken 40 days post-boost (***Figure 3.5-6A***).

Total anti-RabG IgG titres were determined by ELISA against the WT (PVoG) protein, and medium-dose samples sent for quantification of virus neutralising antibody. Over the three doses tested, the ChAdOx2 H270P vaccine did not induce higher titres of anti-RabG IgG (***Figure 3.5-6B***), nor did the medium dose group show any differences in VNA titre between the three constructs (***Figure 3.5-6C***).

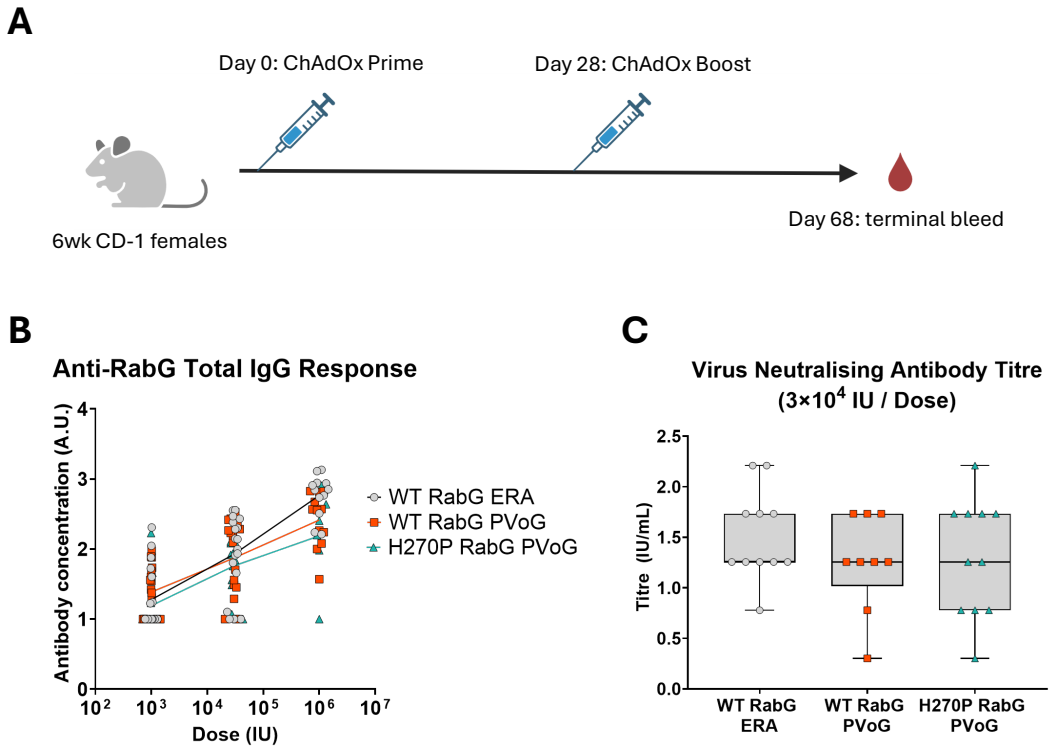


Figure 3.5-6: in vivo screening of ChAdOx2-vectored H270P.

(A) Immunisation and blood sampling schedule for ChAdOx2 RabG-immunised CD-1 mice. Schematic created using BioRender.com.

(B) Post-boost total IgG responses to the WT RabG antigen, as measured by ELISA, raised against different doses of the ChAdOx2 RabG vaccines. Points represent individual mice. Lines connect the mean response at each dose group for each vaccine construct.

(C) Post-boost Virus Neutralising Antibody titres for mouse samples from the middle dose group in (B) (3 ×10^4 IU). Points represent individual mice. Grey boxes represent the inter-quartile range for each vaccine, error bars represent the full range of responses and horizontal black lines represent the median response.

3.5.4 Refinement of the RabG Mutant Screen

I hypothesised that the failure of the H270P mutation to improve the immunogenicity of RabG may have been because the single mutation only partially stabilises the pre-fusion conformation. Combinatorial RabG mutants were therefore synthesised for screening, results of which are discussed in the following section.

Whilst the combinatorial mutants were being produced, it was noticed that only one of the tested single-mutants, V273P, conveyed some kind of expression advantage over the WT (***Figure 3.5-5C***). This was at odds with the pre-fusion stabilisation data which showed there were a considerable number of RabG mutants capable of improving stability.

The possibility that the lack of any apparent enhancement to expression conferred by mutation may have been an artefact of the *in vitro* screening assay developed in *Section 3.5.1* was considered. It was postulated that transient transfection of Expi293F cells, developed for high levels of protein expression, may result in saturation of the cell surface with antigen, limiting the ability to detect improvements to expression.

A titration experiment was therefore conducted in which the amount of WT RabG DNA used in the transfection was varied, whilst keeping the total amount of transfected DNA constant using an empty pENTR4 expression vector to act as 'filler' DNA. Surface expression of WT RabG was indeed saturating when using >10% the total amount of transfected DNA (***Figure 3.5-7A***) suggesting increases to expression levels conveyed by mutation may not have been detected. After fitting a 4-parameter curve to the log-transformed titration data, an EC_{50} value of 2.9% RabG DNA was determined (95% CI = 1.8 – 4.5%) (***Figure 3.5-7A***). Subsequent screens of RabG mutants were therefore performed using 2% the original amount of RabG-encoding plasmid, within the dynamic range of the dose-response curve for the WT.

The WT-normalised expression levels of mutants that appeared to stabilise the pre-fusion conformation were compared for their 2% and 100% RabG Transfections. Whilst these mutants appear to homogeneously express at the approximate level of the WT (i.e. 1×) for the 100% DNA condition, using 50-fold less DNA reveals large differences in expression levels that are not simply the product of increased variation (***Figure 3.5-7B***).

To further avoid the possibility of cell surface saturation, the mutants described above were screened at an earlier timepoint of 24 h post-transfection, as well as the 48 h timepoint used in *Section 3.5.2*. Plotting the normalised expression values of each mutant at 24 and 48 h reveals that when comparing expression the WT, the 24 h timepoint yields greater relative-expression values than at 48 h (***Figure 3.5-7C***). This suggested that mutations conveying improved expression of RabG may be better detected at the earlier timepoint and that with a longer incubation period, expression levels of all the mutants start to homogenise.

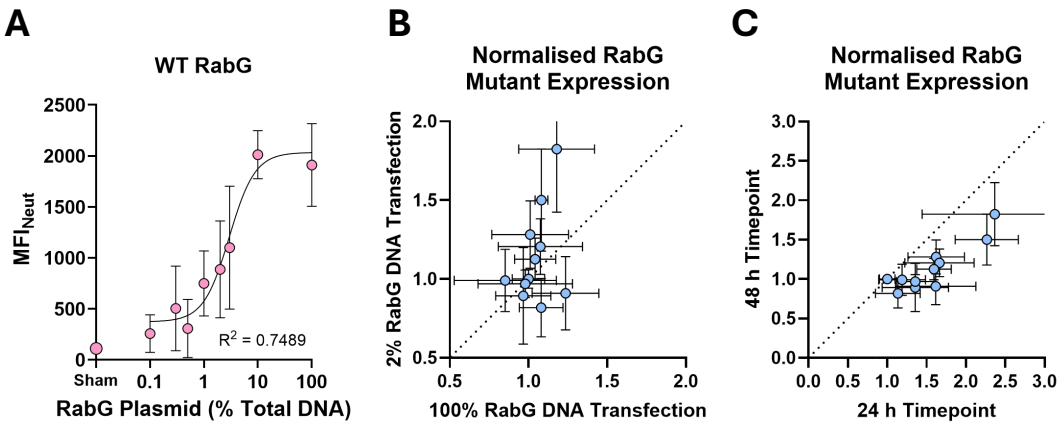


Figure 3.5-7: Refinement of the RabG in vitro expression assay.

(A) XY plot displaying RabG antigen expression, measured using the median fluorescence intensity of transfected cells stained with the RVC20 mAb conjugated to AlexaFluor647, as a function of the amount of RabG DNA used in the transient transfection. 100% RabG Plasmid corresponds to a DNA concentration of 1 µg/mL transfected cells. The sham condition used 100% non-RabG plasmid DNA (see methods). Data points represent the average MFI_{Neut} values across all technical replicates (n = 6 per dose). Where NanoGlo luciferase values indicated a failure of transient transfection for any replicates, data was excluded from the analysis. These exclusions led to smaller sample sizes for the 0.5% condition (n = 3) and 1% condition (n = 5). The plotted line and corresponding R^2 value represent a 4-parameter sigmoidal curve fitted to the log-transformed DNA dose data. Curve fitting was conducted in GraphPad Prism.

(B) XY plot displaying the expression levels of the 10 single, untagged mutants selected for design of combinatorial double mutants (discussed in *Section 3.5.5*) transfected using 100% RabG DNA and 2% RabG DNA. Relative expression values displayed were calculated as described in (**Figure 3.5-1A**) comparing to WT RabG transfections using 100% and 2% RabG DNA correspondingly. Data points represent average values across technical replicates for each mutant (n = 4 for all variants except WT, L271Q, H270P_L271Q, V272P_H419L, R264I_L271Q, H270P_H261L_H419L where n = 8, and H270P where n = 12). Error bars represent the standard deviation calculated across technical replicates. Dotted line represents $y = x$.

(C) XY plot displaying the relative expression levels of mutants in (B) sampled at 24 h and 48 h post transfection with 2% RabG DNA. Data points represent average values across technical replicates for each mutant (replicates as per (B)). Error bars represent the standard deviation calculated across technical replicates. Dotted line represents $y = x$.

3.5.5 Stability and Expression Screening of the RabG Mutation Combinations

Using a cut-off expression value of >70% WT expression, 10 pre-fusion stabilising mutations from the untagged panel (H270P, H261L, R264I, D266P, I268N, L271Q, V272P, S379R, M396T, H419L) and one mutant from the GFP-tagged panel (V273P) were selected to construct 43 double-mutants and 3 triple-mutants (***Figure 3.5-5***, coloured data points). These mutants, summarised in *Appendix II*, were investigated to determine if pre-fusion stabilising effects and/or improvements to RabG expression may be additive.

Combinatorial mutants were screened alongside their single-mutant parents. After the optimisation of the expression assay (preceding section), expression differences between the single-mutant constructs were apparent. Although combining mutants did not always produce an additive effect with respect to expression levels, double-mutants containing the L271Q mutation saw considerable boosting (***Figure 3.5-8A***). The acid-stabilising effects of individual mutants, however, were additive for a number of mutant pairs, with 6 double-mutants exhibiting acid-stability ratios >0.8 (***Figure 3.5-8B***). The double mutant L271Q_H419L conveyed the greatest improvement to antigen expression (***Figure 3.5-8C***), the H270P_H419L combination exhibiting the joint-highest acid stability score (***Figure 3.5-8D***).

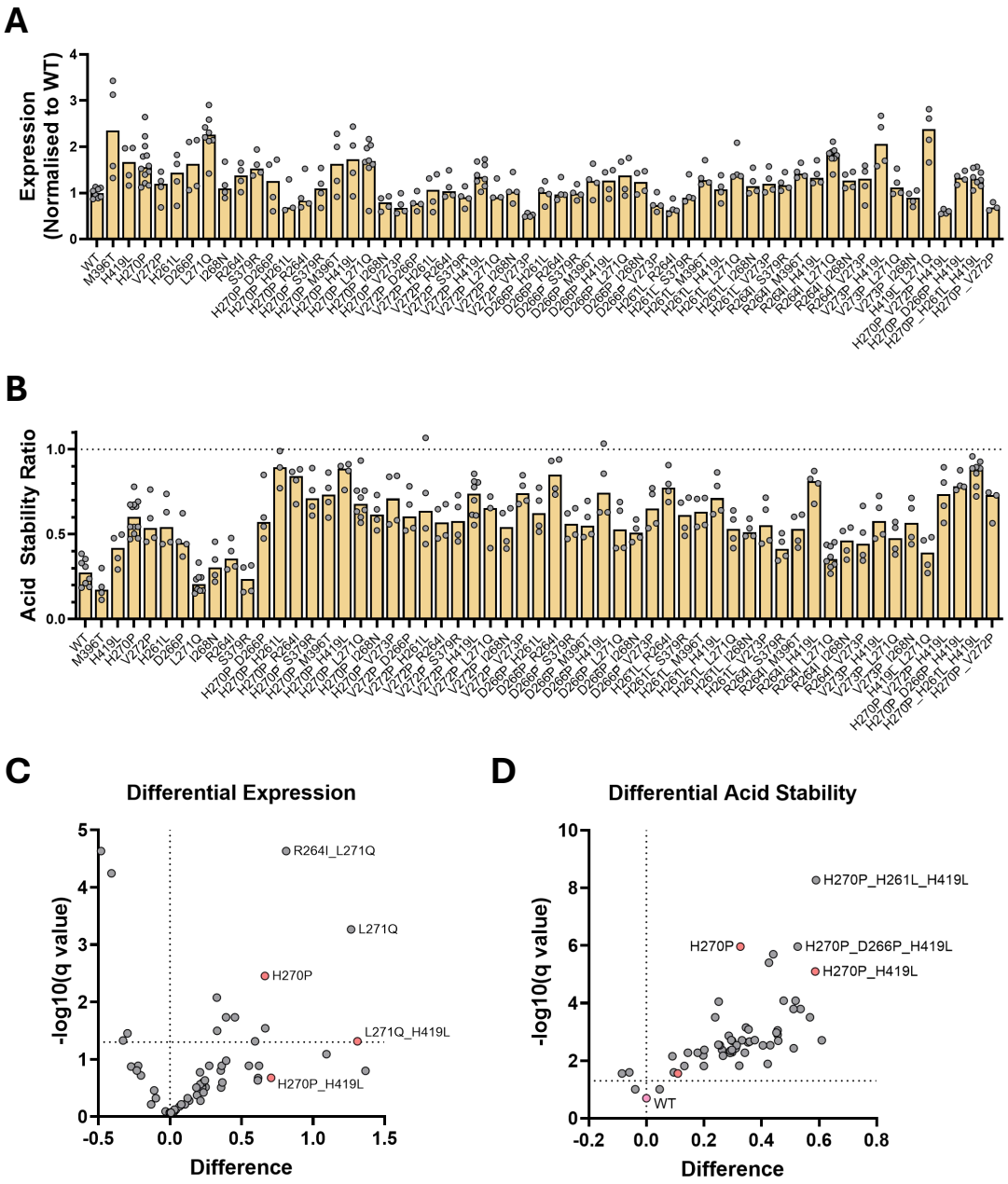


Figure 3.5-8: RabG double mutant panel screening.

(A) Expression levels of RabG double mutants and their single-mutant parents. Values are reported as fold-changes relative to the WT RabG, with the average of the WT replicates set to an expression value of 1. Data points represent technical replicates. Bars represent median values for each mutant. All transfections performed with 2% RabG DNA.

(B) Acid stability ratios of double mutants and their single-mutant parents. Data points and bars as in (A).

(C) Volcano plots displaying the effects of mutation on expression, relative to the WT.

(D) Volcano plots displaying the effects of mutation on acid stability, relative to the WT.

For (C) and (D), data points represent individual RabG variants. Differences are plotted such that positive values correspond to greater expression or acid stability in relevant graphs. Comparisons to the WT were made by multiple unpaired t-tests with Welch's correction, assuming individual variance for each mutant and implementing a false discovery rate of 5% using the two-stage step-up method developed by Benjamini, Krieger and Yekutieli. Differences are plotted such that positive values correspond to greater expression and acid stability in relevant graphs. Horizontal dotted lines represent a significance cut-off of $p < 0.05$. Red data points correspond to mutants selected for *in vivo* screening.

3.5.6 Mutants that Improve Expression and/or Acid Stabilisation Do Not Improve the Immunogenicity of RabG Using an mRNA Vaccine Platform

RabG double mutants were successfully identified that improved *in vitro* expression relative to the WT and conveyed pre-fusion stabilisation effects greater than their parent single mutants. Whether these mutations may also enhance the immunogenicity of a vaccine based upon them was therefore considered. Though the H270P mutant did not show improvement of a ChAdOx2 RabG immunogen, the L271Q_H419L and H270P_H419L mutants out-perform this single mutant with respect to expression and pre-fusion stability, respectively.

As discussed in *Section 3.3.2*, I hypothesised that use of a ChAdOx2-based platform may not be appropriate for detecting improvements to expression of the RabG antigen conferred by these mutations. Given this, the H270P_H419L and L271Q_H419L double-mutants were screened *in vivo* using an mRNA platform. Their immune responses were compared to the WT RabG construct and the H270P single mutant that represented the best single mutant, but that did not prove advantageous when administered via an adenovirus.

Coding sequences were inserted into a mRNA expression plasmid and the WT construct first used to assess transcription efficiency, antigen expression and immunogenicity in mice. *In vitro* transcription of the RabG transcript yielded a single-stranded mRNA transcript of the correct length (2 kb) with high purity (***Figure 3.5-9A, B***). The pilot mRNA prep was subsequently used to transiently transfect adherent HEK293T cells and produced detectable levels of cell surface-expressed RabG at 48 h post-transfection (***Figure 3.5-9C***).

Similar to the refinements considered for the *in vitro* RabG mutant screening assay in *Section 3.5.4*, it was important to select an mRNA vaccine dose on the steep part of the mRNA dose-immunogenicity response curve, to maximise sensitivity to differences between constructs. A pilot mouse experiment was therefore designed using the WT RabG mRNA construct. Groups of 6-week-old female CD-1 outbred mice were given doses of 12, 4, 1.3, 0.44 and 0.15 μg mRNA (n = 4 per group), administered

intramuscularly on day 0 with boosting on day 14. Post-prime samples were taken on day 13 and post-boost samples taken on day 28 (***Figure 3.5-9E***).

To determine a suitable mRNA dose, four-parameter logistic curves were fitted to the log-transformed pre-boost and post-boost responses. Anti-RabG IgG titres were determined by ELISA (***Figure 3.5-9D***). A vaccine dose of 0.2 µg induced responses on the steepest part of both dose-response curves and was subsequently used for comparisons between the RabG mutants and the WT.

Data from the pilot experiment was used for a power calculation which indicated the need for 12 mice per group to provide 80% power to detect an effect of the specified magnitude (see method *3.4.8*).

12 animals per vaccine were immunised at 0.2 µg/dose for each of the four constructs, using the same regimen as the pilot experiment. Post-prime and post-boost samples were analysed by ELISA to determine total anti-RabG IgG titres (***Figure 3.5-9F***) and virus neutralising antibody (VNA) titres determined for the post-boost samples (***Figure 3.5-9G***).

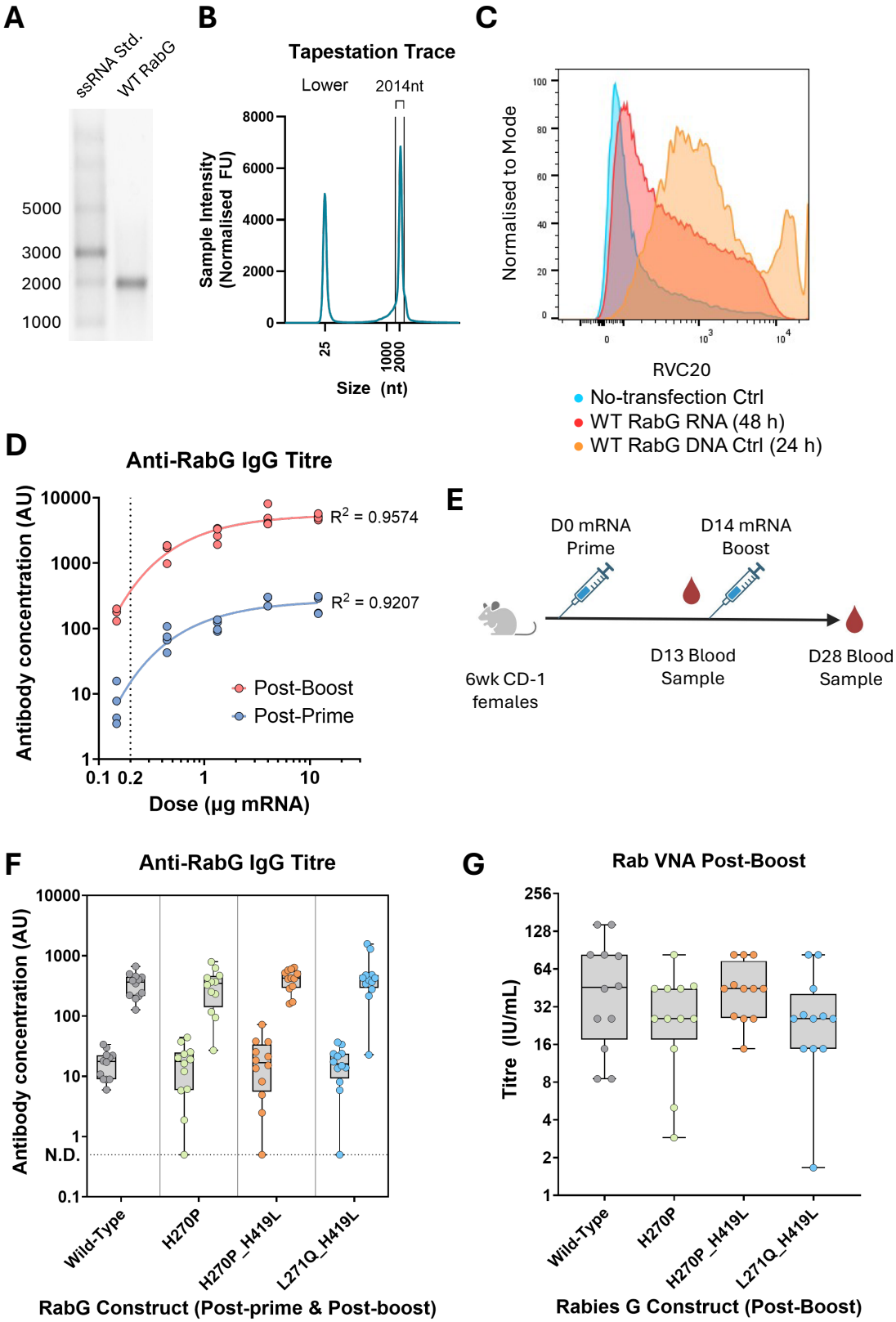

A
ssRNA Std.
WT RabG
5000
3000
2000
1000
B
Tapestation Trace
Lower
2014nt
Sample Intensity (Normalised FU)
8000
6000
4000
2000
0
25
1000
2000
Size (nt)
C
Normalised to Mode
RVC20
No-transfection Ctrl
WT RabG RNA (48 h)
WT RabG DNA Ctrl (24 h)
D
Anti-RabG IgG Titre
Antibody concentration (AU)
R2 = 0.9574
R2 = 0.9207
Post-Boost
Post-Prime
Dose (µg mRNA)
E
D0 mRNA Prime
D14 mRNA Boost
6wk CD-1 females
D13 Blood Sample
D28 Blood Sample
F
Anti-RabG IgG Titre
Antibody concentration (AU)
N.D.
Wild-Type
H270P
H270P_H419L
L271Q_H419L
RabG Construct (Post-prime & Post-boost)
G
Rab VNA Post-Boost
Titre (IU/mL)
Wild-Type
H270P
H270P_H419L
L271Q_H419L
Rabies G Construct (Post-Boost)

Figure 3.5-9: RabG mutant mRNA vaccine production and screening.

(A) RNA agarose gel of WT RabG mRNA vaccine construct produced by in vitro transcription with ssRNA ladder (NEB: N0362S).
(B) Tapestation trace for WT RabG mRNA produced by *in vitro* transcription, re-graphed in GraphPad Prism. 'Lower' peak represents Tapestation 25 nt standard peak. Median transcript size for WT RabG construct calculated automatically on Tapestation (Agilent Technologies).
(C) Histogram representing fluorescence intensity in 670/30 filter after staining transfected cells with RVC20 mAb conjugated to AlexaFluor 647. Positive control cells (orange) were transfected with plasmid 100% RabG DNA as described in *Section 3.4.7*.
(D) Post-prime (blue) and post-boost (red) total IgG responses to WT RabG, as measured by ELISA, plotted as a function of mRNA vaccine dose. Data points represent individual mouse responses. Dose response curves were determined by fitting of a 4-parameter curve to doubly log-transformed data, with corresponding R^2 values for each curve also calculated. Curve analysis was performed using GraphPad Prism. The dotted vertical line demarcates the vaccine dose selected for further mouse experiments.
(E) Immunisation and blood sampling schedule for RabG mRNA-immunised CD-1 mice. Schematic created using BioRender.com.
(F) Post-prime and post-boost total IgG responses to WT RabG, as measured by ELISA, for mice immunised with different RabG mutant mRNA vaccines at 0.2 µg/dose. N.D. = No detectable response
(G) Virus neutralising antibody titres determined for the same mouse samples in (E) at the post-boost timepoint only.

For (E) and (F), data points represent individual mouse responses, grey boxes represent the inter-quartile range, error bars display the response range and horizontal black lines show the median for each group.

To better understand the quality of the anti-RabG response induced by each construct, VNA : total anti-RabG IgG (tIgG) ratios were calculated and compared between groups (***Figure 3.5-10A***). The relationships between these two metrics were also analysed by plotting each animal's VNA titre against its tIgG titre (***Figure 3.5-10B***). Fitting linear regression models to each vaccine group's responses with a fixed x-intercept for all groups permitted the comparison of response 'quality' by comparing the slopes of each regression line. Responses raised by all three RabG variants were not significantly different to those induced by the WT sequence (***Figure 3.5-10B***).

The differences between the mean responses for each vaccine group were compared to the WT with respect to tIgG titres pre- and post-boost, VNA titres post-boost and VNA : tIgG ratios post-boost. For all immunological readouts, ANOVA testing (with correction for multiple comparisons) revealed that no mutant RabG significantly improved upon the quantity or quality of the immune response raised to the WT (***Figure 3.5-10C***). The upper bounds of the 95% confidence intervals for the effect sizes all excluded 3-fold improvements relative to WT. 3-fold is an arbitrary margin, but the upper

limits of the CIs reflect the statistical power of the experiment i.e. the data indicates a large difference is improbable, rather than merely failing to detect a large and biologically important difference due to insufficient replication.

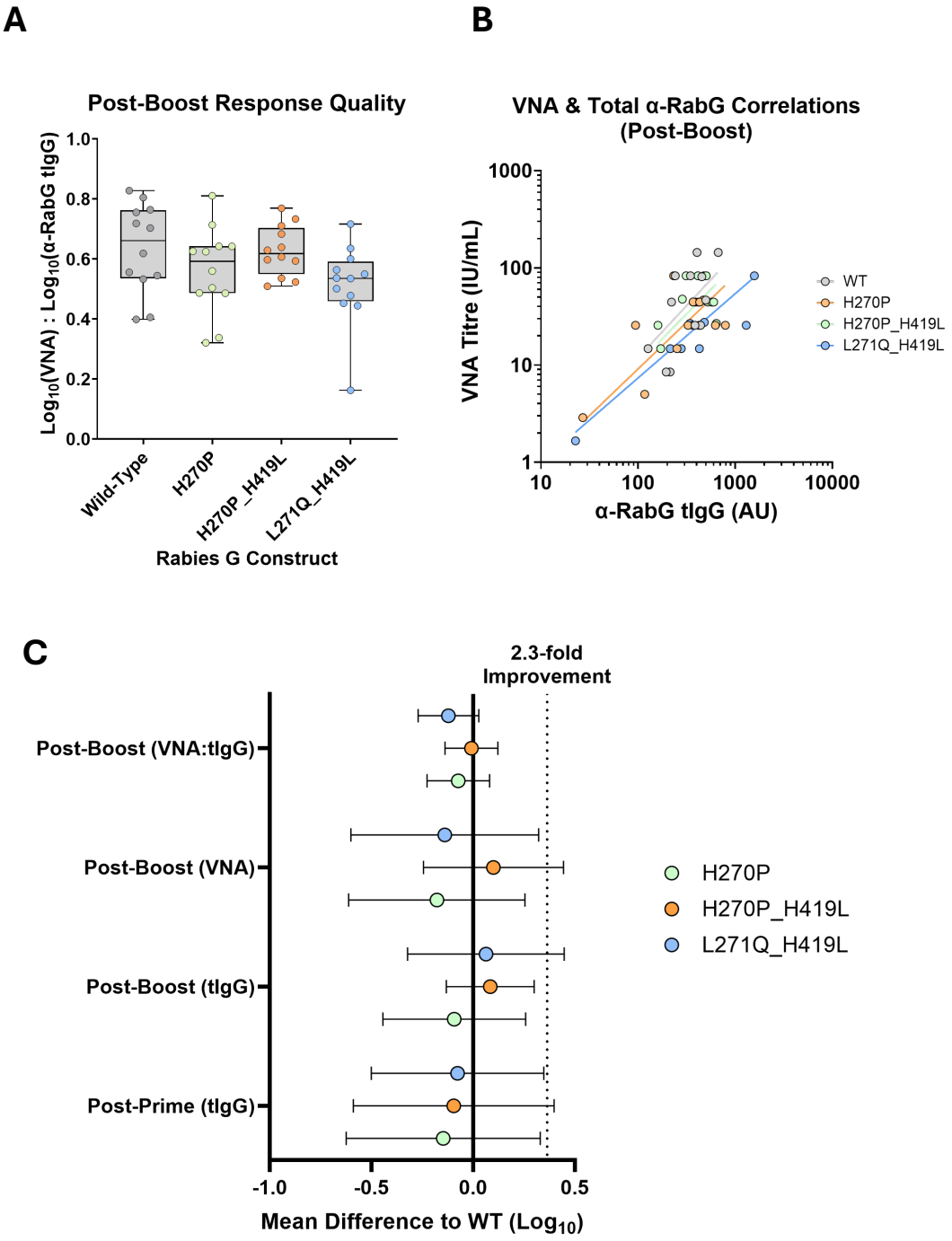


Figure 3.5-10: Immune responses to WT and mutant RabG mRNA vaccines.

(A) Virus-neutralising antibody (VNA) : total anti-RabG IgG (α-RabG tIgG) ratios for animals immunised with different RabG mRNA constructs at the post-boost timepoint. Ratios were calculated using the $\log_{10}$-transformed values for each assay. Data points represent responses for individual mice. Grey boxes represent the inter-quartile range, error bars display the response range and horizontal black lines show the median for each group.

(B) XY plots of the same VNA and tIgG responses as in (A). To determine whether any of the RabG variants affected the quality of the anti-RabG response raised, simple linear regression was conducted on the log-transformed responses for each group with a fixed x intercept ($x = 10$) and the slopes of each line compared. 95% confidence intervals for the slopes of each fit were: WT = 0.9320 to 1.214, H270P = 0.8242 to 1.094, H270P_H419L = 0.9189 to 1.110 and L271Q_H419L = 0.7789 to 0.9546, suggesting no significant differences in the relationships between VNA titre and tIgG titre for all vaccines.

(C) Differences in the mean response values for three mRNA vaccines encoding variants of RabG, relative to the WT mRNA construct. For each immunological readout (Y-axis), geometric means were compared to the WT and differences plotted (circles). A mean difference of 0 therefore represents no change from the WT response. Error bars represent the 95% confidence intervals for each RabG mutant and for each immunological readout, all of which show overlap with $x = 0$, suggesting no significant differences between the WT and any mutant RabG vaccine in any readout. No adjustments for false discovery were made. The dotted line represents a 2.3-fold improvement over the WT. This value represented the fold-change improvement to total anti-RabG IgG and VNA titres conveyed by an H270P mutant RabG mRNA vaccine as reported previously *(Cao* et al*, 2024)*. In all cases, mean differences and confidence intervals were calculated by a one-way Brown-Forsythe and Welch ANOVA with Dunnett's T3 multiple comparisons test. All values are relative to the WT, i.e. positive mean differences correspond to higher induced titres. Statistical analysis was performed using GraphPad Prism.

3.6 Discussion

The RabG mutant screening described above sought to answer whether it might be possible to improve antigen expression and/or the stability of its pre-fusion conformation using a semi-rational mutagenesis approach. Once mutants were identified that could achieve this, the most promising candidates were screened *in vivo* to determine whether they were able to improve the immunogenicity of RabG-based vaccines. The mechanism for this improvement may either be by increasing the quantity of antibody induced or the quality of the antibodies raised.

Of the 73 'single mutants' screened initially, mutations from a range of strategies appeared to stabilise the pre-fusion conformation. The eleven best performers used to design a second set of combinatorial mutants were from four of the six strategy groups first conceptualised. 8 of these mutations, however, targeted the flexible loop between H261 and V273. This highlights the importance of this region in the structural rearrangements from pre- to post-fusion. H270P, a helix-breaking mutation designed to disrupt such

rearrangements, was the most stabilising single mutant and ultimately facilitated the elucidation of the pre-fusion RabG structure by cryo-electron microscopy (Ng *et al*, 2022).

Combining the H270P mutant with a histidine switch-targeting mutation, H419L, located just prior to the transmembrane domain resulted in further stabilisation of the pre-fusion conformation (***Figure 3.5-8D***). Given that H419 is not resolved in any pre- or post-fusion RabG structures (Ng *et al*, 2022; Yang *et al*, 2020; Hellert *et al*, 2020; Callaway *et al*, 2022), it is likely that it does not form part of any rigid secondary structure elements. This might further support the hypothesis that its role in the pre- to post-fusion transition is not mediated by perturbation of secondary structure refolding. Instead, mutating H419L may abrogate RabG's ability to detect the drop in pH that triggers the pre- to post-fusion transition in the WT (Irie *et al*, 2006; Gaudin *et al*, 1993). It follows that the greater acid stability observed by combining the H270P and H419L mutations may be the result of two orthogonal stabilisation mechanisms operating in tandem, though this is speculative.

Ultimately, the H270P mutation did not convey an immunological advantage when administered as a ChAdOx2 or mRNA vaccine. Additionally, combinatorial mutants that out-performed H270P with respect to improving acid stability and expression failed to achieve this when administered as mRNA constructs either. Given the careful selection of an mRNA vaccine dose that did not induce a saturating antibody response in mice, maximising the chances of observing any inter-vaccine differences, this work suggests that improvements to the RabG *in vitro* had no effect on their suitability as vaccine targets.

Two hypotheses were tested in the choice of mutant and design of the mRNA mouse experiment: 1) does a stabilised pre-fusion RabG antigen induce a qualitatively improved antibody response by targeting a more biologically relevant antigen conformation, and 2) could the improvement of RabG's expression, proposed as being determined by the efficiency of successful translation, quantitatively improve the anti-RabG response? On the contrary, it appears from this work that administration of a full-length RabG vaccine candidate, in which the antigen is likely expressed predominantly in the context of a membrane, *does not* benefit from further stabilising the pre-fusion conformation. At the

least, no such benefit is apparent with the degree of stabilisation and expression enhancement achieved here.

This result is in direct conflict with recently published work by Cao and colleagues. Motivated by our published study describing the *in vitro* stabilising effect of the H270P mutation (Ng *et al*, 2022), they present evidence that a H270P mRNA vaccine induces a more potent antibody response than the WT (Cao *et al*, 2024). In their study, Balb/c mice were administered two doses of a lipid nanoparticle mRNA vaccine encoding the WT RabG or the H270P mutant, given at doses of 17.54 μg and 16.23 μg mRNA, respectively. H270P-immunised mice generated 2.3-fold higher anti-RabG tIgG responses and VNA titres (Cao *et al*, 2024). Here, the authors proposed that the mechanism by which H270P conveys an advantage is indeed in the stabilisation of a more immunologically relevant pre-fusion conformation (Cao *et al*, 2024).

Notably, however, Cao's conclusion appeared to be based upon a single experiment with groups of 6 mice, without further replication, and without any examination of the dose-response relationships for the two vaccines. The data presented here investigated three separate RabG mutants with greater numbers of mice in each group and at a low dose to maximise the chances of detecting differences in immune responses raised to the antigen. No significant differences could be detected. For H270P, a 2.3-fold improvement to tIgG and VNA titres induced by the mutant construct fell outside the 95% confidence interval for differences compared to the WT (***Figure 3.5-10C***). It is possible that the improvement Cao and colleagues observed after introducing the H270P mutation was due to chance, with their low number of replicates. Confidence that the true effect of stabilising mutations is indeed null (i.e. no meaningful beneficial effect) is enhanced by the fact that this result was consistent across all constructs tested here, as it seems unlikely that H270P and combination mutations selected using the same screens would have divergent effects.

Perhaps more surprising is the lack of evidence to support the second hypothesis. Given that mutations presented here show significant improvements to the cell-surface expression of RabG *in vitro*, why is no advantage observed *in vivo*? The most likely

explanation is that improvements to antigen expression, whilst statistically significant, are not biologically significant: a ~2-fold improvement may simply not be great enough to improve antibody responses.

Alternatively, the *in vitro* screening method used here may poorly represent the *in vivo* scenario, therefore modelled improvements to antigen expression may translate poorly. After optimisation of the *in vitro* mutant screening assay, differences to antigen expression were most pronounced when cells were transfected with low doses of RabG-encoding plasmid DNA and at a relatively early timepoint of 24 h. How relevant such improvements are *in vivo* may be questioned.

Firstly, antigen expression on the surface of transfected cells persists for longer than 24 h – a recent review of human and animal studies investigating mRNA vaccines suggest antigen expression peaks within 3 days post-administration but may persist past 9 days (Pateev *et al*, 2023). Given that the expression-boosting effects of productive mutants appeared smaller at the 48 h timepoint for the *in vitro* studies, it could be argued that the prolonged period of antigen expression *in vivo* exacerbates this trend.

Secondly, the transfection-based screening assay revealed that using low doses of DNA to transfect cells was required to see significant differences in antigen expression levels. Whether this condition is reflected *in vivo* by the administration of a low dose of mRNA or ChAdOx2-vecotored vaccine is unclear. Its translational relevance might also be questioned given that suboptimal dosing of a human vaccine is nonsensical.

Together, these findings may build a picture outlining the effect of expression-improving mutations of RabG. I propose that the mutations identified here that improve expression do so by increasing the rate of translation per template, but perhaps not the maximum expression level.

Administering low doses of nucleic acids (DNA or mRNA) encoding RabG results in greater antigen expression levels for these mutants soon after administration. Given time, however, expression of the WT antigen 'catches up' to that of the mutants on a timescale that is relevant to *in vivo* antigen expression. The result, therefore, is no observed effect

of mutation on antigen expression which, in this case, is measured by proxy through immunogenicity readouts.

A final, important consideration is that the assumed mechanism of action of these expression-improving mutations operating at the translational level may be unfounded. Were the stabilising mutations acting at the transcriptional level, administration of mRNA vaccines would not capture such an effect. This is not supported, however, by the data presented using the ChAdOx2 platform which *would* capture any DNA-level effects and yet no improvement was observed for the H270P construct. Testing this could be achieved by the *in vitro* transfection of cells with mRNA encoding the WT and relevant mutants and determining whether they influence antigen expression levels.

※

Emerging clinical and pre-clinical data suggests that adenovirus-vectored and mRNA vaccine delivery of WT RabG are highly immunogenic, in that single-dose vaccination typically achieves VNA titres exceeding the correlate of protection (Schnee *et al*, 2016; Zhang *et al*, 2024; Ertl, 2019; Astray *et al*, 2017; Jenkin *et al*, 2022). Although these results are of course encouraging, further enhancement of immunogenicity remains worthwhile, for example to enhance the longevity of responses or to allow reduction in vaccine doses (and hence costs and reactogenicity).

Data presented here suggests, however, that trying to achieve this through RabG engineering is challenging. In the context of pre-fusion stabilisation, mutagenesis strategies capable of such stabilisation do not have an effect on immunogenicity. Successes using this approach for fusion proteins in Class I, including RSV F and SARS-CoV-2 Spike, do not appear to translate to this Class III analogue.

One reason for this failure may simply be that the pre-fusion conformation of RabG is sufficiently stable *in vivo* when expressed in the context of a membrane. Given this work shows pre-fusion RabG can be expressed at pH 7.3 for the WT *in vitro*, it might also be true after its vectored delivery in mice. Stabilisation advantages would, therefore, not convey a benefit in the same way that they have for the Class I fusion proteins.

3.7 Appendix II: Combinatorial RabG Mutants

Combinatorial Mutant	Mutation Strategy 1	Mutation Strategy 2	Mutation Strategy 3
H270P_D266P	HbH Proline	RR1 HbH	
H270P_H261L		His Switch	
H270P_R264I		RR1 HbH	
H270P_S379R		RR2: 376-389	
H270P_M396T		RAIN	
H270P_H419L		His Switch	
H270P_L271Q		RR1 HbH	
H270P_I268N		RR1 HbH	
H270P_V272P		HbH Proline	
H270P_V273P		HbH Proline	
V272P_D266P		RR1 HbH	
V272P_H261L		His Switch	
V272P_R264I		RR1 HbH	
V272P_S379R		RR2: 376-389	
V272P_H419L		His Switch	
V272P_L271Q		RR1 HbH	
V272P_I268N		RR1 HbH	
V272P_V273P		HbH Proline	
D266P_H261L	RR1 HbH	His Switch	
D266P_R264I		RR1 HbH	
D266P_S379R		RR2: 376-389	
D266P_M396T		RAIN	
D266P_H419L		His Switch	
D266P_L271Q		RR1 HbH	
D266P_I268N		RR1 HbH	
D266P_V273P		HbH Proline	
H261L_R264I	His Switch	RR1 HbH	
H261L_S379R		RR2: 376-389	
H261L_M396T		RAIN	
H261L_H419L		His Switch	
H261L_L271Q		RR1 HbH	
H261L_I268N		RR1 HbH	
H261L_V273P		HbH Proline	
R264I_S379R	RR1 HbH	RR2: 376-389	
R264I_M396T		RAIN	
R264I_H419L		His Switch	
R264I_L271Q		RR1 HbH	
R264I_I268N		RR1 HbH	
R264I_V273P		HbH Proline	
V273P_H419L	HbH Proline	His Switch	
V273P_L271Q		RR1 HbH	
V273P_I268N		RR1 HbH	
H419L_L271Q	His Switch	RR1 HbH	
H270P_V272P_H419L	HbH Proline	HbH Proline	His Switch
H270P_D266P_H419L		RR1 HbH	His Switch
H270P_H261L_H419L		His Switch	His Switch

Table 3.7-1: Combinatorial RabG mutants. The mutation strategies from which parent single mutants are derived are shown. HbH Proline = Helix-bend-helix proline mutations, RR1 HbH = Rosetta Redesign 1: Helix-bend-helix, His Switch = Histidine switch, RR2: Rosetta Redesign of Aas 376 – 389, RAIN = Resistant to Acid Induced Neutralisation.

4 Results II: Development of a Workflow for the Isolation of Monoclonal Antibodies Against an Unstable Membrane Glycoprotein

4.1 Statement of authorship

All work reported in this chapter was designed and executed by S.E. with the following exceptions:

Hands-on use of a Beacon Instrument (Bruker Cellular Analysis) at the University of Edinburgh was assisted by Dr Gaynor Campbell (Edinburgh Genome Foundry).

Edinburgh-based FACS instruments were operated by Dr Martin Waterfall (Edinburgh Flow Core Facility).

Mouse immunisations and sample processing for isolation of fresh mouse tissue for the initial Beacon screen were performed by Dr Inga Dry (Roslin Institute, University of Edinburgh) (subsequent work used frozen tissue from mice immunised in Oxford by S.E.).

Re-expression of the monoclonal antibody panel and some mAb characterisation experiments were conducted with laboratory assistance from Francisco Orliacq, under S.E.'s close supervision.

4.2 Chapter Overview

1) A Beacon-based method for isolating anti-gB monoclonal antibodies was established with the intention of screening mAbs against two conformations of the antigen.

2) The experimental 'pipeline' was successfully adapted to work on frozen tissue samples. Optimising sample handling steps upstream and downstream of the Beacon improved hit rates and their successful recovery (***Figure 4.2-1***).

3) 40 new anti-gB monoclonal antibodies were successfully identified, though none bound pre-fusion gB specifically.

4) A transgenic animal model, OmniMouse, raises human-like antibodies to gB after immunisation, but heavy and light chain sequences cannot be re-amplified for mAb isolation.

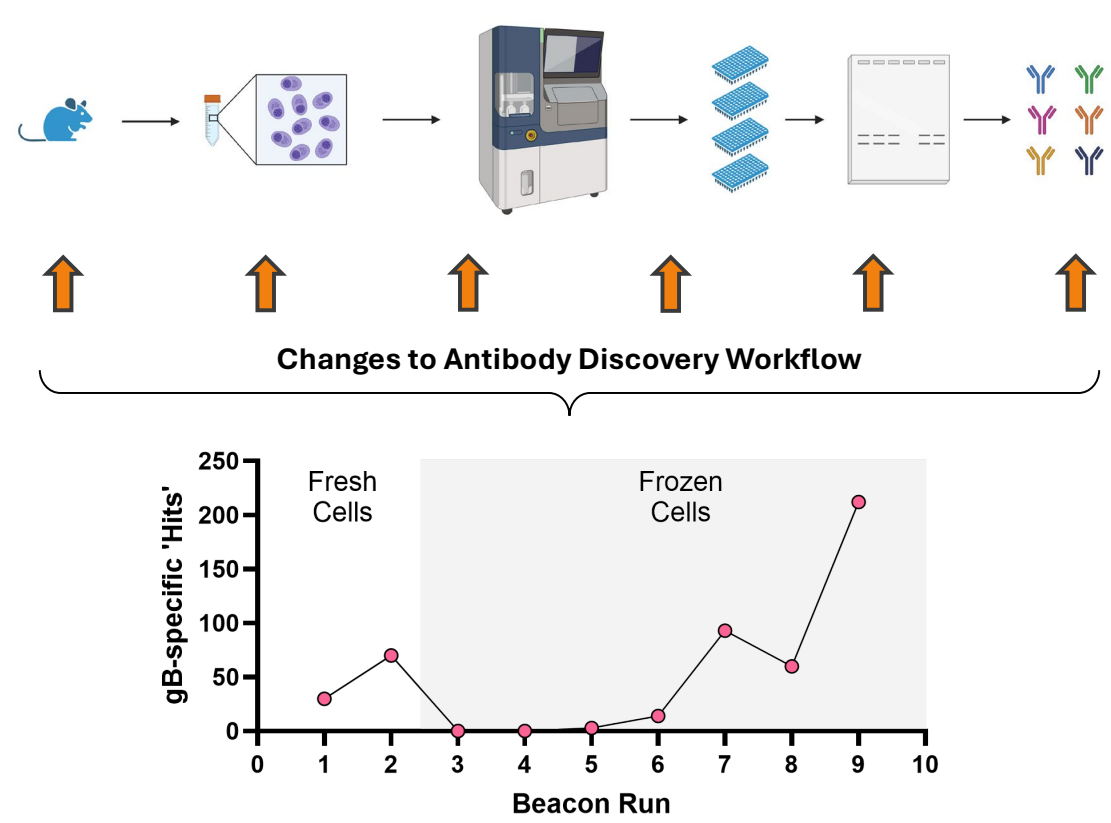


Figure 4.2-1: Chapter Summary.
Optimising a Beacon-based antibody discovery 'pipeline' improves anti-gB hit numbers, even when working from frozen samples. Schematic created using BioRender.com.

4.3 Introduction

The efforts described in *Results I* to try and understand the importance of pre-fusion RabG in generating a protective immune response were possible because of the strong foundational knowledge of the antigen itself. For Epstein-Barr Virus gB, however, understanding of the antibody response against it remains incomplete. Indeed, there is as yet no evidence that pre-fusion-specific anti-gB antibodies exist. In addition, the first successful attempt to stabilise the pre-fusion form of gB has only just been published, though details of the stabilised construct are yet to be fully disclosed (McCallum & Veesler, 2024).

Designing and using immunogens capable of inducing a pre-fusion specific antibody response is therefore difficult given the metastable nature of this conformation. Similarly, making a probe capable of screening for pre-fusion specific mAbs is challenging if the antigen cannot be isolated in this form.

This work therefore sought to try and establish a method for the isolation of pre-fusion gB-specific antibodies. The efforts described avoided any reliance upon stabilising or isolating the pre-fusion conformation of the protein, which in turn would have required an understanding of its structure that did not exist at the time.

To do this, the screening strategy developed would rely upon two considerations regarding the conformation gB adopts. First, expressing full-length gB in the context of a membrane is likely to present antigen in a mixture of pre- and post-fusion conformations. This has been observed for HSV-1 gB expressed within the membranes of vesicles shed from gB-transfected cells (Zeev-Ben-Mordehai *et al*, 2016), and on the surface of pseudotyped HIV virions (Fontana *et al*, 2017). Secondly, expressing WT gB as a recombinant ectodomain results in the full conversion of the protein to the post-fusion conformation.

Using these assumptions, I hypothesised that isolation of pre-fusion specific antibodies would be possible via a dual selection assay. Screening mAbs for binding to membrane gB-expressing reporter cells would determine whether any bind either the pre- or post-fusion conformation of the protein. Using a gB ectodomain-based probe would

subsequently determine whether any mAbs recognise the post-fusion conformation. Antibodies capable of binding only the cell-based probe would indicate preference for binding to the pre-fusion form of gB.

Multiple methods exist for the isolation of mAbs, summarised in ***Table 4.3-1***, and reviewed in detail by Pedrioli and Oxenius (Pedrioli & Oxenius, 2021). Notwithstanding library display technologies, these invariably rely on a screen of B cells from some antigen-exposed source such as an immunised animal or human or a recently infected individual.

Hybridoma-based approaches depend upon the immortalisation of antibody secreting cells (ASCs). Performing limiting dilutions to achieve clonal populations then allows for the screening of culture supernatants for antibody activity of interest. Whilst technically relatively straightforward, its use has declined because of its slow, low-throughput nature and the restricted ability to enrich for ASCs of interest prior to any antigen screening step (Smith & Crowe, Jr., 2015). Though removing the immortalisation steps may speed up the process, screening of B cells *ex vivo* is itself limited by the short lifespan of such cells after isolation (Pedrioli & Oxenius, 2021). Despite its practical limitations, mAb discovery using hybridoma technology has yielded major blockbuster drugs including Adalimumab (Humira) for the treatment of rheumatoid arthritis (Zhang, 2012).

Non-B cell-based methods such as phage display techniques have many advantages not limited to the ability to perform iterative rounds of antibody selection against a target (Alfaleh *et al*, 2020). In addition, such methods prove useful in identifying mAbs against antigens unsuitable for *in vivo* work, such as toxins and venoms (Ledsgaard *et al*, 2018). However, the production of a diverse library of antibody-like sequences and establishment of the selection process is a highly technical and laborious process (Pedrioli & Oxenius, 2021). Phage display efforts have, however, already successfully isolated antibodies capable of neutralising infection of viral targets, including those against viral fusion proteins, summarised elsewhere (Mustafa & Mohammed, 2024).

An approach which is currently frequently used makes use of sorting technologies to enrich a B cell population for those making antibody specific to an antigen of interest.

This is typically done by FACS in which a B cell population expressing cell-surface B cell receptor (BCR) is stained using antigen probes. Sorting for cells capable of capturing the probe allows the user to screen millions of B cells in a single campaign, facilitating isolation of rare antibodies (Pedrioli & Oxenius, 2021). Re-cloning paired Heavy- and Light-chain sequences from these antigen-specific 'hits' by single-cell reverse transcription PCR (RT-PCR) allows isolation of mAbs specific to the antigen of interest. This was recently performed to isolate and characterise antibodies raised in response to a promising new malaria vaccine targeting the *P. falciparum* antigen RH5 (Barrett *et al*, 2024).

FACS-based screening of memory B cells has the advantages of being very high-throughput, relatively affordable and requiring equipment generally available in an immunology laboratory (Pedrioli & Oxenius, 2021). Its accessibility and high throughput have placed FACS-based B cell screening at the centre of mAb discovery research. Many examples exist of neutralising antibodies that have been isolated by this method, including against HIV, RSV and others (Schardt *et al*, 2024; Williams *et al*, 2017; Xiao *et al*, 2019).

Its key limitation, however, is that to use tetrameric antigen probes or their equivalents, one must be able to readily express and purify an antigen of interest in the desired conformation for use as a cell stain. Such a method would therefore not be suitable in this study given the challenges posed by gB's pre-fusion metastability, rendering production of a pre-fusion gB probe greatly challenging without some form of antigen stabilisation.

Screening of plasma cells is an approach complementary to screening of memory B cells. Absence of surface BCR prevents staining and FACS sorting of antigen-specific plasma cells. However, with suitable techniques and equipment, secretion of antibody by plasma cells allows assays of antibody specificity to be performed in solution. Moreover, such assays could extend beyond simple antigen binding to more sophisticated screens using competition, cell binding, binding blockade, or other antibody functions. Screening of plasma cells is thus well suited to isolation of antibodies with rare specificities and against membrane-associated proteins.

Single plasma cell screening technologies have seen significant advances in the last five years, with multiple companies developing mAb isolation platforms better suited to hard-to-target antigens such as membrane proteins. These technologies include the Beacon Optofluidics System (Bruker Cellular Analysis), AbCellera's microfluidics platform (Burman *et al*, 2020), CellCelector (Sartorius Matochko et al., 2022), Cyto-Mine (Sphere Fluidics, Gaa et al., 2021), HiFiBio's CelliGo platform (Gérard *et al*, 2020) and the xPloration platform (OmniAb, omniab.com/technology/screening/xploration/). Though technologies differ, they all rely on the screening of ASCs for ones making antibodies of interest, but with more flexibility over the type of antigen probe used compared to FACS-based approaches.

Technology	Time	R&D Cost	Screening against difficult antigens	Average affinity of isolated mAbs	Ability to identify rare binders	Throughput	Ease	Comments
Hybridoma Screening								Fusion to Myeloma cells is a significant bottleneck. Technology is predominantly used to isolate mouse immunoglobulins.
Memory B and Antibody-secreting cell (ASC) screening								Removing immortalisation steps as in hybridoma screens improves throughput, but ASCs may begin to die.
Antigen-specific FACS-based sorting								Very effective for isolating rare binders. Screening using a membrane-based sorting probe is challenging.
Single ASC Screening								Access to technology and the expense are key barriers to use.
B Cell Replica Methods (& Library Approaches)								Establishing a library screening platform is highly technical, but iterative screens for phenotypes of interest are possible.
Single B Cell repertoire analysis & expansion-guided selection								The reliance on identifying and isolating expanded clonotypes as ones that are likely to be antigen-specific results in the loss of rare binders. Antigen-agnostic screening is possible e.g. target-blind mAb isolation against whole pathogens.

Table 4.3-1: Common approaches for the isolation of monoclonal antibodies, often against specific antigen targets. Colours are subjective scores of each technique's favourability: green = highly favourable, yellow = moderately favourable, red = less favourable. Table adapted from *Pedrioli & Oxenius, 2021*.

At the time of this work, the Beacon Optofluidics system is the only instrument of this type available to purchase and use. The Beacon technology makes use of a microfluidics chip containing thousands of 'nanopens' (~1 nL volume) to screen individual plasma cells in their own microenvironment.

An enriched population of ASCs is first loaded onto the chip such that the bulk cell population occupies channels on the chip pre-flushed with cell culture medium (***Figure 4.3-1***). By passing a voltage over the microfluidics chip, individual ASCs are then guided into their own nanopens by Optical-Electro Positioning (OEP). Here, the electric field is used to generate light patterns resembling cages around single cells. Activation of a photoconductor in solution results in these light patterns gently repelling cells, allowing singly caged cells to be moved around the chip (Le *et al*, 2018). This process allows for the isolation of single cells from the bulk population in the reservoir.

Once the penning process is complete, the reservoir is flushed to remove unpenned cells and screening of the penned ASCs takes place. By filling the channels above the pens with antigen probes, antibody released by the ASCs diffuses out of the pens into the reservoir immediately above the pen opening. Where the antibodies recognise the antigen probe, antibody-probe complexes form. A fluorescently tagged secondary antibody imported concurrently with the probes then begins to accumulate on the probe surface. Fluorescence microscopy images taken at regular time intervals after adding the probes then reveal a halo or 'bloom' of fluorescence above pens containing ASCs making antibodies of interest. Finally, selected cells (i.e. those from pens with blooms) are exported from the chip one-by-one for downstream antibody Heavy (H)- and Light (L)-chain amplification.

Accessing a Beacon instrument comes at a significant cost with respect to both instrument purchase and use of consumables. However, the key advantages of such a technology are the flexibility of probe type that can be used in an assay, and the ability to run multiple assays on penned cells using different probes. Considering the conformational challenges gB presents, the ability to use both a membrane-bound gB probe and a classical protein-

on-bead probe in a dual-selection assay on the Beacon highlighted its suitability over conventional methods.

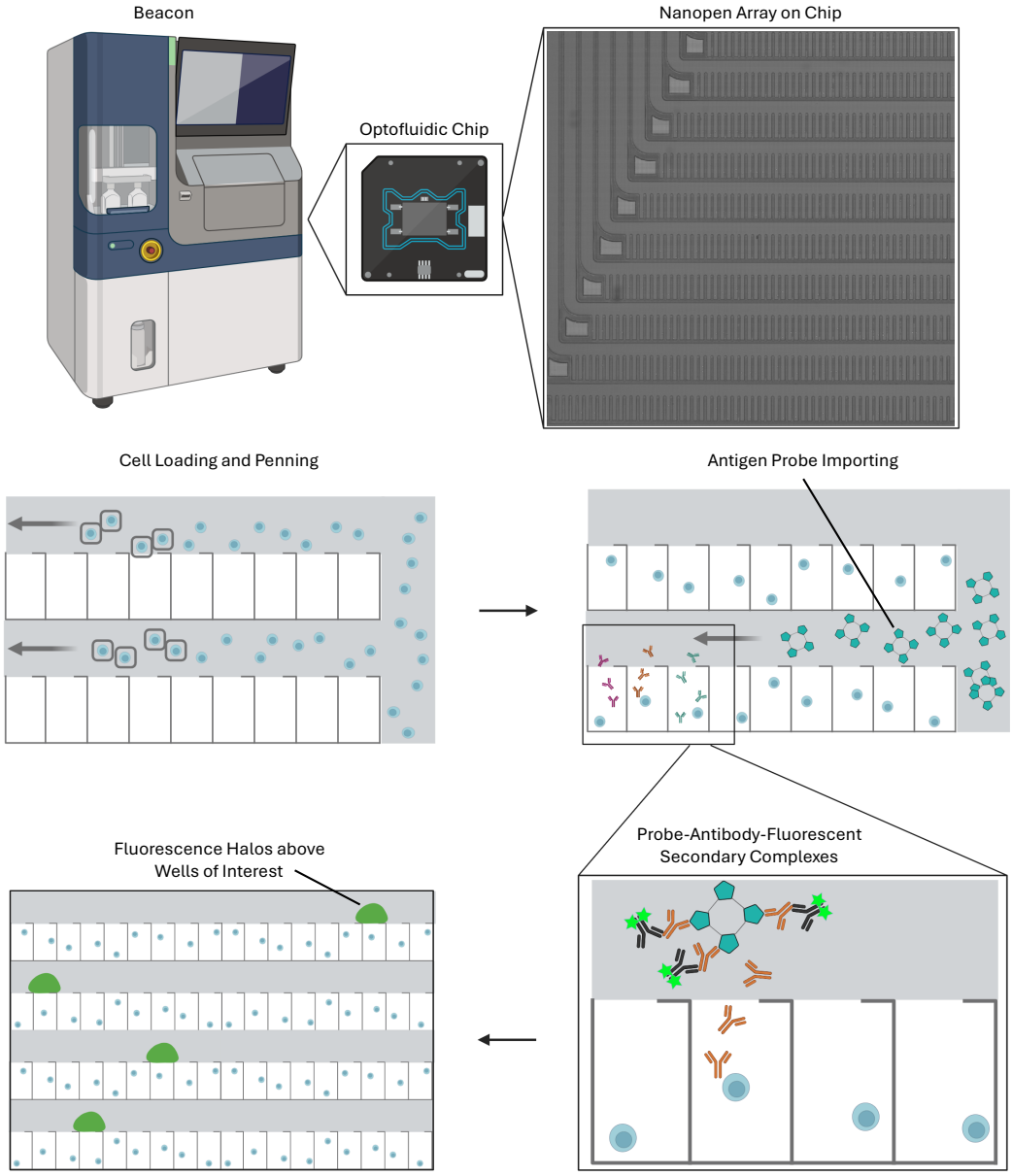


Figure 4.3-1: Plasma cell screening using a Beacon (Bruker Cellular Analysis).
Optofluidics chips, containing thousands of 'nanopens', are loaded with an enriched plasma cell population. Cells are penned by Optical-electro positioning before the import of antigen probes. Antibody secreted by penned plasma cells diffuses into the channel above the pen where it binds and accumulates on the surface of the antigen-coated beads. The localised antibodies are detected by a fluorescent secondary antibody. Time-sequence fluorescence imaging of the optofluidics chip reveals halos of fluorescence above pens containing a plasma cell reactive to the antigen probe, which are selected for exporting from the chip.
Schematic created using BioRender.com

This work therefore sought to make use of a Beacon instrument to isolate conformationally specific anti-gB mAbs whilst optimising steps upstream and downstream of the machine to improve the rates of mAb recovery. To access an instrument, Beacon campaigns were performed in collaboration with the Edinburgh Genome Foundry, which was to our knowledge the only facility offering access to a Beacon for academic researchers across the UK.

Given the need to screen cells at this centralised facility, a secondary objective of this work was to try and adapt the Beacon mAb isolation pipeline for the use of frozen tissue samples (rather than only fresh cells, as recommended by the manufacturer), decoupling the sample acquisition steps from the instrument-dependent steps. Establishing such protocols would therefore improve access to this cutting-edge screening technology for other researchers and projects.

Lastly, this work aimed to establish a pipeline which could be used for the isolation of human mAbs in contexts where antigen-reactive human PBMCs are not available (for example in the early stages of a new disease outbreak, against a recently discovered and poorly immunogenic candidate vaccine antigen, or against some self-antigens). This can be achieved by immunisation of human-IgG-transgenic mice. Several mouse lines have been created, varying in their coverage of the human variable region repertoire and the robustness of the human immune responses they can mount (Chen & Murawsky, 2018; Richardson *et al*, 2023).

Such mice are commercially extremely valuable and, until recently, high-performing human IgG transgenic mice have been inaccessible for academic research. Recently, the 'OmniMouse' has become available for academic use (OmniAb Inc.). These animals have been engineered to express~80% of a variable κ/λ Light-chain repertoire and a full human variable Heavy gene repertoire which is expressed with a rat-derived constant region by the animals (Brüggemann *et al*, 2015). Human variable region repertoires in these animals were first described for the OmniRat model (Osborn *et al*, 2013).

It was reasoned that combining these mice with the plasma cell screening capabilities of the Beacon instrument would provide a powerful method for the isolation of human antibodies against 'challenging' targets, complementary to FACS sorting of antigen-stained human memory B cells (which is already well-established locally). It was therefore decided that this project should investigate the use of these mice, with the goal of developing such a pipeline.

Apart from the mice and the PCR primers to be used, the intended pipeline would be identical to one suitable for isolation of fully murine antibodies from wild-type mice using a Beacon. Establishing use of the Beacon with wild-type mouse samples was therefore an initial goal for work in this chapter. In parallel, I planned to explore immunisation of the OmniMice and recovery of variable region sequences from OmniMouse plasma cells by RT-PCR.

It is important to note that lack of antigen-reactive human PBMCs is *not* a problem for EBV gB, given the prevalence of EBV human infection and the immunogenicity of gB. In the absence of the desire to establish the 'pipeline' described above, it would have been possible to seek human anti-gB mAbs from human samples.

gB-reactive human plasma cells could be obtained either by sorting circulating plasmablasts, soon after EBV infection, or by culture of human memory B cells, as has previously been conducted (Snijder *et al*, 2018). These could then be screened using antibody-secretion-dependent methods, including binding to cell- or virion-associated pre-fusion gB on a Beacon. The decision to work from mouse samples for this project was thus motivated primarily by the Douglas group's desire to establish a versatile pipeline applicable to other challenging targets, rather than this being the only or even the best route to isolate antibodies against this particular target.

4.4 Materials and Methods

4.4.1 Production of Protein and Viral-vectored Immunogens

The gB ectodomain (gBect) immunogen used spans amino acids (AAs) 23-683 of the protein (PDB: 3FVC_A). AAs encoding the WT EBV gB fusion loops ^{112}WY^{113} and ^{193}WLIW^{196} were mutated to HR and RVEA, respectively, analogous residues from HSV-1 gB (Backovic *et al*, 2007). A dual tag was added via a flexible linker (GSGSG) to the C-terminus of gBect, encoding a Spy tag (Zakeri *et al*, 2012) and a C-tag (EPEA). The coding sequence was synthesised by Twist Bioscience pre-cloned into a pTWIST expression vector.

Plasmid DNA encoding gBect was used to transiently transfect Expi293F cells as per *Section 2.1.2*. gBect was then purified on an AKTA Pure protein purification system (Cytiva) using a 1mL CaptureSelect C-tagXL Pre-packed Column (ThermoFisher: 494307201) as per the manufacturer's instructions. Collected fractions containing the purified protein were pooled and buffer exchanged into freezing buffer (50 mM HEPES pH 7.4, 150 mM NaCl, 5% Glycerol (v/v)) using a PD-10 desalting column (Cytiva). Proteins were stored at -80 °C until use.

Viral vectored immunogens encoding full-length gB were generated by the Viral Vector Core Facility (VVCF) using the ChAdOx1 platform (Dicks *et al*, 2012). The gB construct used for production of these vaccines, first described by Garcia et al. encodes the WT gB sequence (GenBank ID: YP_401713.1) with the endoplasmic reticulum (ER) retention sequence ^{836}RRRR^{839} mutated to KKKK to improve cell-surface expression of the antigen (Garcia *et al*, 2013). For adenovirus production, this coding sequence was subcloned into the pENTR4 LPTOS 'entry vector' followed by the pChAdOx1 DEST bacterial artificial chromosome containing the ChAdOx1 genome.

For MVA production, the coding sequence was transferred to an MVA shuttle vector. These cloning steps were performed by Dr Shruti Bakshi, and the resulting DNA was then provided to the VVCF for virus production using previously described methods (Draper *et al*, 2008). All vaccines were stored at -80 °C until use.

4.4.2 Animal Immunisations

Mouse immunisation schedules for experiments in this chapter are shown graphically in relevant figures. Immunisations of mice in Edinburgh to produce fresh splenocyte samples for testing on the Beacon were performed by Dr Inga Dry (Roslin Institute, University of Edinburgh). Female Balb/c mice were administered 3 doses of 50 μg gBect subcutaneously (S.C.) on days 0, 25 and 43. 7-10 days prior to a Beacon campaign, animals were administered a final dose of gB intraperitoneally (I.P.).

Intramuscular (I.M.) administration of vaccines performed at the University of Oxford were given at a volume of 50 μL/dose. I.M. injections were performed under general anaesthetic into the hind limb quadriceps muscles with the vaccine dose administered in halves across each hind limb. gBect protein immunogens used at the University of Oxford were formulated 1:1 (v/v) with and AddaVax oil-in-water adjuvant (InvivoGen) immediately prior to administration. To generate gB-reactive splenocyte samples that would be used on the Beacon, female C57BL/6 were administered three doses of 5 μg gBect in adjuvant I.M. on days 0, 42 and 90 before harvesting tissue 10 days later.

Differences in immunisation regimens between animals immunised in the University of Edinburgh and the University of Oxford were the result of practical limitations on the animal experimental licenses under which mice were regulated in the different institutions. Immunisations at the University of Edinburgh followed an approved regimen used by the Roslin Institute for previous studies of mouse plasma cell responses. Larger doses were used as the license did not permit the use of the AddaVax adjuvant used in studies based in Oxford.

Immunisations of animals that received viral vectored vaccines were also performed at the University of Oxford. ChAdOx1-vectored gB was administered at 1×10^8 infectious units (I.U.)/dose, given I.M. MVA-vectored gB was given at a dose of 1×10^8 plaque forming units (pfu), administered I.M. or intravenously (I.V.) into the lateral tail vein. C57BL/6 mice were administered two doses of ChAdOx1 gB on days 0 and 18, before boosting with MVA-gB on day 54 and culling 10 days later.

To prime OmniMouse animals with a DNA vaccine encoding the full-length WT gB sequence, plasmid DNA was first purified using Phenol:Chloroform:Isoamyl Alcohol (25:24:1, v/v, ThermoFisher: 15593031). The plasmid DNA was administered using the invivo-jetPEI transfection reagent (Sartorius: 101000040) as per the manufacturer's instructions. A DNA : PEI ratio of 6 µg DNA/µL PEI, at a final dose of 15 µg DNA/animal was administered I.V.. After priming with gB DNA, animals were boosted I.M. with MVA gB on day 94 and ChAdOx1-gB on days 126 and 182 before culling 10 days later. Doses for viral vectored vaccines were the same as those described above.

4.4.3 Tissue Processing and Freezing

Spleens from immunised animals were harvested immediately post-mortem and kept on ice before mechanical disruption (using a syringe plunger) within 3 hours to produce a single cell suspension of splenocytes. Cell suspensions were then passed through a mesh strainer (Fisher: 10788201) before red blood cell (RBC) removal steps were conducted.

For samples that underwent RBC lysis (specified in text), strained cell samples were centrifuged at 300 ×G for 5 min before being resuspended in ACK lysis buffer (150 mM NH_4Cl, 10 mM K_2CO_3, 0.1 mM EDTA) for 5 min. RBC-lysed cell samples were centrifuged as above, resuspended in complete RPMI media (RPMI, 10% FBS, 1% L-glutamine, 1% Penicillin Streptomycin) (cRPMI) and passed through a mesh strainer again to remove the RBC 'ghost'. White cell suspensions were counted using a CASY cell counter (Cambridge Bioscience), centrifuged again, and resuspended in freeze media (90% FBS, 10% DMSO). 1 $\times 10^7$ splenocytes were aliquoted into cryovials (1mL/vial). Cryovials were cooled to -80 °C in a CoolCell LX Freezing Container (Merck) at 1 °C/min before being transferred to liquid nitrogen for long-term storage.

For samples that underwent density gradient centrifugation, cell samples suspended in cRPMI were overlayed onto 15 mL Histopaque-1083 (Sigma: 10831) and centrifuged at 400 ×G for 30 min with the brake off. The separated cell layer was subsequently removed with a Pasteur pipette and counted. Samples were resuspended in freeze media, cooled and stored in the fashion described above.

4.4.4 B Cell Enzyme-linked ImmunoSpot (ELISpot) Assay

Total IgG secreting cells and anti-gB IgG secreting cells were quantified by B cell ELISpot using the Mouse IgG ELISpot^{Basic} Kit (MabTech: 3825-2H). 0.45 µm hydrophobic polyvinylidene difluoride (PVDF) filter ELISpot plates (Merck: MAIPS4510) were activated with 70% ethanol for 30 seconds before washing six times with sterile water. Plates were then coated overnight at 4 °C with 5 µg/mL (100 µL/well) of gBect or anti-IgG capture antibody for determining antigen-specific and total IgG responses, respectively.

The following day, frozen cell samples were thawed in a 37 °C water bath, resuspended in cRPMI and allowed to recover for one hour at 37 °C. Meanwhile, coated ELISpot plates were washed five times with sterile PBS and blocked with cRPMI for 30 min. Cells were then added to each well and the total volume topped up to 200 µL with cRPMI. ELISpot plates were cultured for 22-24 h at 37 °C before cells were removed and plates washed 5 times with sterile PBS.

Detection of IgG secreting cell spots was conducted using a biotinylated anti-mouse IgG primary stain before adding a streptavidin-horseradish peroxidase secondary stain as recommended by the manufacturer. Plates were developed for 5-15 min using pre-made 3,3′,5,5′-tetramethylbenzidine (TMB) substrate solution for HRP (MabTech: 3651-10) before washing thoroughly in water and allowing wells to dry. Spot forming units (SFU) were counted using an iSpot ELISpot reader (AID) and images of each well manually checked for aberrant spot identification.

4.4.5 Production and Purification of Recombinant Biotinylated gB Ectodomain for Use as a Protein Probe

The gBect protein used to produce Beacon probes was the same construct as that used in *Section 4.4.1*, but purified using a C-terminal His-Avi tag as previously described (Snijder *et al*, 2018), rather than the SpyTag-Ctag described above for purifying gBect used for immunisation.

Expi293F cells were co-transfected with plasmid DNA encoding gBect and the BirA biotinylation enzyme (5% total DNA, GenBank: ABW71926.1) in a pTT expression

vector using the same transfection protocol described in *Section 2.1.2*. The gBect was purified on an AKTA Pure protein purification system (Cytiva) using a 1 mL HiTrap TALON Crude column (Cytiva: 29-0485-65). After loading transfection supernatant, the column was washed with 5 mL 50 mM HEPES pH 7.3, 300 mM NaCl, 5 mM imidazole before eluting bound protein in 50 mM HEPES pH 7.3, 300 mM NaCl, 250 mM imidazole.

Fractions containing eluted protein were pooled and gBect was further purified by size-exclusion chromatography (SEC) using a Superose 6 Increase 10/300 GL SEC column (Cytiva). Fractions containing gBect were pooled, concentrated using an Amicon 30 kDa MWCO filter (Merck) and stored at -80 °C.

The purity of the gBect protein and the presence of a C-terminal His tag were determined by Coomassie gel and western blot analysis, respectively. Briefly, 10 µL samples from intermediate steps in the purification process, as well as the isolated gBect, were run on two denaturing NuPAGE Bis-Tris (4-12%) polyacrylamide gels (ThermoFisher) for 50 min at 180 V.

One gel was then subjected to staining with Coomassie InstantBlue (SLS) for 1 h before destaining in water overnight.

Samples from the second gel were transferred to a PVDF Trans-Blot Turbo membrane (Bio-Rad) using a Trans-Blot Turbo System (Bio-Rad), as per the manufacturer's instructions. The membrane was subsequently stained overnight using an iBind Western Device (ThermoFisher) and the iBind Flex staining kit (ThermoFisher: SLF2020) as per the manufacturer's instructions.

Stains were diluted in iBind Flex solution (ThermoFisher). Primary staining used an anti-His tag antibody (ThermoFisher: MA1-21315) at a dilution of 1:1000, and an anti-mouse IgG secondary conjugated to HRP (BioRad: 1706516). The stained membranes were detected using SuperSignal West Pico PLUS Chemiluminescent Substrate (ThermoFisher: 34580) as per the manufacturer's instructions. Both the Coomassie gel and western blot membrane were imaged using a ChemiDoc Imaging System (Bio-Rad).

SEC elution fractions were analysed by Coomassie gel using the same method described above.

4.4.6 Flow Cytometry-based Screen of Biotinylated gBect as a Probe Antigen

Biotinylated gBect was conjugated to streptavidin-allophycocyanin (APC) (ThermoFisher: 17-4317-82) by mixing 0.3 µg of protein with 0.24 µL of streptavidin-APC in a reaction volume of 10 µL at 4 °C for 20 min.

Meanwhile, 1 µL samples of mouse serum pooled from animals immunised with 3 doses of gBect or RH5, a *P. falciparum* control antigen, were separately incubated with a single drop of OneComp eBeads (ThermoFisher: 01-1111-41) for 20 min at RT.

1 µL of the newly conjugated gBect-streptavidin-APC probes was then added to each reaction mix and bead samples run on a Fortessa X20 cytometer (BD Biosciences).

4.4.7 Transient transfection of CHO cells to generate a gB-expressing cell probe for Beacon screens

ExpiCHO-S cells were transfected as per *Section 2.1.3* with plasmid DNA synthesised by Twist Bioscience encoding the full-length version of gB with mutated ER retention sequence, as described in *Section 4.4.1* (Garcia *et al*, 2013). Cells were harvested 48 h post-transfection, centrifuged at 300 ×G for 5 min and resuspended to a density of 1 $\times 10^7$ cells/mL in 90% fresh ExpiCHO Expression medium 10% sterile DMSO. 1 mL aliquots of the cell suspension were transferred to cryovials and frozen as per *Section 4.4.3*.

To confirm expression of gB on the surface of freeze/thawed reporter CHO cells, cells were revived by thawing in a 37 °C water bath, resuspending cells in ExpiCHO expression media and allowing them to recover for 1 h at 37 °C. After recovery, 1 $\times 10^6$ cells were washed twice in PBS before staining with an anti-gB antibody, AMMO5 (Snijder *et al*, 2018), at a concentration of 1 µg/mL for 30 min at RT. After washing twice more as above, a secondary stain consisting of a donkey anti-human IgG conjugated to AlexaFluor 647 (Jackson Immuno: 709-605-098) was added to cells at a final antibody

dilution of 1:1000. Samples were incubated and washed as above, before running the fully stained samples on a BD LSRII flow cytometer (BD Bioscience).

4.4.8 Conjugation of Biotinylated Antigen to Streptavidin Coated Beads

Production of gBect-coated assay beads was performed according to protocol MAN-000024_RD supplied by Bruker Cellular Analysis (henceforth referred to as Bruker). Briefly, 600 µL streptavidin-coated assay beads (Bruker: 520-0005) were washed 4 times by centrifuging at 3000 ×G for 5 min, removing the supernatant and resuspending the beads in 1 mL sterile PBS, before finally resuspending the assay beads in 6 mL PBS. 30 µg of the purified biotinylated gBect protein was added to the assay bead mix and incubated on a roller at 4 °C overnight. The coated beads were then centrifuged and washed three times in 1 mL PBS as above, resuspended to a final volume of 480 µL and stored at 4 °C until use.

4.4.9 Isolation of Antibody-secreting Cells by Magnetic-Activated Cell Sorting (MACS)

After removal of RBCs, bulk splenocytes (or bone marrow samples) were subjected to plasma cell enrichment by MACS using the $CD138^+$ Plasma Cell Isolation Kit (Miltenyi: 130-092-530) as per the manufacturer's instructions, with the modification that only the positive enrichment step was performed.

Briefly, 1 $\times 10^8$ cells were mixed with 100 µL CD138 microbeads and incubated for 15 min at 4 °C. Cells were washed in 10mL MACS buffer (cold PBS, 0.5% FBS), centrifuged at 300 ×G for 10 min and resuspended in 500 µL MACS buffer. The cell-bead mixture was then passed over a MS MACS column (Miltenyi) pre-equilibrated into MACS buffer in a MiniMACS Separator (Miltenyi). The sample was allowed to run through the column before the column was then washed 3 times with 500 µL MACS buffer. The retained fraction (plasma cells) was then flushed from the MS column using a plunger and eluted. These cells were loaded onto a second MS MACS column for a full repeat of the column-based steps. The eluted cells from the second column were centrifuged at 300 ×G for 5 min and resuspended to a final concentration of 7 $\times 10^6$ cells/mL in MACS buffer for loading onto the Beacon.

4.4.10 Isolation of Antibody-secreting Cells by Fluorescence-Activated Cell Sorting (FACS)

Homogenised mouse splenocyte samples between 2 ×10^7 and 5 ×10^7 cells were subjected to staining for FACS-based enrichment of plasma cells. Cells were washed twice in 15 mL FACS buffer (Sterile PBS, 0.05% Bovine Serum Albumin) by centrifuging at 350 ×G for 5 min and resuspending the pellet in fresh buffer. After the second wash, samples were incubated with Fc Block for 30 min at 4 °C. 2 µL samples were removed at this stage single-colour staining compensation controls. The remaining staining mix was diluted up to 15 mL and centrifuged as above.

After removing the supernatant and resuspending in 1 mL FACS buffer, cells were stained using the antibody mix described in ***Table 4.4-1*** for 30 min at 4 °C. Cells were then washed twice, as above, before running on a FACS Aria II Cell Sorter (BD Bioscience). For all Beacon campaigns that used FACS, $CD138^{High}$ $B220^{Low}$ plasma cells were sorted by the same gating strategy (***Figure 4.5-4A***).

Plasma cells were sorted into a 5 mL pre-warmed basal media (Bruker) before being centrifuged at 350 ×G for 5 min and resuspended to a target density of 7 ×10^6 cells/mL for loading onto the Beacon. Where cell numbers were limiting, plasma cells were resuspended in a minimum volume of 15 µL required for loading of cell samples onto an optofluidics chip. In all cases, plasma cell samples were loaded onto optofluidics chips by manual import before confirming successful loading and cell distribution across the chip by manually inspecting each field of view (FoV) across the chip.

Fluorochrome	Marker (Supplier: Cat.)	Dilution	Excitation (Filter)
Nil	Fc Block (BD Bioscience: 553142)	1:50	Nil
Live/Dead Fixable Aqua	Live/Dead Stain (ThermoFisher: L34957)	1:1000	405 nm (525/50)
APC-eFluor A780	CD4 (BD Bioscience: 47-0042-82) CD8 (BD Bioscience: 47-0081-82) F4/80 (BD Bioscience: 47-4801-82) GR1 (BD Bioscience: 47-5931-82)	1:150 each	640 nm (780/60)
Alexa Fluor 700	CD45R (B220) (BD Bioscience: 56-0452-82)	1:150	633 nm (710/50)
Phycoerythrin	CD138 (Biolegend: 142503)	1:150	561 nm (586/15)

Table 4.4-1: Staining panel for the enrichment of $CD138^{High}$ $B220^{Low}$ mouse plasma B cells from splenocyte samples. All markers are mouse-specific except the live/dead stain.

4.4.11 Screening and Export of Plasma Cells on the Beacon

After loading of plasma cell samples onto the chip, cells were penned using one of two penning protocols - Live B Cell Penning or Pen Plasma Cells (Bruker) - as specified in ***Figure 4.5-9B***, at which point penned cell counts were performed. Antigen-specific and total IgG assays were subsequently performed by importing the relevant bead/cell-based probes into chip reservoirs and manually confirming a uniform distribution of probes across the chip by inspecting each field of view.

In all cases, an anti-mouse IgG-fluorescein isothiocyanate (FITC) secondary (Jackson ImmunoResearch: 115-546-062) was used at 4 µg/mL. Images were taken at time t = 0 after probe loading and at four subsequent timepoints at intervals of 4 min. Probe-reactive pens were identified automatically by the Beacon before manually inspecting each FoV to remove false positives and include any unidentified hits. Pen hits containing single cells were subsequently selected for pen-by-pen export into a 96-well PCR plate.

Wells of the export plate were preloaded with one of two cell lysis mixes. 10 µL 2× TCL buffer (Qiagen), 10 µL mineral oil (VWR Avantor: 0219483690), as recommended by Bruker, was used as the lysis mix for Beacon runs 1-5. From then on, 4 µL RT-PCR lysis mix (0.5× sterile PBS, 10 mM DTT (ThermoFisher), 8 U RNAsin (Promega: N2111)) was added to each export well, as described in previously published mAb isolation method (Von Boehmer *et al*, 2016). After completion of the export protocol, plates were sealed with foil seals (Biorad: MSF1001), centrifuged briefly and stored at -80 °C.

4.4.12 Reverse Transcription PCR for Antibody Heavy- and Light-Chain Amplification from Wild-type Mice

Two protocols were used for isolation of paired H and L chain sequences from WT mouse-derived single cells export mixes. Methods are compared in the corresponding results section, in ***Figure 4.5-10***.

Originally, RT-PCR steps were conducted as per Bruker's instructions (protocol MAN-000047_RF). After comparison of this method to that published by von Boehmer and colleagues (Von Boehmer *et al*, 2016) (***Figure 4.5-10A***), subsequent RT-PCR

amplifications of H- and L-chains were performed by their protocol, with the minor modification that PCR reaction mixes used 2× DreamTaq Hot Start PCR Master Mix (ThermoFisher: K9011).

For all single-cell samples, γ-, κ- and λ-chain PCR reactions were performed. All primers used in PCR reactions were kept at the same concentrations as the original protocol (Von Boehmer *et al*, 2016). Thermocycler parameters were unchanged from the original protocol. As per the published method, where H- or κ-chains were not successfully amplified by the standard primer sets, PCR reactions were repeated with a second set of primers, termed 'low yield' primers, complementary to rarer V gene fragments.

4.4.13 RT-PCR on OmniMouse-derived Antibody Secreting Cells

Amplification of OmniMouse-derived paired H- and κ L-chain sequences were performed using a RT-PCR protocol supplied by OmniAb. Briefly, plasma cells were first sorted into 5 µL of lysis mix (10mM DTT, 5U RNAsin in sterile PBS) and stored at -80 °C until use. mRNA from lysed cells was then purified using the Dynabeads mRNA DIRECT Purification Kit (ThermoFisher: 61012), as per the manufacturer's instructions, whereby mRNA molecules were annealed to Oligo $(dT)_{25}$-coated magnetic beads and washed. After washing, the mRNA-coated beads were resuspended in 10 µL reverse transcription reaction mix (SuperScript III First-Strand Synthesis System, ThermoFisher: 18080051) and incubated at 50 °C for 45 min.

Beads were then washed with 20 µL 10mM TrisHCl (pH 8.5) before the entire bead sample was used in the first-round PCR amplification reaction of H- and κ L-chain sequences. PCR reactions were performed using the GoTaq Green 2× Master Mix (Promega: M7123). H- and κ L-chain forward primer mixes were added to first round reactions at a final concentration of 0.5 µM, whilst reverse primers (Cγ, Cκ, Cλ) were added at 0.13 µM. Reactions were carried out with an initial melt step at 95 °C for 2 min, followed by 38 cycles of 94 °C for 30 s, 59 °C for 30 s and 72 °C for 1 min, before a final 2 min extension at 72 °C. 1 µL samples of the first-round reaction mix were used to template separate H- and κ L-chain second-round amplifications. Second-round reactions used the same concentration of forward primer mixes. Chain-specific primers were added

at 0.24 μM. Reactions were incubated using the same thermocycle conditions as in round one but with only 36 amplification cycles. λ L-chain reactions were not performed for OmniMouse samples.

Analysis of each PCR reaction was performed by running amplified products on 2% agarose gels. In all cases, 10 μL of the PCR reaction was mixed with 2 μL 6× gel loading dye (NEB: B7024S) and the entire sample loaded into the well of a gel. Gels were run at 120 V for 35 min and imaged on using a ChemiDoc Imaging System (Bio-Rad).

The sequences of all primers used in these reactions are listed in *Appendix III* with the exception of those supplied by Bruker Cellular Analysis.

4.4.14 Sequencing and Synthesis of mAb Heavy- and Light-chains

Unpurified PCR products from the second round of chain-specific amplification reactions were sent for Sanger sequencing (Eurofins Genomics) using the chain-matched reverse primer from the second round of amplification as the sequencing primer. Returned sanger sequences were subjected to antibody sequence alignment using IgBLAST (NIH) to determine each chain's V(D)J gene usage, complementarity-determining region (CDR) sequences and whether sequences would produce functional variable regions.

In cases where alignments identified expression-lethal mutations, original Sanger sequencing chromatograms were inspected manually to determine whether they were the product of a sequencing mis-call. Where reasonable, such mistakes were manually corrected. Three common corrections were made: 1) where the N-terminal sequence of Framework Region (FR) 1 and/or the C-terminal sequence of FR4 were unread, residues were manually added using the germline sequence with highest % alignment in the IgBLAST database as the template sequence. 2) Deletions in framework regions that resulted in frameshift mutations were corrected to germline sequence if they a) introduced a premature stop codon, or b) were the result of a sequencing mis-call identified on manual inspection of the chromatogram trace. 3) Where a point mutation resulted in a premature stop codon, the sequence was corrected to germline.

Where viable paired H- and L-chains were recovered, variable region sequences were synthesised by Twist Bioscience, pre-cloned into chain-matched human IgG vectors generously gifted by Dr Kirsty McHugh and Prof Simon Draper (University of Oxford). AbVec-hIgG1 (GenBank: FJ475055.1), AbVec1.1-IGKC (GenBank: LT615369.1) and AbVec IGLC (GenBank: FJ517647.1) vectors were used for inserting γ-, κ- and λ-chain variable regions, respectively. It should be noted that this resulted in expression of chimeric antibodies, with murine Fv and human constant regions.

In cases where both a κ and a λ light-chain were isolated from a single sample (8 of 111 H/L pairs), both light-chains were cloned into their respective Light-chain vectors and expression of mAb attempted with each.

4.4.15 Expression and Purification of mAbs by Small-scale Transient Transfection

mAbs were expressed by transient transfection of Expi293F cells as described in *Section 2.1.2* with two modifications: H- and L-chain plasmids were co-transfected in a 1:1 ratio by mass, and transfections were performed in 50 mL sterile vented cap tubes (Merck: Z761028), agitated at 210 rpm, 25 mm orbital diameter.

mAbs were isolated by affinity purification on an AKTA Pure system (Cytiva) using a 5 mL HiTrap Protein A HP (Cytiva: 17040301) as per the manufacturer's instructions. Eluted fractions containing IgG were buffer exchanged into freezing buffer (50 mM HEPES pH 7.4, 150 mM NaCl, 5% Glycerol (v/v)) and concentrated using a 30 kDa MWCO spin filter (Merck: UFC903096). All purified mAbs were stored at -80 °C until use.

4.4.16 ELISA-based Screening of Antibody Binding to gBect

ELISAs were performed as summarised in *Section 2.1.5* with protocol-specific steps described in ***Table 4.4-2***.

Protocol step	Description
Coating protein	Recombinant gBect produced in *Section 4.4.1*. Concentration: 2 µg/mL, 50 µL/well.
Blocking incubation	1 h at RT in the dark.
Primary stain	50 µL/well monoclonal antibodies run in duplicate wells at each tested concentration. Concentration: each antibody tested using a 5-point, 4-fold serial dilution series from 2 µg/mL to 3.2 ng/mL, 50 µL/well.
Control conditions	Controls run on each individual plate. Negative control: AMMO1 anti-gH/gL antibody tested in quadruplicate at 2 µg/mL, 50 µL/well. Positive control: 3A3 anti-gB mAb, tested in the same fashion as newly identified antibodies.
Primary incubation	1 h at RT in the dark.
Secondary stain	Goat anti-human IgG (γ-chain specific) secondary conjugated to alkaline phosphatase (Merck: A3187) at a dilution of 1:1000, 50 µL/well.
Secondary incubation	1 h at RT in the dark.
Development	5 min prior to reading.

Table 4.4-2: ELISA protocol for confirming mAb binding to gB ectodomain.

4.4.17 Flow-cytometry-based Screening of Antibody binding to Membrane-expressed gB

Expi293F cells were transiently transfected as per *Section 2.1.2* with plasmid DNA encoding the mutant form of full length gB described in *Section 4.4.1* where the ER retention sequence ^{836}RRRR^{839} is mutated to KKKK (Garcia *et al*, 2013). 48 h after transfection, gB-expressing cells were centrifuged at 300 ×G for 5 min and the cell pellet resuspended in Expi293 expression medium supplemented with 10% DMSO (v/v) to a density of 1 ×10^7 cells / mL before controlled freezing by the same method used in *Section 4.4.3*.

To screen mAbs for their ability to bind membrane-expressed gB, frozen vials of the gB-transfected Expi293F cells were thawed, freezing medium removed and allowed to recover for 1 h at 37 °C in fresh Expi293 media. 2 ×10^5 cells were added to wells of a 96-well plate, centrifuged 300 ×G for 5 min and washed twice with PBS. After the second wash and centrifugation, cell pellets were resuspended in primary stain of each antibody separately. For each mAb, mixes at final concentrations of 5, 0.5 and 0.05 µg/mL diluted in PBS were tested in duplicate (50 µL/well). Staining was performed for 1 h at RT

before washing each cell sample twice with PBS as before. Each cell pellet was subsequently resuspended in a staining mix containing anti-human IgG conjugated to AlexaFluor 647 (Jackson Immuno: 709-605-098) diluted 1:1000 in PBS. After staining for 1 h at RT, cell samples were washed twice again before running on a LSRII flow cytometer (BD Bioscience).

4.4.18 Screening of OmniMouse Antibody Responses by ELISpot and ELISA

Frozen splenocyte samples from WT mice and OmniMouse animals immunised with 3 doses of gBect were subjected to an ELISpot assay to quantify gB-specific plasma cell responses. ELISpots were conducted using the same method described in *Section 4.4.4* with one change: for detection of OmniMouse responses, detection of antibody spots was performed using a minimally cross-reactive, biotinylated anti-rat IgG secondary (BioLegend: 405428). Subsequent staining steps were identical to those previously described.

For screening OmniMouse anti-gB serum antibody titres, ELISAs were performed as summarised in *Section 2.1.5*, with protocol-specific steps described in ***Table 4.4-3***.

Protocol step	Description
Coating protein	Recombinant gBect produced in *Section 4.4.1*. Concentration: 2 µg/mL, 50 µL/well.
Blocking incubation	1 h at RT in the dark.
Primary stain	50 µL/well OmniMouse serum samples after 4 doses of DNA and viral-vectored vaccines encoding gB. Concentration: 3-fold serial dilutions from 1:100 to 1:24300. Each dilution tested in duplicate.
Control conditions	Negative control: OmniMouse serum pool from animals immunised with 3 × 5µg RH5 antigen. Positive control: OmniMouse serum pool from animals immunised with 3 × 5µg gBect protein.
Primary incubation	1 h at RT in the dark.
Secondary stain	Goat anti-rat IgG (Merck: A8438) used at 1:5000
Secondary incubation	1 h at RT in the dark.
Development	20 min prior to reading.

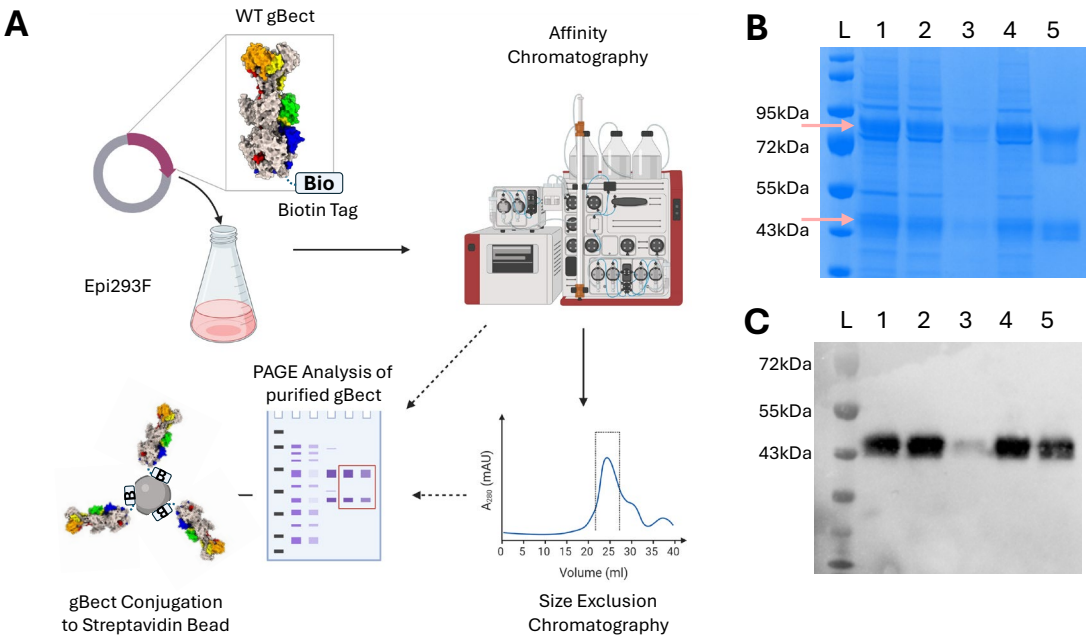
Table 4.4-3: ELISA protocol for determining anti-gB titres in OmniMouse animals.

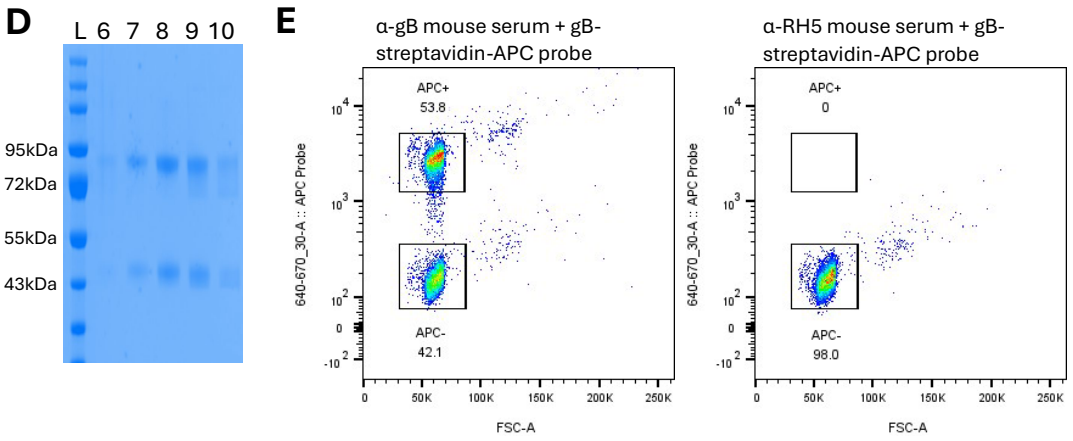
4.5 Results

4.5.1 gB Bead- and Cell-based Probes are Functional on a Beacon Optofluidics Chip

As stated in *Section 4.3*, screening of plasma cells (rather than memory B cells) allows a wider range of screening assays, particularly for membrane-associated targets. In this case, the interest in using a Beacon-based screening method stemmed from the ability to test whether plasma cells, or more accurately antibody secreting cells (ASCs), were capable of secreting antibody against two different forms of the gB protein. This would require the development of probes that used a post-fusion ectodomain of gB (gBect) and a membrane-expressed, full-length version of gB (FL-gB) predicted to present in both the pre- and post-fusion conformation.

Production of the gBect, bead-based probe followed a method similar to those used for the production of FACS probes. Expi293F cells were transiently transfected with plasmid DNA encoding a biotinylated gBect construct before the protein was subsequently purified from the transfected cell culture supernatant by affinity purification (***Figure 4.5-1A***). The purity of the isolated gBect was determined by Coomassie gel (***Figure 4.5-1B***) and the presence of the C-terminal his-tag confirmed by Western blot. As expected, the His-tag was detected on the smaller subunit of gBect, C-terminal to the furin cleavage site that separates the ectodomain into two polypeptide chains after cell-surface expression (Sorem & Longnecker, 2009) (***Figure 4.5-1C***). The protein was further purified by size-exclusion chromatography (SEC) to >90% purity (***Figure 4.5-1D***).


A
WT gBect
Bio
Biotin Tag
Epi293F
Affinity
Chromatography
PAGE Analysis of
purified gBect
gBect Conjugation
to Streptavidin Bead
Size Exclusion
Chromatography
Volume (ml)
B
L 1 2 3 4 5
95kDa
72kDa
55kDa
43kDa
C
L 1 2 3 4 5
72kDa
55kDa
43kDa


D
L 6 7 8 9 10
95kDa
72kDa
55kDa
43kDa
E
α-gB mouse serum + gB-
streptavidin-APC probe
APC+
53.8
APC-
42.1
640-670_30-A :: APC Probe
FSC-A
α-RH5 mouse serum + gB-
streptavidin-APC probe
APC+
0
APC-
98.0

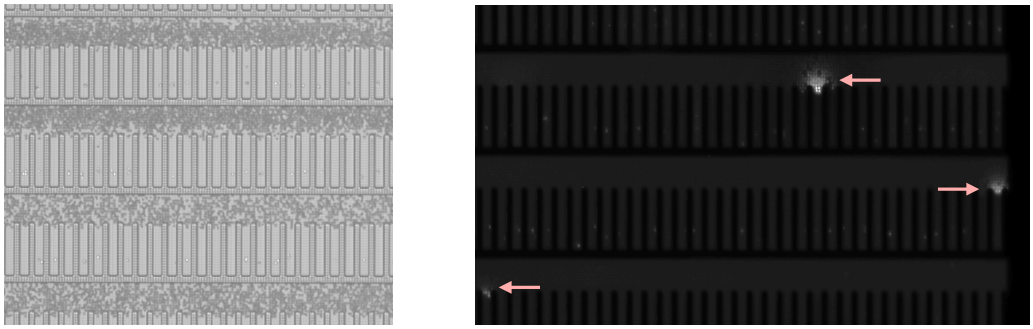

F
G

Figure 4.5-1: Post-fusion gB Beacon probe production.

(A) Production of the gBect bead-based probe for use on the Beacon. Plasmid DNA encoding a His-tagged version of the gBect with a C-terminal biotinylation site was used to transiently transfect Expi293F cells. gBect was isolated from culture supernatant by affinity chromatography. The eluted protein was further purified by size exclusion chromatography before confirming its purity on by PAGE analysis. The biotinylated gBect was finally conjugated to streptavidin-coated latex beads to produce the final Beacon probe. Schematic created using BioRender.com.

(B) Polyacrylamide gel electrophoresis (PAGE) analysis of samples collected throughout the purification process, stained with Coomassie Blue. L = Prestained Protein Standard, Broad Range (10-250 kDa) (NEB: P7719S), 1 = supernatant from gBect-transfected Expi293F culture, 2 = supernatant post-filtration, 3 = wash sample prior to the elution step, 4 = column flow-through upon sample loading, 5 = pooled fractions from the elution step. Expected sizes of the gBect fragments after furin cleavage are ~70 kDa (N-terminal fragment) and ~40 kDa (C-terminal fragment).

(C) Western blot analysis of the samples described in (B). Gel-analysed samples were stained for the presence of a His-tag, inserted at the C-terminus of the gBect construct.

(D) PAGE analysis of eluted fractions isolated from size exclusion chromatography on gBect. L = as per (B) and (C). 6 – 10 = elution fractions corresponding to a SEC chromatogram peak thought to be gBect.

(E) FACS plots showing OneComp eBeads (ThermoFisher) pre-coated with gB-reactive serum (left) and RH5-reactive serum (right). Beads were stained with tetrameric gB probes. Probes were made by mixing biotinylated gBect with streptavidin tetramers conjugated to APC.

(F) Representative light microscopy image of gBect bead probes loaded into the channels of an optofluidics chip. Nanopens are ~3 nm in height.

(G) Representative fluorescence microscopy image from gBect bead assay conducted on a Beacon. Pink arrows point to identified fluorescence halos.

A key limitation of conducting mAb isolation campaigns on a Beacon is cost, both of the instrument itself and of the consumables (notably the single-use chips, which cost ~£4000). As a result of the latter, combined with the design of the instrument which typically 'uses' a whole chip for each run, there is limited ability to perform dedicated method development or quality control runs. Instead, such experiments were conducted via off-chip proxies, where possible, or otherwise embedded within full mAb isolation campaigns in which the primary goal was a full run-through of the ASC screening assay. Given these restrictions, it was important to test the ability of the biotinylated gBect protein prep to capture anti-gB antibody using an off-chip method, to provide confidence that the protein probes would be functional on-chip.

To this end, biotinylated gBect was used to construct mock probe antigen by conjugating a sample of the protein to streptavidin-APC fluorophore tetramers. These probes were used to stain OneComp eBeads (ThermoFisher) pre-incubated with gB-reactive mouse serum or serum from animals immunised with a control *P. falciparum* antigen, RH5. Given the nature of the OneComp eBeads (a pre-mixed population of IgG-capture and capture-negative beads), a functional gBect probe would stain ~50% of the bead

population where beads were coated with antigen-matched serum, whilst an unmatched probe/serum combination would yield a 100% APC-negative population.

Testing the biotinylated gBect protein in this way revealed that the gBect probe was indeed capable of staining serum-coated beads in an antigen-specific fashion, with a ~10-fold difference in signal between populations (***Figure 4.5-1E***). This antigen was therefore used to produce all bead-based probes for Beacon campaigns. For the avoidance of confusion, the OneComp beads and fluorophore-labelled antigen were used purely for this 'QC' assay. For experiments on the Beacon instrument itself, beads were directly antigen-coated (rather than antibody-coated,) and detection used a fluorophore-labelled secondary antibody (rather than antigen).

Though this flow cytometry-based proxy assay did provide some insight into probe functionality, it does not perfectly replicate the assay beads that would be used on the Beacon, nor the on-chip conditions under which the probes will be used. The functionality of these antigen beads would ultimately be determined on-chip in the initial mAb isolation campaigns. Early Beacon runs showed that antigen probes produced by conjugating this biotinylated gBect prep to streptavidin-coated latex beads could be imported onto optofluidics chips at high density with good distribution throughout the channels and without significant clumping when visually screening FoVs (***Figure 4.5-1F***). Early Beacon runs also showed that these beads were capable of capturing gB-reactive antibody secreted by penned mouse ASCs (***Figure 4.5-1G***).

To produce a cell-based FL-gB probe, it was suggested by Bruker that this was done by the generation of a stably transfected, inducible gB reporter cell line. Given that stable cell line generation may take a significant amount of time and that development of a simple, easily transferrable mAb isolation protocol was a key aim of this research, the use of a transiently transfected reporter cells was investigated instead.

Two variants of FL-gB were tested to produce CHO cell probes, the full-length WT form and a mutant version of gB in which the endoplasmic reticulum retention sequence ^{836}RRRR^{839} was mutated to KKKK to improve cell-surface expression (gBmutK hereon)

(Garcia *et al*, 2013). Importantly, the gBmutK mutant does not appear to affect fusogenicity, suggesting the conformation of membrane-expressed antigen is similar to that of the WT gB (likely in the pre-fusion for the most part) (Garcia *et al*, 2013).

Plasmid DNA encoding each version of gB was used to transfect ExpiCHO-S cells and cell samples taken at 24, 48 and 72 h post-transfection (***Figure 4.5-2A***). Transfected cells from each timepoint were then stained with an anti-gB antibody, AMMO5 (Snijder *et al*, 2018), to measure cell-surface expression of the antigen by flow cytometry (***Figure 4.5-2B***). Expression of both FL-gB constructs appeared to peak at 48 h post-transfection, and whilst both the WT gB and gBmutK showed similar median fluorescent intensity values, analysis of each population's fluorescence intensity histograms revealed the gBmutK construct produced a subset of cells expressing gB at levels higher than the WT (***Figure 4.5-2C***), and thus was selected over the WT for making Beacon probes.

Given that these reporter cells would be frozen for storage before their use on a Beacon, a 24 h sample of the gBmutK transfection and a 48 h sample of the WT transfection were also analysed by flow cytometry after being frozen and thawed. Freezing appeared to reduce surface expression by ~50% relative to fresh samples in both cases (***Figure 4.5-2B***). Ultimately, however, loading the gBmutK-transfected CHO cells onto the Beacon revealed a uniform distribution of cell probes in the channels (***Figure 4.5-2D***) and sufficient expression of the antigen for the instrument to detect gB-reactive hits (***Figure 4.5-2E***).

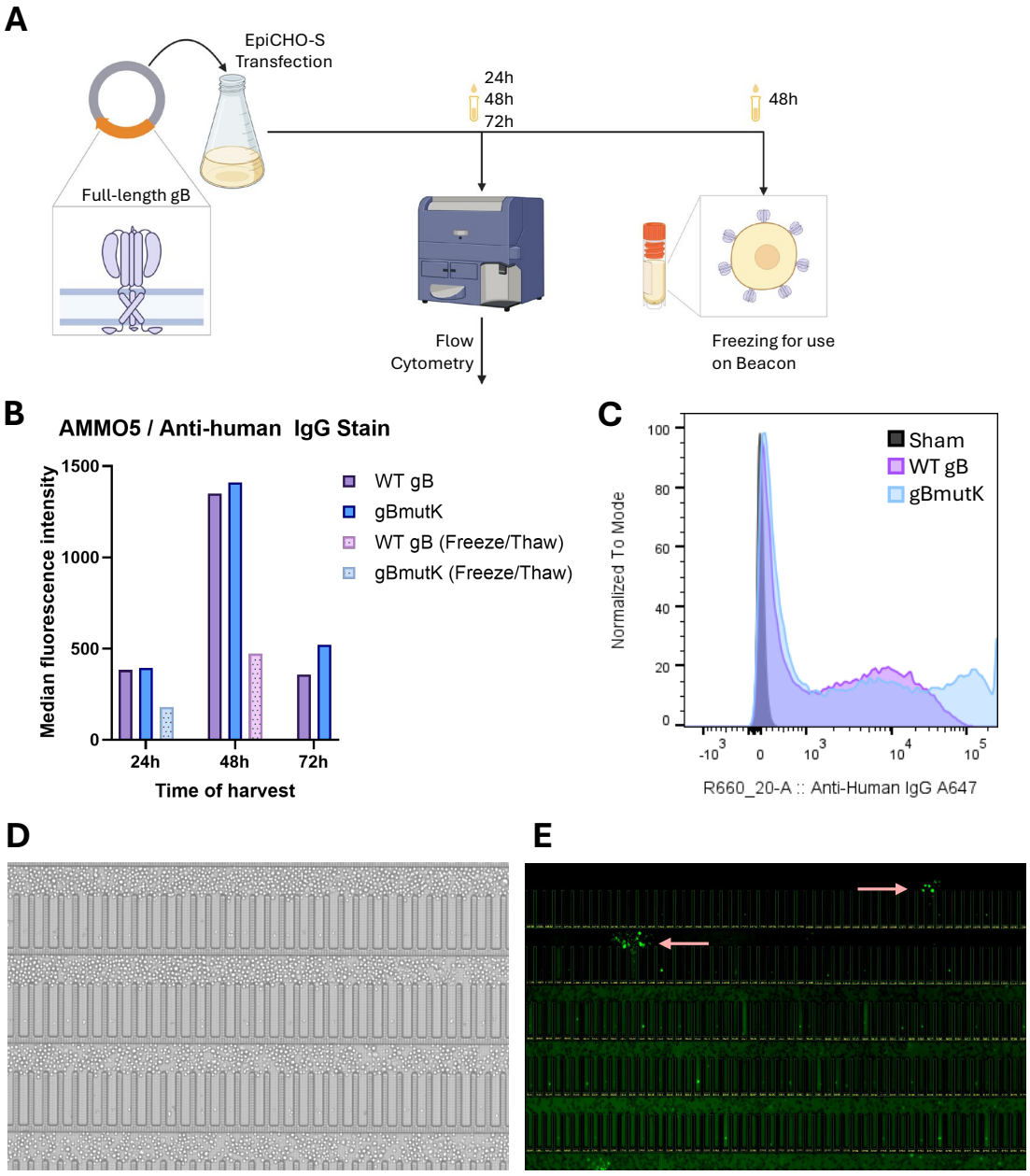


Figure 4.5-2: CHO cell-based gB Beacon probe production.

(A) Plasmid DNA encoding a full-length version of gB was used to transiently transfect CHO cells. Transfected cell samples taken 24, 48 and 72 h post-transfection were tested for gB surface expression by flow cytometry. Transfected cells from the 48 h timepoint were also frozen for use as a gB cell probe on the Beacon.

(B) Histogram showing the fluorescence intensity of cells isolated at the 48 h timepoint expressing FL-gB in the WT form, or gBmutK, stained with an anti-gB antibody. The sham condition represents gBmutK-transfected cells stained with a non-gB specific antibody, 17C7. Each histogram is normalised to its modal value.

(C) Expression levels of gB on the surface of CHO cells transfected with WT FL-gB, or the gBmutK mutant. Samples were stained with AMMO5, as in (B). Bars represent the median fluorescence intensity of each cell population. The different timepoints were analysed by flow cytometry on consecutive days using the identical cytometer parameters.

(D) Representative light microscopy image of gB-expressing CHO cell reporters loaded into the channels of an optofluidics chip. Nanopens are ~3 nm in height.

(E) Representative fluorescence microscopy image from a gB-CHO reporter assay conducted on a Beacon. Pink arrows point to identified fluorescence halos.

4.5.2 Beacon Screens on Fresh Samples Yield Modest Hit Numbers from both FACS- and MACS-enriched Splenocytes

Bruker recommend the use of fresh cells on the Beacon instrument, although they were unable to provide data comparing use of fresh versus frozen mouse cells. Given the unknowns posed by using frozen cell samples for mAb discovery on a Beacon, the Edinburgh-based pipeline was first tested using fresh splenocyte samples from animals immunised on-site with purified gBect protein (***Figure 4.5-3A***). These pilot runs sought to:

1) Investigate two methods for the removal of red blood cells from a bulk splenocyte population. Chemical lysis using Ammonium-Chloride-Potassium (ACK) lysis buffer was compared to density gradient centrifugation using Histopaque-1083.

2) Compare two methods of isolating ASCs from bulk splenocytes: a flow cytometry-based method that sorted for $CD138^{High}$ $B220^{Low}$ classical plasma cells and the MACS-based enrichment of $CD138^{+}$ cells.

3) Determine whether the biotinylated gBect-bead probes were functional on a Beacon by isolating singly penned cells secreting antibody reactive to the probe ('hits' hereon).

Ideally, upstream cell processing steps would yield approximately 1 $\times 10^5$ healthy ASCs with minimal RBC contamination, sufficient cells for two rounds of cell loading in case of erroneous importing in the first instance (most commonly the inadvertent import of air bubbles).

Prior to the first Beacon run, it was predicted that recovered numbers of healthy ASCs would likely be higher after RBC removal by ACK lysis, compared to density gradient centrifugation. Similarly, the MACS-based enrichment method was attempted before the FACS method on account of the fewer processing steps involved, gentler treatment of cells and the shorter time between tissue harvest and chip loading. The first test on fresh mouse splenocytes yielded 4.2 $\times 10^5$ ASCs prior to loading and identified 30 gB-reactive hits. Whilst recovered ASC numbers exceeded the target value, later inspection of these

cells after loading onto an optofluidics chip revealed substantial cell clumping and a poor single-cell penning efficiency of ~40%.

Single-cell penning efficiency is an important metric for 'success' of an antibody discovery campaign on the Beacon. The total number of antigen-specific, single-cell hits is inherently limited by the 'sample size' of single cells being assayed. Higher single-cell penning efficiencies permit the screening of a greater number of cells, improving the chances of finding hits. Greater penning efficiencies therefore improve the number of hits isolated per chip, the significance of which is underlined by each chip's price. Efficiently penning *single* cells is particularly important when considering downstream antibody H- and L-chain amplification by RT-PCR. Isolating paired H/L-chains is predicated on having samples that only contain a single sequence for each.

An equivalent number of bulk splenocytes were subjected to density gradient centrifugation to understand whether this method better separated white cells from RBCs. After isolating the white cell layer, the sample was split into two for enrichment of ASCs by MACS and FACS. The two populations of ASCs were then loaded onto the same optofluidics chip, one after the other. This allowed for the two methods to be compared on a single optofluidics chip by assaying the cell populations simultaneously, whilst keeping track of which pens contained cells from each parent population.

Screening two differently enriched cell populations on a chip necessitates one population being loaded and penned before the other. Given this, it was important to ensure there were enough empty pens remaining on the chip after the first loaded population to allow for a 'pseudo-independent' loading of the second sample. Each cell population's penning was therefore limited to a maximum pen number of 7000, 35% the chip's total, so that even for the second round of penning, available pens were at a two-fold excess.

The removal of RBCs by density gradient centrifugation detrimentally affected recovery of ASCs overall compared to the ACK lysis method (***Figure 4.5-3B***), yielding approximately 4-fold fewer ASCs at the point of chip loading. From the same starting population of white cells, the MACS process showed greater recovery of ASCs than FACS-

enriched cells (***Figure 4.5-3B***), however the latter were penned on the chip with comparable efficiency despite this (***Figure 4.5-3C***). The FACS-enriched population also yielded a greater number of penned IgG secreting cells and gB-reactive IgG secretors compared to the MACS process (***Figure 4.5-3D***).

These data indicated that the FACS enrichment method marginally outperformed the MACS protocol with respect to penning and hit rates but yielded fewer ASCs overall. On inspection of the chip after loading, both populations showed less RBC contamination than the ACK-lysed population tested previously (***Figure 4.5-3E-G***), although at considerable expense to total ASC recovery numbers.

In general, all combinations of RBC removal and ASC enrichment methods tested proved successful in isolating some gBect-reactive hits, but it appeared that further optimisation may increase efficiency of hit isolation.

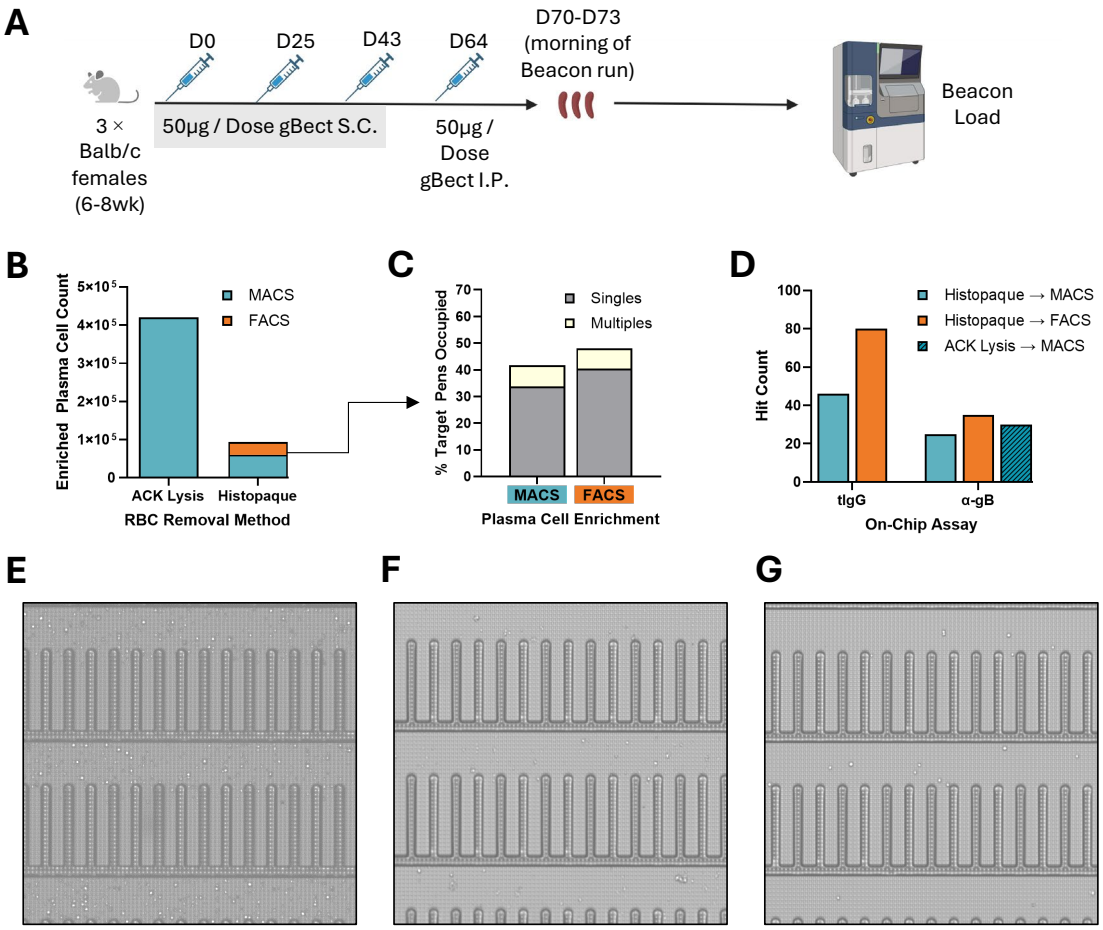


Figure 4.5-3: Beacon runs on fresh mouse splenocytes.

(A) Immunisation regimen for the generation of gB-reactive plasma cells used in fresh sample Beacon campaigns. Female balb/c mice were administered 3 doses of gBect protein subcutaneously (S.C.) before a final dose given intraperitoneally (I.P.) the week before spleens were harvested. Schematic created using BioRender.com.

(B) Total numbers of plasma cells isolated from a single mouse spleen after the removal of red blood cells by ACK lysis or Histopaque gradient density centrifugation. Colours represent the plasma cell enrichment method used. For the Histopaque-treated sample, splenocytes isolated from a single animal were split into two before each half was subjected to a plasma cell enrichment method.

(C) Penning efficiencies of single and multiple cells for plasma cell populations isolated by Histopaque gradient density centrifugation, followed by MACS (blue) or FACS (orange) enrichment. MACS- and FACS-enriched populations were loaded and penned sequentially on the same optofluidics chip. Penning of each population was limited to a maximum of 7000 pens of the 20000 available to permit penning of both samples. 100% pen occupancy therefore represents 7000 pens.

(D) Total number of pens containing an IgG secreting cell (tIgG) or an anti-gB IgG secreting cell (α-gB) as measured using IgG capture beads (Bruker) and custom gBect beads, respectively. Bars represent assay readouts for the populations penned in (B), enriched by MACS (blue) or FACS (orange). For comparison, the gB hit count for the ACK-lysed cell sample is also included (blue, hashed)

(E) Representative light microscopy image of plasma cells enriched by MACS after ACK lysis. Pens are ~3nm tall. RBCs appear as 'messy' grey particles in the reservoirs.

(F) Representative light microscopy image of plasma cells enriched by MACS after Histopaque gradient density centrifugation.

(G) Representative light microscopy image of plasma cells enriched by FACS after Histopaque gradient density centrifugation.

4.5.3 FACS and MACS Plasma Cell Enrichment Methods Isolate Subtly Different Cell Populations to Capture IgG-Secreting Cells

The slightly increased penning efficiency of the FACS-enriched cells presented above does not explain the increased total IgG (tIgG) and anti-gB (α-gB) hit numbers isolated compared to those of the MACS-enriched cells (***Figure 4.5-3D***): improving the total number of penned ASCs by 8% is unlikely to produce a ~two-fold increase to tIgG hits.

Two explanations for this as-yet unexplained advantage were considered. First, the resulting improvements to tIgG and α-gBect hit recoveries may be the result of greater cell viability of the imported cell population. Provided dying or recently dead ASCs remain structurally intact, penning efficiencies may not accurately predict the number of IgG-secreting cells given that the proportion of these cells healthy enough to secrete antibody may differ. Given that both the MACS- and FACS-enriched populations were >90% viable immediately prior to loading onto the chip, there was little evidence to support this, however.

A second possible explanation lies in the difference between the two cell populations isolated by each method. Whilst the MACS protocol recommended by Bruker isolates $CD138^{+}$ cells from bulk splenocytes, a marker that is also expressed on a range of precursor B cells (Wilmore *et al*, 2017; Nutt *et al*, 2015), the gating strategy used for FACS more stringently captures mature plasma cells characterized by a $CD138^{High}$ $B220^{Low}$ phenotype (Wilmore *et al*, 2017; Nutt *et al*, 2015; Wang *et al*, 2016).

To test this hypothesis, a flow cytometry-based assay was developed that could interrogate the differences between the two populations being enriched. A pool of splenocytes from mice immunised with the control antigen RH5 were first subjected to ACK lysis and frozen. After thawing, FACS was performed to isolate two populations: a $CD138^{High}$ $B220^{Low}$ population was sorted to replicate the FACS-based enrichment process tested in *Section 4.5.2* alongside a $CD138^{High}$ $B220^{High}$ population (***Figure 4.5-4A***). Whilst the $CD138^{High}$ $B220^{Low}$ cells would accurately represent the population enriched by FACS prior to Beacon loading, the combination of the two populations would approximate the $CD138^{+}$ cells enriched by the MACS process.

Sorted cells from the two populations were then screened by B cell ELISpot, staining for IgG (tIgG ELISpot hereon) to determine the proportion of IgG-secretors in each (***Figure 4.5-4A***). Whilst both populations contained IgG-secreting cells at a greater proportion than in unenriched splenocytes, the $CD138^{High}$ $B220^{Low}$ gating strategy better enriched for ASCs than a combined $CD138^{+}$ gate would (***Figure 4.5-4A***). Thus, the improved hit rate observed when screening FACS-enriched cells on the Beacon may be the result of a better-defined plasma cell/ASC population.

The $CD138^{+}$ MACS enrichment method used a plasma cell enrichment kit (Miltenyi: 130-092-530) in which steps that deplete non-plasma cells are omitted, as recommended by Bruker. The full MACS protocol was also investigated to determine whether it yielded a cell population that contained a higher population of IgG secretors. Using samples from the same frozen splenocyte pool as above, cells were subjected to either the full MACS protocol (enrichment and depletion steps) or just the enrichment steps. Samples of each population were then screened by tIgG ELISpot alongside the cell populations that would otherwise have been discarded at each step; that is, the retained fraction of the depletion step and the flow-through from the enrichment step.

As expected, the enrichment-only condition significantly increased the proportion of IgG-secreting cells when compared to the bulk splenocyte population. Surprisingly, however, the addition of a depletion step was worse overall than just enriching for $CD138^{+}$ cells (***Figure 4.5-4B***). Furthermore, taking the size of each population into account by reporting total IgG-secretor cell numbers in each population rather than as proportions, it became clear that both the enrichment and the depletion steps result in significant losses to IgG-secreting cell numbers (***Figure 4.5-4C***). Given these findings, there was little evidence to justify the inclusion of a depletion step should a MACS-based enrichment process be used upstream of future Beacon screens.

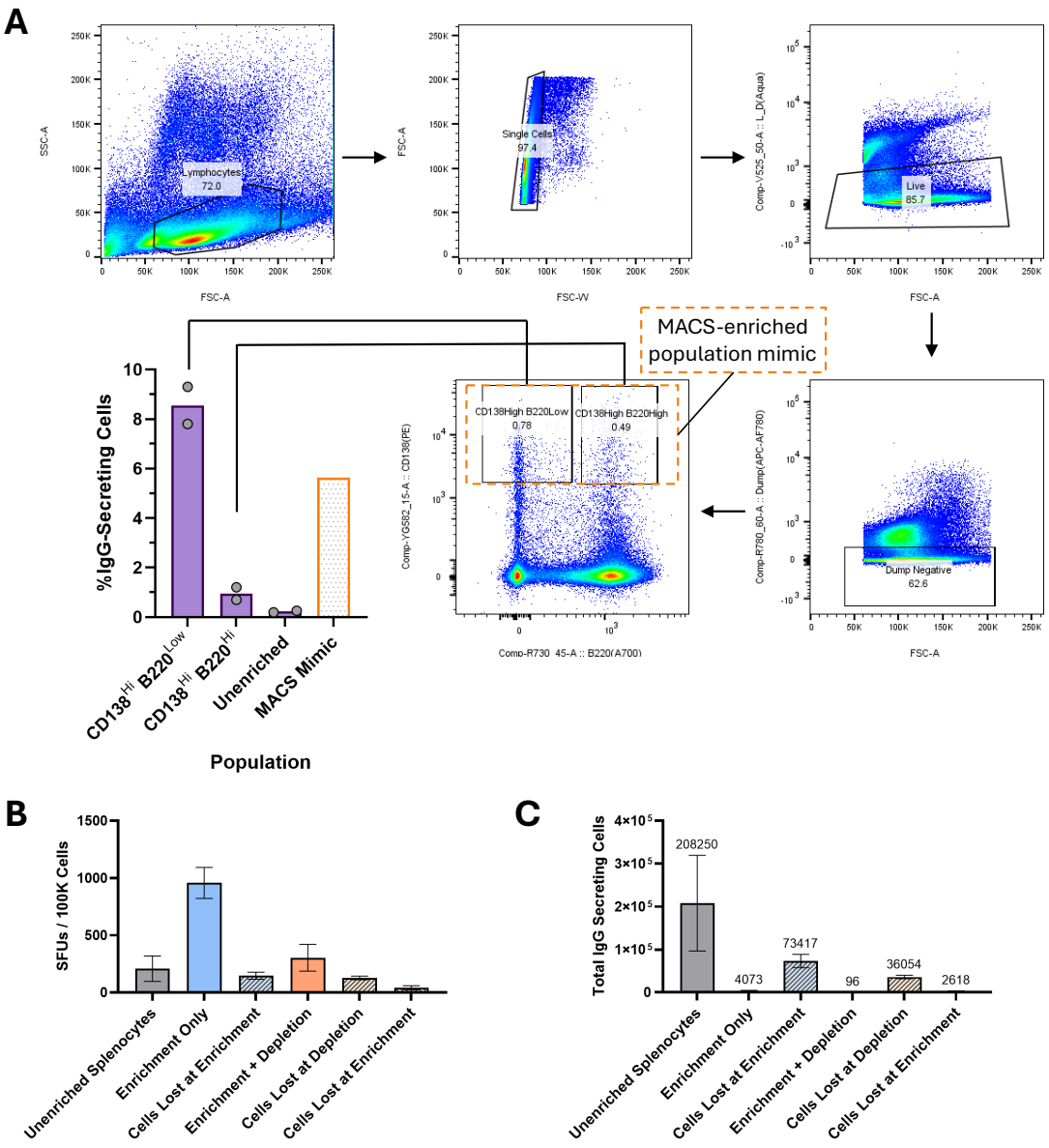


Figure 4.5-4: Antibody secreting cell numbers in different B cell populations.

(A) Flow cytometry gating strategy used for the isolation of two sorted populations, CD138^{Hi} B220^{Low} and CD138^{High} B220^{High}, from animals immunised with three 5µg doses of RH5 protein in AddaVax. The dotted orange box represents an approximation of the population enriched by the MACS protocol used upstream of the Beacon (CD138^{+} enrichment only). Total IgG-secreting cell numbers for both populations were determined by B cell ELISpot, alongside the parent, unenriched splenocyte population. By weighting the proportions of IgG-secreting cells in each of the two enriched populations by their respective sizes, an approximation of the responses in a MACS-enriched plasma cell sample was calculated ('MACS Mimic').

(B) Proportions of IgG-secreting cells, measured as spot forming units per 100,000 cells, for populations of splenocyte-derived cells collected at each stage of a MACS enrichment protocol. Unenriched splenocytes (grey bar) are included for comparison. Blue bars represent populations collected after performing CD138^{+} enrichment steps only. Orange bars represent those collected after performing non-plasma cell depletion and CD138^{+} enrichment steps. Hashed bars correspond to populations that would otherwise be discarded during plasma cell isolation protocols.

(C) IgG-secreting cell responses as in (B), scaled by each population's respective size. Number values represent the total number of IgG-secreting cells in each population.

4.5.4 Beacon Campaigns on Frozen Cell Samples Reveal MACS-Based Enrichment of Plasma Cells Out-Performs FACS Despite RBC Contamination

Early cell processing optimisation showed that the use of density gradient centrifugation followed by FACS enrichment of $CD138^{High}$ $B220^{Low}$ cells produced the cleanest ASC samples and thus resulted in better penning efficiencies and final hit numbers on the Beacon. When considering the efficiency of sample use, however, the removal of RBCs by gradient centrifugation performs significantly worse than the ACK lysis protocol, yielding a fraction of the number of isolated plasma cells. Although the number of plasma cells which are actually penned by the instrument is quite small (less than 20,000), the concentration of cells required for loading of the chip is very high (7×10^6/mL) and a volume of 15 µL is required. Each experiment thus requires ~100,000 isolated plasma cells, and substantial plasma cell losses would require the use of prohibitive (and potentially unethical) numbers of mouse spleens.

Given the intended goal of adapting this pipeline to using frozen cells, that are themselves likely to yield fewer healthy plasma cells than analogous fresh samples, it was decided that the benefits conveyed by the gradient density centrifugation in terms of sample cleanliness did not justify the inefficiency of cell recovery.

Frozen splenocytes used hereon were therefore subjected to ACK lysis prior to freezing. For the first tests, splenocyte samples were pooled from female C57BL/6 mice immunised with three doses of gBect administered with an AddaVax adjuvant (***Figure 4.5-5A***). The first campaign on frozen cells used the FACS enrichment method after recovering thawed cells at 37 °C for 1 hour. After isolating plasma cells, a sample was stained with trypan blue and counted immediately prior to loading. Though cells remained >90% viable up to this stage, it was immediately clear that the thawing and enrichment method chosen had detrimentally affected plasma cell functionality: only one IgG^+ penned cell was identified across the optofluidics chip (***Figure 4.5-5E***). Closer analysis of the fluorescence time course images also showed that most penned cells rapidly began to autofluoresce, further suggesting that plasma cells were dying, visualised in real-time on the chip.

Given that cells appeared healthy up until the point of cell penning, cell death was suspected to be being caused by events during penning. To pen cells by OEP, a voltage of ~5 V must be passed across the fluidics chip and as a result cells are exposed to an electric field for ~1 hour. Though this voltage appeared to be well tolerated by cells from fresh samples, it was suspected that combining the voltage exposure with the added fragility of recently-thawed cells might be resulting in cell death.

As the observed effect might result from the poorer membrane integrity of frozen and thawed cells, splenocytes were subsequently allowed to recover overnight at 37 °C in complete RPMI media before FACS (***Figure 4.5-5B***). From the same size of starting splenocyte population, overnight recovery marginally improved the total number of enriched plasma cells compared to the 1-hour recovery condition (***Figure 4.5-5C***). In addition, despite a poorer penning efficiency, recovery appeared to increase the number of IgG secreting cells, albeit still at a substantially lower frequency than observed for fresh cell samples (***Figure 4.5-5E***).

A high proportion of penned cells still showed rapid autofluorescence, despite the overnight recovery. I subsequently hypothesised that the combination of FACS and exposure to on-chip voltage may still affect cell health, and thus a third screen of frozen splenocytes was conducted, in which overnight recovery was followed by MACS enrichment. Despite the RBC contamination issue discussed earlier, which clearly affected cell penning compared to the FACS treatment (***Figure 4.5-5D***), MACS-enriched cells showed a lower propensity to autofluoresce on-chip and ultimately yielded more IgG- and anti-gB-secreting cells than either FACS campaign (***Figure 4.5-5E***).

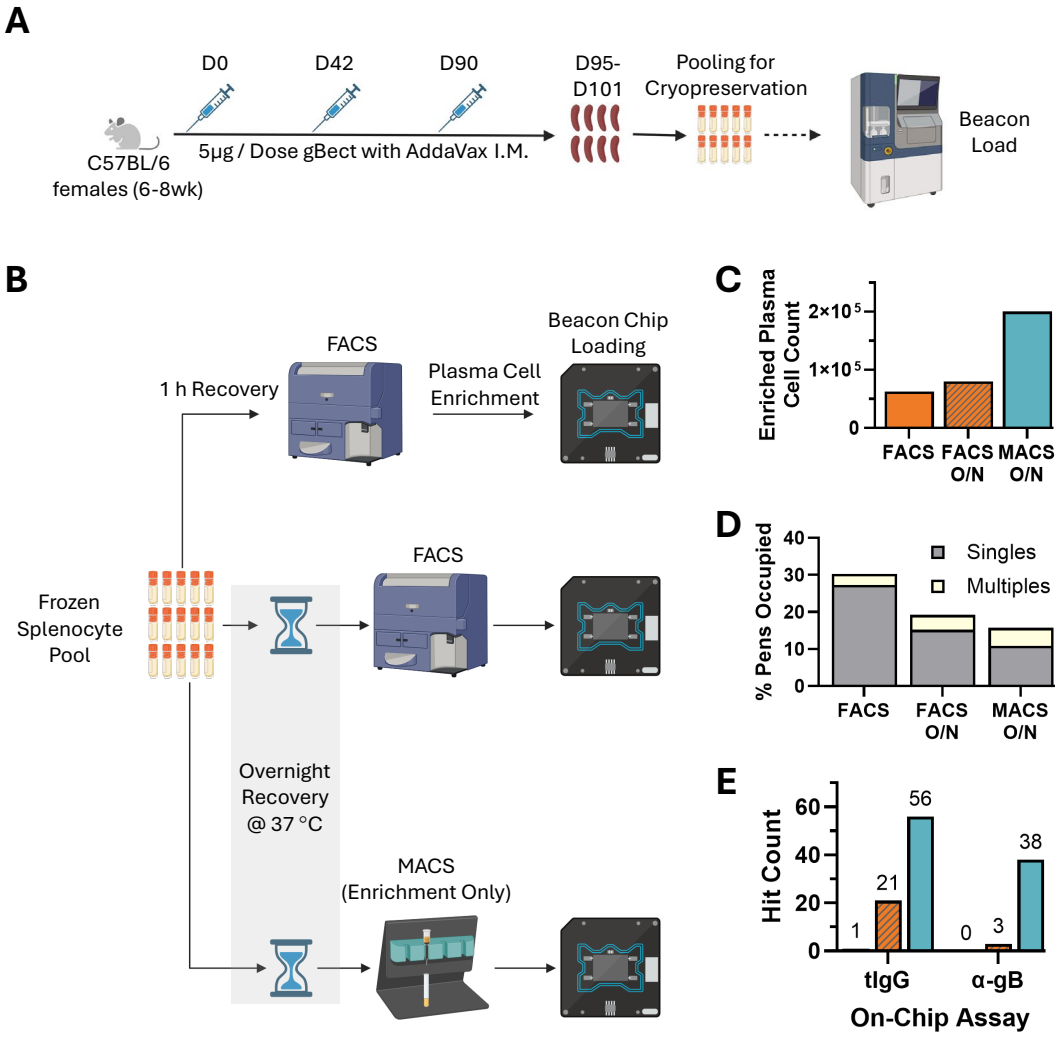


Figure 4.5-5: First Beacon screens on frozen splenocyte samples.

(A) Immunisation regimen for the generation of frozen gB-reactive plasma cell pools used on the Beacon. Female C57BL/6 mice were administered 3 doses of gBect protein in AddaVax adjuvant intramuscularly (I.M.) before culling 5-11 days after the final boost. Splenocytes were subjected to ACK lysis and pooled prior to freezing.

(B) Experimental design of the first three Beacon campaigns using frozen cell samples. Vials of the frozen splenocyte pool were thawed at 37 °C before recovering in complete RPMI media. Recovered samples were enriched by FACS or MACS, as indicated, and immediately loaded onto an optofluidics chip.

(C) Total number of live plasma cells enriched from 1 $\times 10^8$ splenocytes by FACS with 1 h recovery (FACS), FACS with overnight recovery (FACS O/N) or MACS with overnight recovery (MACS O/N), immediately prior to chip loading.

(D) Efficiencies of single-cell and multiple-cell penning for the plasma cell populations described in (C).

(E) Total number of pens containing IgG secreting cells and anti-gB IgG secreting cells for the cell populations treated by FACS (orange), FACS after overnight recovery (orange, hashed) and MACS (blue).

Schematics were created using BioRender.com.

It was therefore concluded that whilst MACS enrichment of plasma cells does not remove RBCs as efficiently as FACS, the gentler process provided a substantial health benefit when screening cells from frozen samples. Subsequent frozen cell campaigns were performed with MACS enrichment.

4.5.5 An Added MACS Step Successfully Removes RBC Contaminants from Frozen Samples

Although ACK lysis is a commonly used and effective way of removing RBCs, some inevitably remain. The previous experiments had shown that enriching plasma cells by MACS fails to remove these residual RBCs, hindering the Beacon's ability to pen single cells. The mechanism by which RBCs impede the penning process is simply by overcrowding the chip reservoirs, such that the instrument is unable to identify single cells for penning that are suitably far apart from one another. Whilst one solution would be to load plasma cell samples at a lower density, this would come at the expense of loading fewer plasma cells overall and thus was not expected to improve the overall number of cells penned.

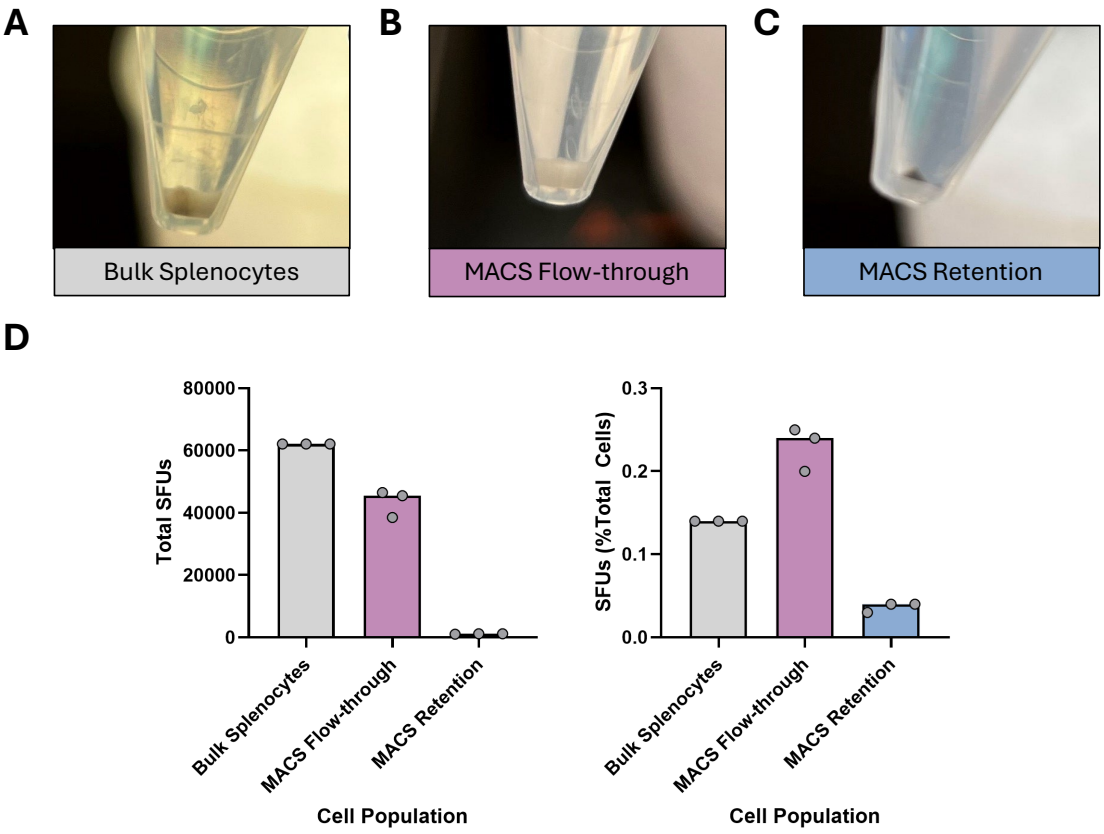
It was therefore imperative to identify a better method for removing RBCs from the frozen cell samples. Early fresh and frozen cell campaigns using MACS revealed that a seemingly minor population of RBCs observed in the bulk splenocyte population would ultimately outnumber enriched plasma cells in the pre-load sample as much as 12:1 (data not shown).

This suggested that the MACS process may inadvertently enrich for RBCs as well as plasma cells. Given that the only selection maker used, CD138 (Syndecan-1), is not expressed by RBCs (Motta *et al*, 2023), it seemed unlikely that this enrichment was marker-specific. On that basis, the possibility that RBCs were being enriched non-specifically by the magnetic column was considered. Whist no literature was identified that actively studied RBC enrichment by a magnet-based method, oxygenated haem groups within erythrocytes are weakly diamagnetic (Zborowski *et al*, 2003), warranting further investigation of this as the root cause.

A simple protocol modification was investigated to remove contaminant RBCs: by passing the bulk population of recovered splenocytes through a MACS column *prior to the staining of CD138$^+$ cells*, residual RBCs binding non-specifically to the magnet matrix could be removed before the pulldown of the target ASC population. To test this, a representative population of frozen splenocytes, harvested from mice immunised with RH5 was subjected to a MACS pulldown with no cell staining. On inspection of the cell pellets from centrifuged samples of bulk splenocytes, the MACS flow-through population and the retained fraction, the MACS column treatment appeared to markedly reduce the presence of RBCs in the flow-through population (***Figure 4.5-6A-C***).

Both the flow-through sample, theoretically containing the CD138$^+$ plasma cells, and the retained fraction, intended to contain RBCs, were then screened by tIgG ELISpot. The MACS treatment did result in the loss of some ASCs, likely from repeated centrifugation and wash steps, however most ASCs could be recovered from this fraction (***Figure 4.5-6D***). The cell population that bound non-specifically to the magnetic matrix of the MACS column did not contain many ASCs and so, by depleting the RBC population, the proportion of IgG secreting cells in the bulk cell population was greater than that of the bulk splenocyte comparator (***Figure 4.5-6D***).

The use of a 'dummy' MACS column to remove RBCs was therefore incorporated into the Beacon pipeline. Comparing the loaded population of plasma cells to previous populations enriched by MACS and FACS, the additional processing step greatly reduced RBC contamination relative to the original MACS protocol and did not produce as many cell clumps as were observed after FACS enrichment (***Figure 4.5-6E-G***).


A
B
C
Bulk Splenocytes
MACS Flow-through
MACS Retention
D
Total SFUs
80000
60000
40000
20000
0
Bulk Splenocytes
MACS Flow-through
MACS Retention
Cell Population
SFUs (%Total Cells)
0.3
0.2
0.1
0.0
Bulk Splenocytes
MACS Flow-through
MACS Retention
Cell Population

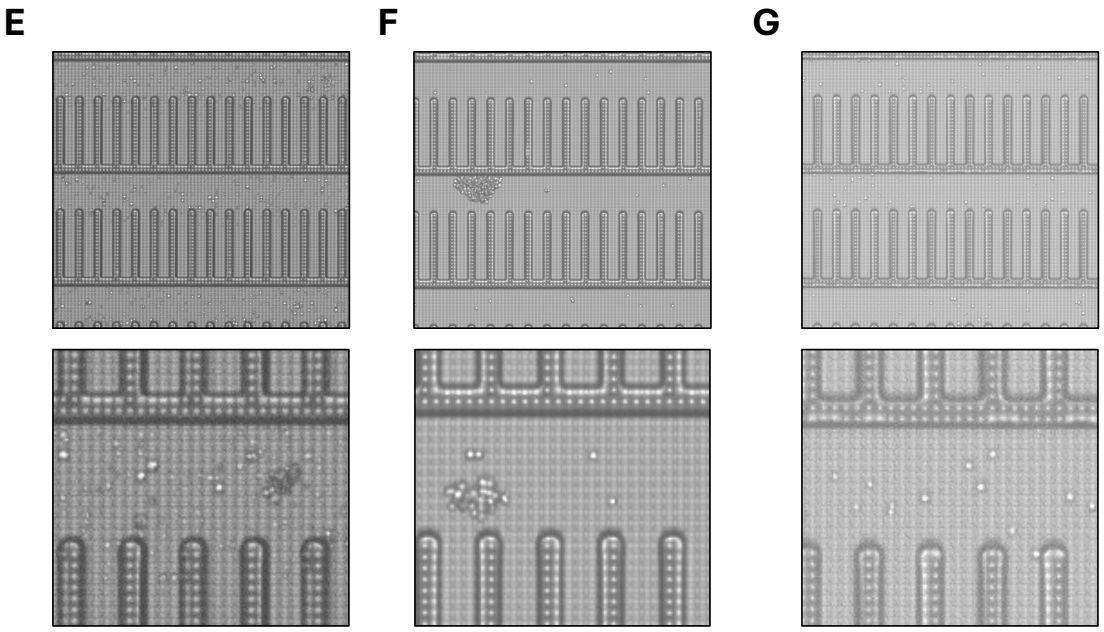

E
F
G

Figure 4.5-6: Red blood cell removal by an added MACS protocol step.

A) A cell pellet of bulk splenocytes derived from a pool of frozen cells isolated from mice immunised with three 5µg doses of RH5 in AddaVax adjuvant. Splenocyte pools were treated by ACK lysis prior to freezing.
B) The splenocyte cell pellet from (A) after passing the cell sample through a MACS MS column prior to any staining step.
C) The cell pellet of the fraction of the bulk splenocyte population in (A) retrained by the MACS MS column.
D) Total IgG ELISpot responses of the populations imaged in (A), (B) and (C), represented as the total number of IgG spot forming units in the population (left) and as a proportion of each population (right). Dots represent technical replicates performed for each cell sample. Bars represent the median of technical replicates.
E) Representative overhead light microscopy images of plasma cells isolated by MACS-based $CD138^{+}$ enrichment from frozen splenocytes pre-treated by ACK lysis. RBCs appear as 'messy' grey particles. Pens are ~3 nm tall.
F) Representative overhead light microscopy images of plasma cells isolated by FACS ($CD138^{High}$ $B220^{Low}$) from frozen splenocytes pre-treated with ACK lysis.
G) Representative overhead light microscopy images of plasma cells isolated by MACS-based $CD138^{+}$ enrichment after being passed through a MACS MS column to remove RBCs, prior to any staining step. Plasma cells were isolated from frozen splenocytes pre-treated with ACK lysis.

4.5.6 Bone Marrow Samples Pen More Efficiently than Splenocyte Samples, but Yield Fewer gB-Reactive Hits on the Beacon

The focus of the first six Beacon campaigns was to refine the methods used to isolate and screen plasma cells. Splenocyte samples used in these runs were isolated from animals immunised with gBect protein. Though this provided a source of gB-reactive plasma cells for the establishment of an effective discovery pipeline, the nature of the immunogen used makes these samples unsuitable for the discovery of pre-fusion conformation-specific antibodies.

To address this, female C57BL/6 mice were immunised with viral-vectored vaccines encoding the full-length gBmutK antigen. By this delivery method, it was hypothesised that the antigen may adopt the pre-fusion conformation given its expression in the context of a membrane *in vivo*. Animals were immunised intramuscularly with two doses of a ChAdOx2-vectored gB vaccine before being boosted once with a modified vaccinia Ankara (MVA)-vectored vaccine administered either intramuscularly (I.M.) or intravenously (I.V.) (***Figure 4.5-7A***).

Splenocyte and bone marrow samples were isolated and pooled across mice immunised by the same regimen and their total IgG and anti-gB responses measured by B cell ELISpot. With respect to both readouts, splenocyte pools yielded comparable responses

to those of a pool isolated from mice immunised with three doses of gBect in AddaVax, equivalent to tissues used in the original Beacon campaigns (***Figure 4.5-7B***). However, I.V. administration of the MVA booster raised substantially higher bone marrow tIgG and anti-gB responses than either the I.M. boosted mice or those given a protein immunogen (***Figure 4.5-7B***).

Bone marrow and splenocyte cell samples were ultimately pooled by tissue across both the I.M- and I.V.-boosted groups to produce 'pooled pools' large enough to use in Beacon campaigns. Given that pooled pools were a 1:1 mixture of cells from each group, it was expected that Beacon readouts using these cells would represent the 'average' responses across the two boosted groups (***Figure 4.5-7B***). However, testing the bone marrow pooled pool revealed a far lower proportion of gB-reactive IgG-secreting cells than anticipated (***Figure 4.5-7C***). Though it is unclear why such a disparity between the ELISpot and Beacon readouts was observed in bone marrow responses, the success of mAb discovery campaigns is determined by how many gB-reactive hits are observed on the Beacon. Subsequent campaigns were therefore conducted with the splenocyte pooled pools that yielded 3 times more gB-reactive hits (***Figure 4.5-7C***) than the bone marrow sample, despite a 20% lower overall penning efficiency.

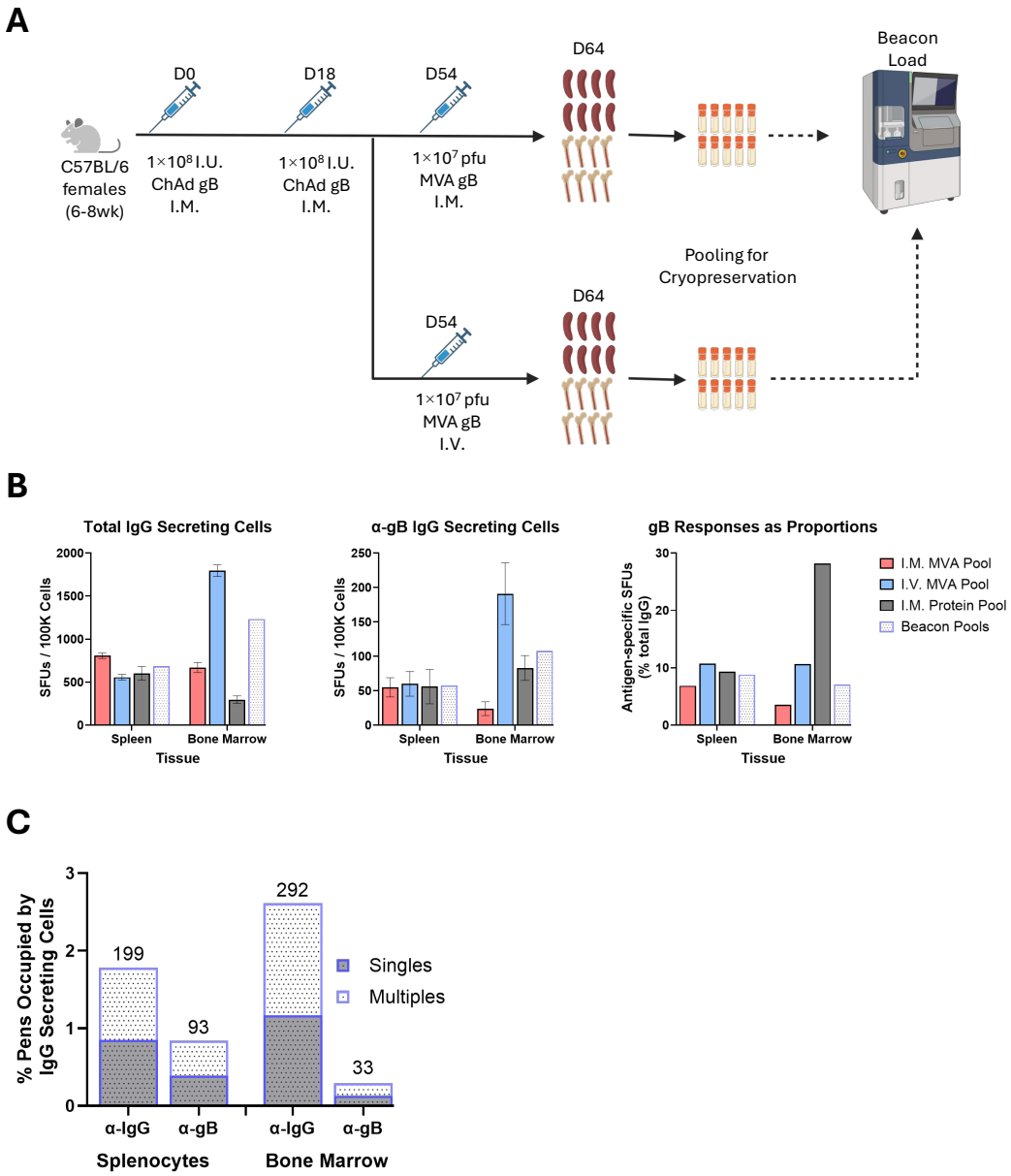


Figure 4.5-7: Beacon screens on spleen and bone marrow tissues.

(A) Immunisation regimen for the generation of frozen gB-reactive plasma cell pools used on the Beacon. Female C57BL/6 mice were administered two doses of a ChAdOx2-vectored full-length gB vaccine, administered intramuscularly (I.M.), before boosting with a modified vaccinia Ankara (MVA)-vectored full-length gB vaccine, administered I.M. or intravenously (I.V.). Animals were culled 10 days after the final boost at which point spleen and bone marrow samples were collected and separately pooled across animals of the same immunisation regimen. Schematic created with BioRender.com.

(B) Total IgG-secreting and anti-gB IgG-secreting cell responses of spleen and bone marrow pools from animals immunised by the regimens in (A), as well as a comparison group immunised with three 5 µg doses of gBect protein with an AddaVax adjuvant, administered I.M.. Bars represent the mean of three technical replicates. Error bars represent the standard deviation across technical replicates. The estimated responses of 'pooled pool' samples, produced by combining cells from the I.M. and I.V. MVA pools in a 1:1 ratio, are also shown as they represent approximate responses of samples loaded on the Beacon ('Beacon Pools').

(C) On-chip hits identified using IgG capture beads (Bruker) and gBect beads for pooled pool splenocyte and bone marrow samples derived from viral vectored gB-immunised animals.

4.5.7 The 'Live B Cell Penning' Algorithm is Less Efficient than 'Pen Plasma Cells' but can be Supplemented by Performing an Extra Round of Penning

Cells are imported into pens using proprietary 'penning algorithms'. The details of these algorithms are unclear, in part because they are not made public by Bruker, but also because of their reliance on machine learning tools for their refinement.

Discussions with Bruker did not offer a clear answer as to which of the two B cell penning algorithms implemented by the Beacon, 'Live B Cell Penning' and 'Pen Plasma Cells', was superior. As a result, a comparison experiment was conducted using the original splenocyte pool from animals immunised with gBect protein (***Figure 4.5-5A***). After MACS-based enrichment and loading, the two penning algorithms were used to pen cells across different halves of an optofluidics chip. The Pen Plasma Cells algorithm was able to pen more single cells over than Live B Cell penning, despite a poorer selectivity for penning single cells over multiples (***Figure 4.5-8***).

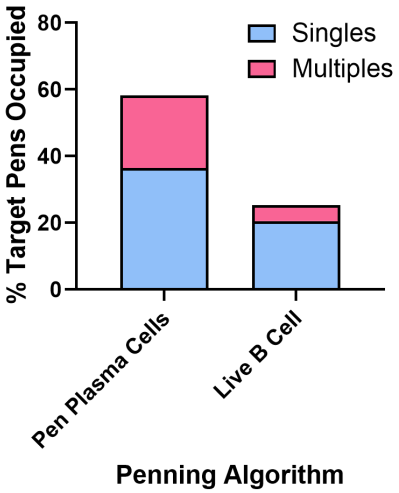


Figure 4.5-8: Comparing antibody secreting cell penning algorithms.
Penning efficiencies of enriched plasma cells, isolated from animals immunised with three 5 µg doses of gBect with an AddaVax adjuvant by ACK lysis and MACS. After loading the plasma cell sample onto the chip, fields of view (FoVs) 0-13 were penned using the Pen Plasma Cells algorithm, whilst FOVs 14-27 were penned using the Live B Cell algorithm. Bars represent the proportion of available pens (½ chip) successfully filled with a single cell or multiple cells for each algorithm.

Beacon campaigns were largely performed using the Pen Plasma Cells algorithm. However, it was subsequently communicated by Bruker that this algorithm is poorly implemented on the larger 20,000-pen (20K) chip compared to the 11,000-pen (11K) version: pens on the margins of the chip are inaccessible due to configuration differences. Use of a 20K chip for a final Beacon campaign on frozen splenocyte samples that integrated all the method improvements described above was therefore performed using the Live B Cell penning algorithm.

To minimise the effect of its seemingly poorer efficiency, two rounds of penning were performed, increasing the number pens successfully loaded with a single cell from 54% to 68%. It should be noted that this first-round penning efficiency is substantially higher than previous runs using this algorithm (***Figure 4.5-8***). This is likely the result of increasing familiarity with the entire experimental pipeline between the initial algorithm comparison and later runs, streamlining the process.

4.5.8 Integrating Method Improvements to Screen for Conformationally-specific Anti-gB mAbs Identifies >200 Single Cell Hits

The improvements made across the Beacon campaigns sought to address the added challenges posed by using frozen cell samples (***Figure 4.5-9A***), and hence to greatly enhance the utility of the Beacon instrument for investigators working at sites remote from the Edinburgh facility.

The 'success' of each campaign can be summarised by two key metrics:

1) The percentage of pens on a chip successfully penned with a single cell. Described briefly in *Section 4.5.2*, this reflects the ability to isolate a clean population of intact plasma cells and ultimately determines the 'sample size' of the gB reactivity assays; the more single cells penned, the more cells can be screened for a phenotype of interest.

2) The percentage of pens on the chip which contain a single cell capable of producing an IgG reactive to a gB probe. This is a product of both the ability to pen cells efficiently and the antigen-specific reactivity of the cell sample used.

Mapping these data across the Beacon campaigns performed highlights the additional challenge posed by working with frozen cells, as well as the effects of the method improvements implemented (***Figure 4.5-9B***). Incorporating the MACS-based RBC removal step resulted in the single largest increase to the penning efficiency of any campaign on splenocyte-derived plasma cells. By the sixth attempt using frozen cell samples, an overall penning efficiency of 80.6% (68.6% single cells) was achieved, matching target figures recommended by Bruker for fresh sample campaigns.

Across the ten campaigns performed, approximately 260 single cell, gB-specific hits were successfully identified and exported, with 212 of those from the final three splenocyte runs (which used splenocytes from animals immunised with the viral-vectored full length gB). Of these, 95 were reactive to gB ectodomain, 154 were reactive to both ectodomain and gB-expressing CHO cells, and 11 hits were identified as being singly reactive to the CHO cell reporter.

A

Use of fresh samples on the Beacon works but is impractical.
✓ Use frozen samples.

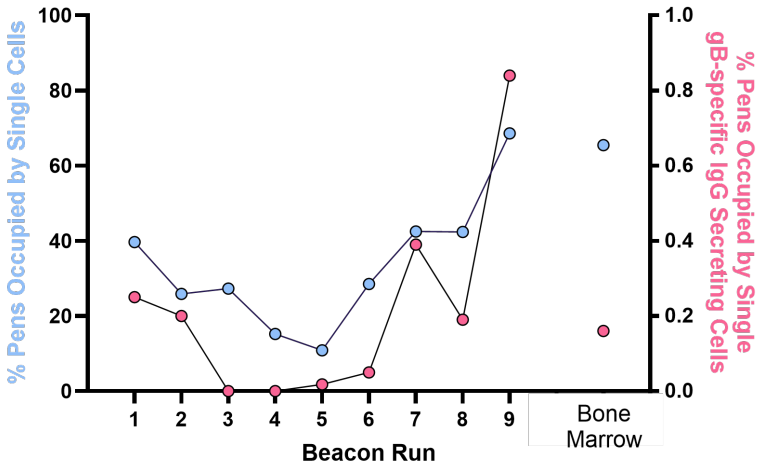
Enriching frozen samples by FACS results in cell death.
✓ Enrich plasma cells by MACS.

The MACS method inadvertently enriches for RBCs.
✓ Introduce an additional processing step to remove RBCs prior to ASC enrichment.

Splenocytes and bone marrow samples contain gB-reactive ASCs.
✓ Using a Beacon-based readout for gB hit discovery rates, splenocytes outperform bone marrow samples.

The 'Pen Plasma Cells' algorithm pens ASCs more efficiently than the 'Live B cell penning' but is poorly implemented on 20K chips.
✓ Perform two rounds of penning with the Live B cell penning algorithm.

B



gB Immunogen(s)	P	P	P	P	P	P	V	V	V	V
Enrichment Method	M	B	F	F	M	M	M	M	M	M
Penning Algorithm	LB	PP	PP	LB/PP	PP	PP	PP	PP	LB	PP
Chip Size	11	20	20	11	11	11	11	11	20	11
Rounds of Penning	1	1	1	1	1	1	1	1	2	1
Frozen Samples			×	×	×	×	×	×	×	×
RBC Removal									×	

Figure 4.5-9: Refinement of the Beacon-based antibody discovery pipeline.

(A) Flowchart of the methodological challenges encountered during adaptation of a Beacon-based mAb discovery pipeline to use of frozen cells and implemented solutions.

(B) Global summary of the Beacon campaigns conducted in this research tracking two metrics: single-cell penning efficiency (blue), and the number of single-cell gB-reactive hits isolated in each run, represented as a percentage of total number of pens to account for differing chip sizes (pink). Parameters of each Beacon run are tabulated below including:

- gB immunogen(s): P = protein in adjuvant, V = viral-vectored.
- Plasma Cell enrichment method: M = MACS $CD138^{+}$ enrichment, F = FACS $CD138^{High}$ $B220^{Low}$ enrichment, B = both MACS and FACS on one chip.
- Penning algorithm: LB = Live B Cell Penning, PP = Pen Plasma Cells.
- Optofluidics chip size (1000s of pens).
- Rounds of cell penning.
- Use of fresh or frozen cell samples.
- Inclusion of the MACS-based RBC removal step.

4.5.9 A Published RT-PCR Protocol Recovers Paired H/L-Chains from Single-Cell Hits with Greater Efficiency than the Beacon Method

The single plasma cells secreting IgG reactive to either or both gB probes would ultimately be subjected to reverse transcription PCR to isolate paired H- and L-chain sequences. However, an initial test of the RT-PCR reagents and protocol supplied by Bruker failed to efficiently amplify paired chains. H-chain sequences were only amplified from 5 of 40 hits exported from the Beacon (isolated in Beacon runs 1 - 3, data not shown).

Given the precious nature of the single-cell samples exported from the Beacon campaigns, the method recommended by Bruker was compared to a previously published protocol from the laboratory of Michel Nussenzweig ('Nussenzweig protocol' hereon) (Von Boehmer *et al*, 2016). Differences between the protocols are highlighted graphically (***Figure 4.5-10***).

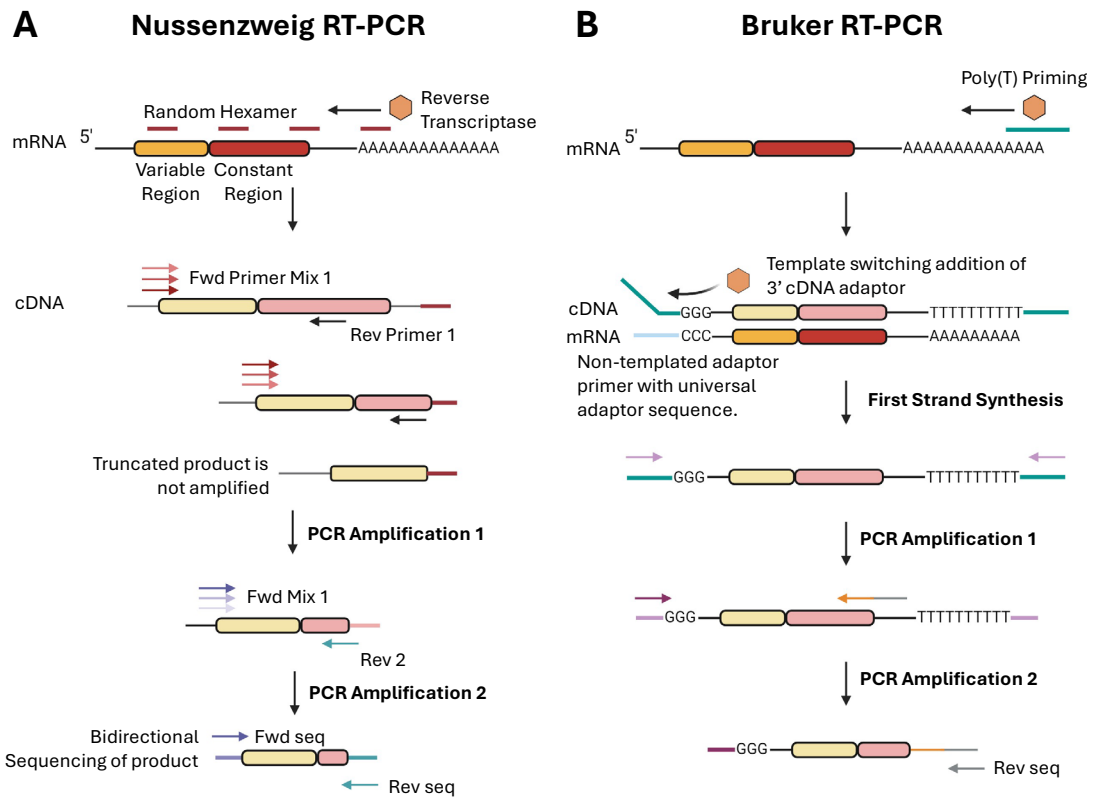


Figure 4.5-10: Comparison of reverse transcription PCR methods.

(A) Schematic representation of the Nussenzweig reverse transcription PCR (RT-PCR) protocol *(Von Boehmer* et al*, 2016)*. The reverse transcriptase step is primed using random hexamers capable of binding anywhere on the heavy (H) or light (L) chain mRNA transcript. After synthesis of the first cDNA strand, H- and L-chain sequences are amplified in separate PCR reactions using chain-specific primers sets. Sets are comprised of a single reverse primer that binds in the conserved constant region of the Ig chain and equimolar mixes of forward primers specific to different framework region 1 sequences that may be incorporated in any mouse IgG. Only cDNA templates spanning the framework and constant regions contain primer binding sites and are successfully amplified. A second chain-specific amplification, using similar primer sets nested internally to the first set, further amplifies H and L chain variable regions, which are ultimately sequenced bidirectionally.

(B) Schematic representation of the Bruker-supplied RT-PCR protocol. A poly(T) primer facilitates reverse transcription from the 3' of any polyadenylated transcript. At the 3' end of the nascent cDNA strand being synthesised the reverse transcriptase enzyme incorporates a non-templated tri-deoxyguanosine (GGG) handle. Addition of a second primer with a 3' CCC adaptor facilitates a template switching of the reverse transcription reaction: re-docking of the reverse transcriptase enzyme leads to an extension of the original cDNA molecule at the 3' end to incorporate a universal adaptor sequence. Subsequent PCR amplification of cDNA makes use of the universal primer binding sites incorporated at the 5' and 3' ends. Amplicons from the first PCR are then used to template separate H- and L-specific PCR reactions that make use of a reverse primer specific to the constant region of the Ig chain. Amplified H and L chains are sequenced in the reverse direction.

Schematics created with BioRender.com.

The two amplification strategies were tested on dummy export plates prepared by FACS-sorting CD138^{High} B220^{Low} cells isolated from mice immunised with three 5 µg doses of the protein RH5. Cells were sorted such that an approximate two-fold serial dilution from 100 to 1 cell per well was achieved (***Figure 4.5-11***). This design could therefore assess the ability of each method to successfully amplify IgG chains from samples with multiple copies of a H- or L-chain template, down to the single-cell level.

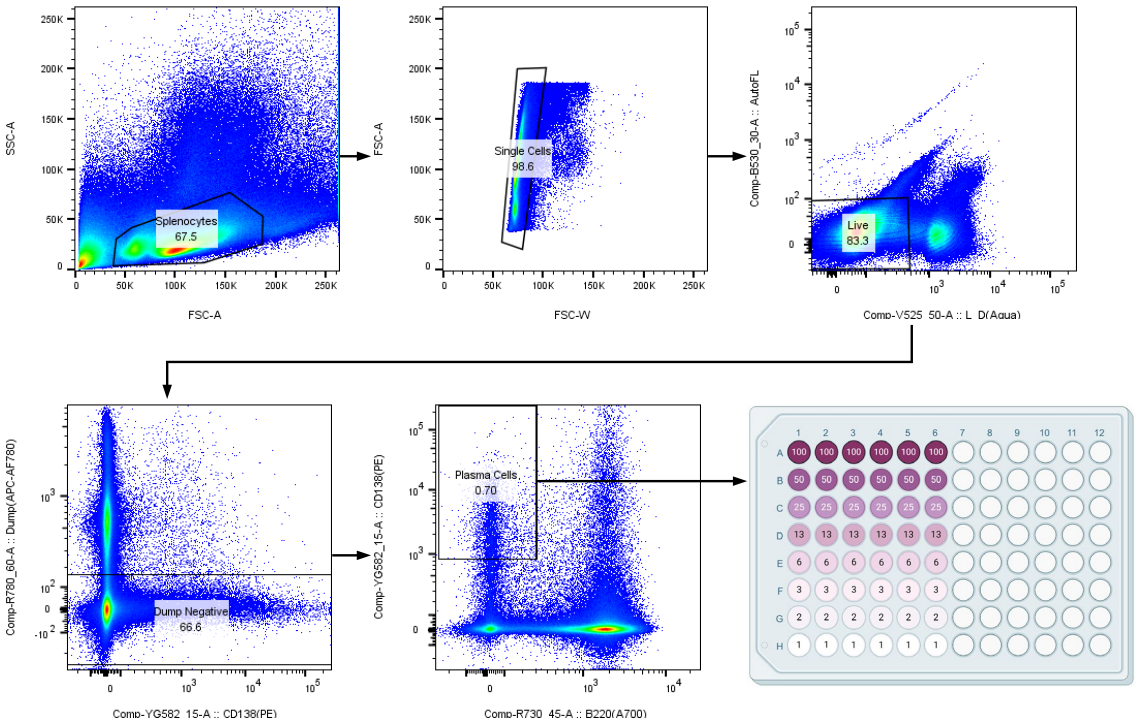
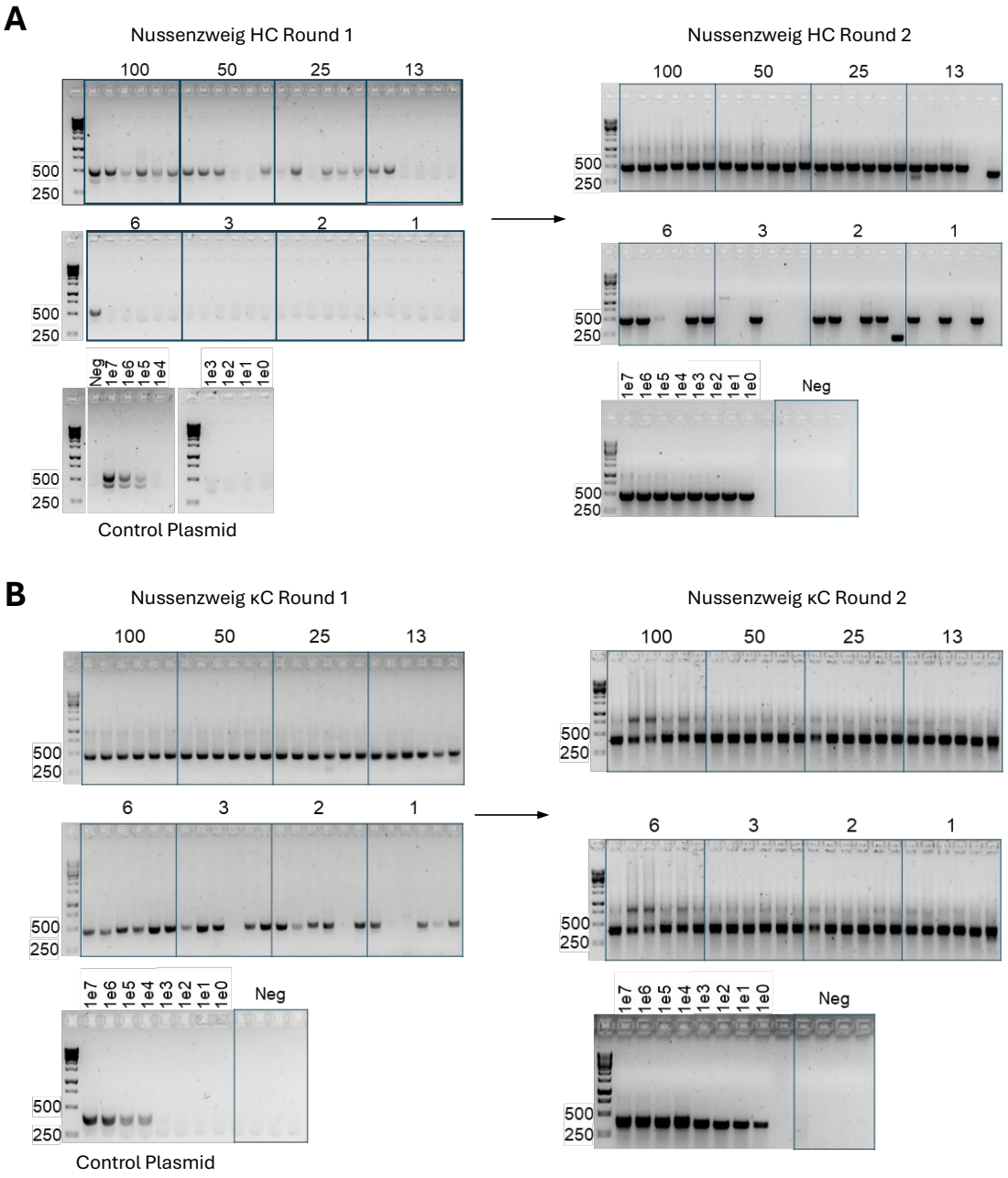


Figure 4.5-11: FACS-based generation of dummy Beacon export plates for RT-PCR optimisation. FACS gating for the isolation of plasma cells from bulk splenocytes harvested from animals immunised with three 5µg doses of RH5 protein in AddaVax adjuvant. Plasma cells were sorted into 96 well plates pre-filled with 4 µL of the lysis mix used for exporting plasma cells from the Beacon. Numbers in the wells of the plate graphic represent the number of plasma cells sorted into each well to generate an approximate 2-fold dilution series from 100 cells per well to a single cell.

Across both Heavy- and Light-chains, the Nussenzweig protocol was better able to amplify sequences than the Bruker protocol (***Figure 4.5-12***). As was observed with the initial test of the Bruker method, both methods showed better recovery of L-chains than H-chains. This finding is perhaps not surprising considering that ϰ and λ Light-chains may be expressed across different classes of immunoglobulin (Ig) (Charles A Janeway *et al*, 2001) and thus could be amplified from cells expressing any Ig class. For the H-chain amplification, however, primer sets are IgG-specific. Though this effect was observed across both protocols, it was more pronounced for the Bruker method (***Figure 4.5-12C***).

Subsequent RT-PCR amplifications were therefore conducted using the Nussenzweig method (Von Boehmer *et al*, 2016).



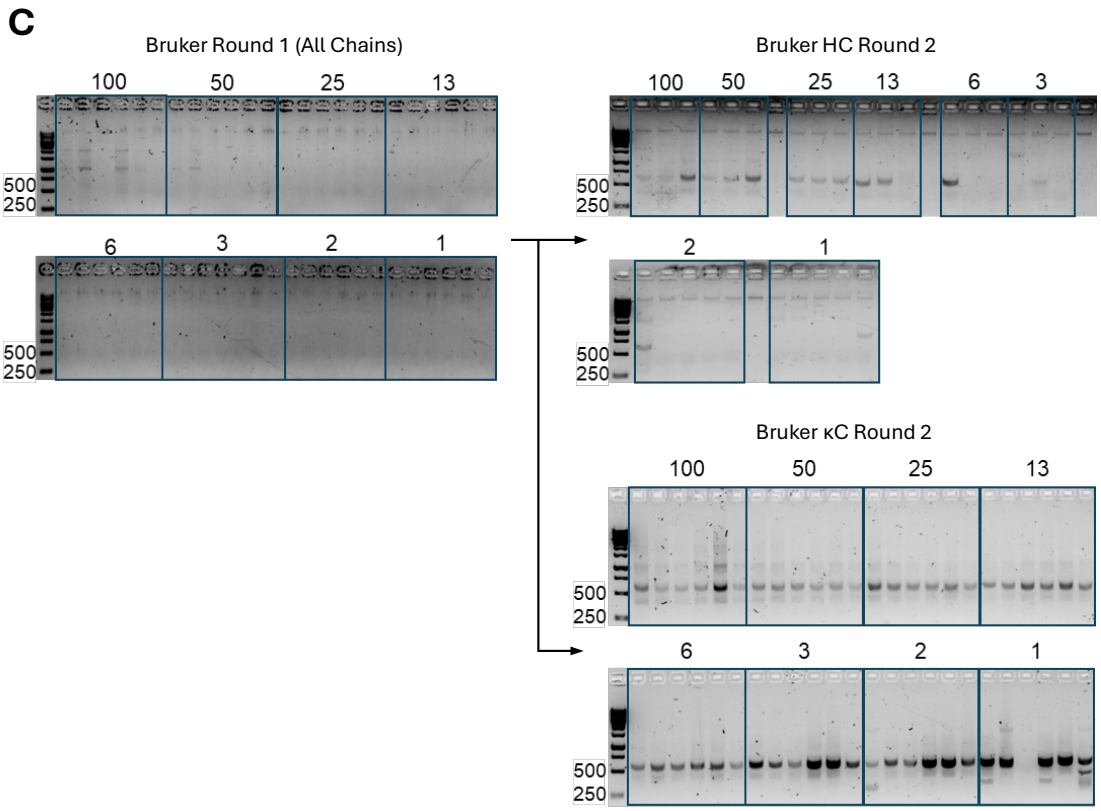


Figure 4.5-12: Comparison of mAb chain recovery rates after RT-PCR by two different methods.

(A) Agarose gel images of heavy chain PCR amplifications conducted on cDNA samples from dummy export plates after Reverse transcription (RT) using the Nussenzweig protocol *(Von Boehmer* et al*, 2016)*. Numbers above each gel lane correspond to the number of plasma cells sorted into the well of the dummy plate, on which the RT was performed. Gels represent amplified PCR products using the outer primer set of round 1 (left-hand gels) and the inner primer set of round 2 (right-hand gels). Heavy chain amplicons are expected to be ~550 bp and ~500 bp after the first and second rounds of amplification, respectively. Negative control wells represent full PCR reactions conducted without a cDNA template, using a sample of the first-round reaction mix as a mock template for the second round. Positive control samples represent PCR reactions conducted using a plasmid DNA template encoding the AMMO5 IgG heavy chain *(Snijder* et al*, 2018)*. Numbers above positive control wells represent the total copy number of each plasmid in the PCR reaction. As with the negative controls, a sample of the first-round reaction mix was used as template in the second round, mimicking the method used for real samples.

(B) Agarose gel images of κ-light chain PCR amplifications conducted on cDNA samples from the same dummy export plate as the heavy chain reactions. Gels represent PCR products after round 1 (left) and round 2 (right) PCRs, as for the heavy chain gels. κ-light chain amplicons are expected to be ~500bp and ~450bp after the first and second rounds of amplification, respectively. Negative controls are as for the heavy chain. Positive controls were designed in the same fashion as for the heavy chain, using a plasmid DNA template encoding the κ-light chain from a previously-published mAb against the rabies glycoprotein, 17C7 *(Sloan* et al*, 2007)*.

(C) Agarose gel images of PCR amplifications conducted on cDNA samples from dummy export plates after RT using the Bruker protocol. Numbers above each gel lane correspond to the number of plasma cells sorted into the well of the dummy plate, on which the RT was performed. Gels represent amplified PCR products using the universal primer set of round 1 (left) and the inner primer set of round 2, specific for the IgG heavy chain (top right) and the κ-light chain (bottom right). Due to the limited availability of heavy chain PCR reagents supplied by Bruker, heavy chain amplifications were performed on in triplicate for samples derived from 3 – 100 cells, and with 5 replicates for the 1- and 2-cell samples.

4.5.10 A Panel of 40 gB-Specific mAbs Show Diverse V/J Gene Usage with 3 mAbs Showing Preferential Binding to Recombinant gB Ectodomain

RT-PCR reactions were performed on a total of 239 gB-reactive, single-cell hits exported from the Beacon. From these reactions, paired H- and L-chain sequences were recovered for 115 cells, and 62 IgG monoclonal antibodies were successfully re-expressed (***Figure 4.5-13A***).

The purified mAbs were subjected to two gB binding assays to confirm their ability to recognise either one or both conformations of the antigen. An ELISA-based screen assessed binding to gBect, mimicking the bead-based Beacon probe for post-fusion binding (***Figure 4.5-13B***). A flow cytometry assay measured binding to membrane-expressed gB by staining gB-transfected Expi293F cells with each mAb separately (***Figure 4.5-13C***).

Three new mAbs (ECO12, ECO38 and ECO48) appeared to show conformational preference for the post-fusion form of gB evidenced by their deviation from the roughly linear relationship traced by the rest of the panel on an XY plot of ELISA and flow binding results (***Figure 4.5-13D***). Interestingly, a previously published antibody, 3A3, known to be capable of neutralising EBV infection of both B cells and epithelial cells *in vitro* (Zhang *et al*, 2022), displayed a similar binding pattern.

Despite successfully re-expressing five mAbs identified as only binding the cell-based gB probe on the Beacon, it was not possible to reproduce this conformational preference after their isolation and re-expression. When evaluated by ELISA and FACS, the mAbs isolated from cells that appeared singly positive on the Beacon either bound both cell-associated gB and the post-fusion ectodomain (2/5 mAbs) or neither form of the antigen (3/5 mAbs). Possible explanations for the disparity in behaviour on the Beacon and after re-expression are discussed further below.

The 40 mAbs successfully isolated against gB employed a diverse array of V/J gene pairings in their Heavy- and Light-chains (***Figure 4.5-13E***), as well as in their combinations of H and L V gene segments (***Figure 4.5-13F***). Using splenocyte samples

pooled from multiple animals is likely to have conveyed a benefit in this respect, with no two mAbs in the panel being clonally identical.

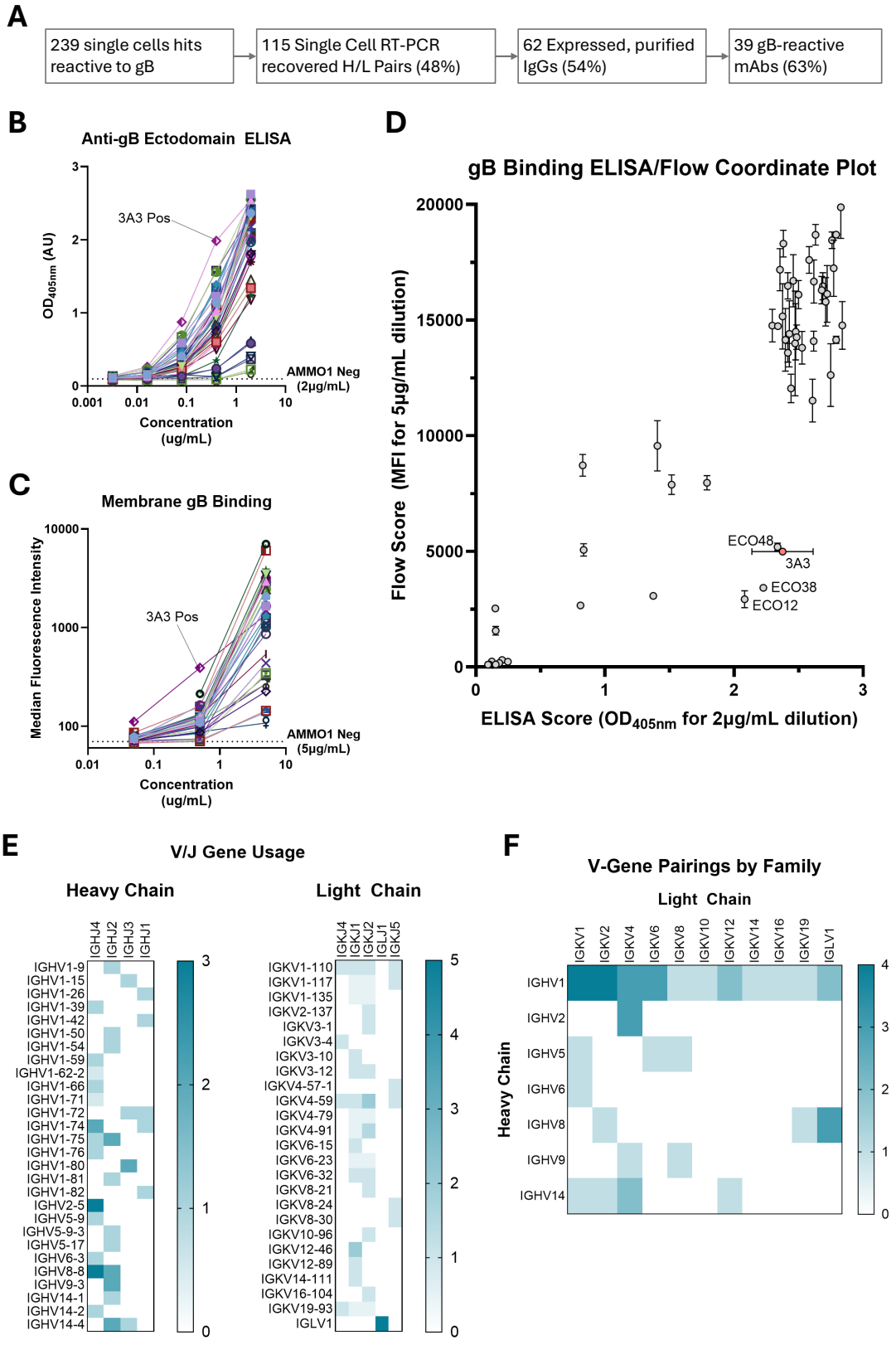


Figure 4.5-13: Anti-gB mAb sequence variability and antigen binding behaviour.

(A) Flowchart representing successful recovery rates at each stage of the mAb discovery pipeline downstream of exporting cells off the Beacon.

(B) ELISA readouts for each gB-reactive mAb successfully re-expressed downstream of the Beacon. Each mAb was used to detect gBect coated onto an ELISA plate as a primary stain, before detecting with an anti-human IgG secondary antibody conjugated to alkaline phosphatase. Each mAb was tested at 5 different concentrations. A previously-published anti-gB neutralising antibody, 3A3 was included as a positive control *(Zhang* et al*, 2022)*. AMMO1, a gH/gL-reactive mAb was tested at the highest concentration as a negative control for gB binding. Values represent the $OD_{405\,nm}$ readouts for each staining condition, averaged across two technical replicates.

(C) Flow cytometry-based readouts for each gB-reactive mAb tested in (B). Expi293F cells expressing gB on their cell surface membrane were stained with each mAb in the panel at three different concentrations. The ability to bind gB was measured by detecting the mAb primary stain with an anti-human IgG secondary antibody conjugated to AlexaFluor 647. As for the ELISA assay, 3A3 was included as a positive control, whilst AMMO1 was used as a measure of background staining. Values represent the median fluorescence intensity for each staining condition, averaged across two technical replicates.

(D) XY plot of each mAbs ELISA and flow assay readouts at the highest staining concentration. Values represent the average across two technical replicates. Error bars represent half of the range between technical replicates.

(E) Heavy and Light chain V- and J-gene fragment usage of the gB-reactive mAb panel.

Heatmaps were created using Geneious Biologics.

4.5.11 Human IgG-transgenic Mice Raise Antibody Responses to gB Vaccines, but Amplification of the Heavy-chain Sequences is Challenging

As explained in the chapter introduction (*Section 4.3*), the key reason for the use of mouse rather than human samples for the work in this chapter was that the Douglas group wished to develop a pipeline for isolating human-like mAbs from human IgG transgenic mice. Such a tool would be of significant value for early-stage research into new or challenging mAb targets unsuitable for isolation from human samples on the basis of safety, amongst other considerations.

That said, the clinical relevance of mouse-derived antibodies is limited by their inherent immunogenicity in humans (Lonberg, 2008), and human antibodies may also provide more relevant insights into the mechanistic basis of control of a pathogen by the human humoral immune response. To try and combine the practical benefits of mouse-based mAb discovery with the clinical suitability of identifying human-derived antibodies, use of a human IgG transgenic mouse line, OmniMouse (OmniAb), was investigated.

The OmniMouse transgenic model expresses a full repertoire of human V_H gene fragments and a majority of the human ϰ and λ Light-chain repertoire (***Figure 4.5-14A***), inserted

into the mouse genome by random integration. Though the V_H segment and the Light-chain are human, the Heavy-chain constant region is rat-derived (Osborn *et al*, 2013), resulting in a chimeric human-rat antibody (***Figure 4.5-14A***).

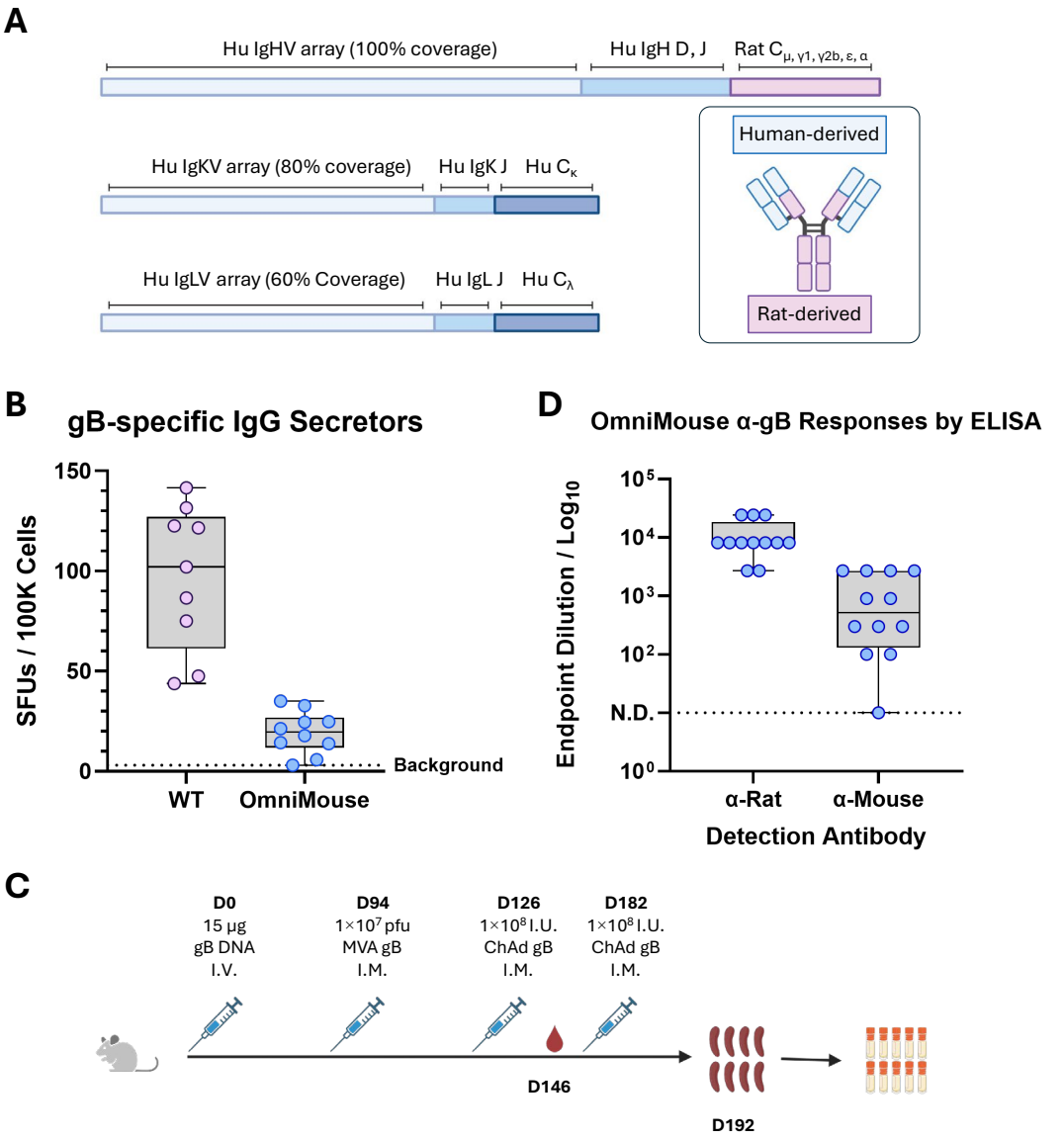


Figure 4.5-14: Investigating OmniMice as transgenic animals for human-like mAb isolation.

A) Schematic representation of the human heavy- and light-chain V(D)J repertoire encoded by the OmniMouse transgene. Sequences encoding the variable regions of the heavy and light chains are human-derived (blues), whilst constant region sequences are rat-derived (pink). A cartoon representation of an OmniMouse IgG antibody shows which regions of the antibody are derived from human or rat Ig sequences (box).

B) gB-specific ELISpot responses from WT (pink) and OmniMouse (blue) animals after immunising with three 5 µg doses of gBect protein in AddaVax adjuvant. As in (B), WT-derived IgG was detected using an anti-mouse IgG secondary antibody, whilst OmniMouse-derived IgG was detected using an anti-rat IgG secondary. Data points represent individual animal responses. Grey boxes display the inter-quartile range. Black lines represent the median response whilst bars represent the range. The background response (dotted line) was determined by plating samples in wells that were not coated with antigen and taking the highest SFU value of all samples tested to represent the upper limit of the non-specific response.

C) Regimen for 12 OmniMouse animals immunised with full-length gB DNA and viral-vectored immunogens. Serum samples taken 146 days post-prime were investigated for their anti-gB IgG responses by ELISA.
D) gB-specific IgG titres from 12 OmniMouse animals (blue points) after immunisation with plasmid DNA encoding full-length gB, administered intravenously, followed by boosting with MVA- and ChAdOx2-vectored full-length gB vaccines, given intramuscularly. Anti-gB titres for each OmniMouse were determined using the anti-rat and anti-mouse secondary antibodies used in (B) to stain for IgG encoding rat-derived or mouse-derived Fc regions, respectively. Grey boxes display the inter-quartile range. Black lines represent the median response whilst bars represent the range.

Two cohorts of OmniMouse animals were immunised with gB constructs. First, transgenic animals were given three doses of gBect administered with AddaVax (InvivoGen) by the same regimen used for immunisation of WT mice discussed earlier (***Figure 4.5-5A***). Importantly, whilst immunisation regimens and mouse strains were matched, the nature of the OmniMouse's rat-derived heavy constant region necessitated the use of different staining antibodies for the WT and transgenic mice: anti-mouse Fc and anti-rat Fc, respectively. Endpoint gB-specific responses measured by B cell ELISpot showed ~5-fold greater responses in WT animals than the transgenics (**Figure *4.5-14B***).

The endogenous mouse constant region locus is not silenced in the OmniMouse. As a result, it was suggested that a recombination event between the inserted rat sequence and the mouse locus may produce human-mouse chimeric antibodies, rather than human-rat ones. A second cohort of OmniMouse animals, immunised with a DNA and viral-vectored vaccines encoding full-length gB (***Figure 4.5-14C***), were investigated to determine whether antibodies expressed a mouse or rat Fc region. Performing an ELISA on serum samples taken after the third vaccination showed animals express antibodies detectable with a minimum-cross reactivity anti-mouse Fc secondary, but only at titres ~10-fold lower than those detectable with a minimally cross-reactive anti-rat secondary (***Figure 4.5-14D***).

The nature of the OmniMouse IgG construct(s) described above complicates the isolation of Heavy-chain sequences on account of the species-specific primer sets required for their amplification. Using a set of human/rat primers and protocol designed by OmniAb for this purpose, RT-PCR reactions were performed on dummy plates of OmniMouse-derived $CD138^{High}$ $B220^{Low}$ plasma cells sorted in a similar fashion to those described in *Section 4.5.9* (***Figure 4.5-11***). Though L-chain fragments could readily be amplified at

the single-cell level, amplification of H-chain fragments was unsuccessful. On the occasion where amplicons were visible, reaction products were too short to be real Heavy-chains (expected size ~750 bp) (***Figure 4.5-15***). Extensive troubleshooting involving the testing of multiple rat- and mouse-derived CH1 reverse primers, as well as the substitution of OmniAb-supplied primer sets into the Nussenzweig protocol (see *Section 4.4.12*) all proved to be unsuccessful (data not shown).

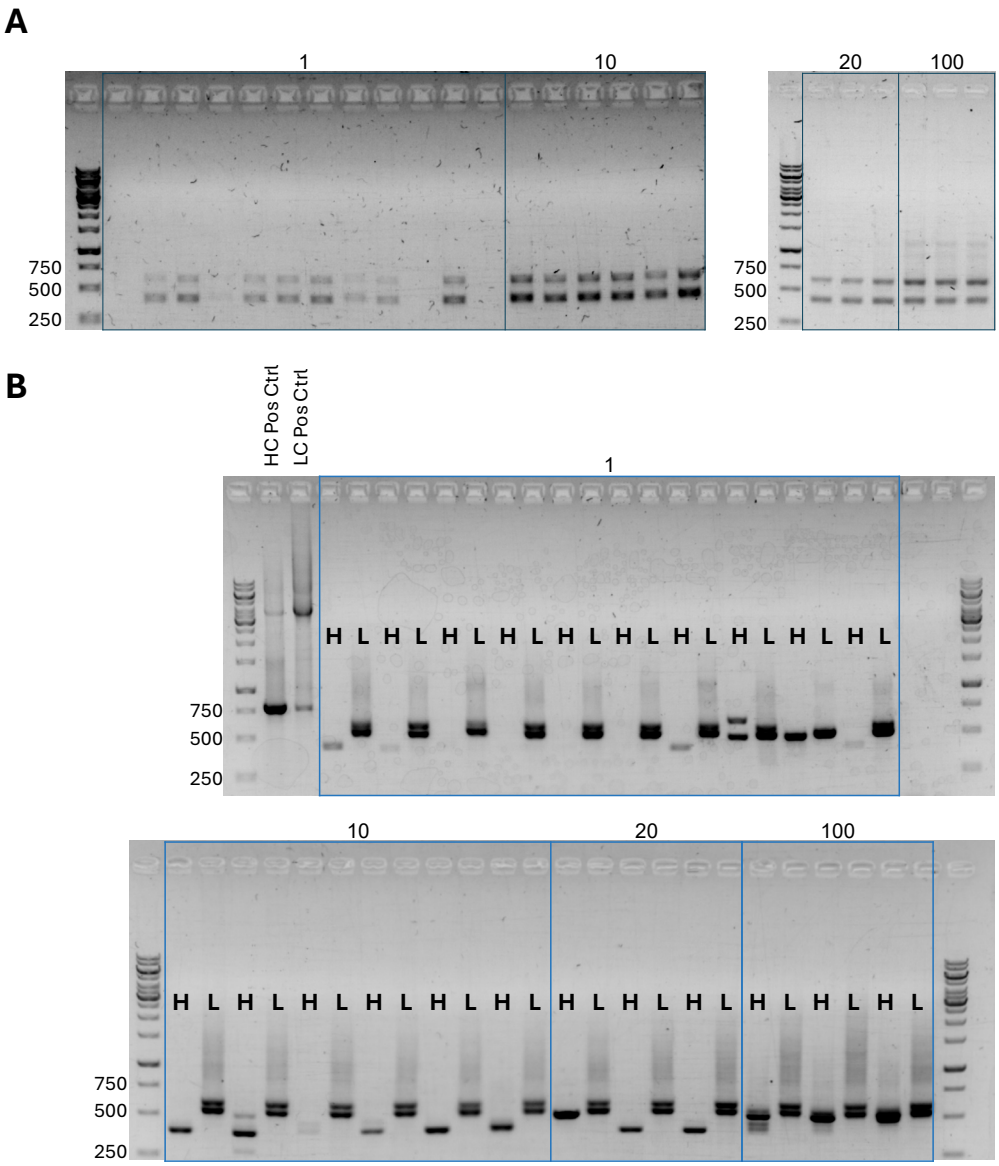


Figure 4.5-15: RT-PCR of OmniMouse antibody heavy- and light-chain sequences.

(A) 2% agarose gel electrophoresis images from first-round PCR reactions on OmniMouse-derived CD138^{High} B220^{Low} plasma cells sorted into dummy plates as in **Figure 4.5-11**. Numbers above each gel lane correspond to the number of plasma cells sorted into the well of the dummy plate, on which the RT was performed. PCR reactions were carried out using a protocol supplied by OmniAb. First-round heavy- and light-chain amplifications were conducted in a single reaction. Each lane in (A) therefore represents the products of the heavy and light chain reactions. Expected chain sizes are ~780 bp and ~610 bp for successfully amplified heavy and light chain sequences, respectively.

(B) 2% agarose gel electrophoresis images from second-round PCR reactions using reaction products from (A). Heavy- and κ Light-chain amplifications were conducted in separate reactions. Paired H- and L-chain products are loaded into consecutive lanes on the gel for each sample. Expected chain sizes are ~520 bp and ~510 bp for successfully amplified heavy and light chain sequences, respectively. Positive control conditions represent second-round H- and L-chain amplification reactions using plasmid DNA templates encoding complementary sequences to selected primers in the H- and L-chain amplification mixes, spaced 750 bp apart.

Given these challenges, work to adapt the Beacon pipeline to OmniMouse-derived mAb discovery was discontinued. Ultimately, the difficulties experienced here, which appeared specific to the Heavy-chain of the OmniMouse IgG molecules, strongly suggests the chimeric rat/human transgenic constructs were the cause. Further work using OmniMouse animals for antibody discovery therefore require better characterisation of the true nature of the IgG molecules these animals express, and the development of efficient new primer sets for H- and L-chain amplification.

4.6 Discussion

The work discussed in this chapter sought to develop a method for the isolation of mouse monoclonal antibodies against gB, an example of a classically hard-to-target antigen. The conformational instability of the antigen did not permit the use of standard mAb isolation techniques such as FACS-based isolation of antigen-specific B cells using tetrameric antigen probes. A Beacon-based pipeline was therefore adapted to identify mAbs that bound to one or both conformations of gB using two probes: a protein-on-bead post-fusion probe and a cell-based reporter expressing full-length gB in the context of a membrane.

After isolating a modest number of gB-reactive hits from fresh mouse splenocyte samples, efforts focused on adapting the method to the use of frozen cell samples. Probably as a result of their poorer viability compared to fresh cells, the use of frozen tissues required adding an overnight recovery step between thawing of the sample and loading it onto the instrument. In addition, the use of a FACS-based method for enriching plasma cells, which proved successful for fresh samples, was unusable on the grounds that FACS-enriched cells could be observed dying in real time on the optofluidics chip.

Upon reverting to a MACS-based plasma cell enrichment protocol, further method development was required to address the significant red blood cell contamination of plasma cells loaded onto the chip. Rectifying this by the addition of a MACS-based erythrocyte depletion step meant frozen plasma cells could efficiently be loaded onto a chip, penned and screened for antigen-reactivity without the viability issues observed for the FACS method.

Changes to the upstream and on-chip steps in the Beacon pipeline yielded clear improvements in the ability to detect gB-reactive hits across the campaigns. However, without robust head-to-head comparisons of each method modification, it is not possible to attribute effect sizes to any one change that was implemented. The nature of mAb discovery on the Beacon makes such experiments challenging. Whilst it could be argued that a 'gold standard' design would involve multiple Beacon runs, each on a fresh chip and changing only one parameter between otherwise-identical runs, even this design has important limitations. Given the innate variability in the density and distribution of cells and or/probes observed after loading, robust inter-chip comparisons would require significant replication to detect differences above the noise, at vast expense.

Considerable thought was put into possible designs for intra-chip comparisons that might avoid the inter-chip variability issues described above; however, these too are imperfect. Single-chip experiments suffer from the fact that the comparison step must necessarily be performed sequentially, rather than in parallel. Two examples considered here included investigating different penning algorithms and the on-chip performance of cells enriched by MACS or FACS. In both cases, loading cells onto the chip must be performed in two steps, one after the other, either to pen each population using a different algorithm, or simply because the populations themselves are different. Given that loaded cell populations are exposed to an on-chip voltage, which appears to affect viability, accounting for any effects on cell performance resulting from the different lengths of time each population spends on-chip is nontrivial.

These technical challenges, combined with the constraints imposed by the Beacon's cost of use, ultimately meant that methodological comparisons were performed pragmatically,

using the best experimental designs achievable at reasonable expense. Each Beacon campaign served not just as an optimisation experiment but simultaneously as an attempt to successfully isolate as many gB-reactive hits as possible. That said, the implementation of the method modifications ultimately improved the recovery of antigen-specific, single-cell hits from 0 in the first two campaigns on frozen cells to >150 in the final attempt.

Improvements to the mAb discovery pipeline were not limited to steps before and on the Beacon instrument. Performing RT-PCR amplifications of Heavy- and Light-chains on the single-cell hits exported form the Beacon ultimately showed that the method supplied by Bruker failed to amplify H-chain sequences with reasonable efficiency. Replacing this method with a published alternative (Von Boehmer *et al*, 2016) improved H-chain recovery rates from ~12% to between 48% and 65% across the exported sample plates.

Though it is not possible to definitively attribute the observed differences to a single mechanistic step in the amplification processes, priming of the reverse-transcription (RT) should be considered as a possible cause. The poly(T) priming of RT step in the Bruker protocol is an effective way of restricting cDNA synthesis to that derived from mRNA templates specifically (Zucha *et al*, 2021). However, this method relies on the presence of a Heavy/Light-chain-encoding mRNA template that remains fully intact, from poly(A) sequence to the 5' of the variable region, for successful amplification. Given that the plasma cells used here were subjected to freezing and thawing, MACS enrichment and screening on the Beacon, one may reasonably assume that mRNA quality is suboptimal.

Priming the reverse-transcription reaction with random hexamers, however, as is the case for the Nussenzweig protocol (Von Boehmer *et al*, 2016), is not predicated on the presence of a fully intact mRNA template with a poly(A) tail. Instead, this method requires only the variable and CH1 regions of the antibody chain sequence to remain intact to produce a cDNA product spanning the primer binding sites required for all downstream PCR reactions (***Figure 4.5-10A***).

Other differences in the two protocols may also contribute to their dissimilar efficiencies. As an example, the Bruker-supplied protocol relies on a template switching reaction to

add a universal adaptor at the 3' end of the nascent cDNA strand. I speculate that the efficiency of this reaction, which requires DNA-priming of the reverse transcriptase (classically RNA-primed) may be suboptimal, though this is understudied in the literature. Furthermore, whilst the addition of a universal primer binding site to all cDNA products avoids the requirement of complicated primer mixes that recognise all/any V-gene segment in the genome, this method restricts chain-specific amplification to only the second PCR reaction which may not provide sufficient amplification of H- or L-chain sequences for downstream cloning/sequencing.

Ultimately, the methodological changes implemented throughout the whole pipeline from cell processing to paired H/L sequence isolation facilitated the isolation of 40 distinct anti-gB mAbs. Despite careful consideration taken over the design of the viral-vectored gB immunogens and the dual-probe screening assay, however, attempts to isolate a pre-fusion specific mAb against gB were unsuccessful.

Given that gB-reactive hits were identified that only reacted to the CHO-cell based reporter, suggesting gB binding with conformational specificity, one must consider why there were disparities between the on-chip assay and downstream validation experiments. Failure to re-demonstrate that such mAbs only reacted with one probe is likely related to the following:

1) Fluorescence halos produced by antigen-reactive cells may be extremely faint, fractionally above background fluorescence. Successfully identifying such hits comes at the expense of the instrument's specificity, increasing the probability of misidentifying background or non-specific fluorescence as a true hit. The nature of this problem means cells identified as 'singly positive' are the most likely hits to in fact be the product of a misidentification.

2) In cases where fluorescence halos are particularly bright, cells in adjacent pens may be miscalled as hits themselves. Though automated hit calling is checked manually, in cases where it is unclear whether the observed fluorescence is the

result of a spillover or two adjacent hits, both pens were selected for export. This method risks the misidentification of pens as containing gB-reactive cells.

3) The functionality of each gB screening assay is, in part, a product of each probe's distribution in the channels of the optofluidics chip. Whilst both gB beads and gB-expressing cells were generally well distributed across the chip, and loaded at high densities, regions of marginally lower probe density hinder the instrument's/user's ability to detect positive pens in the local area. These regions would not necessarily be the same across the two binding assays and thus pens that would otherwise have been doubly positive may appear singly positive.

Despite the imperfections of the dual screening assay, the failure to identify any conformationally specific anti-gB mAbs speaks to the rarity of such a population of mAbs, should they exist at all. Failure to find such mAbs is in itself an important consideration with respect to the relevance of pre-fusion stabilisation in gB-based vaccine design, albeit far from definitive evidence that such an approach is not worth pursuing.

Were the sole objective of this work to be the isolation of pre-fusion specific mAbs, it should be reiterated that antibody discovery may have benefited from working on human-derived samples. Any future efforts to exhaustively establish whether pre-fusion specific antibodies exist should certainly include such work, not least for the reason of working in the most biologically relevant context.

Nonetheless, the 40 novel antibodies identified in this chapter represent a valuable new tool for investigation of the antigen landscape of gB and the functionality of antibodies against it. Subsequent characterisation work is described in the following chapters.

4.7 Appendix III: RT-PCR Primer Sequences

Nussenzweig heavy chain round 1 amplification	
IgH PCR 1 1mFH_I	AGGAACTGCAGGTGTCC
IgH PCR 1 1mFH_II	CAGCTACAGGTGTCCACTCC
IgH PCR 1 1mFH_III	TGGCAGCARCAGCTACAGG
IgH PCR 1 1mFH_IV	CTGCCTGGTGACATTCCCA
IgH PCR 1 1mFH_V	CCAAGCTGTGTCCTGTC
IgH PCR 1 1mFH_VI	TTTTAAAAGGTGTCCAGKGT
IgH PCR 1 1mFH_VII	CCTGTCAGTAACTRCAGGTGTCC
IgH PCR 1 1mFH_VIII	TTTTAAAAGGGGTCCAGTGT
IgH PCR 1 1mFH_IX	CGTTCCTGGTATCCTGTCT
IgH PCR 1 1mFH_X	ATGAAGTTGTGGYTRAACTGG
IgH PCR 1 1mFH_XI	TGTTGGGGCTKAAGTGGG
IgH PCR 1 1mRG* (γ Reverse)	AGAAGGTGTGCACACCGCTGGAC

Nussenzweig κ light chain round 1 amplification	
Igκ PCR 1 1mFK_I	RGTGCAGATTTTCAGCTTCCTGCT
Igκ PCR 1 1mFK_II	TGGACATGAGGGCYCCTGCTCAGT
Igκ PCR 1 1mFK_III	CTSTGGTTGTCTGGTGTTGAYGGA
Igκ PCR 1 1mFK_IV	GTTGCTGCTGCTGTGGCTTACA
Igκ PCR 1 1mFK_V	GTATCTGGTACCTGTGG
Igκ PCR 1 1mFK_VI	TGCCTGTTAGGCTGTTGGTGCT
Igκ PCR 1 1mFK_VII	GCTCAGTTCCTTGGTCTCCTGTTGC
Igκ PCR 1 1mFK_VIII	TGGGTGCTGCTGCTCTGGGT
Igκ PCR 1 1mFK_IX	CAGTTCCTGTTTCTGTTARTGCTCTGG
Igκ PCR 1 1mFK_X	TGCTCTGGTTATATGGTGCTGATGGG
Igκ PCR 1 1mRK* (κ Reverse)	ACTGAGGCACCTCCAGATGTT

Nussenzweig λ light chain round 1 amplification	
Igλ PCR 1 1mFL_I	ACTTATACTCTCTCTCCTGGCTCTC
Igλ PCR 1 1mFL_II	CTCTTCTTCTTCTTTGTTCTTCATTGCT
Igλ PCR 1 1mRL* (λ Reverse)	GTACCATYTGCCTTCCAGKCCACT

Nussenzweig heavy chain round 2 amplification (& sequencing primers)	
IgH Seq PCR 2mFG*	GGGAATTCGAGGTGCAGCTGCAGGAGTCTGG
IgH Seq PCR 2mRG* (γ Reverse)	GCTCAGGGAARTAGCCCTTGAC

Nussenzweig κ light chain round 2 amplification (& sequencing primers)	
Igκ Seq PCR 2mFK*	GAYATTGTGMTSACMCARWCTMCA
Igκ Seq PCR 2mRK* (κ Reverse)	TGGGAAGATGGATACAGTT

Nussenzweig λ light chain round 2 amplification (& sequencing primers)	
Igλ Seq PCR 2mFL_A*	CAGGCTGTTGTGACTCAG
Igλ Seq PCR 2mFL_B*	CAACTTGTGCTCACTCAG

Igλ Seq PCR 2mRL* (λ Reverse)	CTCYTCAGRGGAAGGTGGRAACA

Nussenzweig heavy chain round 1 amplification (low yield)

IgH PCR 1 Low Yield 1mFH_XII	GGCAGTGGTTACAGGGGTC
IgH PCR 1 Low Yield 1mFH_XIII	TGCTCTTTTAAAAGATGTCCAGTGT
IgH PCR 1 Low Yield 1mFH_XIV	TGTTCACAGCCTTTCCTGGT
IgH PCR 1 Low Yield 1mFH_XV	GCTTGGCAGCAGCTCTA
IgH PCR 1 Low Yield 1mFH_XVI	TCTGCATGCTGACATTCCCA
IgH PCR 1 Low Yield 1mFH_XVII	TGTTGTCAGCCCTTCCTGG
IgH PCR 1 Low Yield 1mFH_XVIII	ACACCTTTAAATGGTATCCAGTGT
IgH PCR 1 Low Yield 1mFH_XIX	GGCAGCTGCCCAAAGTRYCC
IgH PCR 1 Low Yield 1mFH_XX	CTTTWWMAAGGKRTSCAKTGT
IgH PCR 1 Low Yield 1mRG* (γ Reverse)	AGAAGGTGTGCACACCGCTGGAC

Nussenzweig κ light chain round 1 amplification (low yield)

Igκ PCR 1 Low Yield 1mFK_XI	GCTGTTTTGTATACCTGGG
Igκ PCR 1 Low Yield 1mFK_XII	CTCAGCTCCTGTTGCTGTGGC
Igκ PCR 1 Low Yield 1mFK_XIII	CCTCATATTTTTGCTGCTATGGG
Igκ PCR 1 Low Yield 1mFK_XIV	TGCTTTTCTGGATTTCAGCCTCCAG
Igκ PCR 1 Low Yield 1mFK_XV	TCAACTTCTGCTCTTCCTGCTGTTC
Igκ PCR 1 Low Yield 1mFK_XVI	CTAGCTCYTCTCCTCAGYCTTCTTCTCCTC
Igκ PCR 1 Low Yield 1mFK_XVII	GTGTMTGGTGCTBRTGGG
Igκ PCR 1 Low Yield 1mFK_XVIII	STGYTGHTGYTCTGG
Igκ PCR 1 Low Yield 1mFK_XIX	GGGTATCTGGTACCTGTGG
Igκ PCR 1 Low Yield 1mRK* (κ Reverse)	ACTGAGGCACCTCCAGATGTT

Table 4.7-1: Primer sequences (5' – 3') for PCR amplifications as per Von Boemer et al. *(Von Boehmer* et al*, 2016)*.

OmniMouse heavy chain round 1 amplification

IgH VH1_24 PCR 1	GGACTGCACCTGGAGGATC
IgH VH1_VH7_4 PCR 1	ATGGACTGGACCTGGAGGATC
IgH VH2_5 PCR 1	CATCCCTTCATGGGTCTTGTC
IgH VH2_26 PCR 1	GCTACACACTCCTGCTGCTGACC
IgH VH3 PCR 1	ATGGAGTTTGGGCTGAGCTGG
IgH VH3_07 PCR 1	ATGGAATTGGGGCTGAGCTG
IgH VH3_09 PCR 1	ATGGAGTTGGGACTGAGCTGGA
IgH VH4 PCR 1	TGAAACACCTGTGGTTCTTCC
IgH VH4_39 PCR 1	TGAAGCACCTGTGGTTCTTCC
IgH VH6 PCR 1	ACAATGTCTGTCTCCTTCCTCATC
IgH VH1-18, VH1-45, VH1-46, VH1-69 PCR 1	CCATGGACTGGACCTGGAG
IgH VH1-58 PCR 1	CACTATGGACTGGATTTGGAGG
IgH VH2-70 PCR 1	TCCACGCTCCTGCTACTGAC
IgH VH3 (VH3-13,15,20,53,64,66,72,73,74 outer) PCR 1	ATGGAGTTTGGGCTGAGCTGG
IgH VH3-21 PCR 1	ATGGAACTGGGGCTCCGCT
IgH VH3-43 PCR 1	ATGGAGTTTGGACTGAGCTGG
IgH VH3-48 PCR 1	ATGGAGTTGGGGCTGTGC

IgH VH3-49 PCR 1	ATGGAGTTTGGGCTTAGCTGG
IgH VH4 (VH4-61 outer) PCR 1	TGAAACACCTGTGGTTCTTCC
IgH VH4-59 PCR 1	ATGAAACATCTGTGGTTCTTCCTTC
IgH VH5-51 PCR 1	ATGGGGTCAACCGCCATC
IgH Rat gamma CH2 R1a (γ Reverse)	CTTTGGGGGGAAGATGAAGACAGATG
IgH Rat gamma CH2 R1b (γ Reverse)	CTTTGGCGGGAAGATGAAGACAGATG

OmniMouse κ light chain round 1 amplification

Igκ HuVκ1 PCR1	ATGAGGGTCCCCGCTCAG
Igκ HuVκ116 PCR1	GACATGAGAGTCCTCGCTCAG
Igκ HuVκ3 PCR1	ATGGAAGCCCCAGCTCAG
Igκ HuVκ3_15 PCR1	CCAGCGCAGCTTCTCTTC
Igκ HuVκ4_1 PCR1	ATGGTGTTGCAGACCCAGGT
Igκ HuVκ5_2 PCR1	TCCCAGGTTCACCTCCTCAG
Igκ HuVκ2 PCR1	ATGAGGCTCCCTGCTCAGC
Igκ HuVκ6-21 PCR1	GTTGCCATCACAACTCATTGGG
Igκ Human R1 (κ Reverse)	GTTTCTCGTAGTCTGCTTTGCTCA

OmniMouse heavy chain round 2 amplification

IgH VH1, VH7-4 PCR2	TCTTCTTGGTGGCAGCAGC
IgH VH2 PCR2	TCACCTTGAAGGAGTCTGGTCC
IgH VH3_07 VH3_23 FR1 PCR2	AGGTGTCCAGTGTGAGGTGC
IgH VH3_09 FR1 PCR2	AAGGTGTCCAGTGTGAAGTGC
IgH VH3_11 3_30 3_33 FR1 PCR2	AGGTGTCCAGTGTCAGGTGC
IgH VH4 PCR2	GCTCCCAGATGGGTCCTG
IgH VH6 PCR2	ATCTTCCTGCCCGTGCTG
IgH VH1, VH7-4 (VH1-18, VH1-45) PCR2	TCTTCTTGGTGGCAGCAGC
IgH VH1-46 PCR2	TCTGCTTGCTGGCTGTAGC
IgH VH1-58 PCR2	TCTTCTTGGTGGGAGCAGC
IgH VH1-69 PCR2	TCTTTGTGGTGGCAGCAGC
IgH VH2 (VH2-70) PCR2	TCACCTTGAAGGAGTCTGGTCC
IgH VH3_07 VH3_23 FR1 (VH3-13,15,20,21,48,53,64,66,72,73,74) PCR2	AGGTGTCCAGTGTGAGGTGC
IgH VH3_09 FR1 (VH3-43) PCR2	AAGGTGTCCAGTGTGAAGTGC
IgH VH3-49 PCR2	AGGTGTCCAATGTGAGGTGC
IgH VH4 (VH4-59, VH4-61) PCR2	GCTCCCAGATGGGTCCTG
IgH VH5-51 PCR2	CTGGCTGTTCTCCAAGGAGTC
IgH Rat gamma CH1 R2 (γ Reverse)	GGACAGGGCTCCAGAGTTCC

OmniMouse κ light chain round 2 amplification

Igκ HuVκ1 PCR2	TCAGCTCCTGGGGCTCCT
Igκ HuVκ1_13 PCR2	TCAGCTCCTGGGGCTTCT
Igκ HuVκ3 PCR2	TCTCTTCCTCCTGCTACTCTGG
Igκ HuVκ4_1 PCR2	TCTGTTGCTCTGGATCTCTGG
Igκ HuVκ5-2 PCR2	TCCTCCTCCTTTGGATCTCTG
Igκ HuVκ1-27 PCR2	TCAGCTCCTGGGACTCCT

Igκ HuVκ2 PCR2	CTGGGGCTGCTAATGCTCTGG
Igκ HuVκ6-21 PCR2	CTGCTGCTCTGGGTTCCAG
Igκ Human R2 (κ Reverse)	CCTGGGAGTTACCCGATTGG

Table 4.7-2: Primer sequences (5' – 3') for PCR amplifications of OmniMouse-derived human/rat transgenic IgG heavy and κ light chains.

5 Results III: Characterisation of the Binding and Function of a Mouse Monoclonal Antibody Panel Against gB

5.1 Statement of Authorship

All work reported in this chapter was designed and executed by S.E. with the following exceptions:

Western blot analyses were performed by Orthi Onupom under S.E.'s supervision.

Peptide mapping ELISAs, competition ELISAs and neutralisation assays were conducted with help from Francisco Orliacq, under S.E.'s supervision.

The mAb and Fab panels were expressed and purified with assistance from Francisco Orliacq and Orthi Onupom, under S.E.'s supervision.

Production of GFP-tagged virus was performed with assistance from Francisco Orliacq and Dr Rameswara Segireddy.

5.2 Chapter Overview

1) The anti-gB mAb panel bind a variety of epitopes on the post-fusion gB surface, the presentation of which are generally unaffected by antigen glycosylation state.

2) Cluster analysis reveals anti-gB antibodies recognise four 'antigenic sites' on the ectodomain, three of which are near the crown of the post-fusion structure, whilst the fourth is on Domain II.

3) The majority of mAbs in the panel are not potently neutralising. Neutralising mAbs disproportionately recognise antigenic Site 4 but are rare.

5.3 Introduction

5.3.1 Antibodies Against EBV gB

Most of the mouse monoclonal antibodies isolated against gB in *Results II* bound both soluble recombinant gB ectodomain and cell-associated full-length gB, without clear preference for one form or the other. Three newly isolated mAbs, ECO12, ECO38 and ECO48, appeared better able to bind to gBect than membrane-expressed gB, and none showed the opposite trend. Efforts to further characterise the binding of these antibodies therefore largely focused on study of the ectodomain and, by its nature, the post-fusion conformation.

The antibody responses to HCMV and HSV-1/2 gB have been sufficiently studied to characterise major epitopes. As described earlier in ***Table 1.4-1***, these regions are referred to as antigenic domains (AD) and functional regions (FR) for HCMV and HSV anti-gB mAbs, respectively. How antibodies against EBV gB interact with the ectodomain is poorly understood. Only a handful of monoclonal antibodies against EBV gB have been isolated prior to this study. Characterisation of their gB binding and functionality have been performed to varying extents, summarised in ***Table 5.3-1*** and discussed in detail later.

mAb	Origin	Isolation	Structural Characterisation	*In vitro* Neutralisation Capability	Comments	Ref
CL55	Mouse (strain unknown)	Hybridoma	None	Non-neutralising		(Wu *et al*, 2005; Chesnokova & Hutt-Fletcher, 2011)
AMMO5	Infected individuals	FACS of gBect tetramer-positive Memory B cells	gB-derived peptide ^{410}PSPPAPSAAR^{419} represents shortest linear epitope recognised by AMMO5. Alanine scanning reveals P413, P415, and R419 as key interactors (Hong *et al*, 2022). Residues in an unresolved loop between DII and DIII. Does not compete with 3A3 for gBect binding (Zhang *et al*, 2022).	On SVKCR2 epithelial cells: complete neutralisation (EC_{50} ~ 0.2 μg/mL) On HNE1 epithelial cells: complete neutralisation (EC_{50} = 0.13 μg/mL) Partial neutralisation of Raji (~50% at 100 μg/mL) and Akata B cells (~60% at 100 μg/mL)	3 non-neutralising anti-gB mAbs also identified, but not characterised further.	(Snijder *et al*, 2018)
3A3	gBect-immunised rabbits	FACS of gBect tetramer-positive Memory B cells	Cryo-EM structure of gBect complexed by 3A3 reveals binding site on DII.	On HNE1 epithelial cells: complete neutralisation (EC_{50} = 0.08 μg/mL) On Akata B cells: complete neutralisation (EC_{50} = 2.97 μg/mL). Proposed to block gB's interaction with cell-surface NRP1.	11 non-neutralising anti-gB mAbs also identified, but not characterised further.	(Zhang *et al*, 2022)
3A5			Cryo-EM structure of gBect complexed by 3A5 reveals binding site on DIV.	On HNE1 epithelial cells: complete neutralisation (EC_{50} = 0.31 μg/mL) On Akata B cells: complete neutralisation (EC_{50} = 4.90 μg/mL). Proposed to block gH/gL-gB interaction.		
8A9	Mouse (Balb/c)	Hybridoma	Both mAbs bind recombinant DII by ELISA and compete for binding of gBect by Surface Plasmon Resonance (SPR).	On Akata B cells: complete neutralisation (EC_{50} = 0.75 μg/mL).	8A9 exhibits cross-reactive binding to rhesus lymphocryptovirus (rhLCV) gB.	(Hong *et al*, 2022)
8C12				On Akata B cells: complete neutralisation (EC_{50} = 5.39 μg/mL).		

Table 5.3-1: Summary of binding and *in vitro* neutralisation characteristics for published anti-gB monoclonal antibodies.

5.3.2 Methods for the Mapping of Epitopes

Techniques commonly used to characterise antibody binding epitopes are summarised in ***Table 5.3-2***. With respect to gB-mAb interactions, epitope mapping has been conducted by methods including peptide scanning and mAb binding to recombinant domains in gBect (Hong *et al*, 2022), ELISA-based antigen binding competition and cryogenic electron microscopy (Cryo-EM) studies of gBect-Fab complexes (Zhang *et al*, 2022).

In this project, antibodies were first tested for their ability to bind denatured fragments of gBect that are produced after furin cleavage (Sorem & Longnecker, 2009). This served as a low-resolution binning tool, in which mAbs were tested for binding of epitopes in the 40 or 70 kDa denatured protein fragments. mAbs capable of this were then screened against a peptide array spanning the length of gBect to try and define their precise binding sites.

The full panel was also subjected to a competition assay in which nearly all ~1600 pairwise combinations of antibodies were screened. Here, a simple and affordable ELISA-based method was developed following the testing of three possible assay configurations. Exploratory analysis of the competition matrix was used to identify communities of antibodies with similar competition profiles.

ELISA competition data was then compared to that generated by a surface plasmon resonance (SPR)-based biophysical screening instrument, the LSA (Carterra). The LSA is capable of measuring thousands of competition interactions in a single, days-long campaign. After coating the LSA chip with a mAb panel, samples of antigen pre-mixed with an excess of IgG are flushed over the chip sequentially. This provides 'all-versus-one' competition data with each iteration and is repeated for all antibodies being screened.

Epitope Mapping Approach	Description	Time	Throughput	Ease	Specialist Equipment?	Resolution	Linear Epitope Detection	Conformational Epitope Detection	Cost	Comments
Peptide Array	Antibody (Ab) binding assay against partially overlapping peptide fragments ~20AA long covering the entire length of the antigen (Ag).									~800AA protein (~ EBV gB) requires 100-peptide array to be screened with each mAb in a panel. Higher resolution of epitopes requires secondary screening with shorter peptides or by a different method.
Fragment Binding Assays	Standard laboratory assays investigating Ab binding to Ag or recombinantly expressed Ag fragments (native or denatured). E.g. ELISA, Western Blot.									Fragmented Ag may not properly fold, restricting ability to detect real conformational epitopes. Objective scoring of positive binding may be challenging.
Bacteriophage / Bacterial / Yeast Display	Protein fragment library expressed on phage / cell surface allows for panning-based approach to identifying Ab epitopes.									Establishing display system is time consuming. Protein fragments capable of adopting secondary / tertiary structure permit some conformational epitope screening, but at the expense of resolution.
Structure-guided mapping	Purification of Ag-Ab complexes for high-resolution structure elucidation by X-ray crystallography or Cryo-EM.									High-resolution structures enable comprehensive epitope foot printing. Epitopes containing flexible regions and PTMs are difficult to solve.
Mass Spectrometry (MS)	Cross-linking of Ag-Ab complexes followed by proteolysis to generate fragment library for MS, or mapping deuterium exchange rates at Ag surface with and without bound Ab.									Well suited to linear / flexible epitopes. May capture conformational / discontinuous epitopes but does not determine structure. Ag post-translational modification e.g. glycosylation of epitopes may be captured, as for HIV gp120 (Behrens *et al*, 2016). Can be used to map polyclonal responses (Ständer *et al*, 2021).

Epitope Mapping Approach	Description	Time	Throughput	Ease	Specialist Equipment?	Resolution	Linear Epitope Detection	Conformational Epitope Detection	Cost	Comments
Nuclear Magnetic Resonance (NMR)	Comparing differences in NMR spectrum of the Ag with and without complexing Ab allows for deduction of interacting residues.									Temporal resolution of Ag-Ab complexes in solution captures dynamic nature of interaction (Gershoni *et al*, 2007). Typically limited to proteins <30 kDa (Wüthrich, 1990).
Label-free biosensing	Biophysical characterisation of Ag-Ab interactions e.g. Surface Plasmon Resonance, Biolayer Interferometry.									Resolution of epitope mapping dependent on: a) Ability to express folded Ag fragments recombinantly, or b) Ability to generate Ag mutants to map epitopes e.g. by alanine scan, or c) Ability to determine binding competition with antibodies binding known epitopes. Multiplexed platforms permit rapid generation of competition data for Ab panels (Säfsten, 2009) e.g. LSA Carterra.
Deep Mutational Scanning	Mutagenesis of Ag to generate cell-expressed library for screening of Ab binding. Downstream sequencing of depleted mutants reveals key sites of Ag-Ab interaction.									Construction of Ag mutant library is time consuming. Well suited to membrane-expressed Ag. Agnostic of epitope structure provided mutations are sufficiently tolerated to permit mutant Ag expression.
Computational Approaches	*In silico* prediction of Ag-Ab interaction.									Online tools for protein-protein interaction modelling readily available e.g. AlphaFold3 (Abramson *et al*, 2024). Predicted Ag-Ab binding invariably requires validation a laboratory method.

Table 5.3-2: Common approaches to the characterisation of antigen-antibody binding sites, their advantages and disadvantages. Compiled with general guidance from recent review literature *(Hu & Irving, 2023; Hamed* et al*, 2023)*.

5.3.3 Glycosylation in the Context of the Anti-gB Response

The glycosylation of viral proteins is known to play key roles in protein folding, viral packaging, immune evasion and cell entry (Bagdonaite & Wandall, 2018). As its name suggests, gB is extensively glycosylated post-translation. Treatment of gB with EndoH or PNGase F glycosidases produces a large shift in the masses of both the 40 kDa and 70 kDa ectodomain fragments on a denaturing gel, confirming the presence of high mannose N-linked glycans at multiple sites (Reimer *et al*, 2009). In total 9 such sites have been identified across gBect (Joel Allen, unpublished) of which 7 were independently identified in a separate study (Zhang *et al*, 2018) (***Figure 5.3-1***).

Though early evidence suggested that EBV gB does not undergo O-linked glycosylation (Reimer *et al*, 2009), a more recent study has identified five threonine residues that may be glycosylated (***Figure 5.3-1***). Three exist in the unresolved N-terminus of the protein, one in the central helix of DIII and the last in DV, closely matching the profiles of HCMV and VZV gB (Bagdonaite *et al*, 2016).

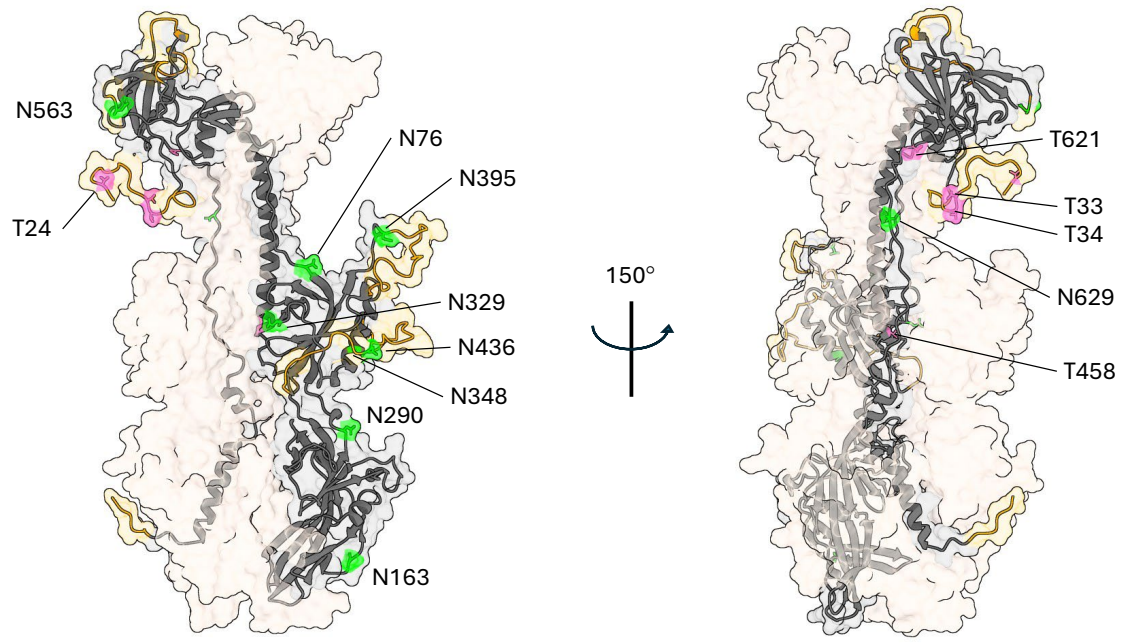


Figure 5.3-1: Glycosylation sites on EBV gB.
The EBV gB ectodomain (PDB: 3FVC) in the post-fusion conformation. A single protomer in the trimeric structure is shown as a grey ribbon. Remaining promoters are beige surfaces. 9 N-glycosylation sites (green) and 5 O-glycosylation sites (pink) are labelled. Flexible loops (yellow) that were not resolved in the Cryo-EM structure have been modelled using the MODELLER plug-in in ChimeraX *(Šali & Blundell, 1993)*. These loops are not proposed as being structurally accurate but are to help with the illustration of glycosylation sites within them.

The role glycosylation might play in shielding against the anti-gB antibody response is only partially understood. A study of polyclonal sera from mice and rabbits immunised with gB suggested that gB binding was similar between the glycosylated and N-deglycosylated forms, the latter generated by PNGase F treatment (Hong *et al*, 2022). Only three mAbs have been screened in a similar fashion, 8A9, 8C12 and AMMO5, none of which showed glycan-dependent changes to gBect binding (Hong *et al*, 2022).

Though these data suggest that antibodies are not raised against epitopes masked by N-glycan, they are limited by the number of mAbs with which glycan-dependent epitopes may be interrogated. To better study this, the binding of all 40 mAbs isolated in this work were tested for differential binding to glycosylated and N-deglycosylated gB.

5.3.4 *In Vitro* Neutralisation Assays to Study Anti-gB mAb Functionality

EBV's nature as an obligate human pathogen complicates its study in animal models. The *in vivo* protection conveyed by 3A3, 3A5 and AMMO5 described above was elucidated using a mouse model engrafted with human hematopoietic stem cells. These animals are thus capable of producing the human-derived B cells necessary for EBV infection (Zhang *et al*, 2022; Guo *et al*, 2019a).

Given these technical challenges, multiple *in vitro* neutralisation assays have been developed as surrogates. Commonly used assays make use of GFP-tagged EBV strains that allow for the detection of infected cells by flow cytometry or fluorescence microscopy. Two widely used cell lines have been generated to produce GFP-tagged virus: the 2089/293 epithelial-derived cell line (Delecluse *et al*, 1998) and Akata B cells (Kanda *et al*, 2004).

Production of the 2089/293 cell line made use of a hygromycin B resistance cassette to stably transfect HEK293 cells with the EBV genome and a constitutively expressed GFP gene. Infectious virus is produced by transiently transfecting these cells with plasmid DNA encoding glycoprotein B and BZLF1, a transcription activator that triggers reversion from the latent to the lytic life cycle (Delecluse *et al*, 1998).

Akata-BX1 cells were developed by transfecting cells with bacterial artificial chromosomal DNA encoding the EBV genome with an inserted GFP gene to produce a stable episome (Kanda *et al*, 2004). Infectious virus is produced by the addition of anti-human IgG to culturing Akata cells. Cross-linking B cell receptors on their surface induces the lytic virus lifecycle (Kanda *et al*, 2004; Takada, 1984; Daibata *et al*, 1990).

More recently, a third EBV-GFP-producing cell line has been developed using Akata BX1-cell derived virus to infect a nasopharyngeal carcinoma line, CNE2, and subsequently using these cells to produce virus with B cell tropism (Zhang *et al*, 2018). Though this cell line has not been widely used, CNE2-derived virus was used to characterise the *in vitro* neutralisation capabilities of 3A3, 3A5 (Zhang *et al*, 2022), 8A9 and 8C12 (Hong *et al*, 2022).

Given the EBV tropism is determined by the cell type from which virus was derived (Borza & Hutt-Fletcher, 2002), epithelial cell-derived virus is commonly used to infect B cells *in vitro*, and vice versa. That said, Akata cell-derived virus is occasionally used for infection of B cell lines (Li *et al*, 2022).

The B cell lines infected in these assays vary. Common targets include Raji cells (Snijder *et al*, 2018; Edwards *et al*, 2024; Zhu *et al*, 2021; Li *et al*, 2022) and EBV GFP^- Akata 4E3 cells (Hong *et al*, 2022; Zhang *et al*, 2022; Li *et al*, 2022). Few studies have compared different susceptible B cell lines with respect to EBV infection. Li and colleagues, however, have shown Raji and Akata 4E3 cells are more susceptible to EBV infection than two comparator B cell lines Su-DHL8 and U266B1 (Li *et al*, 2022). The proportion of GFP^+ cells seemed to correlate with complement receptor 2 (CR2) surface expression, the cognate binding partner of gp350 in B cell infection (Sathiyamoorthy *et al*, 2014). Greater

infection rates suggest the Raji B and Akata 4E3 lines are preferable for study of antibody neutralisation *in vitro* (Li *et al*, 2022).

In similar fashion, epithelial cell lines used in EBV infection assays are inconsistent across the literature. SVKCR2 cells, the most common epithelial line used, have been engineered to constitutively expresses CR2 (Li *et al*, 1992), enhancing gp350-mediated infection. However, given this expression artificially provides a receptor present on B cells, and the understanding that gp350 is involved in B cell infection and appears non-essential to epithelial cell entry in natural infection (Hutt-Fletcher, 2007), this cell line's relevance to *in vivo* conditions may be questioned (Li *et al*, 2022). Other epithelial lines tested include AGS (Bu *et al*, 2019), HeLa (Cui *et al*, 2021), HNE1 (Zhang *et al*, 2022; Hong *et al*, 2022), HEK293 cells (Escalante *et al*, 2020) and HEK293T cells (Li *et al*, 2022).

Published comparison of these cell lines with respect to EBV infection is, again, limited. HEK293T cells have, however, been compared to AGS and U2OS lines with respect to susceptibility to EBV-GFP infection and CR2 expression. HEK293T cells were infected with high efficiency relative to their other cell lines and showed low levels of CR2 expression (Li *et al*, 2022). The authors suggest that this cell line may better mimic a wild-type epithelial cell phenotype, that may include such low levels of CR2/CD21 expression (Birkenbach *et al*, 1992; Fingeroth *et al*, 1999). As a result, HEK293T cells may be better suited for use *in vitro* than alternative lines.

How the use of different cell lines may influence the neutralising capacity of EBV-targeting mAbs is unclear. Repeat neutralisation assays on AMMO5, performed by the original identifiers (Snijder *et al*, 2018) and in its uses as a comparator mAb (Zhang *et al*, 2022) show reasonable concordance despite different B and epithelial cell lines being used. Similarly, characterisation of five mAbs targeting gp42, gp350 and gH/gL has been performed against three B cell and four epithelial cell types. This revealed each mAb's EC_{50} values for B cell entry and epithelial cell entry were consistent to within one order of magnitude across different lines (Zhao *et al*, 2024), though the extent to which this is true of anti-gB mAbs is unknown.

Evidence to date therefore suggests that discrepancies between mAb neutralising potencies caused by using different susceptible cell lines are fairly minor. Perhaps more relevant is the choice of cell lines that a) are reasonably susceptible to EBV infection, and b) somewhat resemble a wild-type phenotype. For these reasons, *in vitro* neutralisation assays in this work used GFP-expressing virus derived from 2089/293 epithelial cells to infect Raji B cells, and from EBV-GFP$^+$ Akata cells to infect HEK293T epithelial cells.

5.3.5 Investigating Complement-dependent Anti-gB Antibody Functionality

Whether anti-gB antibodies can protect against EBV challenge *in vivo* has only been investigated for 3A3, 3A5 and AMMO5 (Zhang *et al*, 2022). The humanised mice described above were administered with 20 mg/kg antibody one day prior to EBV challenge and once weekly following it. All three antibodies prevented weight loss in animals relative to animals administered a non-EBV mAb and showed significantly higher survival rates over the 60-day follow-up (Zhang *et al*, 2022). Animals given 3A3 or 3A5 showed EBV DNA genome copies below detectable levels for the duration of the study. Animals given any of the three anti-gB antibodies had no splenomegaly at post-mortem, whilst the control group showed signs of lymphoproliferative disorder (Zhang *et al*, 2022).

AMMO5's ability to protect 4/6 humanised mice in the lethal challenge experiment (Zhang *et al*, 2022) appears at odds with its poor ability to neutralise infection of B cells *in vitro* (Snijder *et al*, 2018). One explanation for this discrepancy is the inability of such neutralisation assays to capture possible Fc-mediated effector functionality of antibodies, some (but possibly not all) of which may be active in this mouse model. The mechanisms by which anti-gB antibodies that are not directly neutralising may contribute to protection against human herpesvirus infection were summarised in *Section 1.4.5*. As mentioned, however, very little evidence exists for such functionality against EBV.

Establishing assays to measure ADCP and ADCC responses *in vitro* for EBV research was not possible in the timeframe of this study. The possible role of complement-dependent enhancement of neutralisation was, however, explored *in vitro*.

5.4 Materials and Methods

5.4.1 Expression and Purification of Recombinant gB Ectodomain

The gBect construct used in characterisation assays was the same as that described in *Section 4.4.1* (PDB: 3FVC_A), ordered pre-synthesised into a pTWIST backbone (Twist Bioscience).

Plasmid DNA encoding the gBect construct was used to transfect ExpiCHO-S cells as per *Section 2.1.3*. Purification of the C-tagged ectodomain was performed as per *Section 4.4.1*.

5.4.2 Expression and Purification of Anti-gB Antibodies in Fab Format

For each gB-reactive antibody in the panel, Heavy-chain sequences were ordered from Twist Bioscience in Fab format. Variable and Constant Region 1 sequences were identical to those used in the synthesis of each mAb: variable regions were mouse-derived, whilst constant regions were human-derived owing to the AbVec vectors used to produce each mAb in the panel (See *Section 4.4.14*).

Each Fab H-chain was modified at the C-terminus to insert an enterokinase site (DDDDK) via a GS linker, and a Twin-Strep II tag ($AGWSHPQFEK(GGGS)_3AWSHPQFEK$, IBA) to facilitate downstream affinity purification.

Coding sequences were pre-synthesised in a pTWIST expression vector and plasmid DNA used to transfect Expi293F cells as per *Section 2.1.2*. Fabs were isolated from cell culture supernatant by affinity purification on an AKTA Pure purification system (Cytiva Life Sciences) using a Strep-TactinXT 4Flow FPLC column (IBA: 2-5023-001), in accordance with the manufacturer's instructions. Elution fractions containing purified Fab were pooled before concentrating using an Amicon 10kDa MWCO spin column (Merck: UFC9010). Concentrated proteins were stored at -80 °C until use.

5.4.3 Western Blot Analysis of the Mouse mAb Panel

1 µg/lane of purified gBect was subjected to denaturing PAGE using the same running conditions as in *Section 4.4.5*. After running, gel contents were transferred to a PVDF membrane (Bio-Rad) using a TransBlot Turbo (BioRad), as per the manufacturer's instructions.

Western blotting was performed using the iBind Flex solution kit (ThermoFisher: SLF2020). After transfer, membranes were blocked for 30 min in iBind solution. Blocked membranes were cut into single-lane strips and each strip stained for 2 h with a different gB-reactive mAb, diluted to 1 µg/mL in iBind solution. The strips of membrane were subsequently placed in an iBind Western Device for overnight staining with an anti-human IgG secondary antibody conjugated HRP (ThermoFisher: A18805), diluted 1:1000 in iBind solution.

Blots were developed using SuperSignal West Pico PLUS Chemiluminescent Substrate (ThermoFisher: 34580) as per the manufacturer's instructions, before imaging using a ChemiDoc Imaging System (Bio-Rad).

An additional membrane strip was stained with gB-reactive polyclonal mouse serum at a dilution of 1:100 to act as a positive control for successful gel loading and membrane transfer of gB. The positive control was treated as above, with the replacement of the anti-human IgG-HRP secondary with an anti-mouse IgG-HRP equivalent (Bio-Rad: 1706516).

5.4.4 Peptide Mapping ELISA

N-biotinylated 20mer peptides, overlapping by 8 amino acids, were designed spanning the length of WT gB (NCBI Ref: YP_401713.1) and synthesised by Mimotopes. Peptides were resuspended in 80% DMSO in water (v/v) upon arrival to a final concentration of 3 mg/mL. Working dilutions of each peptide were made in sterile PBS to 4 µg/mL as single-use aliquots and stored at -80 °C.

Peptide mapping ELISAs were performed using gBect peptides 1-90, spanning the entire ectodomain. Each mAb was tested against the entire array. ELISAs were performed using the method summarised in *Section 2.1.5*. Experiment-specific steps in the protocol are described in ***Table 5.4-1***.

Protocol step	Description
ELISA plate	EvenCoat Streptavidin coated plates (Bio-Techne: CP003).
Blocking incubation	Streptavidin plates are pre-blocked.
Primary stain	Peptide array spanning gBect added to individual wells of ELISA plates at 4 µg/mL, 50 µL/well.
Control conditions	Controls run on each individual plate. Negative control: two wells coated with biotinylated RH5 antigen at 2 µg/mL, 50 µL/well. Positive control: two wells coated with biotinylated gBect antigen at 2 µg/mL, 50 µL/well.
Primary incubation	1 h at RT in the dark.
Secondary stain	Goat anti-human IgG (γ-chain specific) secondary conjugated to alkaline phosphatase (Merck: A3187) at a dilution of 1:1000, 50 µL/well.
Secondary incubation	1 h at RT in the dark.
Development	10 min prior to reading.

Table 5.4-1: ELISA protocol for determining whether anti-gB antibodies could recognise linear peptide epitopes.

5.4.5 Deglycosylation of gB and ELISA Binding Analysis

100 µg and 20 µg samples of the purified gBect described in *Section 5.4.1* were subjected to *in vitro* deglycosylation using PNGase F (NEB: P0704S) under native and denaturing conditions, respectively, as per the manufacturer's instructions. The denaturing reaction was incubated at 37 °C for 1 h prior to heat inactivation at 75 °C for 15 min and storage of the protein mix at -80 °C. gB deglycosylated under native conditions was incubated at 37 °C for 20 h prior to freezing at -80 °C.

1 µg samples of each protein reaction mix were subjected PAGE analysis with Coomassie staining, as described in *Section 4.4.5*, alongside a sample of the untreated protein.

To test each mAb's ability to bind to gBect before and after N-deglycosylation, an ELISA-based experiment was conducted using the method summarised in *Section 2.1.5*. Assay-specific details are described in ***Table 5.4-2***.

Protocol step	Description
Coating protein	Recombinant gBect produced in *Section 2.1.5* in its fully glycosylated form, and after N-deglycosylation under native conditions. Concentration: 2 µg/mL, 50 µL/well.
Blocking incubation	1 h at RT in the dark.
Primary stain	50 µL/well monoclonal antibodies run in duplicate wells at each tested concentration, against both the glycosylated and deglycosylated antigen. Concentration: each antibody tested at 2, 0.2 and 0.02 µg/, 50 µL/well.
Control conditions	Controls run on each individual plate. Negative control: 17C7 anti-RabG antibody tested in quadruplicate at 2 µg/mL, 50 µL/well, against both glycosylated and deglycosylated antigen. Positive control: 3A3 anti-gB mAb, tested as per 17C7.
Primary incubation	1 h at RT in the dark.
Secondary stain	Goat anti-human IgG (γ-chain specific) secondary conjugated to alkaline phosphatase (Merck: A3187) at a dilution of 1:1000, 50 µL/well.
Secondary incubation	1 h at RT in the dark.
Development	4 min prior to reading.

Table 5.4-2: ELISA protocol for determining each mAb's ability to bind gBect in its native, glycosylated state, and after N-deglycosylation with PNGase F.

Antibodies that appeared to show preferential binding to either form of gBect were re-tested using a 2-fold dilution series of staining antibody concentration from 4 µg/mL to 8 ng/mL.

5.4.6 gB Binding Competition ELISA

Three different configurations for a competition ELISA were investigated, shown graphically in ***Figure 5.5-4***. Protocol details specific to each configuration are shown in ***Table 5.4-3***.

All pairwise combinations of the gB-reactive mAbs were tested in duplicate and average $OD_{450\ nm}$ readouts shown.

In the screening of the entire mAb panel by configuration 2, the concentration of Fab used to form gB-Fab complexes was increased to 20 µg/mL to further reduce the risk of unoccupied Fab/mAb binding sites on the gBect trimer. An additional control was included in which a biotinylated version of gBect was added to mAb-coated wells without pre-incubating with Fab, akin to the positive control for antigen capture in configuration 3.

	Config. 1 (Figure 5.5-4A)	Config. 2 (Figure 5.5-4B)	Config. 3 (Figure 5.5-4C)
Coating protein	gBect as per *Section 5.4.1* (4 µg/mL)	mAb (4 µg/mL)	mAb (4 µg/mL)
Blocking incubation	1 h at RT in the dark		
Primary Stain	mAb (10 µg/mL, 50 µL/well)	None	None
Secondary Stain	Fab (2 µg/mL) for 1 h	gBect (2 µg/mL) pre-incubated with Fab TS-II (10 µg/mL) for 1 h at RT.	Biotinylated gBect (2 µg/mL) pre-incubated with Fab TS-II (10 µg/mL) for 1 h at RT.
Control conditions	A mAb/Fab-matched condition represented self-competition control. For each Fab tested, an additional well of the ELISA plate was left unstained with primary mAb, representing a 'no competition' control condition.	A mAb/Fab-matched condition represented self-competition control.	A mAb/Fab-matched condition represented self-competition control. C-terminally biotinylated gBect added to wells without a complexing mAb represented a positive control condition for each mAb's ability to capture the antigen.
Secondary Incubation	1 h at RT in the dark		
Tertiary Stain	Strep-Tactin conjugated to HRP (Fisher: 12698247) at a 1:1000 dilution	Strep-Tactin conjugated to HRP at a 1:1000 dilution.	Streptavidin HRP at a 1:1000 dilution (ThermoFisher: 21130).
Tertiary Incubation	1 h at RT in the dark		
Development	15 min prior to quenching.	30 min prior to quenching.	15 min prior to quenching.

Table 5.4-3: Assay parameters for different competition ELISA configurations.

5.4.7 Competition Analysis Using the LSA Carterra

Competition analysis on the LSA was performed using the pre-mix method provided by Carterra. Chip conditioning and activation was executed as previously described (Barrett *et al*, 2024). The anti-gB mAb panel was subsequently coupled directly to the activated HC30M chip surface at a concentration of 30 µg/mL (~200 nM), diluted in 10 mM sodium acetate pH 4.5, 0.05% Tween-20, for each antibody in the array.

Meanwhile, gB·mAb complexes were generated off-chip for each antibody in the panel by incubating trimeric gBect with antibody at final concentrations of 150 nM and 1.5 µM, respectively. Complexes were made up in LSA running buffer (Tris-buffered saline, 0.01% Tween-20) and left to incubate at RT for 1 h prior to instrument loading.

Antigen-mAb complexes were then injected onto the chip for 5 min followed by a 15 min dissociation phase using running buffer. After each run, complexes were removed from the chip by flushing it with 10 mM glycine solution at pH 2.3, regenerating the array.

To confirm mAbs used to coat the chip were able to capture antigen alone, 150 nM gBect was flushed over the chip in the same fashion as the complexes. The gB-only control condition was repeated 3 more times at regular intervals throughout the protocol to confirm that the array was being regenerated successfully.

Each antibody in the array was coupled to the LSA chip in duplicate. Each mAb was then assessed for its ability to capture antigen alone. To maximise the signal-to-noise ratio for each mAb, the replicate with the highest antigen-only capture signal was used for the competition analysis. This method was chosen on the advice of Carterra technical experts to mitigate the effects of variable coupling efficiency of mAbs to the chip which is stochastic by nature. In cases where neither replicate for a mAb yielded a SPR signal $<$100 response units (RU) for the antigen-only condition, these data were excluded from the competition analysis. For these antibodies, assessing competition can only be performed unidirectionally; that is, where the antibody is part of the gB$\cdot$mAb complex, but not when it is the on-chip ligand.

5.4.8 ELISA-based Competition Assay Cluster and Network Analysis

Raw $OD_{405\,nm}$ readouts for each mAb/Fab pair in reciprocal configurations were averaged to produce a symmetrised competition matrix. The competition heatmap was produced by unsupervised hierarchical clustering in python using the `seaborn.clustermap` package's default single linkage method. The competition dendrogram was produced in python using the `scipy.cluster.hierarchy` package. Clustering was performed using Ward's minimum variance method with a clustering distance threshold of 4.

Network analysis of the competition data was conducted using the python package `networkx`. A competition network was generated from the same symmetrised matrix by first taking the reciprocal of each mAb/Fab pair's readout. By this method, antibodies that do not compete (large $OD_{405\,nm}$ values) are weakly connected, whilst competing ones

(small $OD_{405\ nm}$ values) are strongly linked. mAbs were plotted using the networkx's `spring` layout with default parameters.

5.4.9 LSA-based Competition Assay Cluster and Network Analysis

SPR data were normalised to the antigen-only condition by taking the ratio of each mAb/mAb pair's signal to its most proximal antigen-only control. i.e. a normalised score of 1 represented equivalent capture signal of a gB·mAb complex as the gB-only condition. Negative signals were arbitrarily set to 0 to represent 100% competition.

Where directional data was available – mAb/mAb pairs for which data was considered passable when an antibody acted as the on-chip ligand and as the pre-complexing mAb – competition scores were averaged to generate a symmetrical competition matrix. For unidirectional competition data arising from poor antigen-only capture (described in *Section 5.4.8*) no averaging was necessary and instead, mAbs of this kind were only considered in the pre-complexing configuration.

To generate a competition network from the unidirectional competition matrix, the reciprocal values of each competition score were taken, as in *Section 5.4.8*. Achieving this required 100% competition conditions to be assigned a non-zero value. These were therefore arbitrarily set to 0.01, lower than all real non-zero values in the dataset. As for the ELISA study, competing antibodies were subsequently heavily connected, whilst non-competing antibodies were weakly connected.

Louvain community detection was performed using the `community` python package's default settings.

5.4.10 Cell Culture

Raji B cells, as well as virus-producing cell lines 2089/293 (Delecluse *et al*, 1998) and Akata B cells (Kanda *et al*, 2004) were a generous gift from Prof Claire Shannon-Lowe, University of Birmingham. HEK293T cells were kindly gifted by Prof Chris O'Callaghan, University of Oxford.

Raji and Akata B cells were cultured in RPMI media (Sigma: R0883) supplemented with 10% heat-inactivated foetal bovine serum (FBS, Sigma: F9665-500ML), 1% penicillin streptomycin (Merck: P0781), and 1% L-glutamine (Sigma: G7513) (cRPMI hereon). Akata cell media was further supplemented with G418 sulfate (ThermoFisher: 10131027) at a working concentration of 200 µg/mL. Cultures were maintained between 0.3 – 1.2 $\times 10^6$ cells/mL.

Adherent 2089/293 and HEK293T cell lines were cultured in treated flasks in DMEM (Sigma: D6546) supplemented with 10% FBS, penicillin streptomycin and L-glutamine as above (cDMEM, hereon). 2089/293 culture media was further supplemented with Hygromycin B (Gibco: 10687010) to a final concentration of 50 µg/mL. To passage both cell types, cell culture media was removed from the flask and cells washed with 10 mL of sterile PBS before aspirating. 5 mL of TrypLE (Gibco: 12604013) was added to each flask and incubated for 5 min at RT. Cells were gently detached from the bottom of the flask by tapping before adding 10 mL fresh cDMEM. The resuspended cells were used to seed new flasks at densities of 1.3 $\times 10^4$ cells/cm^2 and 3.9 $\times 10^4$ cells/cm^2 for HEK293T and 2089/293 cells, respectively.

All cell lines described above were cultured in a static incubator at 37 °C, 8% CO_2.

5.4.11 Production of GFP-tagged EBV from Epithelial and B Cell Lines

GFP-tagged EBV was produced from 293/2089 cells and Akata B cells to generate virus with B- and epithelial cell tropism, respectively.

EBV-GFP from 293/2089 cells was produced by co-transfection with plasmid DNA encoding gB and the transcriptional activator BZLF1 (gift from Prof Claire Shannon-Lowe) first described by Delecluse and colleagues (Delecluse *et al*, 1998, 1999). 2089/293 cells were seeded at 50 % confluency in a T-175 flask the day before transfection. Immediately prior to transfection, cells were resuspended by trypsinisation as per *Section 5.4.10* and centrifuged at 300 ×G for 5 min. The cell pellet was resuspended in culture media and a T-175 flask was seeded with 1 $\times 10^7$ cells.

Transfection mixes were made by mixing plasmid DNA, Lipofectamine 3000 and P3000TM enhancer (ThermoFisher: L3000001) as per the manufacturer's instructions, using the lowest recommended ratio of transfection reagent to plasmid DNA. The transfection mix was subsequently added to seeded 2089/293 cells whilst still in suspension, mixed gently, and then left static to incubate for 72 h at 37 °C, 8% CO_2.

GFP-tagged virus from Akata B cells was produced by treatment of cultured cells with an anti-IgG antibody (Daibata *et al*, 1990). Briefly, cultured Akata cells were centrifuged at 300 ×G for 5 min before resuspending cell pellets in fresh culture media to a density of 4 $\times 10^6$ cells/mL. Cells were induced by adding IgG F(ab')2 Goat Anti-Human IgG (MP Biomedicals: 0855049) to a final concentration of 50 µg/mL and incubated for 4 h at 37 °C, 8% CO_2. Induced cell cultures were subsequently diluted with cRPMI to a final density of 1 $\times 10^6$ cells/mL and cultured for 72 h.

For production of virus from both cell types, culture supernatants were harvested and centrifuged at 3000 ×G for 25 min to remove cell debris. Virus derived from 2089/293 cells were then subjected to ultracentrifugation. 1 mL of OptiPrep (Sigma: D1556) was mixed 1:1 (v/v) with .85% (w/v) NaCl, 60 mM HEPES-NaOH, pH 7.4. 1 mL of diluted OptiPrep was overlayed with 10 mL culture supernatant supplemented with bacitracin (100 µg/mL, Sigma: B0125) and centrifuged at 4 °C for 2 h at 20000 rpm in a SW 32 Ti Swinging-Bucket Rotor (Beckman Coulter: 369650). Deceleration was performed with the brake off. The top ~10 mL of each centrifuged tube was removed leaving ~1 mL of medium containing concentrated virus. These were mixed thoroughly by pipetting and pooled.

Virus preps were stored at 4 °C for up to 3 weeks, or frozen at -80 °C.

5.4.12 *In Vitro* Neutralisation Assay

Virus isolated from 2089/293 cells was used to infect Raji B cells using a method similar to one previously described (Sashihara *et al*, 2009). Briefly, 30 µL of virus was mixed 1:1 with monoclonal antibody diluted in cRPMI and incubated for 2 h at RT. Reported mAb concentrations in all figures correspond to the antibody concentration after mixing with virus. 50 µL of each mix was then added to 2 $\times 10^5$ Raji cells in wells of a 96 well plate at

a final volume of 150 µL. Cells were then incubated at 37 °C, 8% CO_2 for 2 h before centrifugation at 300 ×G for 5 min. Virus-containing supernatants were removed and cell pellets resuspended in 200 µL fresh cRPMI for culture at 37 °C, 8% CO_2 for 72 h.

Virus isolated from Akata B cells was used to infect HEK293T cells using a method derived from that of Li et al. (Li *et al*, 2022). 2 ×10^5 HEK293T cells in a volume of 300 µL were used to seed wells of a treated 24 well culture plate and incubated at 37 °C, 8% CO_2 for 4 h. Meanwhile, 200 µL of 1:1 mixtures of Akata-derived virus and mAb were incubated for 2 h at room temperature. Mixes were then overlayed on the seeded HEK293T cells and plates incubated for a further 72 h.

Where complement-dependent enhancement of neutralisation was investigated, guinea pig serum (Merck: 234395) was added to virus-antibody mixes (10% v/v) at the start of the 2 h incubation.

For both assays, cells were washed at the point of harvest with 200 µL sterile PBS before fixation with 2% formaldehyde (Merck: HT5012) for 20 min at RT. Cells were washed a final time in PBS and resuspended to a sample volume of 150 µL. Samples were analysed by flow cytometry using an LSRII cytometer (BD Bioscience) with High Throughput Sampler.

In all neutralisation assays, a no-infection cell culture condition was included to which no virus was added. A positive control for cell infection was also included where virus was incubated with an irrelevant antibody specific to the rabies glycoprotein, 17C7 (Sloan *et al*, 2007), tested at the highest assay concentration of antibody. An example gating strategy and the formula for the calculation of % neutralisation scores are shown in ***Figure 5.5-11A***.

5.5 Results

5.5.1 Beacon-Isolated mAbs Recognise Epitopes in Both Fragments of the Denatured gB Ectodomain as well as Conformational Epitopes

Antigen-antibody interactions were first characterised by using each Beacon-isolated mAb to stain for gBect after denaturing SDS-PAGE. This method sought to bin mAbs into one of four categories: recognisers of the 40 kDa gB fragment, the 70 kDa fragment, both fragments or neither, in which case antibodies were assumed to recognise a conformational epitope lost upon denaturation. Staining was also conducted using 3A3 and 3A5, previously characterised as binders of the 70- and 40 kDa fragments, respectively (Zhang *et al*, 2022) (***Figure 5.5-1A, C***). Staining with gB-reactive polyclonal mouse serum was used to confirm the presence of both antigen fragments on the blot (***Figure 5.5-1C***).

After initial experiments revealed some inconsistency, Western blots were conducted three times for each mAb on different days. This revealed two new antibodies capable of binding the 70 kDa fragment, and eight recognising the other (***Figure 5.5-1B***). Developing Western blot bands had varying intensities, subjectively scored as strong, moderate and weak to better summarise the panel's binding profile (***Figure 5.5-1C***). Where discrepancies were identified between replicate blots for each mAb, a fourth blot was performed (see ECO68, ***Figure 5.5-1C***). Only antibodies that clearly bound a gBect fragment in 3/3 or 3/4 replicates were considered true fragment binders. All raw Western blot images can be found in *Appendix IV*.

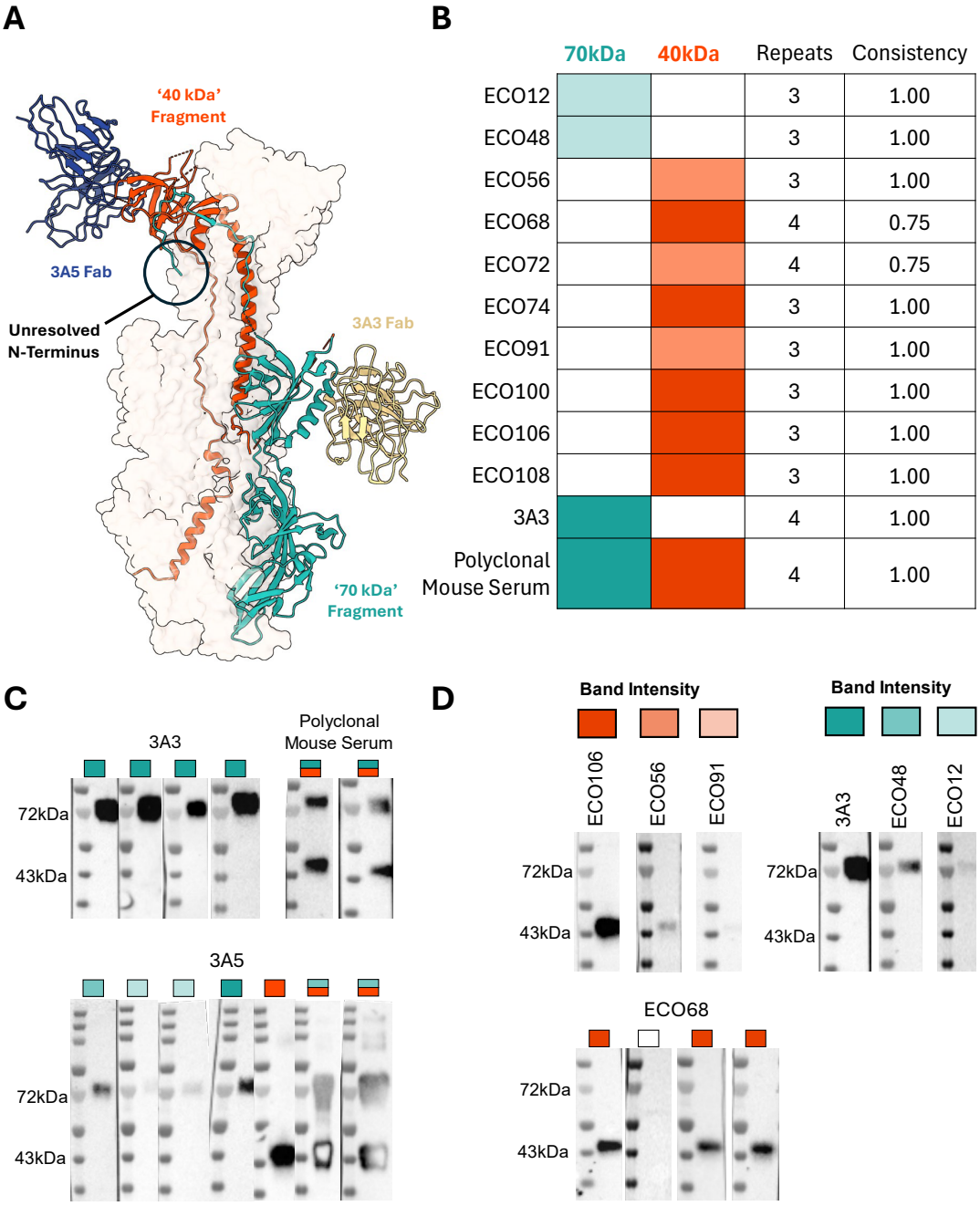


Figure 5.5-1: Anti-gB mAb recognition of denatured gB by Western Blot.

(A) The gB ectodomain (PDB: 7FBI, post-fusion) in complex with two neutralising antibodies: 3A3 (yellow) and 3A5 (navy). For one monomer in the structure, the 40 kDa (orange) and 70 kDa (green) fragments formed after furin cleavage are shown.

(B) Summary of gB binding by mAbs able to recognise the denatured 40 kDa and 70 kDa fragments by Western blot. For each mAb, band intensities were scored by eye as strong, fair or weak. Consistency scores correspond to the proportion of western blot repeats for which mAb successfully stained a gB fragment. Only stains with consistencies ≥ 0.75 were considered true binders.

(C) Raw Western blot images for control conditions 3A3, 3A5 and staining with gB-reactive polyclonal mouse serum. 3A3 and 3A5 were previously identified as 70 kDa and 40 kDa fragment binders, respectively *(Zhang* et al*, 2022)*.

(D) Raw Western blot images showing examples of strong, fair and weak staining of the 40 kDa and 70 kDa fragments. Blots are labelled with the corresponding mAb used as a primary stain. ECO68 is shown as an example of an antibody with staining consistency 0.75.

Though the majority of mAbs showed reproducible staining behaviour, five mAbs, ECO 0, 40, 101, 110 and 112 exhibited inconsistent binding to the 40 kDa fragment, and a sixth mAb, ECO98 bound the 70 kDa band in a similar manner (see *Appendix IV*). Though it is unclear why binding may be inconsistent between repeats, this behaviour was predominantly observed for antibodies that stained only weakly. This suggested that the staining behaviour may be the result of variation in the amount of antigen loaded to lanes of the PAGE gel, efficiency of transfer to the PVDF membrane, a product of varying denaturation extent / re-folding, or in the staining steps. One or any combination of these factors may contribute to whether a weakly staining mAb might produce a visible band on a blot.

Most surprisingly, 3A5 showed substantial variability in its staining of gBect, recognising the 40 kDa, 70 kDa or both fragments across seven repeats (***Figure 5.5-1C***). This conflicts with published binding data in which 3A5 cleanly recognises the 40 kDa band (Zhang *et al*, 2022). One explanation for the staining of both fragments of gBect may be its proximity to the N-terminus of the protein (***Figure 5.5-1A***). Though the Cryo-EM structure shows 3A5 clearly interacts with the 40 kDa fragment, the N-terminus of gB, on the 70 kDa fragment, is proximal to 3A5's variable region, and is only structurally resolved from residue Glu-41. Part of the 3A5 epitope may therefore reside in the 70 kDa fragment.

Overall, only 8 of the new mAbs were found to exhibit such binding to the 40 kDa band, 2 to the 70 kDa band, 24 to neither and 6 that did stain bands albeit inconsistently. This data suggests that the majority of the panel recognise conformational epitopes which cannot be attributed to either fragment using this technique.

5.5.2 mAbs Capable of Binding Denatured gBect Do Not Recognise gB-derived Peptides by ELISA

The ten mAbs that consistently stained fragments of gBect on a Western Blot were further investigated for their ability to bind linear epitopes alongside 3A3, 3A5 and three variably staining mAbs, ECO101, 110 and 112. 20mer biotinylated peptides were designed to span the entire length of gBect with 8 amino acids' overlap between each (90 peptides

in total). Peptide binding ELISAs were subsequently performed using each of the 14 mAbs as a primary stain to map their linear epitopes. Alongside the peptide array, each mAb was also screened against a biotinylated version of gBect protein used to coat additional wells of the plate, and a negative control antigen, biotinylated RH5.

Background staining levels varied between peptides. To identify truly positive binding of mAbs to peptides, all 14 antibodies were analysed together such that the varying levels of background staining would be visible (***Figure 5.5-2A***). Screening the mAbs against the array revealed that only one antibody, ECO12, appeared to bind any peptides above background levels. Though the peptides recognised by ECO12 all clustered within DI of the protein (***Figure 5.5-2B***), this conflicted with structural analysis of this antibody in complex with gBect (discussed in *Results IV*), which showed that its true epitope resides in DII.

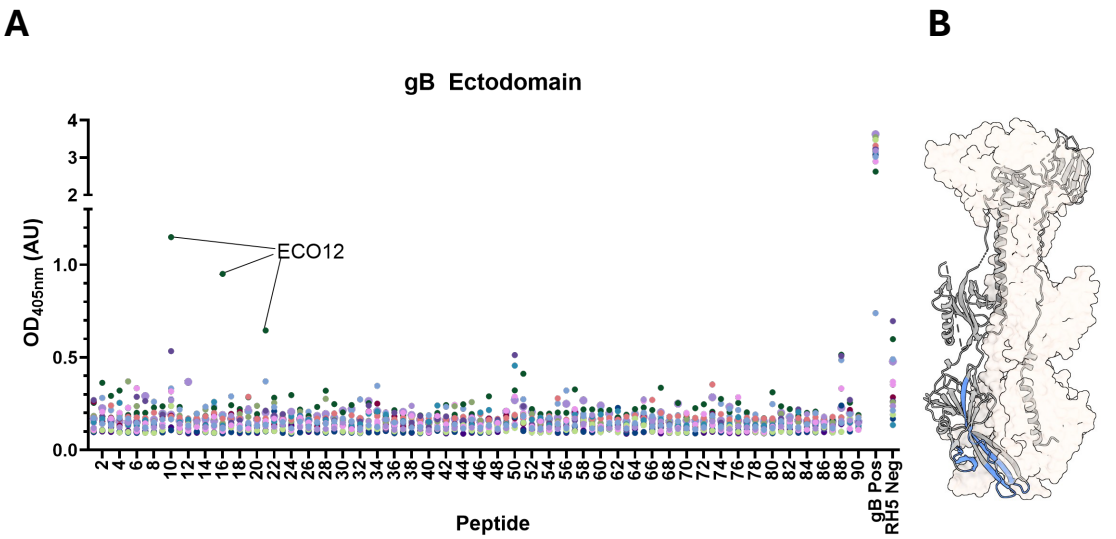


Figure 5.5-2: Anti-gB mAb recognition of linear epitopes in peptide format.

(A) $OD_{405\ nm}$ readouts for 14 mAbs used to stain a peptide array spanning the gB ectodomain in singlicate. mAb stains corresponded to 8 antibodies that recognised the 40 kDa fragment (ECO56, 68, 72, 74, 91, 100, 106, 108), 2 that recognised the 70 kDa fragment (ECO12, 48), three mAbs that inconsistently bound the 40 kDa fragment (ECO 101, 110, 112) and control mAbs 3A3 and 3A5. For each peptide, data points represent an individual antibody. All 15 antibodies were also used to stain a biotinylated gBect control well (gB Pos) to confirm they were able to recognise folded antigen. A negative control condition used each mAb to stain a biotinylated form of the *P. falciparum* antigen RH5.

(B) Peptide sequences positively stained by ECO12 are highlighted (blue) on a monomer of the gB ectodomain (PDB: 3FVC). All three peptides reside in Domain I of the ectodomain.

In summary, while the 14 mAbs screened here appeared to recognise linear epitopes in gB, as determined by Western blot, none appeared to recognise their epitope by peptide ELISA. This discrepancy likely relates to the differing nature of the two assays. Though exposing gB to SDS-PAGE should completely denature the antigen, renaturation or residual secondary structure may be sufficient for mAbs recognising conformational epitopes to stain protein on a blot (Zhou *et al*, 2007). Regarding the ELISA, failure of antibodies to bind peptides may be the result of combination of factors:

1) Were antibodies to in fact recognise conformational epitopes that were not fully denatured prior to Western blot, these mAbs would not efficiently bind peptides by ELISA.

2) Though sequentially identical, complexing of a peptide is associated with a significantly greater entropic cost than binding denatured protein on account of a peptide's greater flexibility (Zhang *et al*, 2012). This may affect mAb binding.

3) Linear epitopes recognised by mAbs may be longer than 20 amino acids. This appears unlikely given previous studies suggesting linear antibody epitopes to be between 4-12 residues (Buus *et al*, 2012).

4) The 'linear' epitopes recognised by these anti-gB mAbs may include post-translational modifications that are not present on synthetic peptides, such as glycans.

5.5.3 Two mAbs Exhibit Variable Antigen Binding Depending on gB's Glycosylation State

As discussed in *Section 5.3.3*, the role of glycosylation in masking antibody epitopes on gBect is only partially understood. The full mAb panel was therefore investigated for ability to bind gBect in its glycosylated form and after *in vitro* N-deglycosylation.

Recombinant gBect, produced in ExpiCHO cells, was first treated with PNGase F to remove N-linked glycans. Deglycosylation reactions performed under native and denaturing conditions showed clear shifts in the masses of the two denatured gBect bands

produced post-furin cleavage (***Figure 5.5-3A***). Band shifts were similar for the denaturing and native deglycosylation reactions, suggesting removal of N-glycans on the folded protein proceeded with comparable efficiency to that of the unfolded protein.

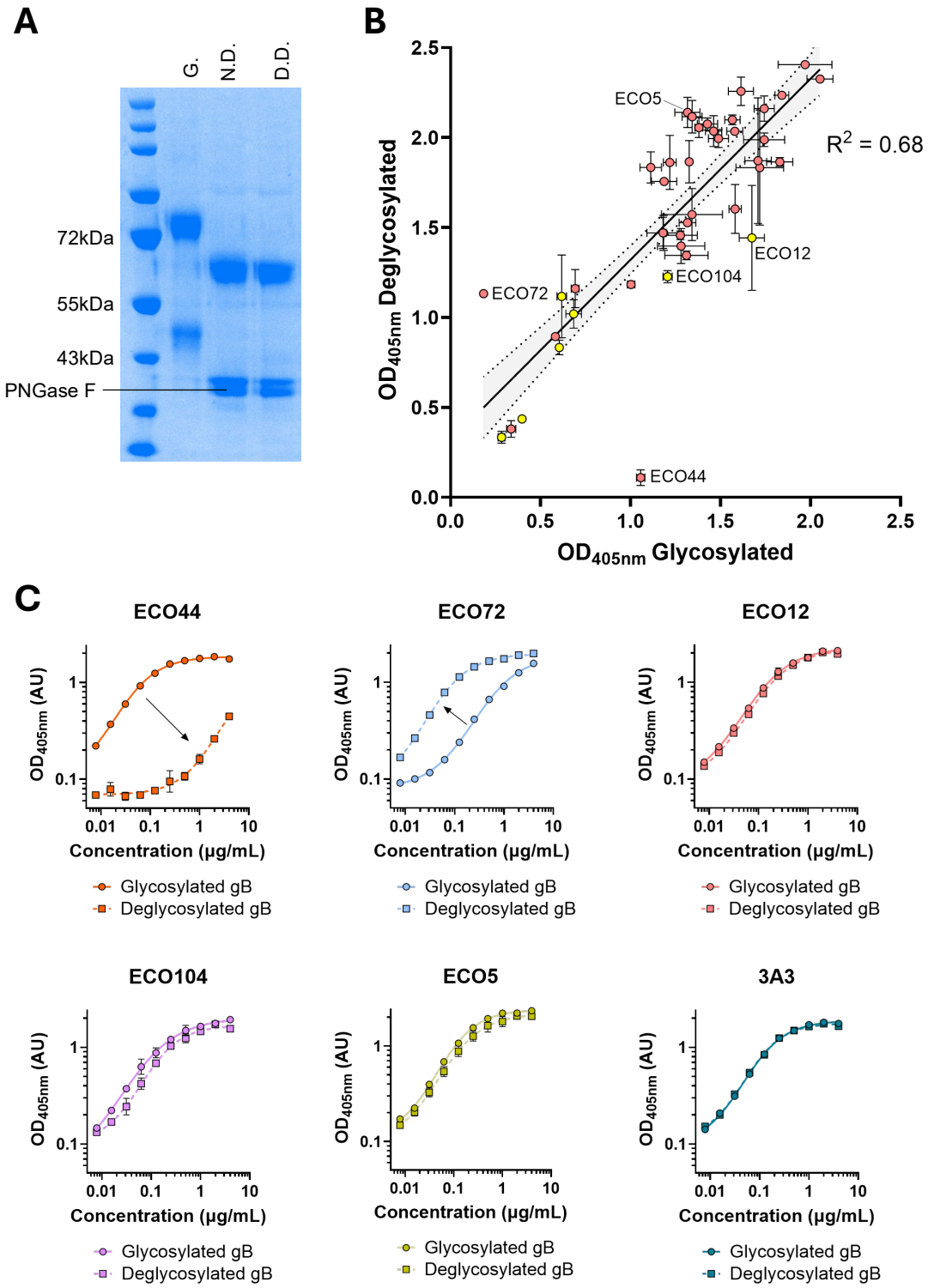


Figure 5.5-3: Glycan dependencies of anti-gB mAbs.

(A) Coomassie gel showing glycosylated gBect ('G.') and gB deglycosylated under native conditions ('N.D.') and denaturing conditions ('D.D.'). The 34 kDa PNGase F band is labelled.

(B) $OD_{405\ nm}$ readouts for anti-gB mAbs used to stain glycosylated gBect and gB N-deglycosylated under native conditions. Data points represent mean values for each mAb used at a final staining concentration of 0.2 µg/mL (red). Where $OD_{405\ nm}$ signals for mAbs binding glycosylated gB were near background, data from the 2 µg/mL staining condition were used instead (yellow circles). Error bars represent half of the range across technical duplicates for glycosylated and deglycosylated gB staining. Plotted line of best fit (solid line) and corresponding R^2 value calculated by simple linear regression with 95% confidence intervals (grey shading). Labelled points were those re-tested as full curves.

(C) Full dilution series for mAbs that deviated most substantially from the line of proportionality in (B) and 3A3. $OD_{405\ nm}$ signals are plotted for each mAb after staining glycosylated gBect (circles, solid lines) and N-deglycosylated gB (squares, dashed lines). Only ECO44 and ECO72 showed substantially different ELISA signals against the glycosylated and deglycosylated forms of the antigen (signal shifts for glycosylated to deglycosylated gB readouts indicated by arrows).

mAbs were subsequently screened by ELISA for their ability to bind gBect from the native deglycosylation reaction as well as the fully glycosylated form. Plotting each mAb's $OD_{405\ nm}$ readouts revealed the majority of mAbs in the panel trace a line of proportionality (***Figure 5.5-3B***). This suggested that the antibodies' recognition of epitopes on gBect were not affected by the presence or absence of N-glycans in the general case.

Two mAbs, ECO44 and ECO72, showed substantial deviation from the line of best fit suggesting their binding was glycan dependent. In addition, three others (ECO5, 12, and 104) may be marginally affected by glycosylation. Such behaviour was further investigated by generating binding curves of mAbs against gBect with and without PNGase F treatment (***Figure 5.5-3C***).

Relative to 3A3, a control mAb that did not exhibit glycan-dependent gB binding, the marginal mAbs' glycan dependencies were insignificant. ECO44's ability to recognise gBect, however, was greatly impaired following deglycosylation. This suggests N-glycans may directly form part of an antibody epitope on gB, or at least that full presentation of ECO44's epitope depends on glycosylation. Conversely, ECO72 showed a greater capacity to bind the deglycosylated antigen than the native form, implying N-glycan dependent epitope masking.

These findings represent the first evidence of gBect's N-glycosylation state playing a role in antigen-antibody binding. That said, the majority of mAbs were unaffected by antigen

N-glycosylation even though the recombinant gBect protein used in these assays was heavily glycosylated at all nine sites (Joel Allen, unpublished). This supports previous work suggesting N-glycosylation does not play a major role in the masking of antibody epitopes, at least *in vitro* (Hong *et al*, 2022). Furthermore, these data do not support the hypothesis that failure of the 14 mAbs screened in *Section 5.5.2* to bind gBect-derived peptides may be explained by the lack of post-translational modifications.

5.5.4 An ELISA-based Competition Mapping Method Reveals Five Distinct Clusters of gB-binding mAbs

Efforts to characterise gBect-mAb interactions by denaturing Western blot or peptide ELISA were unsuccessful for most antibodies in the panel. mAbs were therefore investigated for their ability to compete with one another for gBect binding. Though this method would not necessarily allow for the precise localisation of each mAb's epitope on gB, competition experiments might uncover clusters of mAbs recognising similar or adjacent regions on the antigen. The inclusion of the mAbs 3A3 and 3A5, which have already been structurally characterised, may further assist with the mapping of mAbs onto gB: antibodies competing for binding with 3A3 are likely to bind epitopes on or around DII, whilst those competing with 3A5 may recognise epitopes in DIV (Zhang *et al*, 2022).

Although high-throughput screening technologies exist for epitope binning of this kind, including surface plasmon resonance (SPR), these are expensive and may not be accessible. Three simple, ELISA-based screening methods were therefore investigated as possible alternatives and tested on the anti-gB mAb panel.

The methods differed with respect to their plate coating and staining configurations, illustrated graphically (***Figure 5.5-4***). In all configurations, however, the basis of detection was such that positive signal by ELISA implied two antibodies did not compete. Each method was piloted on a subset of the antibody panel to determine whether it was possible to distinguish between competitive and non-competitive mAb pairings. The self-competition conditions, in which antibodies are tested for their ability to compete with

themselves, represented a 100% competition control and should therefore produce near-background $OD_{405\ nm}$ signals.

Reviewing these across the three assays (by inspecting the central diagonal of the competition matrix), high self-competition $OD_{405\ nm}$ values (imperfect competition) were observed in configurations 1 (***Figure 5.5-4A***) and 3 (***Figure 5.5-4C***). This suggested that these two configurations might be unsuitable for use. Although the explanation for this is not obvious, antibodies appeared unable to saturate their cognate epitope in these configurations, permitting the occupancy of these free sites by mAb/Fab added secondarily. As a result, 100% competition conditions exhibited high signal levels, reducing the ability to differentiate competition from non-competition.

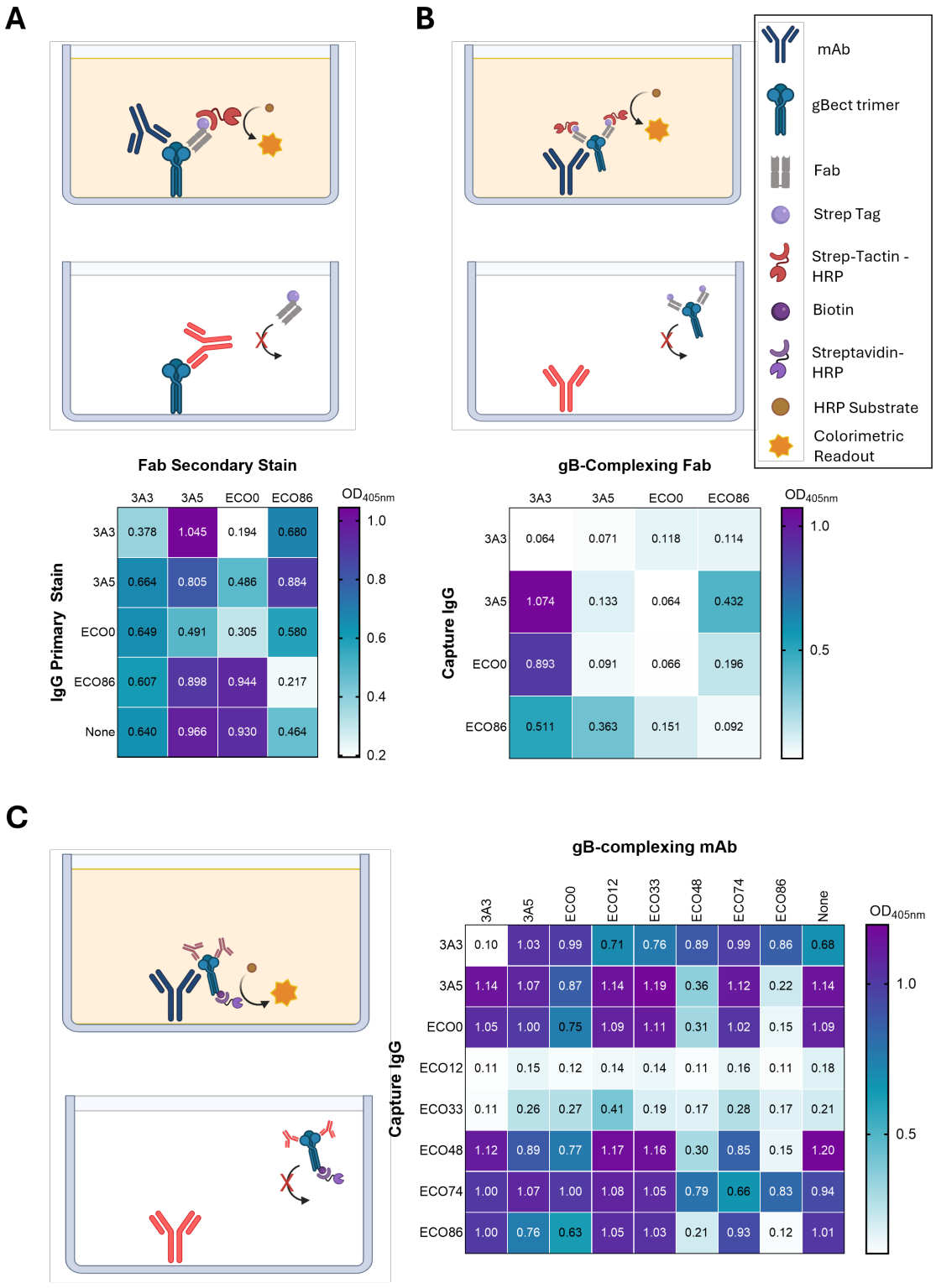


Figure 5.5-4: Assay development for the screening of mAb-mAb competition for gBect binding. Competition ELISA configurations investigated for their ability to differentiate competing mAbs from non-competing mAbs. Three configurations, 1 (panel A), 2, (panel B) and 3 (panel C) are shown graphically. $OD_{405\ nm}$ values, averaged across technical duplicates, are shown in heatmaps for all pairwise combinations of mAb/Fab. For configuration 3, a control condition was included in which biotinylated gBect was added to wells of the ELISA plate in the absence of a complexing mAb ('None') to confirm capture of the antigen by the mAb coated on the plate.

Assay configuration 2, on the other hand, showed low $OD_{405\ nm}$ signals across all four self-competition conditions (***Figure 5.5-4B***). Comparing readouts between reciprocal combinations of mAb and Fab (i.e. paired values either side of the self-competition diagonal) revealed that $OD_{405\ nm}$ values varied depending on which antibody was in the Fab format (***Figure 5.5-4B***). This is perhaps not surprising given Fab binding and therefore detection is not expected to be identical for different Fabs. However, general trends in the competition scores were, by and large, consistent – that is, where a mAb/Fab pairing appeared to compete in one arrangement, the reciprocal Fab/mAb readout showed similar behaviour.

Configuration 2 was therefore used to screen all ~1600 pairwise combinations of antibodies. As was observed in the pilot experiment, analysis of the unclustered heatmap revealed reciprocal mAb/Fab combinations did not produce quantitatively similar $OD_{405\ nm}$ readouts but were similar qualitatively (***Figure 5.5-5***).

Alongside the competition conditions, an additional control was included in which each mAb used to coat ELISA plate wells was tested for its ability to capture biotinylated gBect in the absence of a competing Fab. Captured gBect was directly detected using a streptavidin-HRP conjugate. Studying this control condition across the mAb panel revealed antibodies ECO12 and ECO38 captured gBect poorly, even in the absence of Fab (***Figure 5.5-5***). The reasons for this are unclear given that both mAbs can bind gBect when the antigen is used to coat an ELISA plate (discussed earlier, ***Figure 4.5-13B***). However, one may speculate that the binding mode of these mAbs to gBect requires a degree of flexibility in the antibody that is not afforded when adhered to the well surface. In the context of mAb/Fab competition, this poor ability to capture gBect results in low $OD_{405\ nm}$ values across the entire panel, otherwise interpreted as ECO12 and ECO38 exhibiting competition with all other mAbs. Analysis of the reciprocal arrangements, where ECO12 and ECO38 are instead in the Fab format used to coat gBect, reveals that (as expected) these antibodies each competed with a subset of the panel (***Figure 5.5-5***).

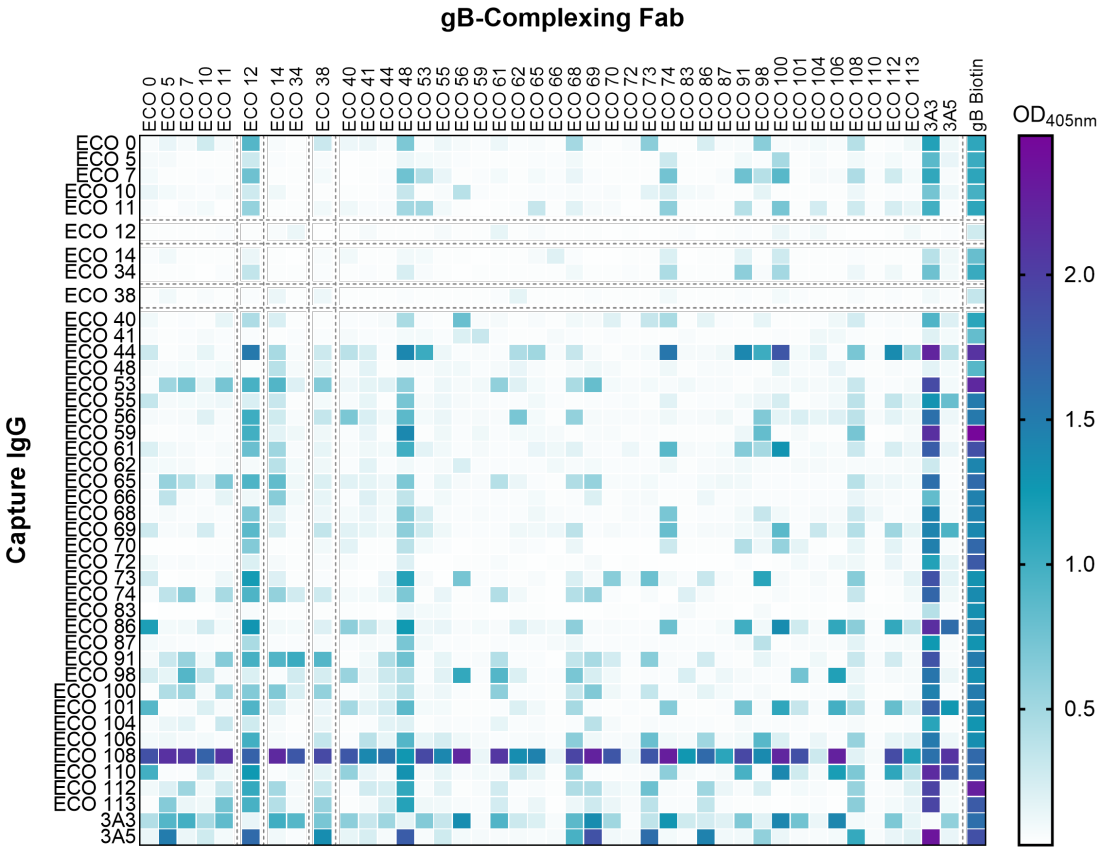


Figure 5.5-5: Unclustered competition heatmap for the full panel of anti-gB mAbs.
$OD_{405\ nm}$ readouts were averaged across duplicate wells from the same experiment for each condition. A positive control condition for antibody capture used direct detection of a biotinylated version of gBect added to wells of the ELISA plate without a complexing Fab, representing a 'no-competition' condition (right most column). Dotted lines highlight the behaviour of two mAbs that poorly capture gBect when used as a coating antibody – ECO12 and ECO38.

Hierarchical clustering was performed using a symmetrised competition matrix where raw $OD_{405\ nm}$ readouts for reciprocal arrangements of each mAb/Fab pairing were averaged. Analysis of the hierarchical clustering was performed using a Ward's method distance cut-off of 4 (***Figure 5.5-6A***). As expected, given their recognition of distant epitopes (Zhang *et al*, 2022), 3A3 and 3A5 populated different clusters. Cluster sizes varied substantially. The competition behaviour of 3A3 appeared particularly rare – analysis of the dendrogram reveals ECO108 and 3A3 to be the most divergent with respect to competition behaviour, followed by the cluster of ECO12, 48 and 98 (***Figure 5.5-6B***).

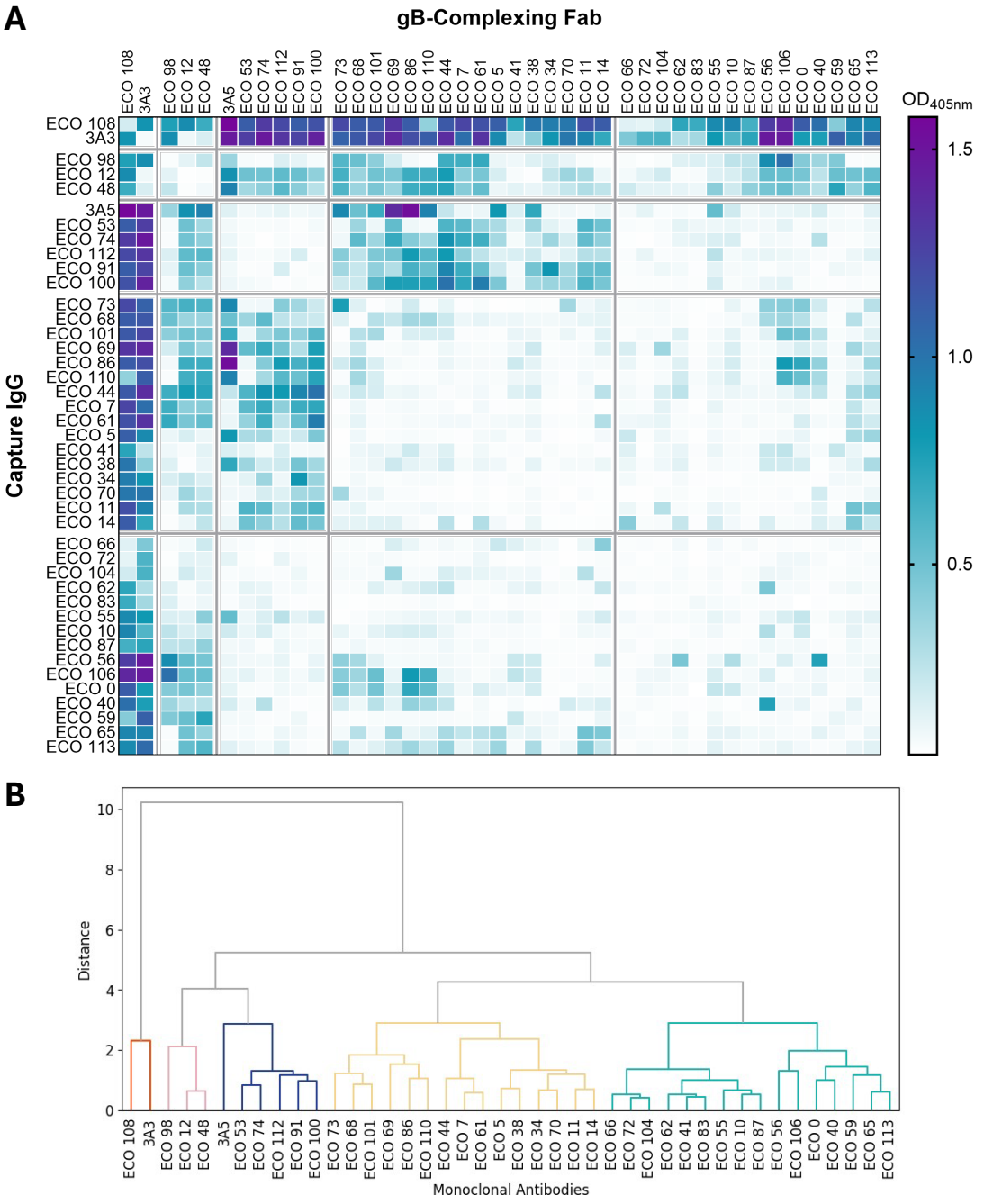


Figure 5.5-6: Cluster analysis of antibody competition by ELISA.

(A) Heatmap of the symmetrised ELISA competition matrix after hierarchical clustering using Ward's minimum variance method. Symmetrisation of competition scores was performed by averaging $OD_{405\ nm}$ readouts for reciprocal mAb/Fab and Fab/mAb configurations. A cluster cut-off distance of 4 was chosen based on inspection of the dendrogram (B), yielding five clusters (separated by grey lines). Antibodies are ordered by linkage distance.

(B) Dendrogram produced from the symmetrised matrix of mAb/Fab competition. Clusters were defined using a Ward's distance cut-off of 4 and are colour-coded.

The relationships between mAbs in the panel were also visualised graphically by an exploratory network analysis (***Figure 5.5-7***). Here, a network was constructed such that connections between antibodies were weighted based on their competition: antibodies that competed with one another were strongly linked. Plotting points using the spring layout reveals strong concordance between the two analysis methods (clustering and network analysis). 3A3 and ECO108 again appear isolated from the rest of the panel, here represented as peripheral location in the network. Given these mAbs do not compete, they are also weakly connected to one another.

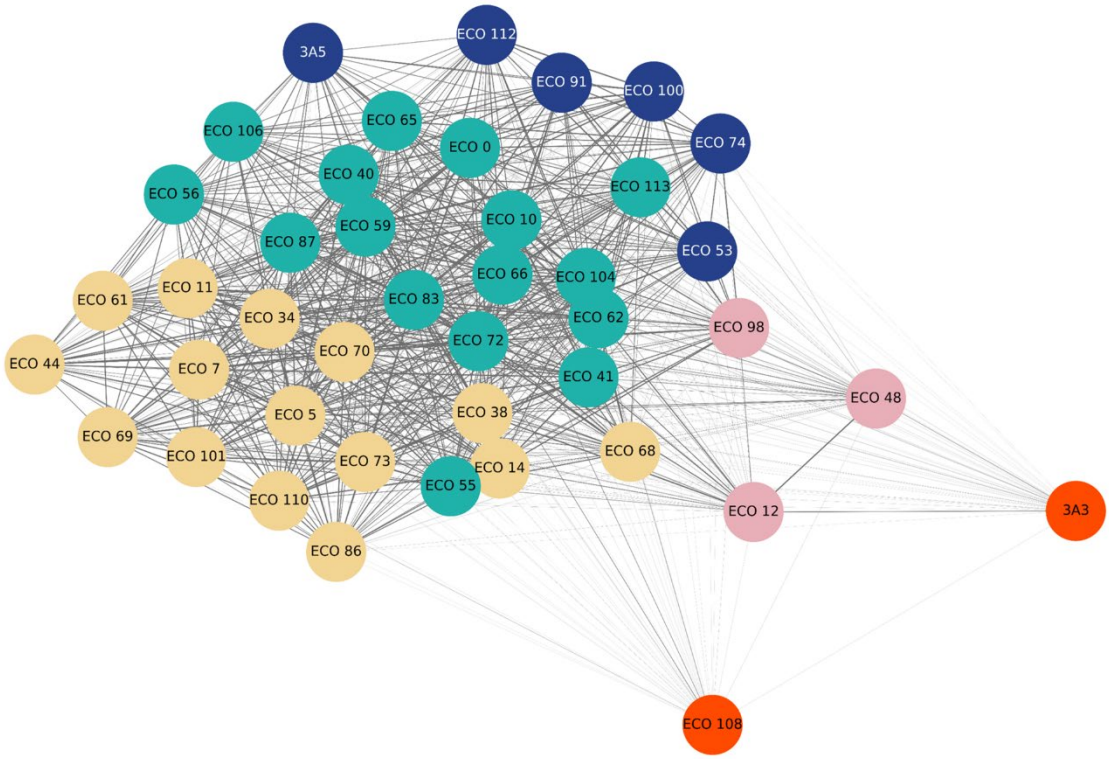


Figure 5.5-7: Exploring antibody competition for gB binding using a network analysis.
Network plot displaying the relationships between antibodies based on the pairwise competition scores. Nodes represent antibodies and are colour-coded as per the dendrogram in **Figure 5.5-6B**. Edges (grey lines) represent the reciprocal of the competition readouts from the symmetrised matrix. Node are positioned using the spring layout – a force-directed method in which nodes repel one another but are connected by spring-like edges whose spring constants are proportional to their edge weight. Iterations of node positions continue until the system reaches near-equilibrium. Heavily connected nodes (antibodies that compete with many others) fall towards the middle of the network. Weakly connected nodes (those that bind rare epitopes and show little competition) are positioned peripherally.

5.5.5 SPR-based Competition Measurements Reveal a Similar Profile to the ELISA-based Method

Competition measurements for antibodies recognising the gBect trimer were also made using an SPR-based method on an LSA Carterra Instrument. This method, orthogonal to the ELISA one above, was intended to serve as a sense-check for antibody competition screening. Ideally, competition behaviour for all mAbs would show similar profiles between the two.

The antibody panel was coupled to an LSA chip and subsequently flushed with trimeric antigen pre-complexed with mAb in a 10-fold molar excess. With this set-up, mAbs that competed for gB binding would produce low or no SPR signal as gB·mAb complexes would not be captured. Conversely, mAbs that did not compete would allow for successful complex capture and therefore give high SPR signals.

For each mAb, gB·mAb complex capture signals were normalised to those of an antigen-only control run as each antibody bound complexes with varying efficiency. Data from reciprocal mAb/mAb arrangements (on-chip ligand or pre-complexing mAb) were then averaged to create a symmetrised competition matrix.

In the cases of ECO12, 34, 48, 56, 61 and 98, antibody coupling on the chip occurred with very poor efficiency. These antibodies were subsequently unable to capture complexes of any kind, including then antigen-only control. Their on-chip ligand data were therefore removed from the larger dataset, meaning competition data for these antibodies was only available in one configuration. In these cases, SPR signals could not be averaged; instead, one-way values were used to construct the matrix.

Unsupervised clustering was conducted using Ward's method on the symmetrised competition matrix in a similar manner to the ELISA-based experiment. Selecting a distance threshold of five revealed a similar profile to the ELISA-based competition map, but with 7 clusters (***Figure 5.5-8A***). Antibodies 3A3, ECO12, ECO48, ECO98 and ECO108 have substantially different competition profiles to the rest of the antibody panel (***Figure 5.5-8B***).

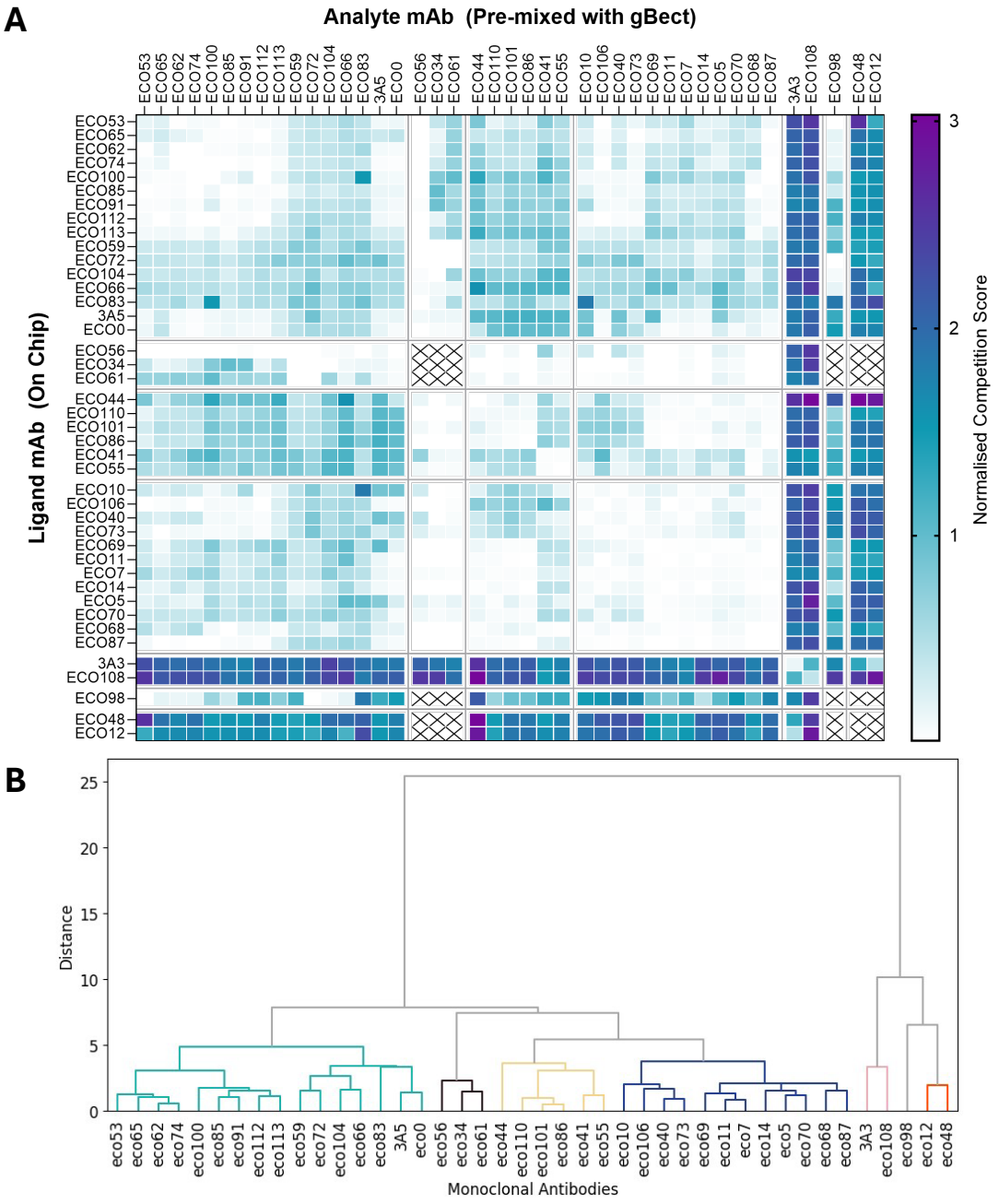


Figure 5.5-8: Cluster analysis of antibody competition by SPR using a Carterra.

(A) Heatmap of the symmetrised SPR competition matrix after hierarchical clustering using Ward's minimum variance method. Symmetrisation of competition scores was performed by averaging singlicate SPR signals for each mAb/mAb pair after normalisation to the signal of an antigen-only run. A cluster cut-off distance of 5 was chosen based on inspection of the dendrogram in (B), yielding seven clusters (separated by grey lines). Antibodies are ordered by linkage distance. For antibodies ECO12, 34, 48, 56, 61 and 98, their chip coupling efficiency was insufficient to yield real competition data with these antibodies acting as the on-chip ligands. For these mAbs, the result is that competition scores are calculated using only those values where these antibodies are used to pre-complex gB. Given this, competition with themselves and one another could not be determined for these antibodies (grey crosses).

(B) Dendrogram produced from the symmetrised matrix of mAb/mAb competition. Clusters were defined using a Ward's distance cut-off of 5 and are colour-coded to best match clusters identified by the ELISA method.

The remaining antibodies fall into larger clusters for which competition behaviour is more heterogeneous – though 'global' competition behaviour is similar between clustered mAbs, analysing individual mAb/mAb competition conditions are not always the same. Both from the cluster analysis and investigating these mAbs' relationships as a network (***Figure 5.5-9***), mAbs across these larger clusters have 'overlapping' competition behaviour; the differences in their competition profiles are not as distinct as for antibodies ECO12, 48, 98 and 108. This would support the ELISA data that suggests most antibodies in the panel bind in ~2-3 epitope regions, at a separate site to the 'rare binders' (3A3, ECO12 etc.).

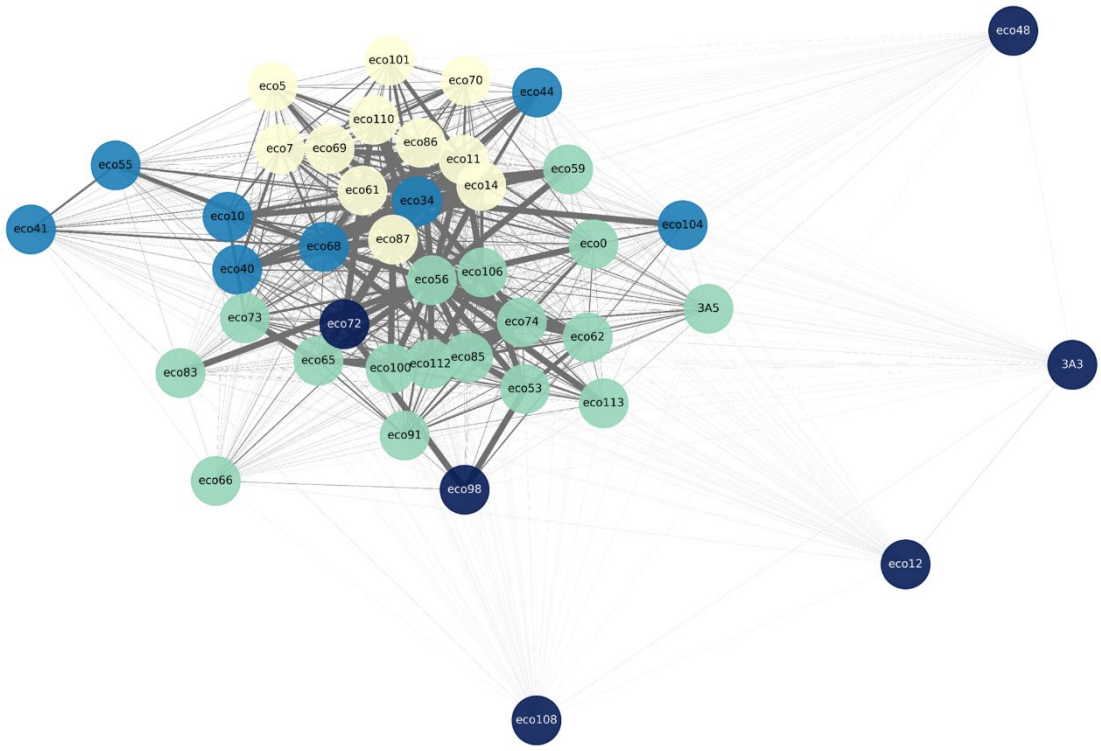


Figure 5.5-9: SPR-based competition interactions plotted as a network.
Network plot constructed using the SPR data for mAb competition after symmetrisation. The network was constructed in the same fashion as **Figure 5.5-7**. However, here nodes are coloured based on their community, determined using the Louvain community detection method, rather than by using their identified cluster. This iterative method assigns antibodies to communities such that a modularity score is maximised, a measure of how similar nodes in a sub-network are if the network is divided. It may represent an alternative method of exploring competition interactions between mAbs.

To assess how well the two assays' findings agree with one another, a correlation analysis was conducted. Competition readouts were plotted for all mAb/Fab pairs tested in the ELISA that were also screened as a mAb/mAb pair by SPR (1250 pairs, ***Figure 5.5-10***). The two assays showed moderate correlation for antibody pairs screened (Pearson $r = 0.4676$, $p < 0.0001$).

mAb/mAb pairs that produced high ELISA readouts (non-competitors) tended to have high SPR readouts (non-competitors). For pairs with low ELISA scores (competitors), corresponding SPR values were more variable. Nonetheless such pairs did generally result in SPR values substantially below the median.

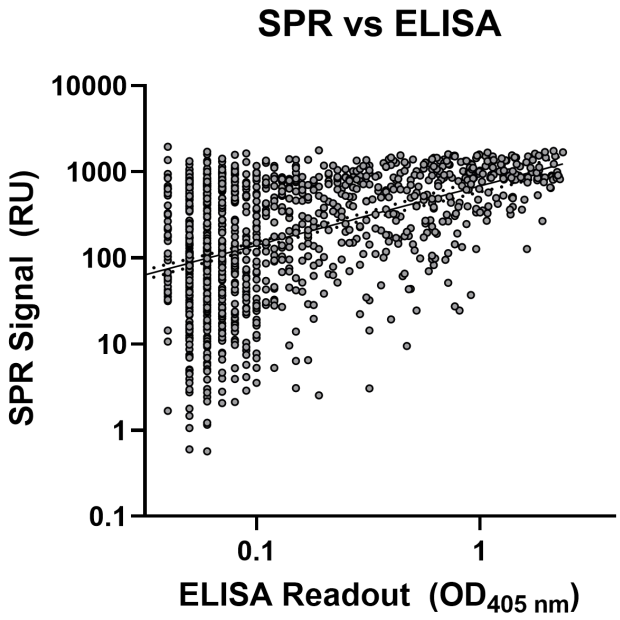
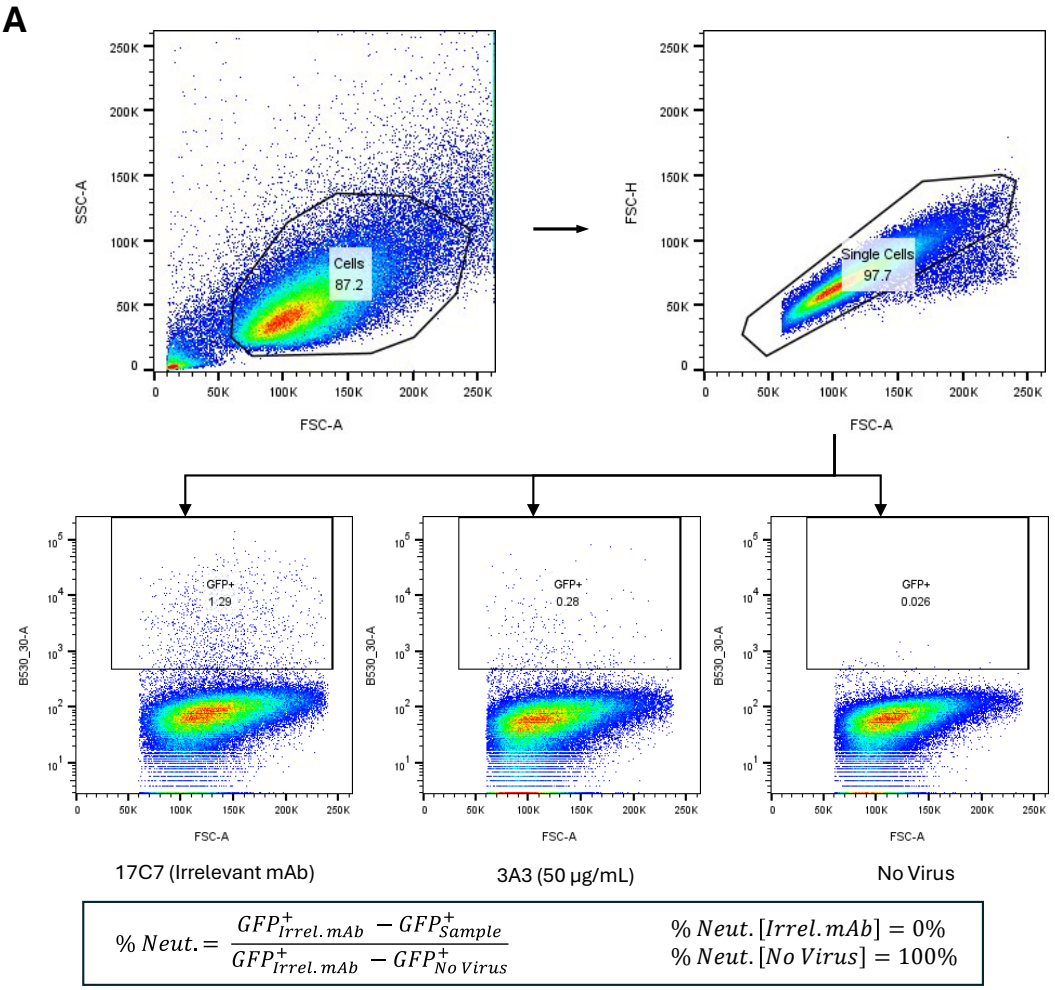


Figure 5.5-10: Correlation between two different competition assays.
XY plot for mAb/Fab pairs tested for binding competition by ELISA and their corresponding mAb/mAb pair tested by SPR. Each point represents a pair of antibodies in a particular orientation. For example, where the ECO0 mAb was used to as the coating antibody for the ELISA protocol, and ECO5 used as the pre-complexing Fab, the ELISA score is plotted against the SPR signal for the condition where ECO0 is coupled to the LSA chip, and ECO5 is the pre-complexing antibody. For both the SPR and ELISA data, large values represent binding, i.e. no competition between mAbs, and low values correspond to competition. Data is representative of all permutations for which ELISA and SPR data existed after exclusion of antibodies that did not couple to the chip (1250 pairs). The line of best fit was calculated by simple linear regression on the log-transformed data in GraphPad Prism ($R^2 = 0.2186$, $p<0.0001$), shown with 95% confidence intervals (dotted lines).

5.5.6 Two New mAbs Efficiently Neutralise *In Vitro* Infection of B Cells and Epithelial Cells by EBV

GFP-tagged EBV was produced from Akata B cells and 2089/293 epithelial cells for the infection of HEK293T and Raji B cells, respectively. Infection assays were performed using methods based on those described elsewhere in the literature (Sashihara *et al*, 2009; Li *et al*, 2022), using flow cytometry to determine the percentage of susceptible cells that expressed GFP. Gating strategies for both neutralisation assays were the same, an example of which is shown (***Figure 5.5-11A***). The raw percentage GFP^+ values for each neutralisation condition were converted into '% neutralisation' scores by normalising the data such that 0% neutralisation corresponded to the $\%GFP^+$ observed in a control condition containing an anti-RabG mAb, 17C7, and 100% neutralisation corresponded to those observed in wells that were not exposed to virus (***Figure 5.5-11A***).

mAbs in the panel were first screened for their ability to neutralise infection of Raji B cells. This assay was performed using a single, high concentration of antibody (50 μg/mL) to act as an initial measure of neutralising capability. Analysis of the normalised neutralisation data revealed four new mAbs, ECO12, 48, 100 and 108, that were able to partially neutralise infection at this concentration (***Figure 5.5-11B***). The majority of mAbs, however, did not neutralise infection but instead appeared to enhance viral entry, as will be discussed later.



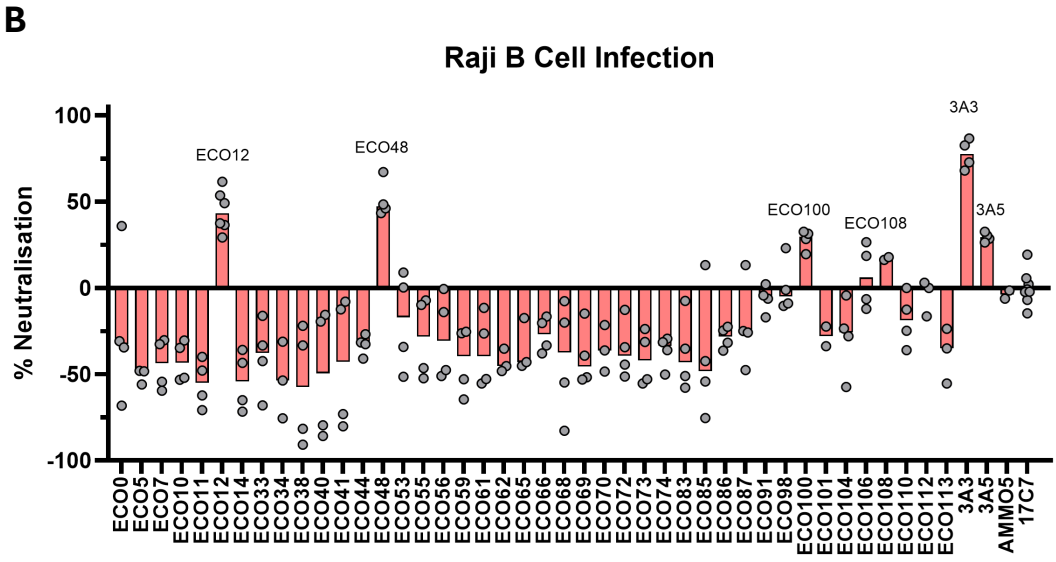


Figure 5.5-11: Neutralisation of in vitro Raji B cell infection with EBV-GFP.

(A) Example gating strategy for all neutralisation assays conducted. Shown are plots for control conditions: 17C7, an anti-RabG antibody used as the '0% neutralisation' condition, 3A3, a previously published neutralising antibody and a no-virus condition, used as the '100% neutralisation' condition. The method of normalisation used to produce '% Neutralisation' scores is shown.

(B) % Neutralisation scores for all mAbs in the panel tested at 50 µg/mL against Raji B cells. Grey data points represent individual wells of the infection assay from two experiments conducted on different days. %GFP⁺ values are normalised to no-virus and irrelevant mAb conditions tested on the same day. Red bars represent the mean values across all normalised replicates. 17C7 was included as the '100% infection' condition.

Due to limited reagent availability (complement and virus), more detailed investigation focused initially on two of the new neutralising mAbs. Two-fold serial dilutions of ECO12, ECO100 and 3A3 were first tested by the same assay, with and without the addition exogenous guinea pig complement. ECO12 exhibited comparable neutralising ability to 3A3 in the absence of complement, whilst ECO100 was less potently neutralising (***Figure 5.5-12A***). The addition of guinea pig complement was performed in a similar fashion to *in vitro* neutralisation studies of HCMV (Loomis *et al*, 2013). For Raji B cell infection, however, exogenous complement inhibited infection in the control RabG mAb condition (***Figure 5.5-12A***), suggesting its activation by a mechanism independent of antigen-specific antibody.

The subsequent testing of ECO108 and 3A5 was therefore performed without complement. ECO108 behaved similarly to ECO100, achieving <50% neutralisation at the highest tested concentration (***Figure 5.5-12A***).

Attempts to characterise the neutralisation ability of ECO48 were hampered by challenges with the production of virus, discussed later. Generation of a neutralisation curve was eventually achieved using a different, less infectious, preparation of virus to that used for the other mAbs (***Figure 5.5-12B***). However, comparing the neutralisation curve of the 3A3 control in this experiment to previous assays, the normalised % neutralisation of 3A3 at all concentrations appears down-shifted. Given this, while ECO48 appears to exhibit comparable potency to 3A3 in this assay, repeat infection assays are required to determine quantitative (EC_{50}) neutralisation potencies. Nonetheless, overall, the four neutralising antibodies' behaviours in dilution series appeared consistent with the initial neutralisation screen of the mAb panel.

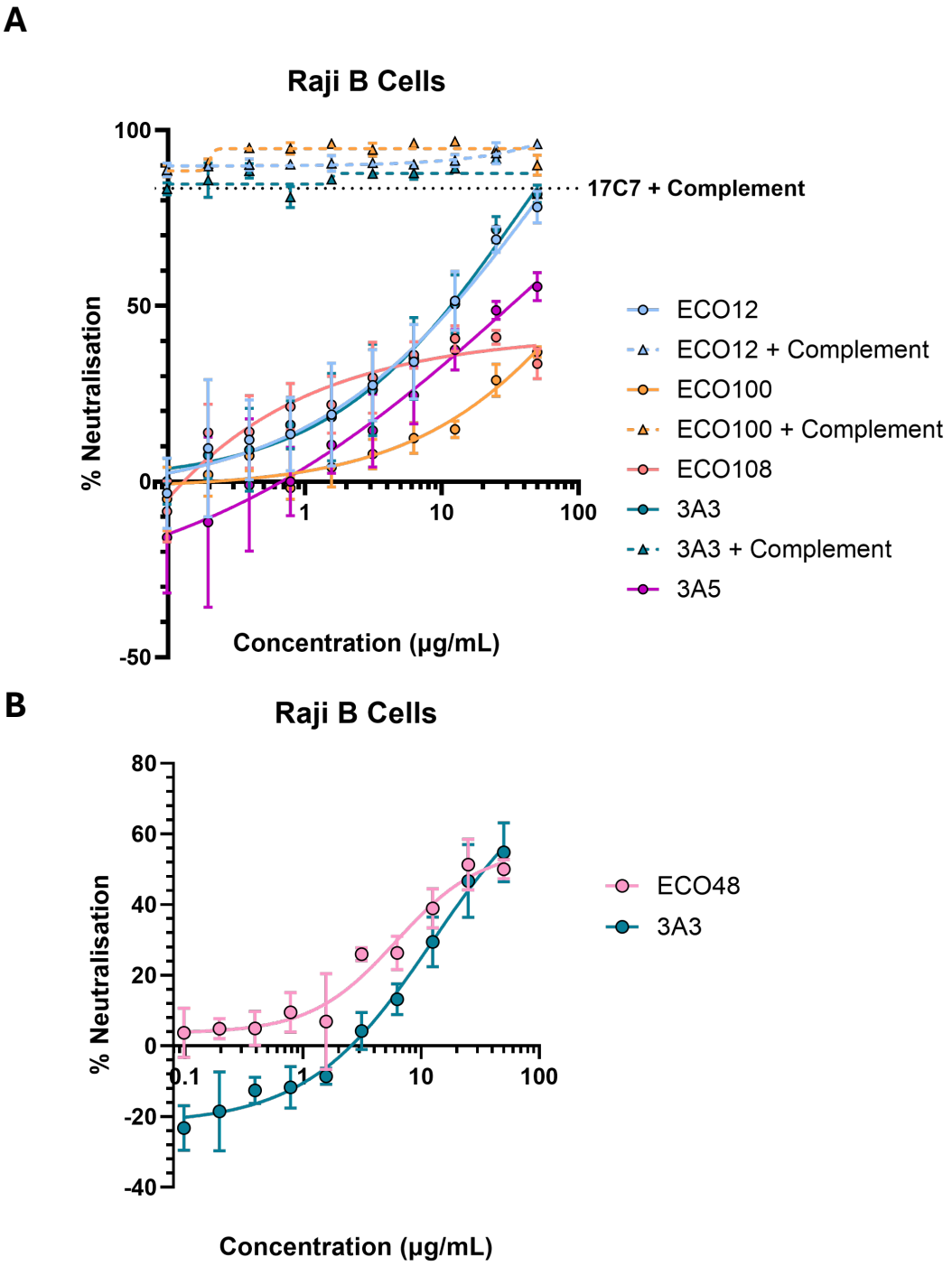


Figure 5.5-12: Dilution series for antibodies capable of neutralising Raji B cell infection in vitro.

A) Neutralisation curves for two newly identified neutralising antibodies, ECO12 and 100, with and without the addition of exogenous guinea pig complement. The previously-identified antibody 3A3 is included positive control. The dotted line represents the % Neutralisation score of an irrelevant mAb, 17C7, with added complement, normalised to no-complement condition. Data points represent mean values across 4 technical replicates except for ECO12 without complement (n = 12) and 3A3 without complement (n = 6).

B) Neutralisation curves for ECO48 and 3A3 without exogenous complement. Data points represent mean values across 4 and 2 technical replicates for ECO48 and 3A3, respectively.

In all cases, error bars represent the standard deviation. 4-parameter curve fitting (lines) was performed for each neutralisation condition in GraphPad Prism.

※

The panel was also screened for neutralising functionality against EBV infection of epithelial cells. By a similar assay to that used for Raji B cell infection, a greater proportion of mAbs in the panel exhibited some ability to neutralise infection (***Figure 5.5-13A***). ECO48 was omitted from this assay, as a result of purification difficulties. Of those tested, ECO12, 100 and 108 were the most potent – ECO12 appeared to be 100% neutralising at this concentration, comparable to 3A3.

These antibodies were investigated in more detail, as for Raji cell infection, in the presence and absence of guinea pig complement. Here, complement activity did appear to be dependent on the presence of an anti-EBV mAb (***Figure 5.5-13B***), with only a mild (20%) infection-inhibiting effect of complement with the non-EBV-specific control mAb. ECO100, in contrast, showed a substantial increase in its potency when administered with complement versus without (***Figure 5.5-13B***). Conversely, complement did not appear to change the potency of ECO12. Where they could be determined, EC_{50} values (mAb concentration required for a % neutralisation score of 50) are summarised in ***Table 5.5-1***.

	On Raji B Cells		**On HEK293T Cells**	
Antibody	EC50 (95% CI) (μg/mL)	EC50 + comp. (95% CI) (μg/mL)	EC50 (95% CI) (μg/mL)	EC50 + comp. (95% CI) (μg/mL)
ECO12	12.1 (9.8 – 15.1)	???	2.4 (2.1 – 2.8)	3.5 (2.4 – 5.8)
ECO100	>50	???	5.8 (2.8 - ???)	0.7 (0.6 – 0.9)
ECO108	>50	Not tested	Not tested	Not tested
3A3	11.5 (9.4 - 14.6)	???	2.4 (1.9 – 3.4)	Not tested
3A5	31.6 (19.8 - ???)	Not tested	Not tested	Not tested

Table 5.5-1: EC_{50} values for all mAbs tested by *in vitro* neutralisation of EBV infection of Raji B cells and HEK293T cells. Values were calculated by interpolating the concentration that would yield a % neutralisation score of 50% using the 4-parameter logistic curves fitted to each dataset in GraphPad Prism. '???' represents where values or confidence limits were incalculable.

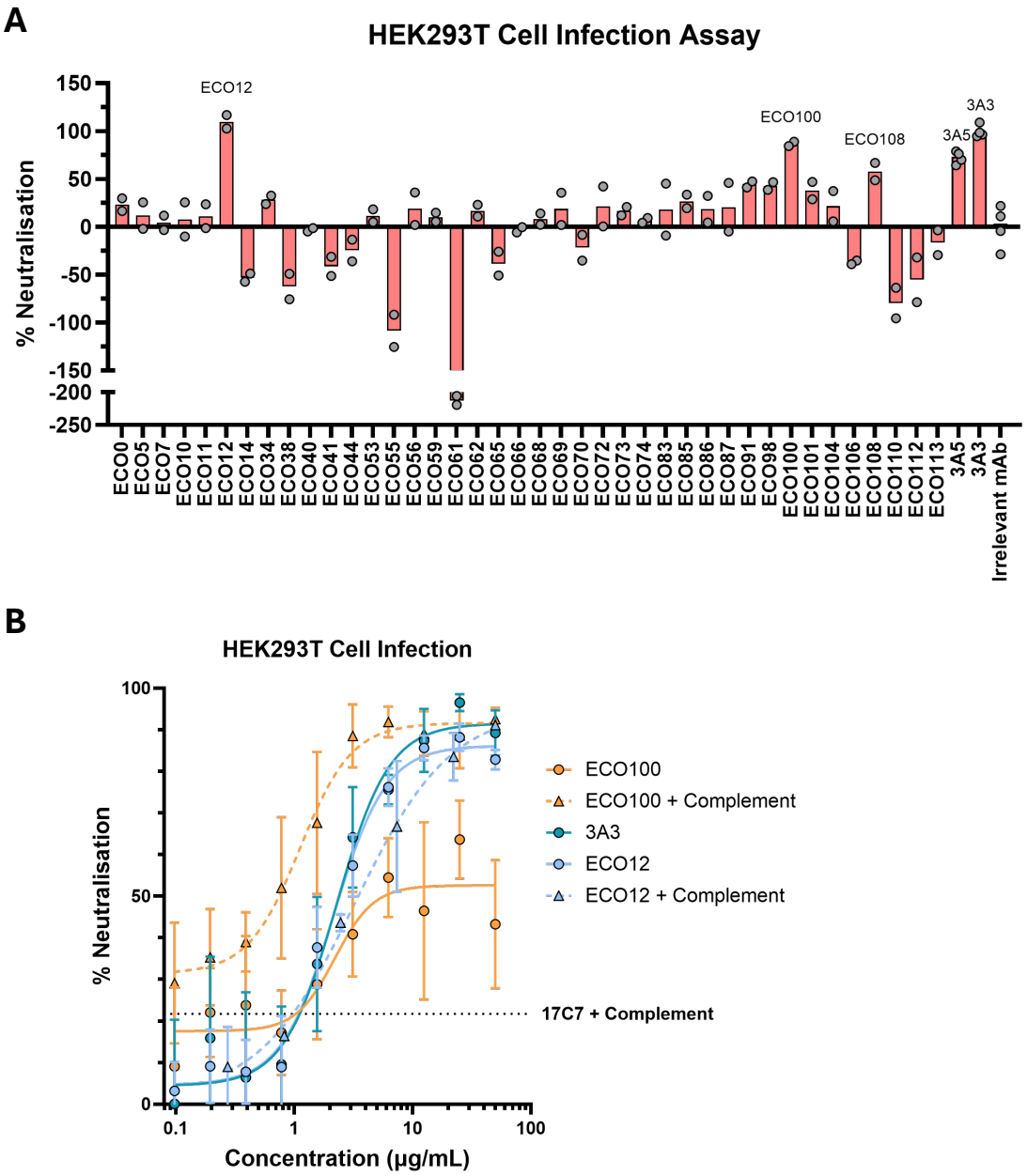


Figure 5.5-13: *In vitro* neutralisation of HEK293T cell infection by EBV-GFP.

(A) % Neutralisation scores for all mAbs in the panel tested at 50 µg/mL against HEK293T cells. Grey data points represent individual wells of the infection assay. %GFP⁺ values are normalised to no-virus and irrelevant mAb conditions. Red bars represent the mean values across normalised replicates. Irrelevant mAb = 17C7.

(B) Neutralisation curves for ECO12, ECO100 and a control mAb 3A3, in the presence (dotted lines) and absence (solid lines) of exogenous guinea pig complement. Data points represent mean values across replicate wells (n = 8 ECO100 ± complement, n = 4 3A3, ECO12, n = 2 ECO12 + complement for each dilution). The dotted line represents the % Neutralisation score of an irrelevant mAb, 17C7, with added complement, normalised to no-complement condition. Error bars represent the standard deviation. 4-parameter curve fitting (lines) was performed for each neutralisation condition in GraphPad Prism.

5.5.7 Apparent Infection Enhancement by Some mAbs in Neutralisation Assays is Not Dose-dependent

Inspection of the initial mAb screens against infection of both epithelial and B cells revealed several antibodies with negative % neutralisation scores, suggesting the possibility that such mAbs may enhance *in vitro* infection by EBV (***Figure 5.5-11B***, ***Figure 5.5-13A***).

Three such mAbs, ECO55, ECO61 and ECO69 were investigated in more detail with respect to Raji cell infection, where this behaviour appeared common across the panel. Serial dilutions revealed that whilst normalised % neutralisation scores of these antibodies were negative across the concentration series, the effect did not appear to be dependent on mAb dose, and error bars were wide (***Figure 5.5-14***). The dilution series for ECO61 was kept separate to those of ECO55 and 69 as assays were performed on different days, with the 3A3 positive control exhibiting notably different behaviour between the two experiments. Interpretation of these findings is discussed below.

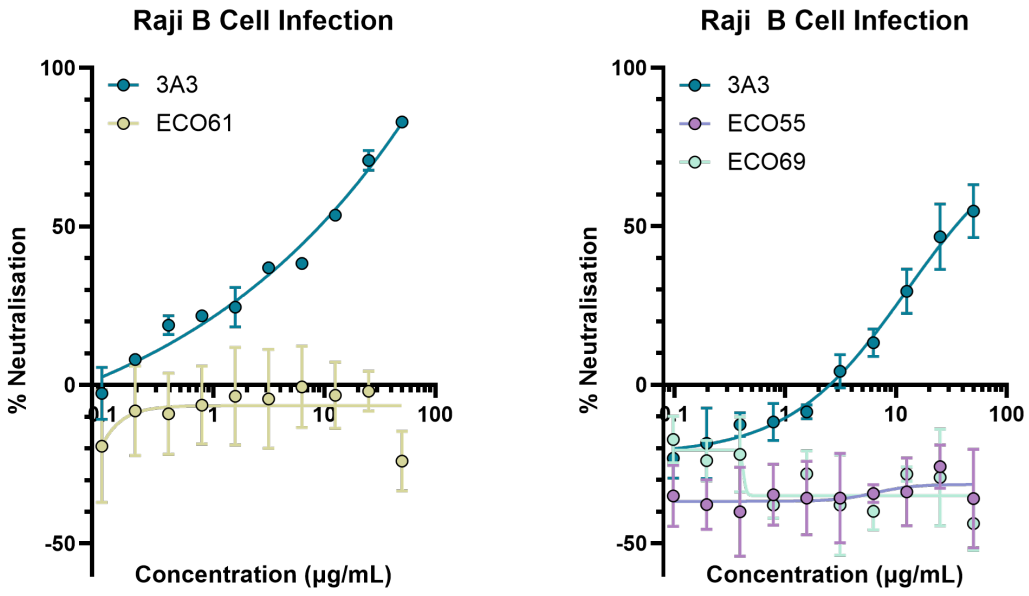


Figure 5.5-14: Antibodies displaying 'enhancement'-like behaviour.
Neutralisation curves for three antibodies, ECO55, 61, and 69 to investigate their possible enhancement of EBV infection in vitro. 3A3 was included positive control for neutralisation. Data points represent mean values across 4 replicate wells for each dilution apart from 3A3 (n = 2). Data from different experiments are plotted on separate graphs to highlight the differences in the 3A3 positive control curve.
Error bars represent the standard deviation. 4-parameter curve fitting (lines) was performed for each neutralisation condition in GraphPad Prism.

5.6 Discussion

5.6.1 Mapping the Antigenic Landscape of gB

The efforts described here to characterise the binding of an anti-gB mAb panel represent the largest conducted so far.

Western blotting suggested that the new mAbs recognise a mixture of linear and conformational epitopes across both furin cleavage fragments in the gB ectodomain. Despite this apparent range in mAb binding sites, only two antibodies recognise epitopes that are substantially modified by the presence or absence of N-glycans. This is somewhat surprising given how extensively gB is N-glycosylated: 9 sites on the ectodomain are consistently modified with diverse high-mannose and complex glycans (Joel Allen, unpublished).

These findings indicate that there are epitopes on the surface of post-fusion gB recognised by both neutralising and non-neutralising antibodies that are not masked by N-glycans. Given, however, that these antibodies were isolated using gB-based probes that we fully glycosylated, it is not possible to fully discount N-glycosylation-based epitope masking on gB as an important immune evasion strategy used by EBV. Were neutralising epitopes masked in this way, the mAb isolation strategy used here would not isolate mAbs against them and so these epitopes would remain uncharacterised, a limitation of this antigen mapping study.

The markedly different conformations of pre- and post-fusion gB may produce a conformationally specific glycan-dependent masking effect: glycans might obscure mAb binding sites in one conformation, not the other. This is speculative, however, and requires in-depth study to determine whether such an effect exists.

※

Analysis of gB-mAb binding competition suggests that antibodies isolated in this work bind diverse epitopes but may be clustered into 5-7 groups based on common competition profiles. To try and characterise these clusters as robustly as possible, two mapping

techniques were employed and results compared across both. Despite some discordance between results from the different techniques, there was overall a reasonably good correlation. For the ~70% of pairs giving concordant results across the two techniques (i.e. doubly positive for competitiveness or doubly negative), the use of the orthogonal techniques provides a high degree of confidence in their 'competitiveness'.

The reasons for the imperfect agreement between the two assays are unknown, though it may well be related to the challenges of working with a trimeric antigen. This necessitated using more complicated competition assays in which a pre-incubation of antigen and antibody 'off-chip' or 'off-plate' was required.

Decorating the gB trimers with antibody (or Fab) was performed with large molar excesses of antibody to saturate binding epitopes on the antigen. It is, however, still possible that epitopes on the trimer remain exposed and, thus, the gB·mAb complex might be captured in the assay despite both mAbs recognising overlapping epitopes.

Studying the correlation between the two assays, where there are mAb/mAb pairs that are ELISA-negative (i.e. competitors), there is spread about the line of best fit with respect to their SPR-based signals. That is to say, some of these antibody pairs appear to be assay double-negatives, whilst others are only ELISA-negative. This would suggest that either the ELISA-based assay is less sensitive to gB·mAb complex capture and, thus, false positives for competition are identified, or that the SPR-based assay is 'leakier', permitting capture of complexes when in actual fact the two mAbs compete.

In both assays, it was not possible to define a clear cut-off value for what was competition and non-competition. Instead, the data are more continuous in nature. To overcome this challenge, methods of analysing both the SPR and ELISA data were developed to better handle continuous datasets rather than a competition/no-competition categorical set that might typically by analysed downstream of the LSA Carterra (Barrett *et al*, 2024).

In this case, competition matrices and network plots were generated using 'competition scores' that may represent clear competition, non-competition or anything in between. This approach permitted clustering analysis on an imperfect dataset to identify patterns

in antibody binding behaviour. Its principal limitation, however, was that conclusions drawn on the competition behaviour of the anti-gB mAbs can only be done at the system level. Diagnosing two mAbs as being definite competitors or definite non-competitors may not be possible for all mAb/mAb pairs, but at least for a large proportion.

Upon studying the mAb panel after clustering analysis, substantial differences in the size of these clusters are evident. This might shed light on which domains are more immunodominant than others, at least for the mouse antibody response. Importantly, the larger clusters contain few antibodies capable of neutralising B cell infection *in vitro*. Instead, antibodies identified as having some effect on EBV infection appear to have markedly different competition profiles to the rest of the panel, suggesting they recognise distinct and rarer epitopes.

Though competition mapping performed here does not reveal the actual binding sites of mAbs on the antigen, antibodies are more likely to compete with one another if their epitopes are overlapping or adjacent to one another. Given this, it appears the major mAb clusters bind to regions of the gB ectodomain that, by and large, do not contain neutralising epitopes.

The cluster analysis performed on data from the LSA Carterra reveals heterogeneity in the competition profiles of mAbs in the larger clusters; mAbs in the same cluster occasionally show competition behaviour that is noticeably different to one another. The ELISA data, however, appears to have identified groups of antibodies that are, by-and-large, homogenous in their behaviour upon inspection of the heatmap.

For the two largest clusters identified by the ELISA method, the most substantial difference between their competition profiles is their competitiveness with antibodies in the group containing 3A5. The ECO0-containing cluster generally competes with that containing 3A5, whilst the ECO5-containing cluster does not.

These findings might permit the first attempt to map antibody binding on the post-fusion structure of gB. Given 3A5's binding to DIV of gB (Zhang *et al*, 2022), mAbs ECO53, 74, 91, 100 and 112 in the same group may recognise epitopes in this domain as well.

This is supported by Western blot data that shows ECO74, 91, 100 and 112 all bind the 40 kDa fragment of gB, containing DIV.

These mAbs' competition with the ECO0-containing cluster suggests the latter bind a region of partial overlap, either in or proximal to DIV. The ECO5-containing cluster does not generally compete with mAbs of the 3A5 group but does with the ECO0 group. This suggests mAbs in the ECO5 cluster recognise remote sites to those of the 3A5 cluster, and sites adjacent to those in the ECO0 cluster. Again, representative mAbs in each of ECO0 and ECO5 clusters recognise the 40 kDa fragment by Western blot, further evidence that the three largest mAb clusters bind somewhere on the 'crown' of the gB ectodomain.

Taken together, these results suggest the existence of three distinct antigenic sites toward the crown of the post-fusion structure, hereby referred to as Site 1, recognised by the 3A5-containing cluster, Site 2, recognised by the ECO0-containing cluster and Site 3, corresponding to the mAbs in the ECO5 cluster (***Figure 5.6-1***). A fourth site distal to all three of these, Site 4, recognised by 3A3, ECO12 and ECO48 is discussed in more detail below.

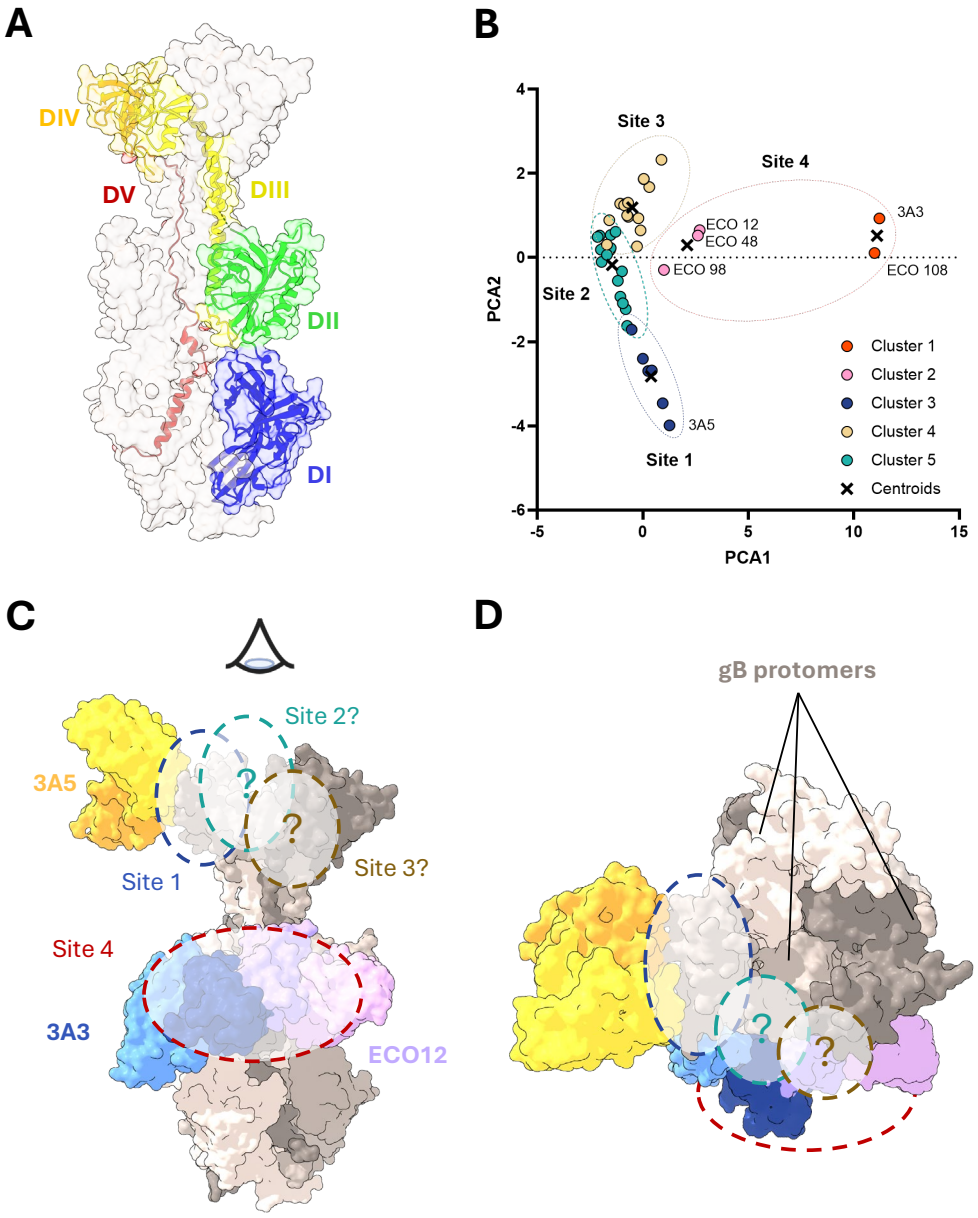


Figure 5.6-1: Proposed antigenic sites on the post-fusion conformation of gB.

(A) The gB ectodomain trimer (PDB: 3FVC). Protomers are shown as surfaces. For a single protomer, domains I (blue), II (green), III (yellow), IV (orange) and V (red) are shown as a surface and a ribbon cartoon. Centroids (black crosses) are shown for each cluster

(B) Competition data generated using the ELISA based method shown in **Figure 5.5-6**, plotted via a principal component analysis plot. Data points represent individual mAbs and are colour coded based on their cluster, identified using Ward's method, as shown in **Figure 5.5-6**. These 5 clusters are proposed to form four 'antigenic sites', dubbed Site 1-4 (dotted circles), based on common features of the competition profiles of the mAbs within them.

(C) Side-view of the post-fusion structure of gB coordinated by three structurally characterised antibodies, 3A5 (yellow), 3A3 (blue) and ECO12 (purple). These structural analyses are the subject of *Results IV*. For clarity, only a single Fab fragment for each antibody is shown on the gB trimer. The antigenic sites on the gB ectodomain are shown. Sites 2 (teal) & 3 (beige) have not been structurally characterised – their locations on the gBect surface can only be inferred by their relative competition with the other antigenic sites. mAbs recognising Site 2 compete with those of 1 & 3, but not 4. mAbs against Site 3 compete with those of 2 only. Together this suggests 2 & 3 are toward the DIV 'crown' of the post-fusion structure, with Site 2 proximal to Site 1, and Site 3 distal to Site 1.

(D) Top-down view of the decorated trimeric ectodomain in (C).

Given the challenges of the competition datasets, an exploratory, alternative analysis framework was investigated, in which the data were analysed using network theory. Taking a similar approach to those employed in the study of social networks (Bedi & Sharma, 2016), graphs were constructed in which antibodies are connected by edges weighted with their competition scores. Performing Louvain community detection on the network subsequently allowed for the identification of mAb communities in an unsupervised manner.

These communities show good agreement with those of the unsupervised clustering approach. Additionally, such analysis permits the plotting of networks using an iterative, force-directed method, the spring layout. Using the magnitude of the competition connections between mAbs, this represents a useful way of visualising antibody competition by 'likeness' scoring. This is used to plot common competition phenotypes at the centre of the graph, and rarer phenotypes at the periphery.

This orthogonal analysis technique provides further support to the notion that antigenic Sites 1, 2 and 3 are overlapping and/or proximal – mAbs in these clusters fall at the heart of the network in a dense, overlapping core. mAbs recognising Site 4, however, are consistently spread around the outside of the network, highlighting their unique competition profiles and, by inference, their remote epitopes relative to the majority of the panel.

5.6.2 Desirability of Improved EBV Production Methods

In trying to determine the potency of the mAbs in this panel with respect to *in vitro* B and epithelial cell infection, significant challenges were encountered. The greatest of these was the difficulty of making large, highly infectious batches of EBV virus from Akata and 293/2089 cell lines.

Despite substantial effort to try and optimise the production of EBV over the course of this work, typical %GFP$^+$ rates for ultracentrifuged virus preps were between 1-2%. Though few studies report raw GFP$^+$ infection rates, other research groups have achieved >30% (Escalante *et al*, 2024). To achieve meaningful neutralisation data with low-titre

virus, hundreds of thousands of flow cytometry events were captured and multiple replicates performed for each mAb to tighten error margins. This not only hampered throughput but required the use of large volumes of virus in each assay.

This work would therefore benefit substantially from improvements to virus production. Possible methods for this include investigating different EBV-producing cell lines such as CNE2-EBV-GFP cells (Zhang *et al*, 2022; Hong *et al*, 2022) or simply concentrating virus preps to higher orders of magnitude (Li *et al*, 2022).

The ability to do this is clearly critical for generating reproducible, high-quality neutralisation data. In this work, the inability to produce such virus prevented direct comparison of neutralising antibodies such as ECO48 and ECO12 given that the control antibody, 3A3, behaved so differently.

5.6.3 The Neutralising Response to gB

The antibodies that appear most potently neutralising, ECO12 and ECO48, compete for gB binding with the previously identified neutraliser, 3A3. This suggests that the three mAbs recognise epitopes in the vicinity of 3A3's structurally-defined epitope on DII (Zhang *et al*, 2022). In contrast, the partially-neutralising ECO108's lack of competition with essentially any other mAb in the panel suggests it recognises a particularly rare epitope, the location of which on gB cannot be reasonably inferred and might therefore not be classified into any of antigenic Sites 1, 2, 3, or 4.

The majority of the mAbs in this work were only tested for their ability to inhibit EBV infection in the absence of complement due to limitations on time. As a result, it is not possible to make general conclusions about the complement-mediated functionality of anti-gB antibodies. The complement-dependent enhancement of ECO100's neutralising ability is the first direct evidence of this phenomenon for an EBV gB-targeting antibody. Interestingly, however, complement's effect on mAb potency did not appear to be uniform. ECO12 showed no evidence of complement-enhanced neutralisation. Further study of the relationship between mAb neutralisation potency, complement and the position of epitopes on gB appears worthwhile.

5.6.4 Anti-gB Enhancement of Infection

A considerable number of anti-gB mAbs tested in the *in vitro* neutralisation assays appeared to have negative % neutralisation scores, implying some mechanism of antibody-induced enhancement of EBV infection. The effects of this do not appear dose-dependent, as might be expected were this enhancement a real phenomenon, however. Studying raw FACS plots suggests that higher %GFP$^+$ scores for some mAbs is not an issue of gating (***Figure 5.6-1***). Instead, however, the enhancement may be caused by a baseline issue – perhaps the 17C7 '0% neutralisation condition' is not at the true 0% mark. This might be supported by the fact that for the Raji cell assay in particular, the majority of the mAbs all fall at approximately -50% neutralisation – it may be the case that this value is the true baseline, though further troubleshooting of the *in vitro* assay(s) is required to prove this.

This phenomenon has not been reported before for anti-gB mAbs. Further characterisation of these antibodies is warranted to better understand this 'enhancement' effect. In particular, mAbs ECO55 and ECO61 display markedly different neutralisation/enhancement profiles to the other mAbs with respect to the HEK293T cell assay. If enhancement of infection were to be validated, understanding where these antibodies bind on the surface of gB is imperative. Such a finding would have significant implications on the pursuit of gB as a vaccine candidate.

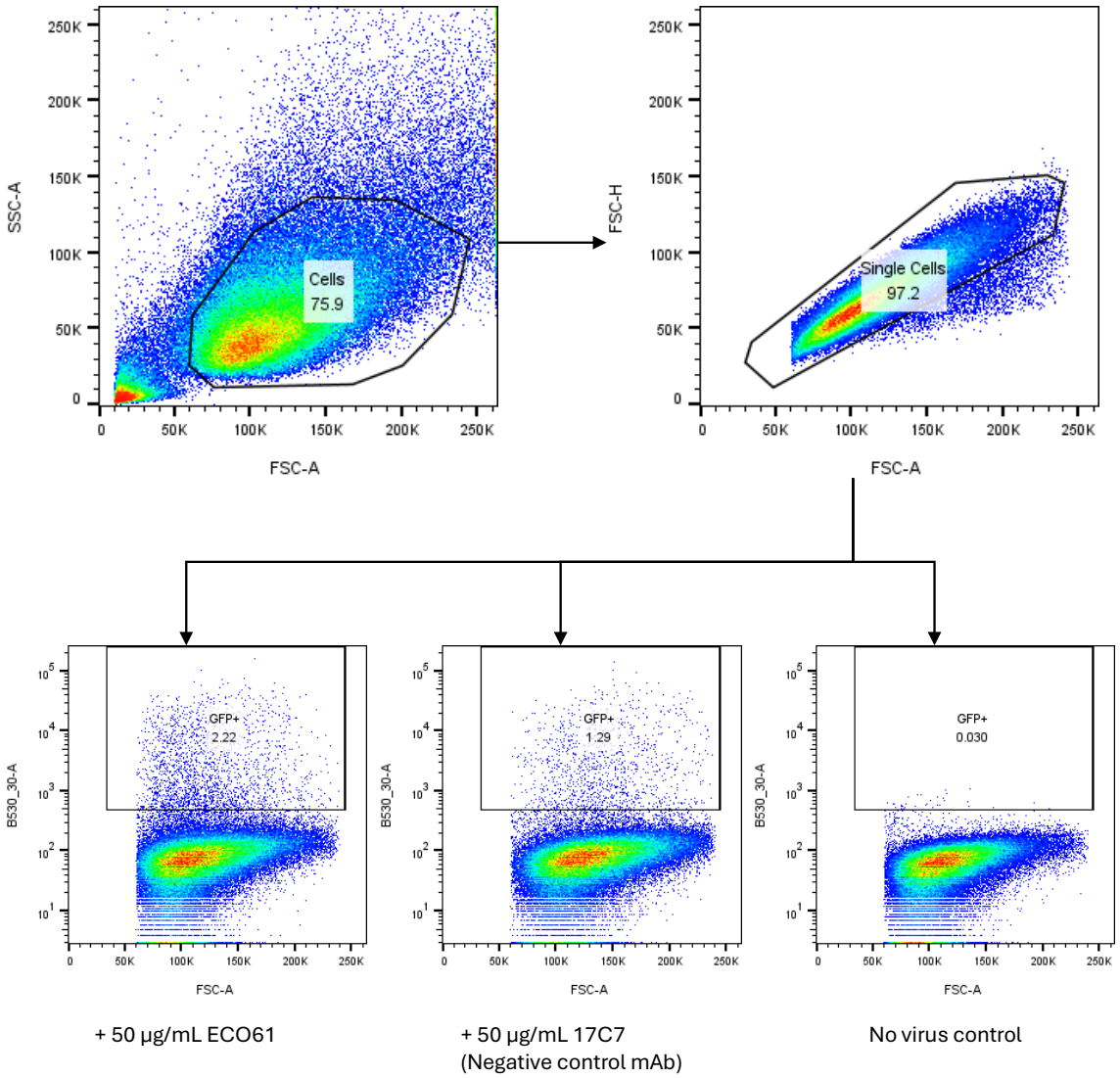


Figure 5.6-2: Example FACS gating for a mAb that 'enhances' in vitro Raji B cell infection.
GFP⁺ gating is shown for three samples (L-R): the ECO61 anti-gB mAb, one that displays enhancement-like behaviour, the 17C7 anti-RabG mAb control condition, used as the '0% neutralisation' normalisation control, and the no-virus condition used to define '100% neutralisation' for neutralisation.

5.6.5 Implications for Pre-fusion Stabilisation

Lastly, these findings should be considered in the context of the uncertainty about means or benefits of pre-fusion HHV gB stabilisation. As discussed in *Results II*, significant efforts were made to generate gB-reactive antibodies to membrane-expressed antigen to maximise the chances of isolating pre-fusion specific antibodies. No such antibodies were isolated. This implies that there truly are few pre-fusion specific epitopes on gB, that efforts to present full-length gB to the immune system by its expression in a membrane *in vivo* were insufficient to induce such antibodies, or that the screening method used was unsuitable for identifying them.

Though the evidence presented does not support a key role for the pre-fusion-specific response, stabilising this conformation may still convey advantages. Principally, if pre-fusion gB better presents neutralising epitopes to the immune system, stabilisation of the former may improve the quality of the antibody response to the antigen without necessarily inducing conformationally specific antibodies. Considering the major structural differences of the pre- and post-fusion conformations for HSV-1 (Vollmer *et al*, 2020; Heldwein *et al*, 2006) and HCMV gB (Liu *et al*, 2021a; Burke & Heldwein, 2015), it is reasonable to assume that EBV gB's pre- and post-fusion forms are also highly distinct from one another. Presentation of different epitopes by these two forms is therefore also feasible.

Little evidence exists to actually support this notion, however. Some of the findings of this work may in fact point to the opposite. Across the mAb panel and its controls, ECO12, ECO48 and 3A3 were some of the few neutralisers. Focussing on these mAbs' abilities to bind gBect by ELISA, and membrane-expressed gB by flow cytometry, these three antibodies form part a cluster of mAbs that poorly bind the latter (***Figure 5.6-2***). If anything, this suggests that a key region of vulnerability on gB, around DII, recognised by these three antibodies is better presented on the post-fusion gB ectodomain than on membrane-expressed gB (presumably pre-fusion). Though improved mapping of neutralising epitopes on gB is required to substantiate these findings, it is perhaps worth noting that potently neutralising antibodies 8A9 and 8C12 also bind DII (Hong *et al*, 2022), highlighting its importance as an antibody target.

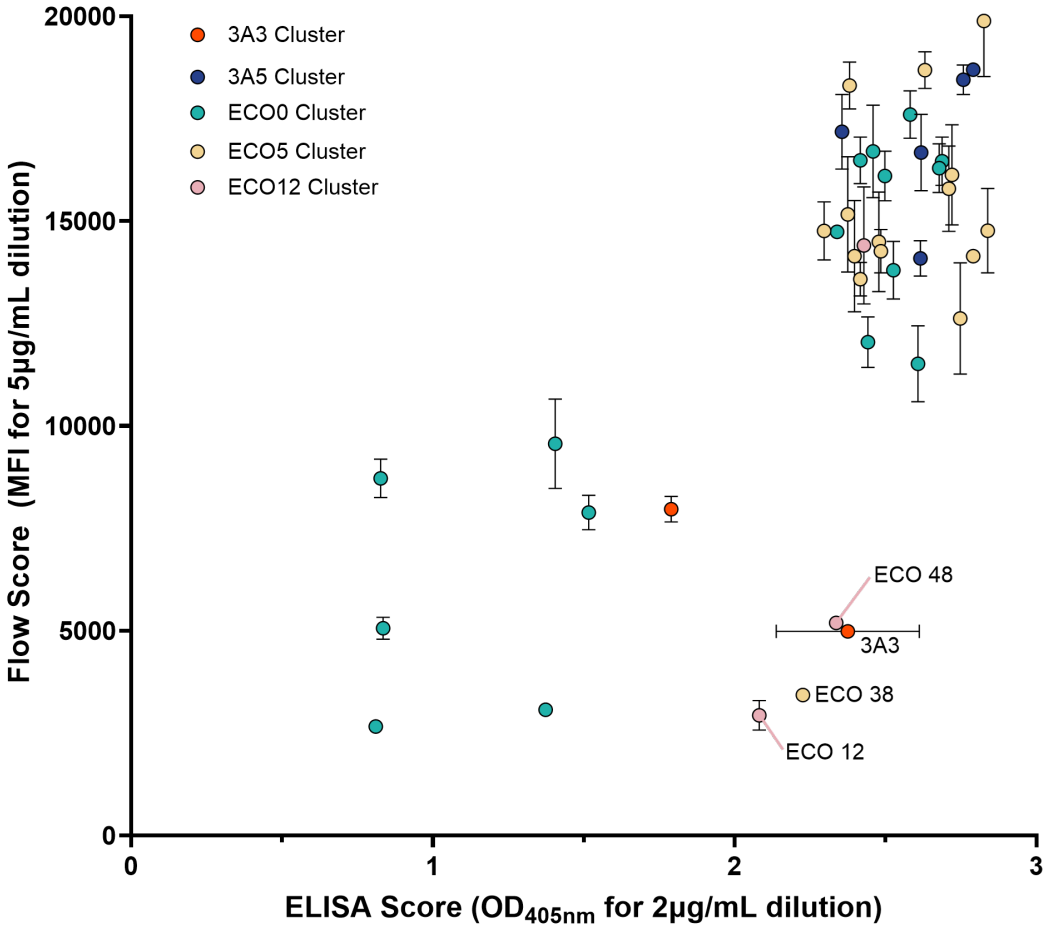
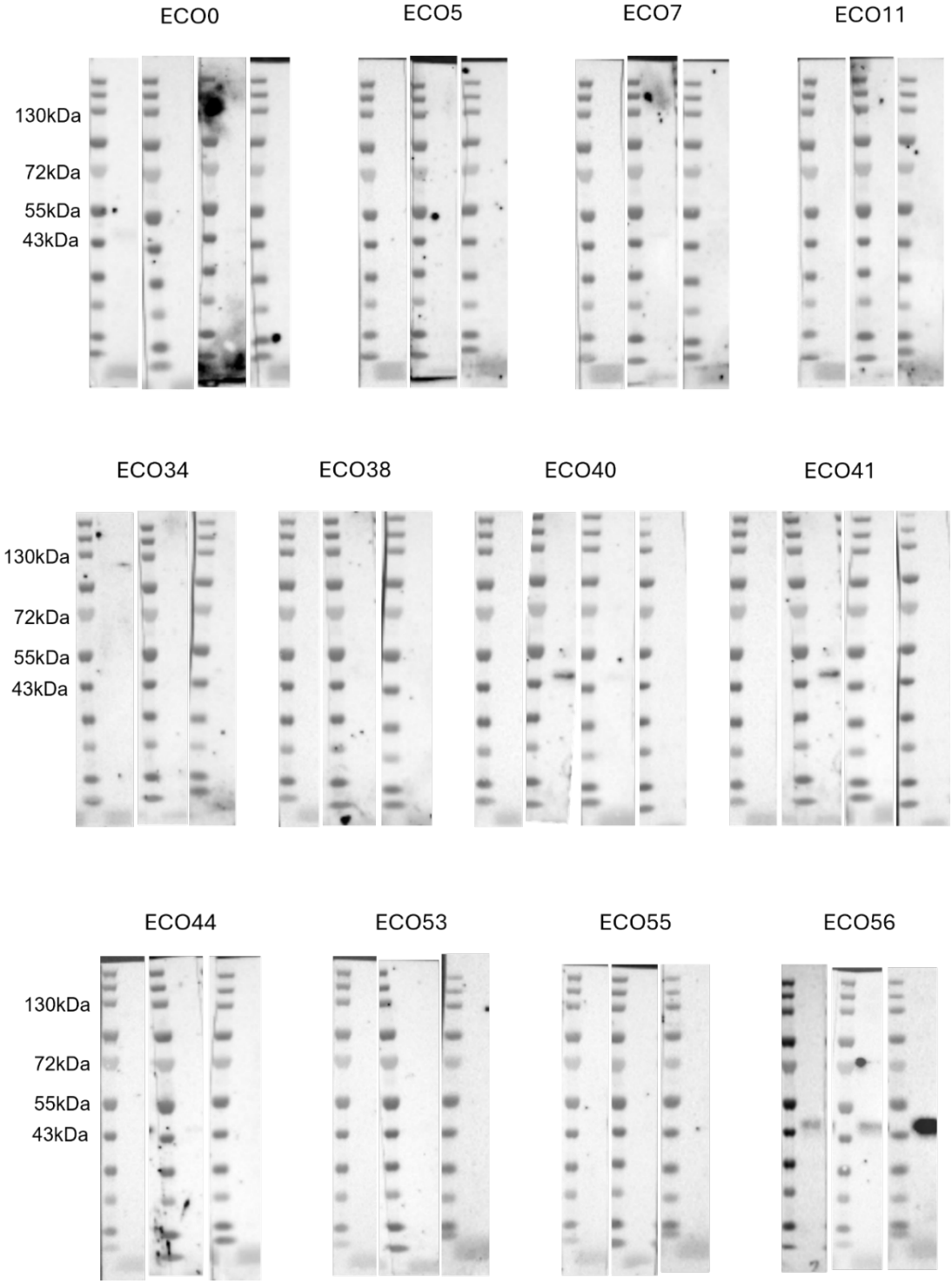
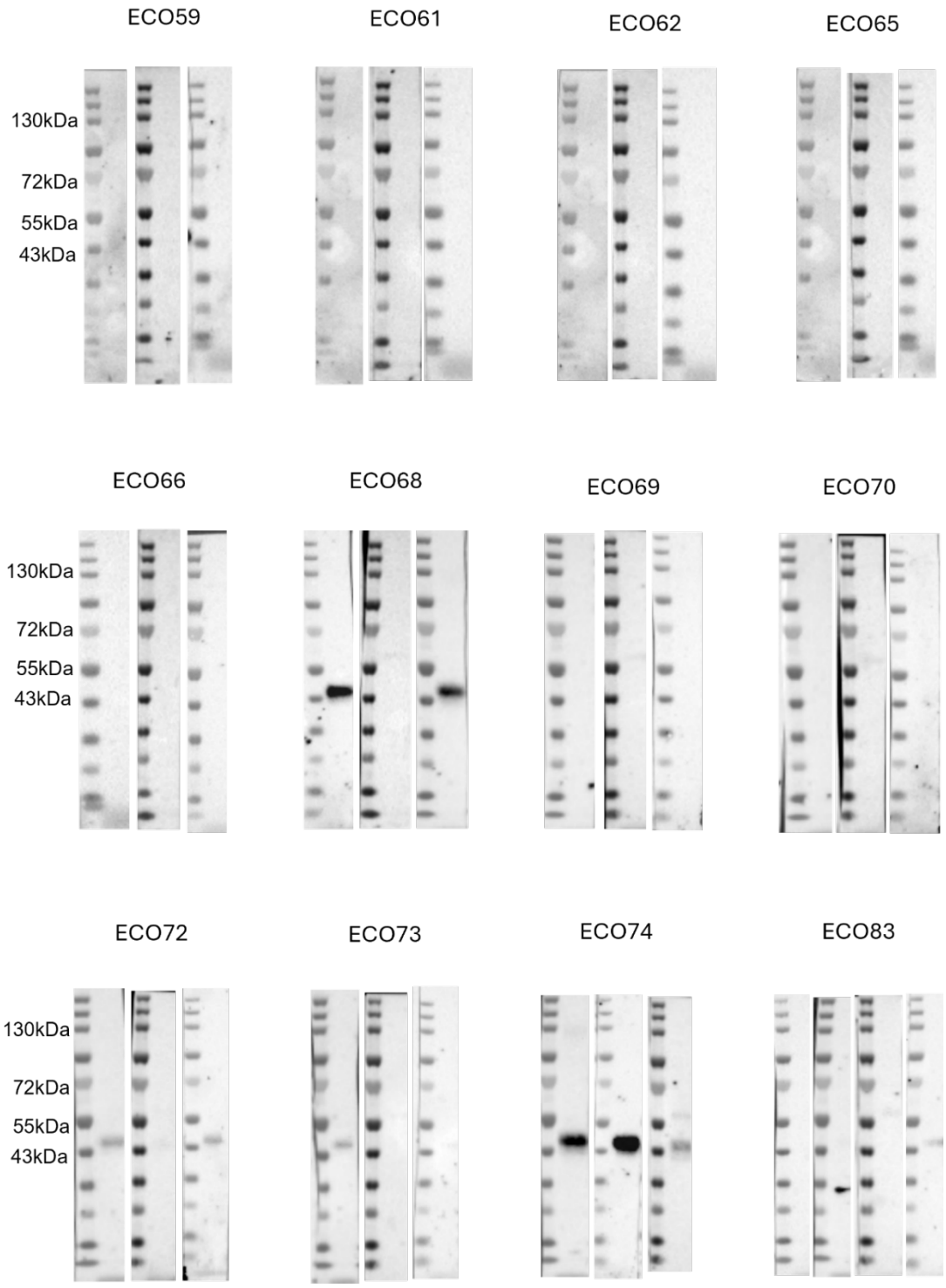


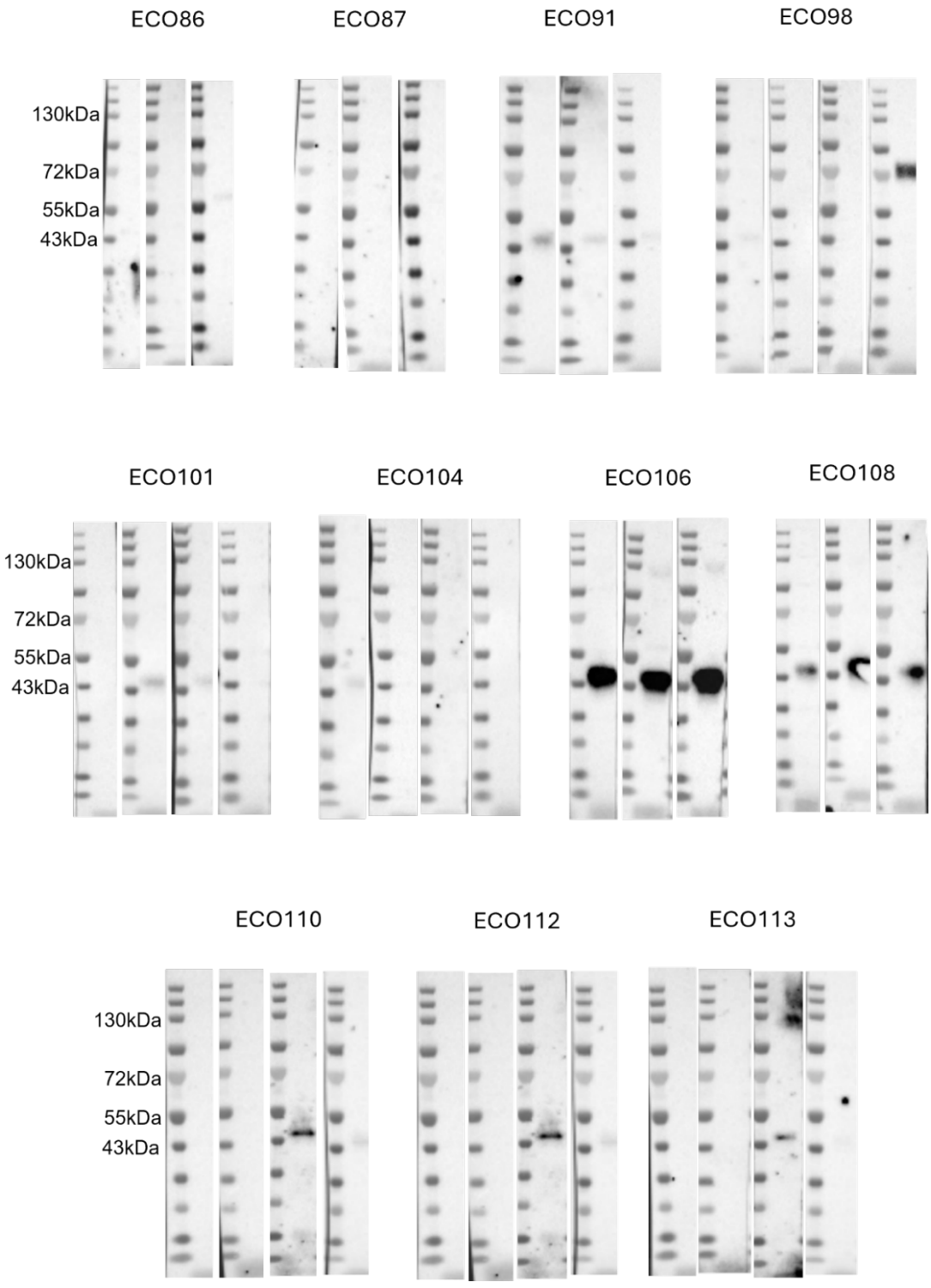
Figure 5.6-3: The relationship between binding of gBect and membrane-expressed gB.
XY plot reproduced from **Figure 4.5-13B** showing the binding capabilities of each mAb against gB expressed as recombinant ectodomain and the full-length antigen expressed on the cell surface membrane. mAbs are colour-coded based on their identified cluster from the ELISA-based competition experiment (**Figure 5.5-6**). Though most antibodies in the panel roughly trace a line of proportionality, mAbs ECO12, ECO38, ECO48 and 3A3 deviate substantially, showing greater ability to bind gBect than membrane-expressed gB.

Until the recently-presented pre-fusion gB structure (McCallum & Veesler, 2024) is fully accessible, understanding differentially exposed neutralising epitopes remains largely speculative. Presenting these two conformations as two different recombinant ectodomain constructs will ultimately facilitate comparison of the pre- and post-fusion antibody responses without the possible confounding of membrane proximity effects. Such studies will help inform the design of gB-based vaccine candidates including whether or not they benefit from being expressed as soluble ectodomains, or if they are amenable to membrane-based expression or any other C-terminal anchor such as a virus-like particle scaffold.

5.7 Appendix IV: Raw Western Blot Images




ECO59
ECO61
ECO62
ECO65
130kDa
72kDa
55kDa
43kDa
ECO66
ECO68
ECO69
ECO70
130kDa
72kDa
55kDa
43kDa
ECO72
ECO73
ECO74
ECO83
130kDa
72kDa
55kDa
43kDa


ECO86
ECO87
ECO91
ECO98
130kDa
72kDa
55kDa
43kDa
ECO101
ECO104
ECO106
ECO108
130kDa
72kDa
55kDa
43kDa
ECO110
ECO112
ECO113
130kDa
72kDa
55kDa
43kDa

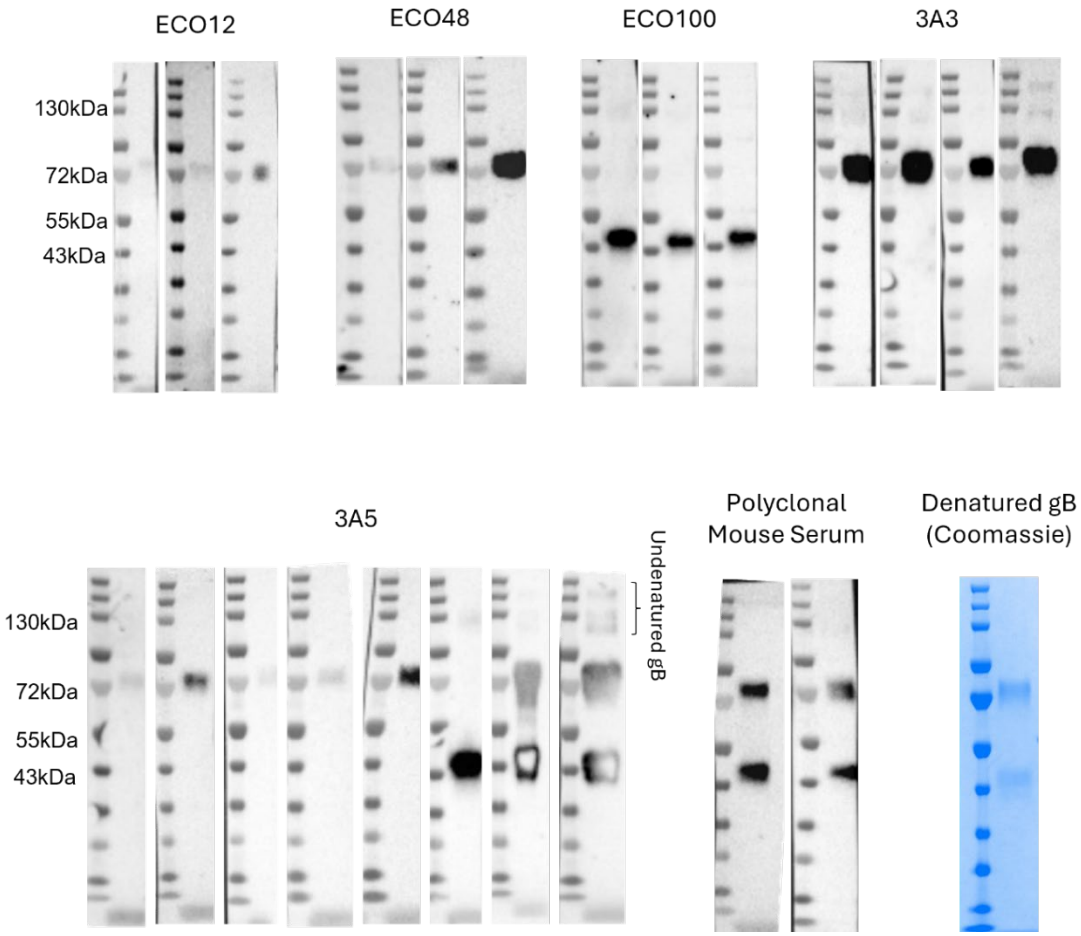


Figure 5.7-1: Raw Western blot images using anti-gB mAbs to stain denatured gBect.
1 µg of gBect was subjected to SDS-PAGE before staining with each antibody. Each blot shows a protein ladder and an adjacent lane to which gB was added. gBect subjected to denaturing conditions separates into two bands of ~70 kDa and ~40 kDa in mass. As a positive control for successful denaturation of the two bands of furin-cleaved gBect, a control membrane was stained with gB-reactive polyclonal mouse serum and detected with an anti-mouse IgG secondary conjugated to HRP. Purity of the protein prep used in all gels was confirmed by Coomassie stain, an example of which is shown.

6 Results IV: Structural Characterisation of Neutralising mAb-gB Complexes

6.1 Statement of Authorship

Work reported in this chapter was designed and executed by S.E. with the following exceptions:

Production of purified Fab and gB proteins were performed with assistance from Francisco Orliacq and Orthi Onupom, under S.E.'s supervision.

Purification of Fab-gB complexes by High-Performance Liquid Chromatography Size Exclusion Chromatography (HPLC-SEC) was conducted by Orthi Onupom under S.E.'s direct supervision.

Negative Stain Electron Microscopy (NSEM) images were generated by Orthi Onupom with consumables and microscope kindly provided by the William Dunn School of Pathology Electron Microscopy Facility.

Preparation of gB-Fab grids for imaging by Cryo-EM was performed by Dr Robert Stass, Division of Structural Biology. Downstream data processing, and model fitting was performed by Dr Robert Stass. Analysis of antigen-antibody interactions and figure generation was conducted by S.E.

The predicted pre-fusion structure of gB generated using AlphaFold 2 was generated by Adam Khan-Qureshi.

6.2 Chapter Overview

1) Complexes of the post-fusion gB ectodomain coordinated by two different Fabs can successfully be produced and imaged by Cryo-EM.

2) Extracting full-length gB antigen from cell membranes in the presence of Fabs permits the isolation of disperse gB·Fab complexes, but these aggregate upon loading of Cryo-EM grids.

3) A high-resolution structure of a new neutralising antibody, ECO12, reveals it recognises a previously uncharacterised site of vulnerability on gB, proximal to that recognised by the 3A3 mAb.

6.3 Introduction

The work described in *Results III* provides further evidence that many antibodies against gB compete with each other to some extent, suggesting they may recognise immunological 'hotspots' on the post-fusion antigen. The competition data suggest that the principal targets of the neutralising antibodies isolated here bound in or near to Domain II, around the torso protein. However, given attempts to identify precise linear epitopes by peptide binding were unsuccessful, pinpointing each mAb's binding site was only possible by inference from competition with antibodies previously characterised structurally.

How antibodies map on the surface of gB is poorly understood. B-cell and antibody repertoire analyses that have sought to characterise the antigenic geography of gB are limited to studies of HCMV (Pötzsch *et al*, 2011; Goodwin *et al*, 2020; Nelson *et al*, 2018b; Perotti *et al*, 2020). The findings of these studies, summarised in ***Table 6.3-1***, do not wholly agree with one another. However, DIV, the crown of the gB ectodomain, is often considered the most dominant antibody target (Baraniak *et al*, 2018b), somewhat supported by the studies referenced below.

Source	Repertoire	Immunodominance of gB domains	Comments	Reference
3 naturally infected individuals.	24 monoclonal antibodies	DII > 'Conformational epitopes' [unspecified binding site] > Unresolved N-terminus > Cytodomain.	No mAbs identified that recognise DIV (AD1) or DI (AD5). DII and N-terminus main targets for nAbs.	(Goodwin *et al*, 2020)
2 Balb/c mice immunised gBect protein in adjuvant.	338 gBect-specific B cells.	DIV > DII >> DI >> 'Unknown' > Unresolved N-terminus.	Unclear how many B cells clones were identical. DI major target for nAbs.	(Perotti *et al*, 2020)
7 naturally infected individuals.	888 gB-specific B cell clones.	'Unknown' > DIV >> DII > DI > Unresolved N-terminus.	Unclear how many B cells clones were identical. DI and DII the main targets of nAbs.	(Pötzsch *et al*, 2011)
19 gB/MF59 vaccinees pre-immunization, 32 gB/MF59 vaccinees post-immunization, 30 chronically infected HCMV patients.	Polyclonal serum samples from individuals screened for binding linear peptides spanning gB.	gB/MF59 vaccinees: Intravirion domain >> 'Other' > DI > Unresolved N-terminus > DII > DIV. Chronically infected individuals: Intravirion domain > 'Other' >> Unresolved N-terminus > DI >> DIV > DII	Antibodies recognising conformational epitopes not detected.	(Nelson *et al*, 2018b)

Table 6.3-1: Studies of the HCMV gB immune responses that have sought to characterise the immunodominance of the antigen's different subdomains.

No such studies have been performed for EBV gB. Additionally, it is unclear how much the immune responses against gB are similar across the human herpesviruses. Their structures, however, are highly homologous (Burke & Heldwein, 2015) and one may speculate that each domain's presentation to the immune system may also, therefore, be similar. Indeed, the structural inferences proposed in *Results III* for the EBV gB mAbs isolated may support the notion that DIV is immunodominant, albeit not targeted by many neutralisers.

Direct elucidation of the structures of gB-mAb complexes could therefore be a powerful tool for understanding the antigenic landscape of gB through direct observation. Though obtaining structures of all mAb-gB complexes is unfeasible, characterising a handful of complexes may better define the binding sites of the different mAb clusters.

Obtaining structures of such complexes is predicated on the ability to express and purify both antigen and antibody (commonly in Fab format). With respect to the former, producing recombinant gB ectodomain has successfully facilitated the determination of post-fusion gB structures for HSV-1 (Heldwein *et al*, 2006), HCMV (Burke & Heldwein, 2015) and EBV (Backovic *et al*, 2009). Thus, the structural elucidation of gB-mAb complexes is viable for the post-fusion conformation at least, evidenced by the successful efforts to characterise gBect binding of mAbs 3A3 and 3A5 (Zhang *et al*, 2022).

The pre-fusion conformation, however, is more challenging. At the time of planning and executing the work reported in this chapter, a high-resolution structure had only been resolved for HCMV gB in this form (Liu *et al*, 2021a). In their work, full-length (FL-) gB was isolated from the virion membrane using a detergent after complexing the antigen with a neutralising antibody, treating the virus sample with a chemical cross-linker and adding a proprietary fusion inhibitor (Liu *et al*, 2021a). Adapting this method for the isolation of pre-fusion EBV gB would be challenging, if not impossible in the absence of the inhibitor.

More recently, a 'pre-fusion like' structure of HCMV gB has been determined for a soluble gB ectodomain variant (Sponholtz *et al*, 2024). Using a structure-guided mutagenesis approach, stabilisation of pre-fusion gB was achieved by introducing two inter-protomer disulphide bonds as well as two cavity-filling mutations to the gBect construct (Sponholtz *et al*, 2024). Even so, the elucidated structure adopted is less compact than that resolved by Liu and colleagues (Liu *et al*, 2021a): DI appears shifted outward relative to the central helix bundle of the trimer (Sponholtz *et al*, 2024). Though production of a pre-fusion like gB ectodomain was achieved, the approach taken relied on pre-existing knowledge of the pre-fusion conformation and therefore may not be transferrable to work on EBV gB.

Prior efforts from the Douglas group to characterise the pre-fusion structures of a Class III fusion protein successfully determined that of RabG (Ng *et al*, 2022). Like the work described by Sponholtz et al., stabilisation was achieved by encoding a pre-fusion stabilising mutation that could be characterised biochemically prior to structural studies (Ng *et al*, 2022). Though this aspect of the stabilisation strategy relied on pre-existing knowledge of a pre-fusion specific mAb (Hellert *et al*, 2020), other aspects of the methodology may be directly transferrable to studying gB. Principally, removing the antigen from the surface membrane pre-complexed with saturating amounts of Fabs may sufficiently stabilise the antigen to permit its structural characterisation.

Here, two pipelines for the determination of gB-Fab complex structures were therefore investigated. First, the isolation of gBect-Fab complexes was performed by HPLC-SEC for imaging by Cryo-EM to determine the binding sites of antibodies to the post-fusion form. Second, to isolate complexes containing pre-fusion gB, the method developed for structural studies of RabG was adapted for use on gB-expressing cells.

6.4 Materials and Methods

6.4.1 Generation of gB-Fab Complexes for HPLC-SEC

Production and purification of gBect was performed as per *Section 4.4.1*. Fab constructs were generated as described in *Section 5.4.2*.

Fab constructs were added to gBect, each at a 3-fold molar excess, for 1 h at RT such that the total amount of theoretical gB·Fab_n complex was ~100 µg. Complexes were then concentrated to a final concentration of 1 mg/mL using a 10 kDa MWCO filter (Merck: Z614033). The reaction mixture was filtered through a 0.2 µm cellulose acetate filter (Corning: 8161) immediately prior to loading onto a 1260 Infinity II Bio-inert HPLC system with Multi-Detector Suite (MDS) (Agilent). gB·Fab_n complexes were then separated from excess Fab using a Bio SEC-5, 500 Å, 7.8 × 300 mm, 5 µm column (Agilent: 5190-2531) with running conditions as per the manufacturer's instructions, using PBS as the running buffer.

Fractions of 0.25 mL were collected into separate vials. Those containing protein complexes were identified using multiple MDS readouts. $UV_{280\ nm}$ absorbance peaks corresponding to gB·Fab_n were identified as those eluting earlier than uncomplexed gBect run as a control condition. In-line dynamic light scattering (DLS) was used to confirm eluted complexes matched the estimated size of gBect·Fab_6: Rh ~8-10 nm based on the reported dimensions of gBect in the literature (Backovic *et al*, 2009). Lastly, protein complex masses were approximated by static light scattering (SLS) calibrated using a Bovine Serum Albumin (BSA, 2 mg/mL) standard as recommended by Agilent (gBect·Fab_6 ~600-700 kDa).

The gB·Fab_n complex fractions were pooled and concentrated using a 10 kDa MWCO filter as before, to a final concentration of 1 mg/mL. Samples were snap frozen using a -80 °C bath of isopropanol and dry ice and stored at -80 °C.

6.4.2 Negative Stain Electron Microscopy (NSEM)

Aliquots of each gB·Fab_n complex were screened by NSEM to confirm the absence of protein aggregates and that complexes were of the right size. Frozen complex samples were diluted ~1:200 and 10 µL used to coat 300-mesh, carbon-coated copper grids (TAAB: C267/100) for 10 min. Excess protein was removed by blotting and grids subsequently stained with 2% w/v uranyl acetate (VWR: 102092-284) for 10 s. Excess stain was removed as above and air dried for 15 min at RT before imaging using a JEOL 1400 Flash 120 kV transmission electron microscope (TEM) (JEOL).

6.4.3 Detergent Extraction of FL-gB and Production of FL-gB·Fab_n Complexes

Expi293F cells were transfected with plasmid DNA encoding the full-length gB construct described in *Section 4.4.7*. After 72 h, 100 mL cultures were centrifuged at 300 ×G for 5 min and cell pellets resuspended in 10 mL freeze buffer (50 mM HEPES, 150mM NaCl, 5% Glycerol, pH 7.4) and frozen at -80 °C.

On the day of extraction, cell pellets were thawed and mixed with 500 µg twin-strep II tagged Fab, three Pierce Protease Inhibitor Mini Tablets (ThermoFisher: A32953) and 1.5% v/v n-octyl-β-d-glucopyranoside (β-OG) (Merck: 494459). Cell lysis and detergent

extract was performed at 4 °C for 2 h on a rocker. The suspension was then treated with 10% v/v Biolock solution (IBA: 2-0205-050) and centrifuged at 3000 ×G for 30 min at 4 °C.

The supernatant containing the detergent-extracted, Fab-complexed gB was then filtered using a 0.45 µm filter (Merck: HAWP14250) on ice. Isolation of the FL-gB·Fab_n complex was then conducted by affinity purification on an AKTA Pure (Cytiva) system using a 1mL Streptactin-XT 4Flow column (IBA: 2-5027-001). Affinity chromatography was performed as per the manufacturer's instructions with the modification that all running buffers were supplemented with 1.5% β-OG.

Eluted fractions from the FL-gB·Fab_n purification were pooled and concentrated as per *Section 6.4.1*. Complexes were stored at 4 °C overnight before further purification by HPLC-SEC the following day in the same fashion described in *Section 6.4.1*.

For samples that were subjected to amphipol exchange, eluted fractions of FL-gB·Fab_n from the affinity purification step were concentrated and mixed with a 3-fold mass excess of amphipol A8-35 (Anatrace: A835). Mixtures were incubated at 4 °C for 50 min before removing excess detergent using a Pierce Detergent Removal Spin Column (Fisher: 11736446) as per the manufacturer's recommendations. The FL-gB·Fab_n complexes were then subjected to overnight incubation and HPLC-SEC as described above.

6.4.4 Cryo-EM Sample Preparation and Data Collection

Cryo-EM grid preparation and data collection were performed by Dr Robert Stass, Department of Structural Biology.

In all cases, gB·Fab_n complexes were plotted onto glow-discharged holey carbon grids (1.2/1.3 µm holes, copper 200 mesh, Quantifoil). Grids were subjected to flash freezing using a Vitrobot Mark IV (Thermo Scientific).

Imaging was performed on a Glacios cryo-TEM (ThermoFisher) to obtain structures of $gB_{3A3\cdot3A5}$ and $gB_{ECO12\cdot3A5}$ at low resolution (~6 Å). The latter complex was then imaged at higher resolution using a Titan Krios G31 cryo-TEM (ThermoFisher).

6.4.5 Cryo-EM Data Processing

Particle picking, 2D classification and 3D model building were all performed by Dr Robert Stass, Department of Structural Biology, using the CryoSPARC software package. For the high-resolution structure of $gBect_{ECO12\cdot3A5}$, Dr Stass produced a final 3D model of the complex to 2.8 Å resolution. A summary of the data collection and processing can be found in *Appendix V*. Downstream analysis of this model was then conducted by S.E.

Analysis of the binding mode between the ECO12 Fab and gBect was performed using the in-built interface function in ChimeraX (Goddard *et al*, 2018) with default interface parameters (1.4 Å solvent-accessible surface (SAS) probe radius, 300 $Å^2$ minimum area). Hydrogen (H-) bonding partners at the interface were determined using the in-built `hbonds` function with default parameters, limiting detection to residues identified at the gB-Fab interface. Interface analysis was independently conducted using the PDBePISA tool (Krissinel & Henrick, 2007) to check the two methods were consistent with one another.

To analyse the binding modes of ECO12 and 3A3, the cryo-EM structure of gBect in complex with 3A3 and 3A5 (PDB: 7FBI) was first superimposed onto the $gBect_{ECO12\cdot3A5}$ model by pairwise sequence alignment using ChimeraX's `matchmaker` command with default parameters.

6.5 Results

6.5.1 A HPLC-SEC-based Method for Purifying gB·Fab Complexes Reproduces the Structure of gBect in Complex with 3A3 and 3A5

Efforts to characterise the binding modes of different Fabs in complex with the gB ectodomain were first performed using 3A3 and 3A5 to serve as a positive control case. Given this structure had previously been elucidated (Zhang *et al*, 2022), confirming the two Fabs do not compete for binding sites on gBect, testing new methods with this combination represented a low risk starting point. Furthermore, efforts to determine the structure of RabG in complex with Fab(s) revealed that multiply decorating the antigen minimised the antigen's tendency to adopt a preferred orientation that would otherwise affect image resolution (Ng & Fedosyuk, unpublished).

Fab-decorated complexes were produced by adding an excess of different Fab molecules to purified gBect and incubating on the benchtop. Reaction mixes were then subjected to HPLC-SEC to separate gBect·Fab_n complexes from unbound Fab and the isolated complexes prepared for imaging by electron microscopy (***Figure 6.5-1A***). The isolation protocol is shown schematically with HPLC-SEC data from a representative case in which gBect·Fab_n were successfully isolated and imaged by NSEM (***Figure 6.5-1B***).

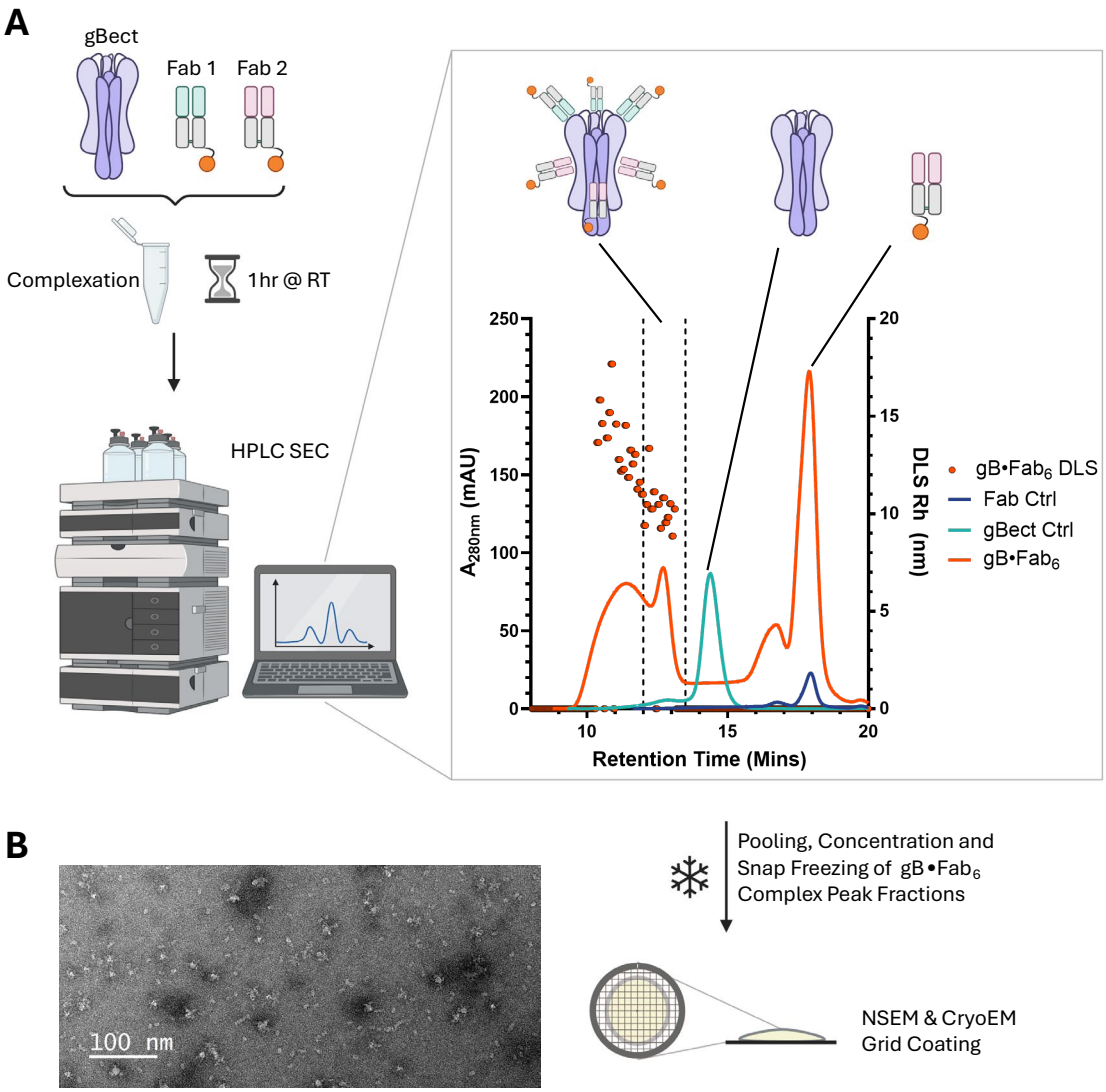


Figure 6.5-1: gBect·Fab complex isolation by HPLC-SEC.

(A) Schematic representation of gBect·Fab_6 complex formation and separation by High-Performance Liquid Chromatography-Size Exclusion Chromatography (HPLC-SEC). A representative set of chromatogram traces from a test campaign of $gBect_{3A3\cdot ECO100}$ is shown in the punchout. $UV_{280\ nm}$ absorbance readouts (lines) are superimposed for runs of the gBect·Fab_6 complex (orange), a gBect control (teal) and a Fab control (dark blue). Particle sizes were measured by dynamic light scattering (DLS) and represented in terms of their hydrodynamic radius (Rh). The Rh values for the gBect·Fab_6 sample are shown (orange circles). Superimposing the control conditions onto that of the complex allows for the identification of which elution peaks correspond to Fab, gB and complex based on their decreasing retention times. Dotted vertical lines represent the range over which eluted fractions of the gBect·Fab_6 run were pooled for downstream imaging. Complexes eluting faster than those isolated are likely to be low-multiplicity aggregates (e.g. dimers / trimers) given their measured Rh values. Similar oligomeric species were consistently observed in HPLC-SEC campaigns, highlighting the importance of relying on both $UV_{280\,nm}$ traces and DLS readouts.

(B) Negative stain transmission electron microscopy (NSEM) micrograph of the $gBect_{3A3\cdot ECO100}$ complexes isolated in (A).

Once the HPLC-SEC workflow had been tested, complexes of $gBect_{3A3\cdot3A5}$ were purified by the same method for downstream structural elucidation. In this case, however, degradation of the SEC column matrix greatly reduced the resolution of the size exclusion chromatography (***Figure 6.5-2A***). Compared to test runs completed prior to this complex, separation between the elution of excess Fab and the complex (assumed to be the heavier peak in ***Figure 6.5-2A***) was greatly diminished.

As a result, determining which eluted fractions contained $gBect_{3A3\cdot3A5}$ was conducted based on DLS measurements of the hydrodynamic radius of the eluted particles. Using a Rh cut-off between ~8 and 11 nm as an estimate for the size of the fully decorated complex, fractions within this window were pooled and their contents investigated by denaturing PAGE with Coomassie stain (***Figure 6.5-2B***). This clearly indicated the presence of Fab and both gBect fragments, suggesting complexes could be isolated despite SEC column degradation.

Screening of the $gBect_{3A3\cdot3A5}$ by NSEM revealed particles were monodisperse in nature and showed little sign of aggregation (***Figure 6.5-2C***). The remaining sample was therefore imaged by cryo-EM. 2D classes used for structural refinement revealed complexes with C_3 rotational symmetry concordant with that of a gBect trimer (***Figure 6.5-2D***). Separate classes resembling a side-on view of gBect doubly decorated with Fabs that appear to bind distal epitopes. 3D model building revealed a 5.6 Å resolution density that closely matched the structure of trimeric $gBect_{3A3\cdot3A5}$ previously published (PDB ID: 7FBI, Zhang et al., 2022) (***Figure 6.5-2E***). Successful reproduction of this complex's structure therefore represented a proof of concept for the isolation and imaging of different gB-based antigen-Fab species.

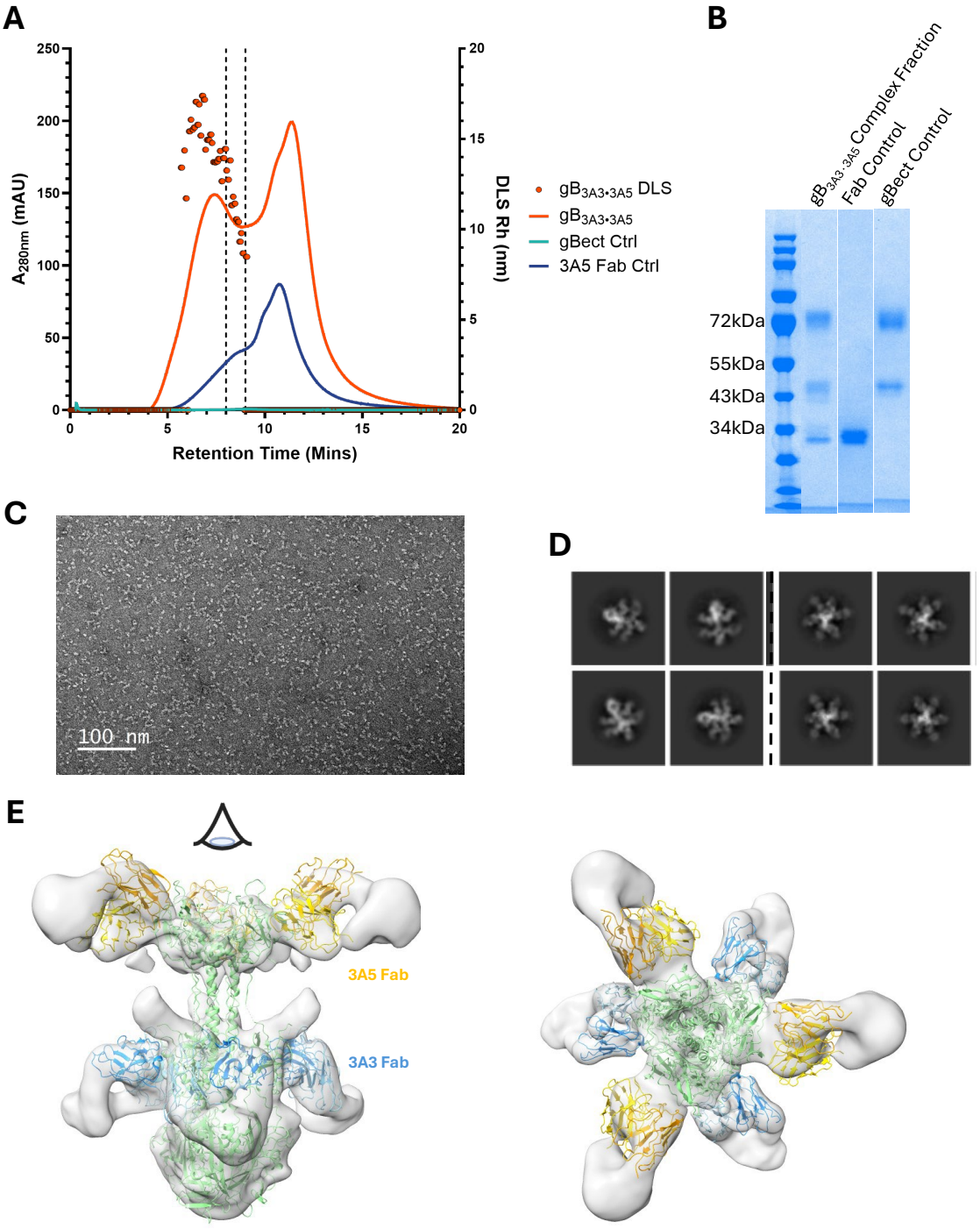

A
250
200
150
100
50
0
A280nm (mAU)
20
15
10
5
0
DLS Rh (nm)
0
5
10
15
20
Retention Time (Mins)
gB3A3•3A5 DLS
gB3A3•3A5
gBect Ctrl
3A5 Fab Ctrl
B
gB3A3•3A5 Complex Fraction
Fab Control
gBect Control
72kDa
55kDa
43kDa
34kDa
C
100 nm
D
E
3A5 Fab
3A3 Fab

Figure 6.5-2: Isolation and structural characterisation of gBect coordinated by 3A3 and 3A5 Fabs.

(A) HPLC-SEC chromatogram for $gBect_{3A3 \cdot 3A5}$ as well as gBect and Fab-only controls. Degradation of the SEC column matrix has greatly reduced its ability to resolve complexes of different sizes. Comparing the chromatogram to that shown in **Figure 6.5-1A** reveals $gBect_{3A3 \cdot 3A5}$ is not being fully separated from excess, unbound Fab, nor does it appear to be fully separated from aggregate species (Rh > 12 nm). Dotted lines represent the range over which eluted fractions were pooled for downstream imaging. Fractions with Rh values between 8 – 12 nm were collected, in line with the estimated size of a multiply decorated gBect complex.

(B) Coomassie-stained reducing SDS-PAGE on a sample of the eluted protein pooled in (A). Relative to control samples of the 3A3 Fab and gBect run separately, the pooled protein fractions from (A) clearly contain both Fab and gBect. This suggested $gBect_{3A3 \cdot 3A5}$ complexes were successfully isolated.

(C) NSEM micrograph of a sample from the pooled fractions thought to contain $gBect_{3A3 \cdot 3A5}$ complexes. Particles are evenly distributed and too large to be Fab alone.

(D) 2D classes identified by Cryo-EM corresponding to a side-on view of $gBect \cdot Fab_6$ (left) and top view (right)

(E) Side-on (left) and top-down (right) view of the isolated $gBect_{3A3 \cdot 3A5}$ complex. Protein models were fitted into electron density by Dr Rob Stass, Department of Structural Biology.

6.5.2 Disperse Complexes of Full-length, Membrane-extracted gB Coordinated by Fabs can be Isolated but Aggregate on Cryo-EM Grids

It has consistently been observed that soluble ectodomains of herpesvirus gB proteins adopt the post-fusion conformation, and that full-length membrane-associated gB proteins also adopt the post-fusion conformation upon detergent extraction from the membrane. To attempt to isolate pre-fusion protein, I therefore sought to stabilise the full-length protein with a potentially 'locking' mAb before detergent extraction.

Though the antibodies isolated against gB in this work were not pre-fusion specific, their binding to gB may still stabilise the pre-fusion conformation. Similarly, for RabG a mAb capable of binding both the pre- and post-fusion conformations is able to lock it in the pre-fusion state (Ng *et al*, 2022). Given their possible role in stabilising pre-fusion gB, the HPLC-SEC pipeline was adapted to investigate whether complexes of the full-length antigen bound to 3A3 and 3A5 could be isolated.

To minimise the risk of membrane-expressed gB spontaneously adopting the post-fusion conformation, the full-length antigen was extracted in the presence of excess Fab (***Figure 6.5-3***). Expi293F cells expressing gB on their cell surface were treated with detergent alongside the 3A3 and 3A5 Fabs. Complexes of $FL\text{-}gB_{3A3 \cdot 3A5}$ were then isolated from bulk cell lysates by affinity chromatography against a TwinStrep-II tag present on both Fabs.

The eluted protein mix was therefore predicted to contain a mixture of unbound Fab and gB·Fab complex, which were subsequently separated by HPLC-SEC chromatography.

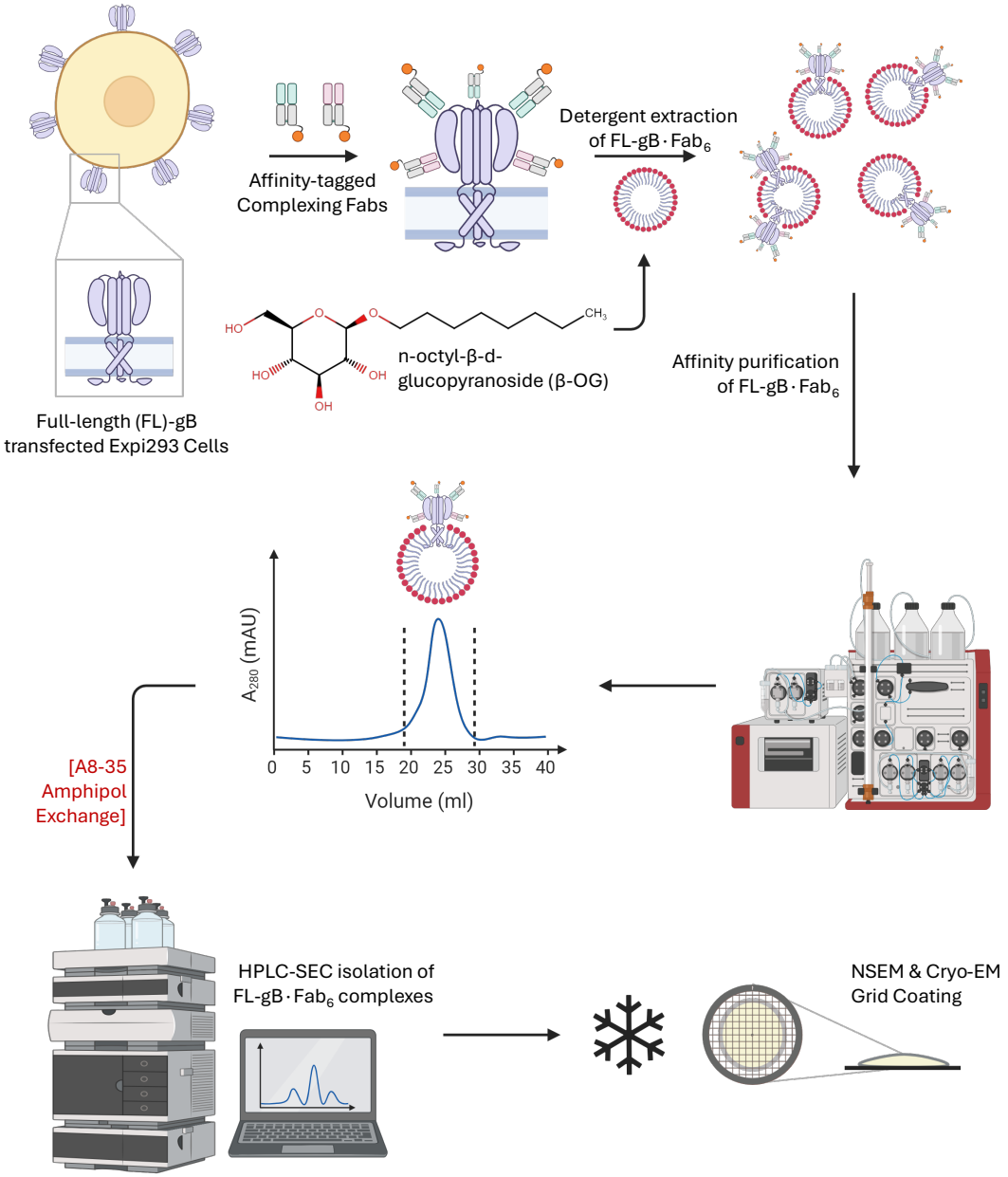


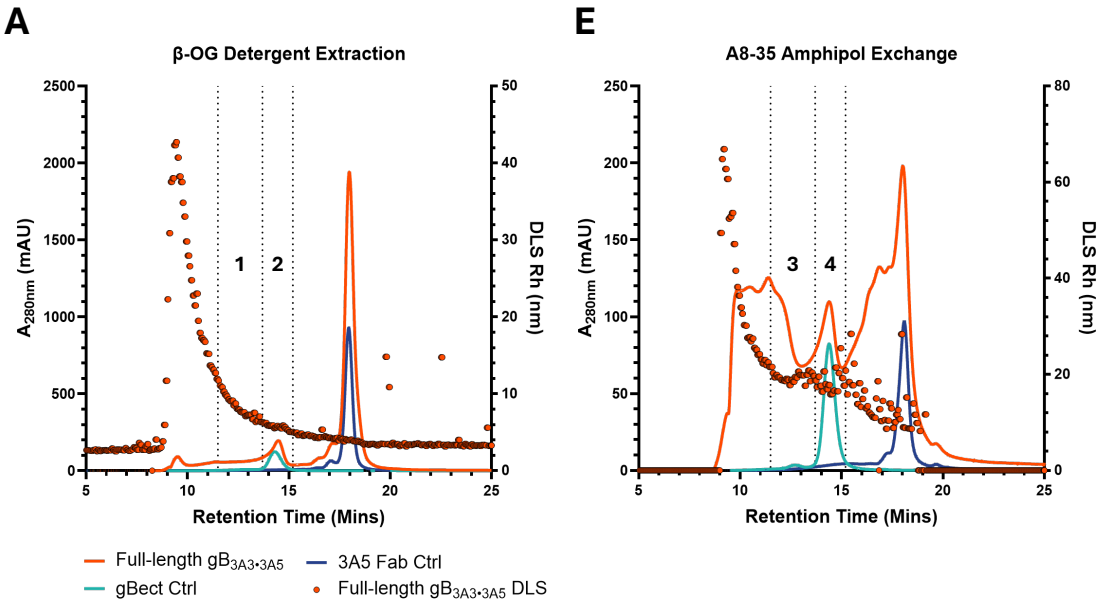
Figure 6.5-3: Membrane extraction of full-length gB for the generation of gB·Fab complexes. Schematic representation of the production of FL-gB · Fab_6 complexes. Expi293 cells transiently transfected with plasmid DNA encoding FL-gB were exposed to β-OG detergent in the presence of excess Fab. Detergent-extracted FL-gB · Fab_6 complexes were subjected to affinity purification against a Twin Strep II tag at the C-terminus of the Fab molecules. Complexes were further separated from excess Fab by HPLC-SEC and eluted fractions containing complexes were frozen for downstream Cryo-EM. A8-35 amphipol exchange was only performed where specified in the text.

The chromatogram of the FL-gB$_{3A3\cdot3A5}$ complex was compared to control runs of gBect and Fab alone (***Figure 6.5-4A***). This revealed a small peak corresponding to a heavy species (~MDa) with a Rh of ~40nm that was assumed to represent aggregate. However, smaller species with Rh between 10-30 nm subsequently eluted followed by a peak that closely matched the elution profile of the gBect control.

Given the effects of the detergent on complex size and its corresponding MDS readouts were unknown, fractions were pooled into two separate populations. DLS and SLS readouts were then used to estimate the Rh and Mw of each peak (***Figure 6.5-4B***). The population of smaller particles that were pooled had a Rh approximately as expected for a gBect trimer and had a complex mass similar to that predicted for gB·Fab$_6$ (~630 kDa). This population was therefore screened by NSEM, revealing evenly distributed particles (***Figure 6.5-4C***). These particles closely resembled those observed by NSEM for the successfully characterised gBect$_{3A3\cdot3A5}$ complex (***Figure 6.5-2C***). Though this appeared promising for imaging complexes by Cryo-EM, attempts to blot the complexes onto carbon grids resulted in particle aggregation, preventing imaging (***Figure 6.5-4D***).

Given particles appeared homogenous and non-aggregated up to the point of NSEM, it was reasoned that aggregation was induced during Cryo-EM grid preparation. This phenomenon was not observed for gBect-based complexes, suggesting that the transmembrane domain (TMD), C-terminal domain (CTD) and/or the detergent were instrumental in triggering aggregation.

The choice of detergent is well documented as an important consideration for Cryo-EM imaging of membrane-extracted proteins (Li, 2022; Egri *et al*, 2023). Study of the pre-fusion RabG·Fab$_6$ complex showed that exchanging the β-OG detergent for A8-35 amphipol prior to HPLC-SEC avoided complex aggregation (Ng *et al*, 2022). This strategy was therefore tested on the FL-gB$_{3A3\cdot3A5}$ complex. Inspection of the HPLC-SEC trace, however, indicated higher levels of protein aggregation than when the detergent was not exchanged (***Figure 6.5-4E***).



B

Membrane Extraction	Peak	Mean Elution Time (min)	SLS-Estimated Mw (kDa)	DLS-Estimated Rh Mean & Range (nm)	Imaging
β-OG	1	12.8	N/A (insufficient signal intensity)	8.3 (6.3 – 11.9)	None
	2	14.5	500	5.7 (5.4 – 6.3)	NSEM & Cryo-EM
β-OG with A8-35 Exchange	3	13.0	1400	19.4 (17.6 – 21.6)	None
	4	14.5	600	18.5 (15.8 – 25.5)	NSEM

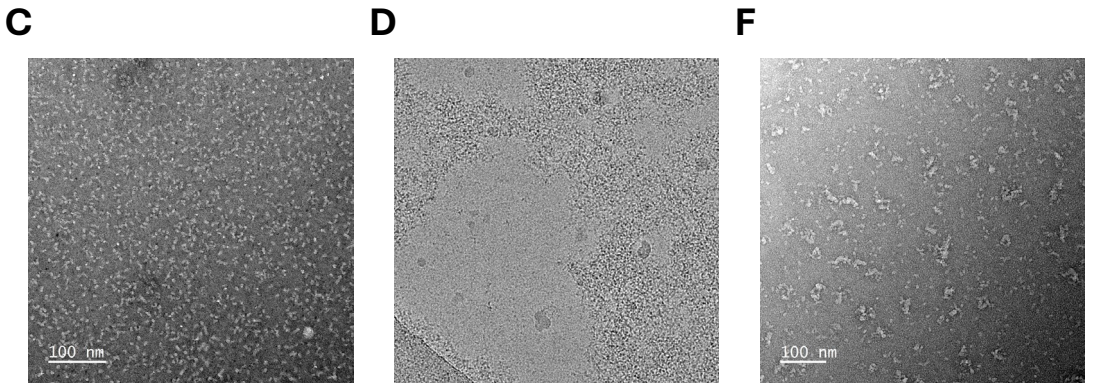


Figure 6.5-4: Pilot membrane extraction of full-length gB complexed with 3A3 and 3A5.

(A) HPLC-SEC chromatogram of the FL-gB$_{3A3\cdot3A5}$ complex overlayed with those of gBect- and Fab-only controls. Numbered windows correspond to the peaks analysed in (B) by SLS and DLS.

(B) Summary table displaying the physical properties of particles corresponding to isolated peaks from the HPLC-Sec. For both attempts, membrane extraction of FL-gB was performed in the presence of 3A3 and 3A5.

(C) NSEM micrograph of FL-gB$_{3A3\cdot3A5}$ after detergent extraction with β-OG. Particles are monodisperse and of a similar size to those of gBect$_{3A3\cdot3A5}$ that were successfully imaged by Cryo-EM.

(D) Protein aggregates of FL-gB$_{3A3\cdot3A5}$ formed after blotting onto Cryo-EM grids and flash freezing.

(E) HPLC-SEC chromatogram of FL-gB$_{3A3 \cdot 3A5}$ complex isolated after performing A8-35 amphipol exchange on complexes prior to HPLC-SEC. As in (A), numbered windows correspond to the peaks analysed in (B).
(F) NSEM micrograph of FL-gB$_{3A3 \cdot 3A5}$ complexes exchanged into A8-35 amphipol. Particles are larger than those that were not exchanged into A8-35, are unevenly sized and irregularly distributed.

Samples from two elution peaks corresponding to smaller particles were pooled to avoid selecting aggregates. Mean Rh and molecular weight (Mw) calculations revealed that the smaller of these peaks were of the correct approximate size (***Figure 6.5-4B***). However, imaging by NSEM revealed particles were highly heterogenous in shape and size, and far larger than previous complexes (***Figure 6.5-4F***). These findings indicated that amphipol exchange was detrimental to the isolation of stable FL-gB·Fab complexes.

Although isolating gB from cell membranes appears feasible using β-OG, further investigation is required to better understand how to maintain particle stability on a Cryo-EM grid.

6.5.3 A Doubly Fab-decorated gBect Complex Reveals the Binding Site of the ECO12 Neutralising Antibody

Given the difficulty in preparing suitable grids with full length gB, and the success of imaging of gB ectodomain with 3A3 and 3A5, characterisation of the interaction between the most potent newly identified neutralising mAb, ECO12, and gB focused on using the gB ectodomain.

Analysis of the competition data described in *Results III* revealed that the ECO12 mAb competed for gBect binding with 3A3, but not 3A5. 3A3 was therefore substituted with ECO12 to maximise the chances of obtaining a new stable complex.

HPLC-SEC analysis revealed a broad peak corresponding to particles larger than the gBect control condition (***Figure 6.5-5A***). Smaller particles corresponding to a Rh cut-off window of 9-12 nm had an estimated mean mass of 577 kDa, similar to that expected for a gBect·Fab$_6$ complex (~630 kDa). These were pooled and subjected to low-resolution Cryo-EM. Downstream analysis of the 2D classes revealed particles with apparent C_3 symmetry, congruent with that of trimeric gBect (***Figure 6.5-5B***).

3D model building was performed to 5.8 Å resolution. This revealed complexes of gBect decorated with 3A5 toward the DIV 'crown' of the ectodomain, in accordance with previous structural studies (*Section 6.5.1* and Zhang et al., 2022). ECO12 appeared to recognise an epitope around the 'torso' of the ectodomain, more toward the MPR and TMD than 3A5 (***Figure 6.5-5C***). Overlaying the high-resolution structure of gBect in complex with 3A3 onto the density map revealed that ECO12 bound a new epitope at the same 'latitude' as that of 3A3 but rotationally offset from it (***Figure 6.5-5D***).

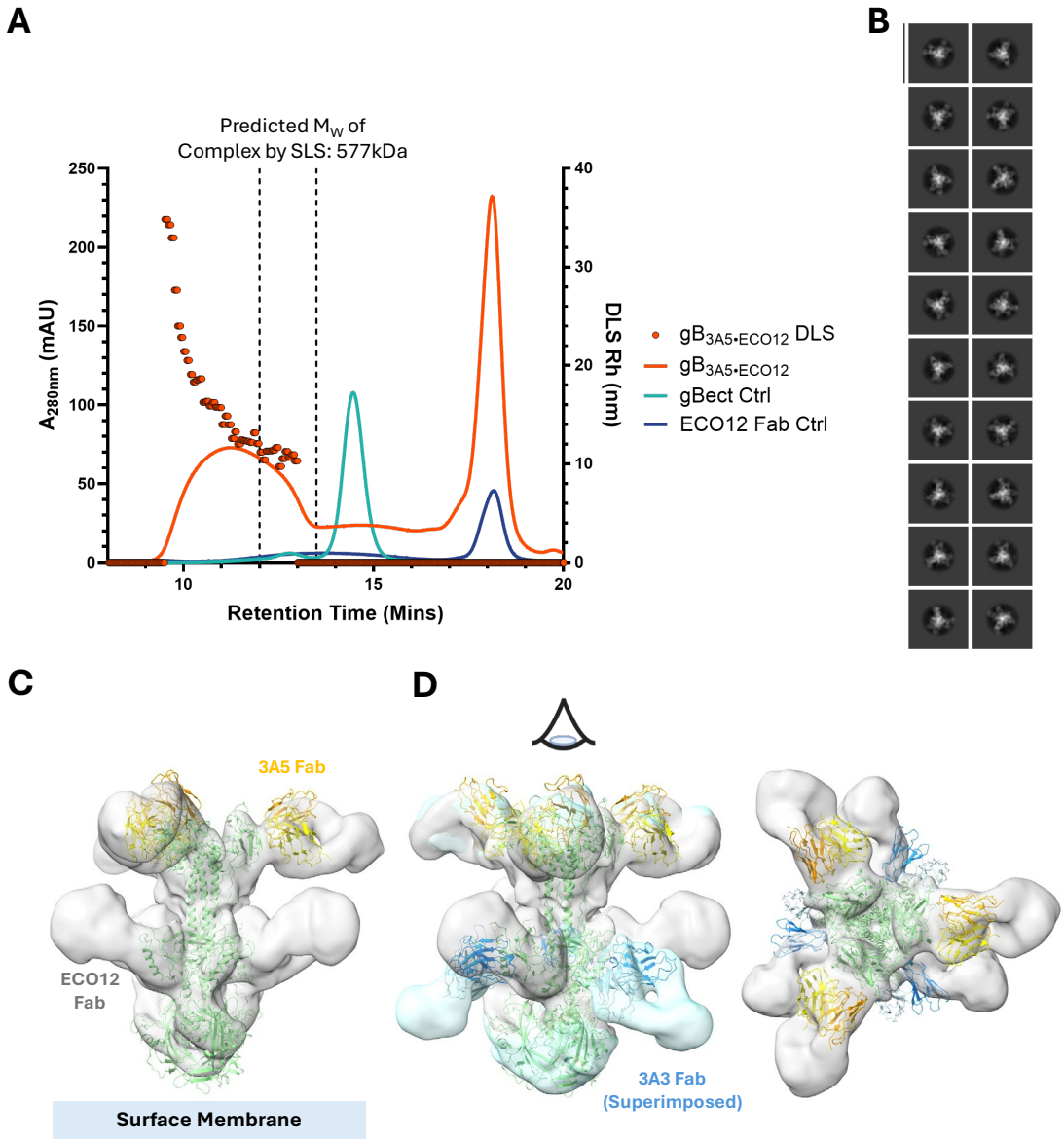


Figure 6.5-5: of gBect coordinated by ECO12 and 3A5 Fabs.

(A) HPLC-SEC chromatogram of the $gBect_{ECO12 \cdot 3A5}$ complex overlayed with those of gBect- and Fab-only controls. Dotted lines represent the window in which fractions were pooled for downstream imaging. SLS-based complex mass approximation for particles in the window is shown.

(B) 2D classes determined for the $gBect_{ECO12 \cdot 3A5}$ complex. C_3 symmetrical particles are identifiable.

(C) Side-on view of the isolated $gBect_{ECO12 \cdot 3A5}$ complex electron density with fitted protein model of gBect and 3A5 Fab.

(D) Electron density of the $gBect_{ECO12 \cdot 3A5}$ complex with fitted models of gBect and 3A5. The 3A3 Fab model is shown superimposed on the gBect map. Viewing the models from above reveals the ECO12 electron density is rotationally offset from that of the superimposed 3A3.

Protein models were fitted into electron density by Dr Rob Stass, Department of Structural Biology.

A 2.8 Å resolution Cryo-EM structure was subsequently obtained to better understand ECO12's interaction with gBect (***Figure 6.5-6A***). Interrogation of the binding site between the Fab and gBect revealed ECO12 made extensive contacts to residues with two loops in DII (***Figure 6.5-6B***), raw electron density and model fitting for which are shown in *Appendix VI*. 11 residues of the ECO12 heavy chain appear to interact with gBect, whilst only 5 light chain amino acids do.

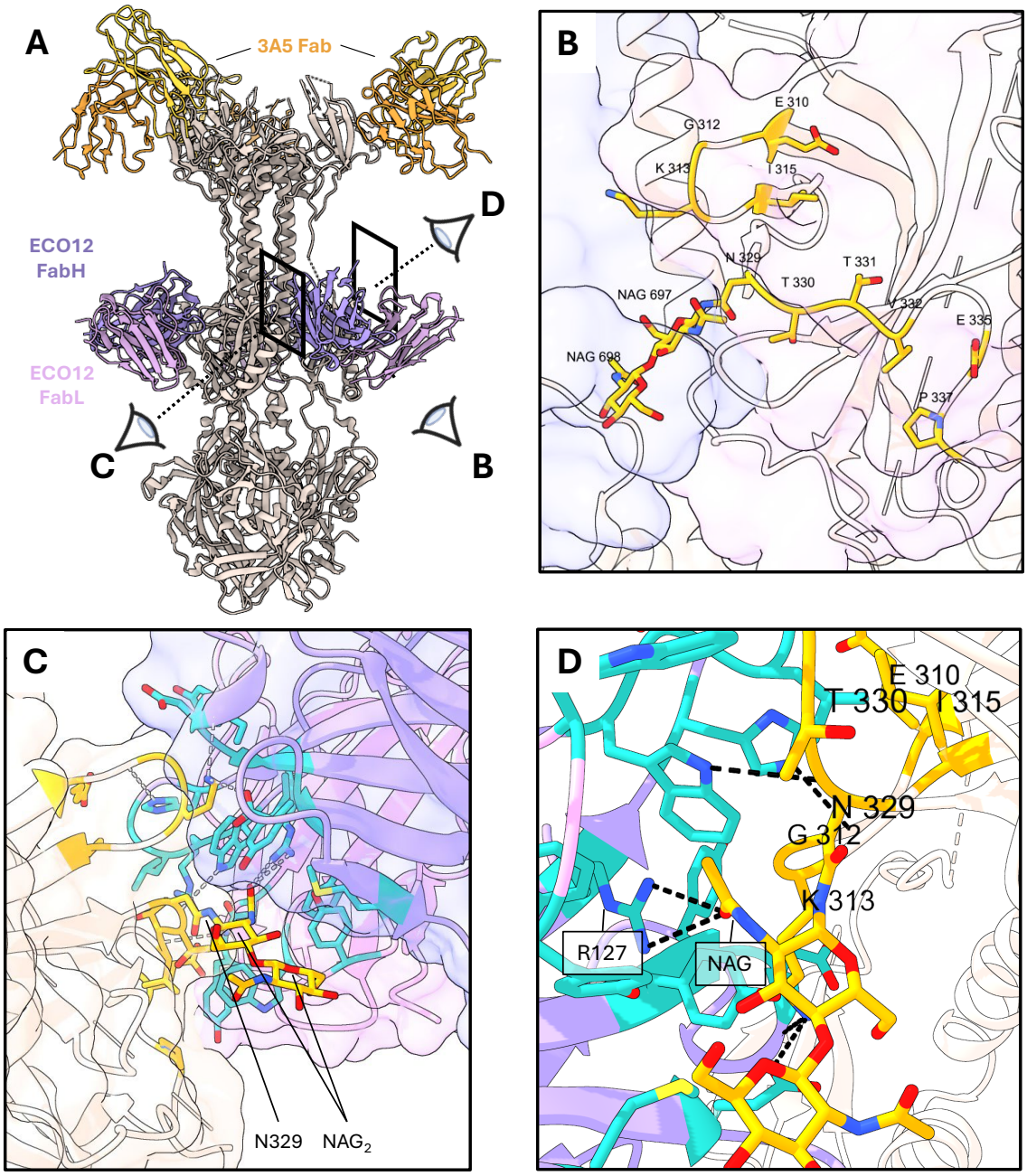

A
3A5 Fab
ECO12
FabH
ECO12
FabL
D
C
B
B
E 310
G 312
K 313
I 315
N 329
T 331
T 330
NAG 697
V 332
E 335
NAG 698
P 337
C
N329
NAG2
D
E 310
T 330
I 315
N 329
G 312
K 313
R127
NAG

Figure 6.5-6: Structural characterisation of the ECO12 epitope.

(A) 2.8 Å resolution model of the $gBect_{ECO12\cdot 3A5}$ complex. The post-fusion gB trimer (beige) is shown complexed by three ECO12 (purple) and three 3A5 (yellow) Fabs. 3A5 binds to the crown of the post-fusion conformation, distal from the membrane. ECO12 recognises an epitope in the torso of the structure, within DII.

(B) Front-on view of the ECO12 epitope on the gB ectodomain. The ECO12 heavy (purple) and light (pink) chains are shown as semi-transparent surfaces. Residues on gBect that interact with ECO12 (yellow) are labelled. Densities corresponding to two N-acetylglucosamine (NAG) moieties (697, 698) were resolvable on account of their complexation by ECO12, restricting the conformational flexibility of these glycan residues.

(C) Side-on view of the ECO12-gBect interface. The side chains of interacting residues on gBect (yellow) and the ECO12 Fab (turquoise) are shown. Hydrogen bonding pairs between antigen and Fab are shown (grey dotted lines).

(D) Side-view of the ECO12-gBect interface from the opposite angle to (C). Hydrogen bonds (dotted black lines) are shown including those between NAG-697 and R127 in the ECO12 heavy chain.

Interacting residues at the antigen-Fab interface were identified using ChimeraX's in-built interface tool. Hydrogen bonding partners were identified using ChimeraX's H-bonds tool.

The ECO12 Fab is predicted to make seven hydrogen bonding interactions with gBect (***Figure 6.5-6C***). Of these, two are formed between Arg-127 of the ECO12 heavy chain and the N-acetylglucosamine (NAG) group branching from Asn-329 on gBect (***Figure 6.5-6D***). This is perhaps surprising given ECO12's binding of gBect is largely independent of gBect's N-glycosylation state (see *Section 5.5.3*).

Electrostatic interactions between ECO12 and gBect are also likely contributors to binding. Study of the antigen at the interface reveals that whilst much of the surface is made up of electron rich amino acids and negatively charged residues, gB Lys-313 forms a solitary, positively charged knob (***Figure 6.5-7A***). This residue is likely to form extensive electrostatic interactions with a concentrated pocket of negative electrostatic potential formed by residues Asp-59, Tyr-60, Tyr-61 and Asp-80 on the ECO12 Heavy-chain (***Figure 6.5-7B***). gB Lys-313 is also able to form a hydrogen bond with ECO12-H Asp-80.

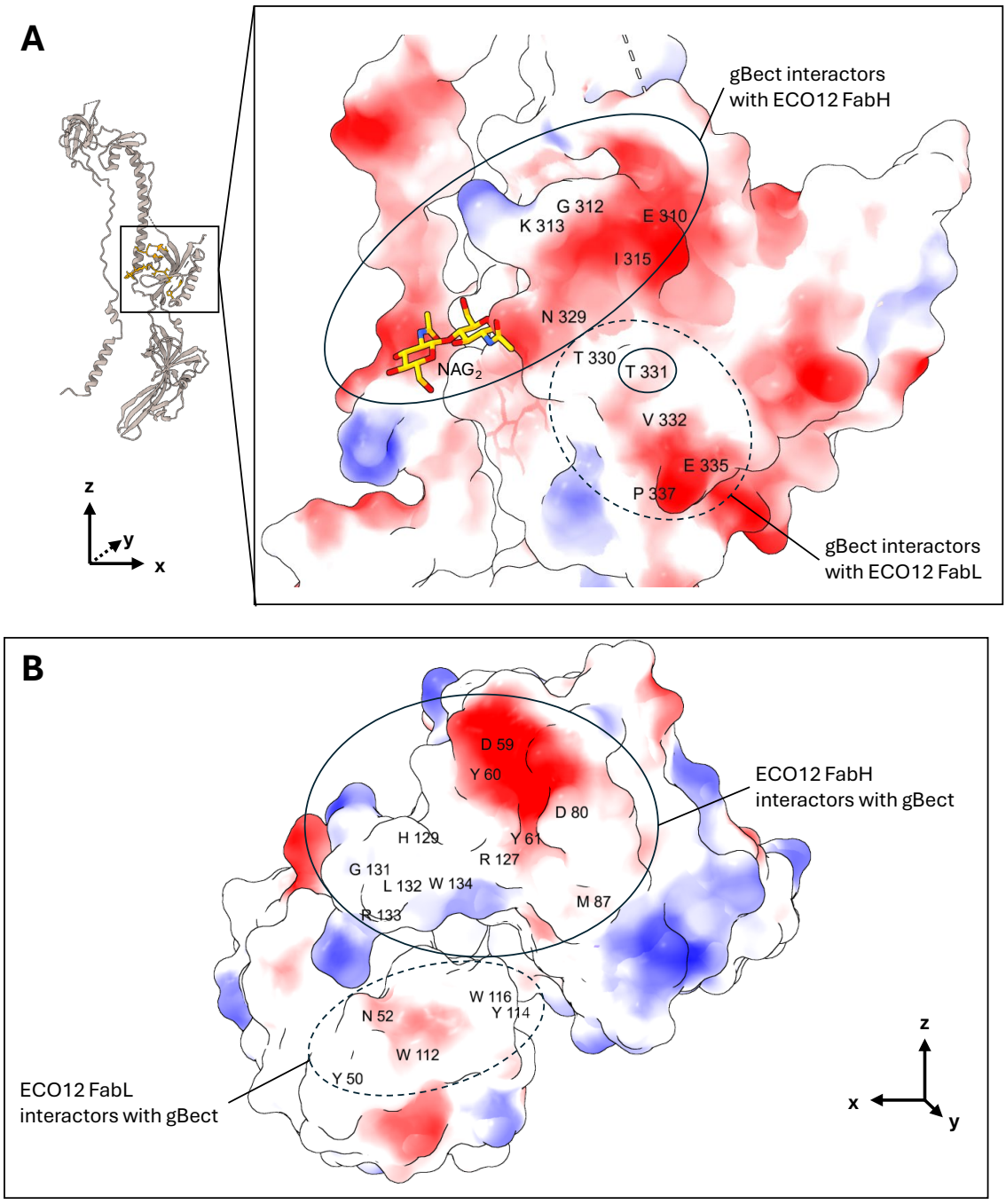


Figure 6.5-7: Electrostatic interactions between gB and ECO12.

(A) Electrostatic potential map of the gBect surface at the ECO12 interface. Residues identified as interacting with ECO12 are labelled. Circles highlight which residues interact with the ECO12 heavy chain (solid) and the light chain (dotted). Concentric circles imply interaction with both chains.

(B) Electrostatic potential map of ECO12 Fab heavy and light chain surfaces interacting with gBect. Residues identified as interacting with gBect are labelled. Circles highlight residues on the heavy (solid) and light (dotted) chains that form bonding interactions with gBect.

3D axes are shown to illustrate the orientation of the Fab with respect to gBect. That is, the two potential maps are shown after rotation about the z axis.

The high-resolution structure of the $gBect_{ECO12\cdot3A5}$ complex also permitted better characterisation of the competition between 3A3 and ECO12. The structure elucidated here was overlayed with the previously published structure of $gBect_{3A3\cdot3A5}$ (PDB: 7FBI, Zhang et al., 2022) using a computational pairwise sequence alignment tool (alignment RMSD = 1.3 Å, ***Figure 6.5-8A***).

This structural overlay therefore allowed for the superposition of the 3A3 Fab onto the structure solved here, to within <1.5 Å of its true binding site. Analysis of the pseudo-triply decorated complex revealed that ECO12 and 3A3 recognising the same gBect monomer do not compete with one another, binding entirely separate epitopes (***Figure 6.5-8B***). However, when considering Fab binding to the trimeric form of the antigen, the mode of partial competition is revealed (***Figure 6.5-8C***). Though the epitopes of the Fabs are distinct, 3A3 and ECO12 disrupt one another's binding in a 'back-to-back' fashion, sterically hindering access the other's epitope without directly recognising it (***Figure 6.5-8D***).

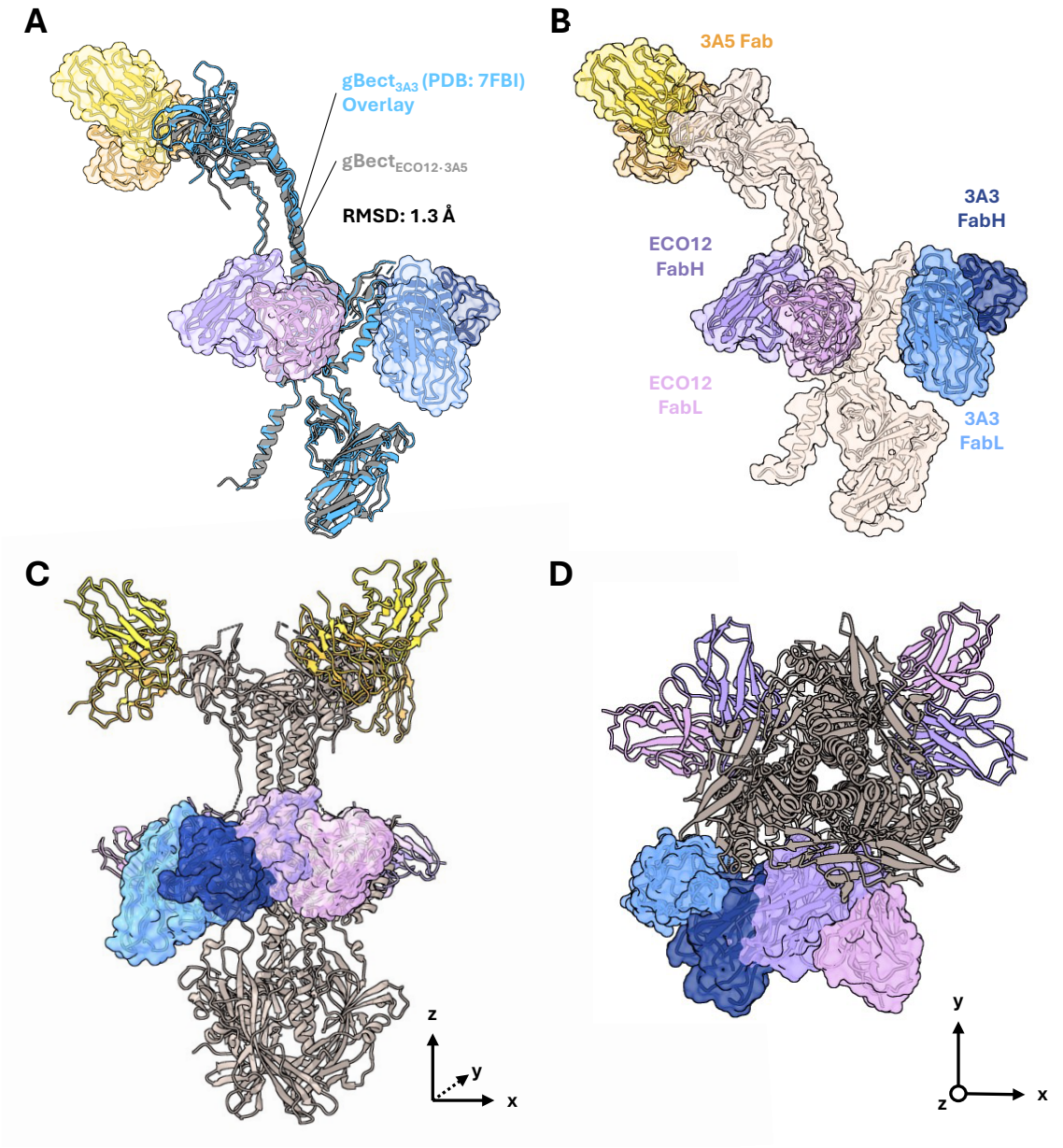


Figure 6.5-8: Structural comparison of the 3A3 and ECO12 epitopes on post-fusion gB.

(A) Structural of the $gBect_{3A3}$ structure resolved by Zhang et al. (PDB: 7FBI, 3A5 Fab removed) *(Zhang* et al*, 2022)* overlaid on that of $gBect_{ECO12·3A5}$ using ChimeraX's in-built matchmaker command. The Root Mean Square Deviation (RMSD) of the structural overlay is shown.

(B) Surface plot of monomeric gBect decorated with ECO12, 3A5 and pseudo-decorated with 3A3 Fab. ECO12 and 3A3 Fabs recognising the same gBect monomer do not compete with one another for antigen binding.

(C) Side-on view of the gBect trimer decorated with ECO12, 3A5 and pseudo-decorated with 3A3. The ECO12 Fab (blue) competes for binding of gBect with the 3A3 Fab (pink) bound to the adjacent protomer.

(D) Top-down view of the gBect trimer in (C) showing the ECO12 Fab competes with the 3A3 Fab coordinating the protomer anticlockwise to that of ECO12.

6.6 Discussion

This work describes the successful implementation of a method for characterising complexes of gBect with multiple Fabs by Cryo-EM. First testing its suitability with a previously published complex of gBect coordinated by antibodies 3A3 and 3A5 represented a proof of concept. Given the high similarity between the structure elucidated here and that reported in the literature (Zhang *et al*, 2022), the method was subsequently used to study the binding of a new Fab, ECO12.

ECO12 appeared to recognise a new neutralising epitope within DII of the gB ectodomain. Of the handful of anti-gB antibodies that have been well characterised, four of the most potent neutralisers, ECO12, 3A3 (Zhang *et al*, 2022), 8A9 and 8C12 (Hong *et al*, 2022) all recognise epitopes in DII. Though it remains to be seen whether the latter two bind different epitopes to ECO12 and 3A3 (binding was determined by domain-specific ELISA, not structurally), current evidence lends support to the notion that DII represents both an important region for gB function and, likely related to this, a site of vulnerability.

There is still only a limited understanding of what role(s) DII plays in gB-catalysed membrane fusion. A bimolecular complementation study of HSV gB suggests DII is an important site of interaction with gH/gL (Atanasiu *et al*, 2007). For EBV, however, it has alternatively been suggested that gB-gH/gL interactions involve residues in DIII, DIV and DV (Plate *et al*, 2011).

Zhang and colleagues instead suggest 3A3 may act by inhibiting gB's interaction with a putative cognate cell surface receptor, NRP-1 (Zhang *et al*, 2022). Mutagenesis of the 3A3 epitope revealed a reduced ability of fluorophore-conjugated NRP1 to bind gB-expressing HEK293T cells (Zhang *et al*, 2022).

NRP1's role in EBV infection is poorly understood and the suggestion it may interact with gB is somewhat at odds with understanding of herpesvirus entry mechanisms: gB proteins are more commonly thought to interact with receptors indirectly, through accessory proteins (gH/gL complexes). At the time of writing, only one study was

identified in the literature that sought to characterise gB-NRP1 interactions in the context of viral infection. Wang and colleagues show that NRP1 interacts with gB between residues 23 and 431 (40 kDa fragment, DI-DIII, Wang et al., 2015). In addition, pre-exposure of EBV virions to soluble NRP1 receptor reduced infection rates of nasopharyngeal cancer-derived epithelial cell lines (Wang *et al*, 2015).

The roles that each domain in the gB ectodomain play in fusion require further study to confidently infer the mechanism of neutralising antibodies that bind them.

Efforts to isolate complexes of full-length gB bound by Fabs were unsuccessful. How antibodies map on to the pre-fusion structure is therefore another important but unanswered question, though this may soon change given the recent development of a pre-fusion stabilised gB ectodomain (McCallum & Veesler, 2024). In the absence of structural data, which is yet to be fully published, computational models of pre-fusion EBV gB are an imperfect but perhaps useful tool.

To this end, two computational models of the pre-fusion structure of gB were generated using AlphaFold 2 (Jumper et al., 2021) and SWISS-MODEL (Waterhouse *et al*, 2018). In both cases, models were generated using a template structure of the pre-fusion HCMV gB, solved to 3.6 Å (PDB: 7KDP, Liu et al., 2021). Though gB proteins across the HHVs share only ~30% sequence homology, their post-fusion structures are remarkably well conserved (Burke & Heldwein, 2015). In the absence of more related structures, this template therefore represents the best match to that of pre-fusion EBV gB.

The two models display high levels of concordance with respect to the global positioning of each domain (***Figure 6.6-1A, B***). Though this is true of the domain structures as well, differences are evident, particularly in secondary structure predictions across DI and DII. Nevertheless, these models are sufficiently consistent to map the ECO12 binding site (***Figure 6.6-1C***) in DII as being at the membrane-distal apex of the protein. This is further supported by the pre-fusion structure of gB published recently, which shows DII is not proximal to the membrane (McCallum & Veesler, 2024).

ECO12's disproportionately poor ability to bind membrane-expressed, full-length gB, presumed to be predominantly pre-fusion, is thus unlikely to be caused by membrane-associated steric hindrance. To investigate the alternative possibility that its preference for post-fusion gB may be the result of changes to its epitope, the surface conformations and electrostatics of the ECO12 post-fusion gB binding site (***Figure 6.6-1D***) were compared to those of the two prefusion models (***Figure 6.6-1E, F***).

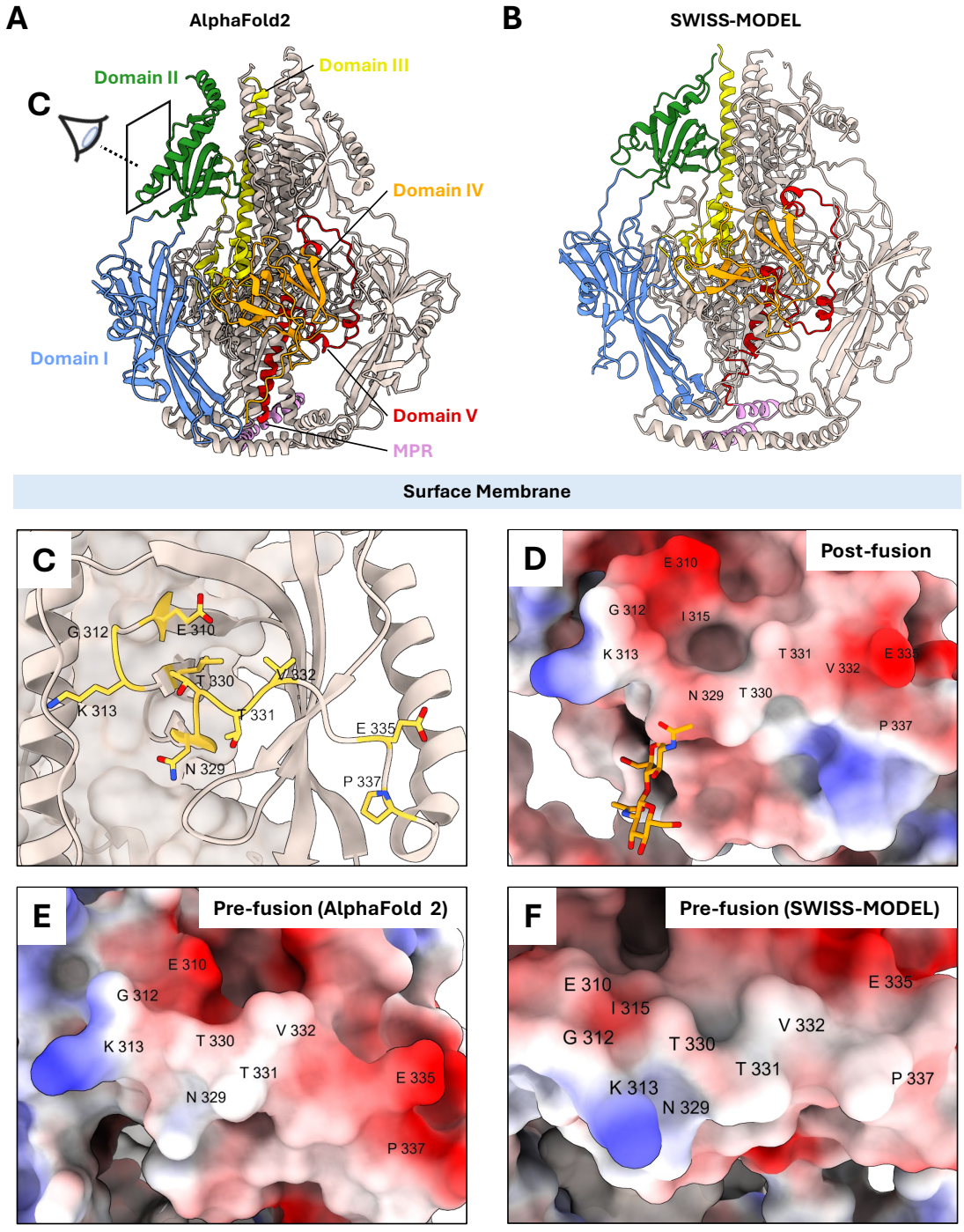


Figure 6.6-1: Modelling the ECO12 epitope on pre-fusion gB.

(A) Pre-fusion structural model of EBV gB generated with AlphaFold 2 *(Jumper* et al*, 2021)* using the pre-fusion structure of HCMV gB as a template (PDB: 7KDP, *(Liu* et al*, 2021a)*). Model generated by Adam Khan-Qureshi. Domains I (blue), II (green), III (yellow), IV (orange) and V (red) are coloured for a single protomer of the trimer. The large flexible loops between T380 and T437 have been removed from both models for clarity.

(B) Pre-fusion structural model of EBV gB generated with SWISS-MODEL *(Waterhouse* et al*, 2018)* using the same template as in (A). Domains are coloured as in (A).

(C) Residues identified as interacting with ECO12 in the post-fusion gB structure described in **Figure 6.5-6** (yellow) are labelled on the pre-fusion model shown in (A).

(D) The electrostatic potential map of ECO12 epitope surface on the post-fusion structure of gB, as in **Figure 6.5-7**, is re-displayed for ease of comparison to those of the pre-fusion models. Glycan moieties branching from N329 are shown as sticks (orange).

(E) Electrostatic potential map of the ECO12 epitope surface for the AlphaFold2 model of pre-fusion gB.

(F) Electrostatic potential map of the ECO12 epitope surface for the SWISS-MODEL model of pre-fusion gB.

Overall, residues identified as interactors on the post-fusion gB structure adopt similar positions with respect to one another in both pre-fusion models. However, clear differences can be observed that may impact antigen-Fab binding for pre-fusion gB:

1) The orientation of the positively charged Lys-313 side chain with respect to the antigenic surface. At the post-fusion gB-ECO12 interface, Lys-313 forms both hydrogen bonding and salt bridging interactions with the Fab heavy chain, predicted using the PDBePISA tool (Krissinel & Henrick, 2007). In addition, the residue is almost completely buried at the interface. Should the orientation of Lys-313's side chain in the pre-fusion conformation impair the formation of H-bonds and/or salt bridges with ECO12, burial of the positively charged -NH_3^+ group would likely carry a heavy enthalpic penalty, reducing the strength of Fab binding.

2) In the AlphaFold2 model of pre-fusion gB, Ile-315 is oriented away from gB's surface which may prevent its interaction with residues on ECO12. Ile-315 is not predicted to form H-bonding or salt bridging interactions with the Fab, however.

3) Whilst there are general differences to the relative positions of each residue on pre- and post-fusion gB, this is most obvious for ^{330}Thr-Thr-Val^{332}. These residues are located across the binding sites of the Heavy- and Light-chains of the ECO12 Fab. Changes to their relative positions may restrict access of these residues to both Fab chains.

A final important consideration is the possible effects of the N-glycosylation of Asn-329. NAG groups attached to this residue make contacts and H-bonds with the ECO12 heavy chain for the post-fusion structure of gB. It is not possible to position these groups on the pre-fusion models, however. Whether they play a role in ECO12's differential binding of the two conformations therefore remains unclear.

This apparent preference for post-fusion binding by ECO12 should be scrutinised in more detail before it is considered conclusive, primarily because it is intuitively odd that a neutralising antibody would be somewhat post-fusion specific. It is important to consider the design of the mAb isolation campaigns as context. Animals from which these mAbs were isolated were immunised with full-length gB using viral vectored platforms. gB would therefore have predominantly been presented to the immune system in the context of a membrane and, because of this, in the pre-fusion conformation for the most part. Isolating an antibody that either cannot bind its epitope if gB is expressed in a membrane or that recognises a site not presented (/less well presented) on pre-fusion gB would therefore appear to be counterintuitive.

These uncertainties about 3A3's and ECO12's recognition of pre-fusion gB may be clarified with the publication of the pre-fusion gB ectodomain construct developed by McCallum and Veesler (McCallum & Veesler, 2024). Such work may ultimately provide evidence for the mechanisms by which these antibodies neutralise infection.

In this study, the authors present a new model for how the pre- to post-fusion transition may occur. First, protomers in the pre-fusion trimer interchangeably adopt one of two conformations they term 'open' and 'closed' (McCallum & Veesler, 2024), a reference to how tightly the DIII central helical bundle aligns to z-axis of the trimer. With all trimers in the closed position, the rotations and 'flips' of other domains that constitute the pre- to post-fusion transition are now possible. These follow the order of a DI/DII flip, DV rotating and finally DII flipping once again (McCallum & Veesler, 2024).

McCallum & Veesler subsequently investigated 3A3 binding by modelling the Fab onto their pre-fusion structure. They observe that 3A3 may only be capable of binding pre-

fusion gB in the 'all-closed' configuration (McCallum & Veesler, 2024). Given this, deducing the basis for which 3A3 could be a fusion inhibitor, and thus neutralise infection, is not trivial – it is from this closed position that the structural rearrangements normally commence (McCallum & Veesler, 2024).

One might therefore speculate that 3A3 may neutralise by the following possible mechanisms:

1) Though 3A3 permits (or even 'encourages'?) adoption of the closed protomer configuration in the pre-fusion structure, necessary for procession to the post-fusion, its steric effects may prevent downstream structural changes from occurring.

2) The importance of the open configuration of pre-fusion gB protomers is not fully recognised – 3A3's prevention of gB protomers adopting this form might disrupt structural changes in ways that are not obvious from McCallum & Veesler's proposed mechanism (McCallum & Veesler, 2024).

3) Perhaps the nature of 3A3's neutralisation is not, in fact, to do with preventing structural transitions, but instead related to either inhibiting gH/gL signalling to gB or preventing gB binding a cell surface receptor such as NRP1 (should this be important to fusion).

In summary, understanding of how 3A3 interacts with pre-fusion gB is not yet sufficient to deduce exactly how the mAb prevents viral infection, but successfully stabilising pre-fusion gB will surely enable such studies for this and other antibodies.

Future work characterising the immunological landscape across gB should focus on three areas in which current understanding is limited. First, a greater number of structures showing where mAbs bind on the gB surface would help characterise hotspots of antibody targeting. These may be areas targeted by neutralising antibodies, but perhaps just as importantly, also those that are recognised by non-neutralisers given that these mAbs appear to be the majority of those isolated (this work, Zhang et al, 2022; Snijder et al,

2018). Second, publishing the sequence of the stabilised pre-fusion construct will facilitate the characterisation of antibody-antigen interactions with respect to both conformations of gB. Third, mechanistic studies that define the mode of action of different anti-gB mAbs should be overlayed onto structural information. This would improve understanding of the functions each domain of gB plays in fusion.

Ultimately, this understanding may guide next-generation gB-based vaccine design focused on enhancing the antibody response to sites of vulnerability on the antigen.

6.7 Appendix V: Data Collection and Processing for the gBect$_{ECO12\text{-}3A5}$ Complex

	gBect$_{ECO12\text{-}3A5}$
Voltage (kV)	300
Electron exposure (e^-/ Å^2)	50
Defocus (μM)	1.5-3.3
Pixel size (Å^2)	0.7303
Symmetry imposed	C_3
Final particle images (no.)	182,954
Map resolution (Å)	2.8
FSC threshold	0.143

Table 6.7-1: Summary of data acquisition and processing for the gBect$_{ECO12\text{-}3A5}$ complex after imaging on a Titan Krios G31 cryo-TEM.

6.8 Appendix VI: Electron Density at the gBect-ECO12 Interface

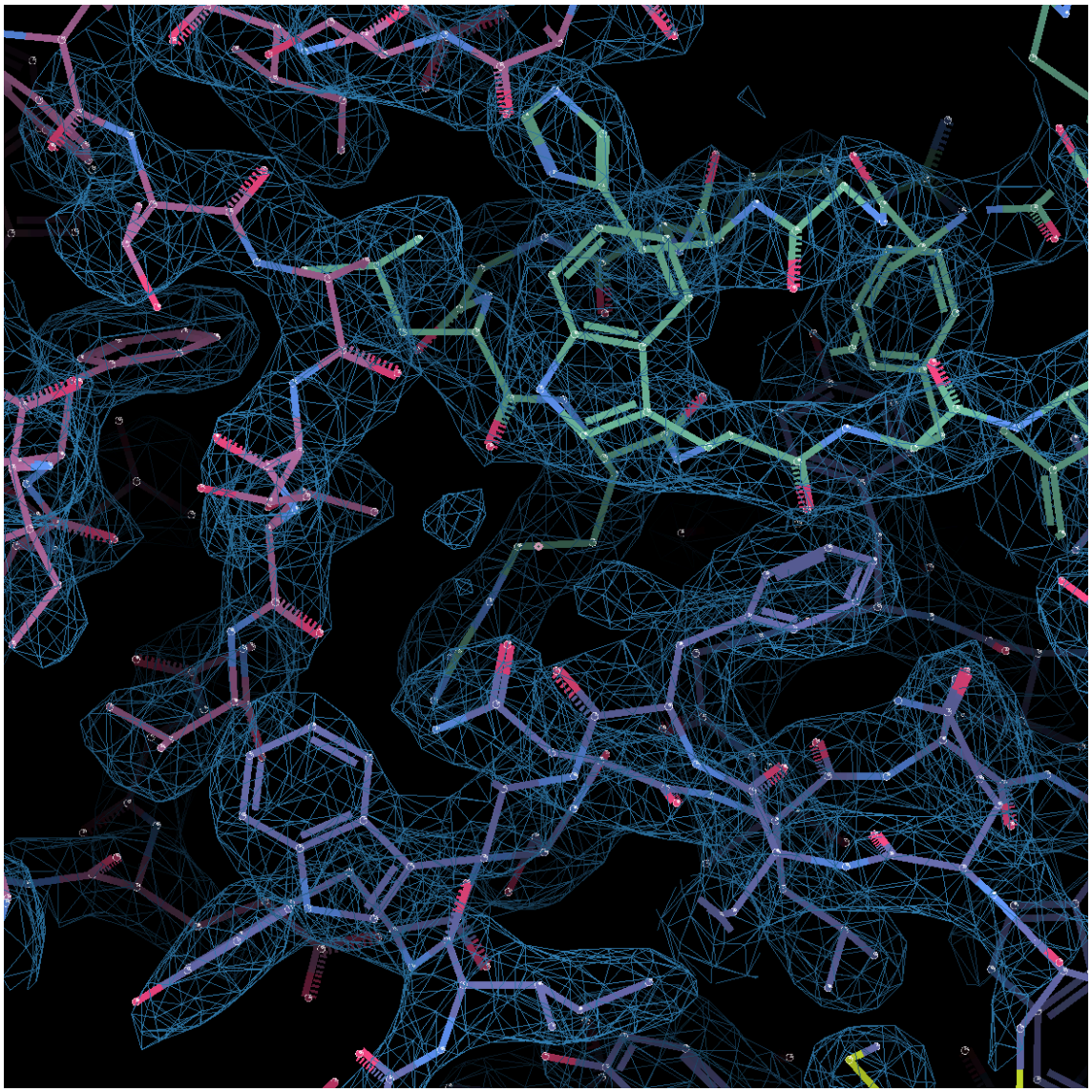


Figure 6.8-1: Electron density at the gBect-ECO12 interface.
Representative view of the Cryo-EM density displayed as a mesh around the model of the $gBect_{ECO12\text{-}3A5}$ complex at the ECO12 binding site. gB (red), the ECO12 Fab heavy chain (green) and the ECO12 Fab light chain (purple) are shown as sticks. Oxygen (pink) and nitrogen (blue) atoms in the model are displayed on all protein chains.
Image provided by Dr Rob Stass.

7 Concluding Remarks

7.1 Summary of Findings

7.1.1 Rabies Virus Glycoprotein

The part of this project relating to the rabies fusion protein, RabG, sought to understand whether RabG could be modified to improve its immunogenicity in a mouse model. To achieve this, structure-guided mutagenesis was conducted and mutants of RabG selected for two characteristics: the ability to improve cell-surface expression and/or to stabilise the pre-fusion conformation *in vitro*.

Mutants capable of improving expression and pre-fusion stabilisation were successfully identified, however screening these *in vivo* revealed none were able to improve the anti-RabG immune response. This was true when considering both a quantity-driven approach, i.e. does antigen engineering simply induce a greater antibody response, and a quality-driven approach – could antigen engineering raise greater titres of virus-neutralising antibodies specifically.

This is not to say that the mutant forms of RabG did not induce protective antibody responses. Even at low (~0.2 µg) doses, RabG constructs were able to induce neutralising antibody in mice. Rather, these findings speak to the potent immunogenicity of the RabG in its wild-type form, a feature of the antigen that would appear difficult to improve upon.

Pre-fusion conformationally specific neutralising antibodies against RabG exist, such as RVC20 (Hellert *et al*, 2020). Despite this, improving the stability of RabG had no effect on virus neutralising antibody titres in mouse studies presented here. Together, these observations suggest one of two explanations. First, though these pre-fusion specific epitopes are sites of vulnerability on RabG, it may be that they play a minor role in the induction of a protective antibody response; other neutralising epitopes clearly exist that are not pre-fusion specific. Second, it may simply be that the WT form of RabG is sufficiently stable under physiological conditions to present these epitopes to the immune system.

The pre-fusion form of RabG was detectable on the surface of transfected cells at pH 7.3 *in vitro*. It therefore seems likely that RabG expressed as a full-length construct in the context of a membrane *in vivo* would be capable of doing the same. On this premise, efforts to stabilise the pre-fusion conformation would convey little immunological benefit were the antigen to be delivered by a viral or mRNA vector, as was performed here.

The choice of these vaccine platforms to study pre-fusion RabG may appear an odd choice given this proposed explanation for the lack of improvement. Determining if pre-fusion stabilisation confers any benefit immunologically might best be done using protein-based immunogens that can definitively be characterised as being either pre-fusion or post-fusion.

Though this alternative appears intuitive, structural studies of a soluble RabG ectodomain at basic pH (~8.0) with no pre-fusion stabilisation suggest it adopts some kind of intermediate structure between pre- and post-fusion (Yang *et al*, 2020). In addition, lowering the pH to just 6.5 produces a fully post-fusion structure (Yang *et al*, 2020). Thus, generating protein vaccines that are 100% pre- or post-fusion under physiological conditions, under which variations in pH may well occur, is non-trivial.

Furthermore, expression of soluble RabG ectodomain does not produce trimeric antigen, but rather monomers (Yang *et al*, 2020). Given that three antigenic sites on RabG, III, IV and 'a', are all near to the protomer interface (Shi *et al*, 2022), it is likely that a monomeric antigen would poorly recapitulate the immunogenicity of the native antigen. Additionally, the interface itself may present conformational epitopes that would inherently be absent from a monomeric immunogen.

Lastly, the practical impact of this research should be considered. It is critical that next-generation rabies vaccines induce a protective antibody response after a single dose given the financial constraints discussed earlier in this thesis. Whether or not a pre-fusion stabilised RabG construct appeared advantageous when administered as a protein-based vaccine, such platforms are not amenable to single-dose administration, typically

requiring boosting. Additionally, expressing properly folded RabG for use as protein-based vaccines is both challenging and expensive (Ertl, 2019).

Whether or not such soluble protein studies could show that a conformationally specific immune response was superior to a non-specific one, its clinical relevance is minimal if viable vaccines do not utilise these immunogens. That is to say: this work suggests that pre-fusion stabilisation did not improve immunogenicity of RabG in mice in the context of clinically relevant vaccine platforms.

A perhaps more surprising result from the RabG work described in *Results I* is that quantitative improvements to the *in vitro* of expression RabG through mutagenesis did not improve immunogenicity. The most likely explanation is perhaps that the magnitude of the *in vitro* expression improvement observed is simply not large enough to have an effect *in vivo*. This suggests that the *in vitro* screen does not perfectly represent the conditions of a real immunisation.

Alternatively, the failure of improvement of expression to induce greater immune responses might be explained by considering expression kinetics. The *in vitro* screen used here measured RabG expression at 24 and 48 h post-transfection, at which time points expression improvements were observable. Antigen expression *in vivo* after mRNA delivery, for example, may persist for days longer than this period, however (Hassett *et al*, 2024; Pateev *et al*, 2023; Cui *et al*, 2024). It may therefore be the case that whilst mutagenesis is able to convey transient improvements to RabG expression over the WT, given sufficient time, WT expression may catch up. This could explain why overall anti-RabG titres are comparable in the animal studies described.

To summarise, the work described here suggests that the WT RabG is a potently immunogenic antigen when administered using viral vectored and mRNA-based platforms. This supports other animal and clinical data investigating similar platforms for RabG delivery (Zhang *et al*, 2024; Napolitano *et al*, 2020; Wang *et al*, 2016, 2018; Jenkin *et al*, 2022).

Improving pre-fusion stabilisation does not appear to convey any immunological benefit. This contradicts a previous study suggesting that the H270P mutant induces a stronger neutralising response than the WT in mice (Cao *et al*, 2024). This study, however, relied on a single animal experiment with six mice in each group. In the work presented here, the same RabG constructs were tested as mRNA vaccines using larger experimental groups and performing a more comprehensive statistical analysis of the effect(s) of mutation on antibody response. The inability to reproduce this significant improvement to total anti-RabG IgG and virus neutralising antibody titres favours the argument that the initial findings by Cao and colleagues may have been due to chance.

It should also be considered that work in this thesis identified a combinatorial double mutant of RabG that conveyed greater pre-fusion stabilisation than the H270P construct, and still no immunological improvement was observed. The inability to detect any differences in this carefully designed, better powered set of animal experiments may suggest that possible future strategies to stabilise RabG are unlikely to yield significant gains.

7.1.2 Epstein-Barr Virus Glycoprotein B

The studies relating to glycoprotein B sought to characterise its antigenic landscape and so facilitate future study of its pre-fusion conformation and decision-making about whether the pre-fusion conformation would be important for a gB-based vaccine. At the time of planning of this experimental work, little was understood about the structures of the pre-fusion gB across the human herpesviruses. This restricted the ability to perform structure-guided mutagenesis by methods similar to those conducted on RabG, necessitating adoption of a different approach.

Rather than attempt to stabilise the pre-fusion conformation through changes to the antigen itself, efforts were made to isolate antibodies against gB that may help identify pre-fusion-specific epitopes and possibly lock the protein in this form, facilitating structural study. Such an approach had the considerable advantage of relying less on pre-existing structural knowledge.

The challenge, however, was to develop a method of isolating antibodies against gB in its unstable conformation. To this end, viral-vectored immunogens of the full-length antigen were administered to mice such that gB presented to the immune system was expressed in the context of a membrane. This approach does not guarantee expression of pre-fusion gB exclusively – some gB may spontaneously adopt the post-fusion form even in a membrane, whilst some cleaved ectodomain may also be produced. Instead, however, this approach represented a reasonable attempt to present pre-fusion gB to the immune system without relying on additional stabilisation, strategies for which were unknown at the time.

A second challenge that arose during design of this work was how to screen antibody secreting cells (ASCs) for those that produced conformation-specific anti-gB binders. Given the barriers to working with pre-fusion gB directly, a two-step screening method was developed in which mAbs were tested for their ability to bind the post-fusion ectodomain or a membrane-expressed gB probe. Using a Beacon Optofluidics instrument, ASCs from immunised mice were assayed against these two probes in series. It was hoped that such an approach would permit the identification of ASCs making antibody against one or both conformations of gB.

Though 40 gB-reactive antibodies were successfully re-expressed and characterised, none were able to recognise the pre-fusion conformation specifically. This finding speaks to two possible explanations. First, it may be that immunising animals with unstabilised gB, even using viral vectors for membrane-based antigen expression, does not result in presentation of pre-fusion gB to the immune system. Should this be the cause of the failure to isolate pre-fusion specific mAbs, without advances in antigen stabilisation techniques, this issue is unavoidable..

Alternatively, or indeed additionally, pre-fusion specific antibodies may represent an extremely rare population, if they exist at all. In this case, the primary limitation of the strategy employed here is throughput: isolation of more mAbs improves the ability to detect rare populations. In the final campaign on the Beacon instrument, ~100 gB-reactive ASCs were identified on a single optofluidics chip. This yield may well be

sufficient to identify such antibodies were multi-chip runs conducted, albeit at considerable consumable cost.

This associated cost of using the Beacon was both a both a challenge and a motivator for aspects of the strategy. Over the 18-month period of working on the Beacon, substantial optimisation and adaptation of the antibody discovery workflow was conducted. The resulting workflow permitted reasonable hit rates from frozen mouse samples. In addition, changes to steps upstream and downstream of the Beacon substituted protocols reliant on expensive, proprietary reagents or kits with readily available, off-the-shelf alternatives. Together, the changes implemented addressed two inhibitory costs of using a Beacon for antibody discovery: instrument purchase and expensive consumables.

※

A final, important consideration with respect to work on the Beacon is the choice of mouse-derived samples for this project, due to the research group's desire to develop a pipeline for mouse mAb isolation. Given the ubiquitous nature of EBV in the human population, antibody discovery from human sources is probably a preferable approach for this particular antigen. Human antibody discovery likely has more direct biological and clinical relevance than mouse antibody discovery on account of avoiding problems with reactogenicity. In addition, human antibody discovery may be better suited to isolating rare or phenotypically different populations of antibodies to those raised in mice given the fundamental differences in their immune systems (Mestas & Hughes, 2004). Whether this is beneficial for pre-fusion specific anti-gB mAb discovery is impossible to predict but worth considering, nonetheless.

The decision to work on mouse-derived samples was made with two considerations in mind. Working with mice holds substantial practical advantages to working with human samples. By its nature, mouse work permits more exploratory study than human work. In this case, it was thought that the ability to immunise animals with a full-length gB immunogen could focus the immune response on the antigen of interest, in its relevant

conformation. Relying on samples from infected individuals, on the other hand, has the disadvantage that only a small number of circulating B cells and/or plasma cells may be gB-specific.

Secondly, as discussed above, the pipeline established was designed to allow other researchers to access the Beacon technology. Whilst EBV antibody discovery is amenable to working from human samples, many other targets are not. Developing a workflow that could be adapted for work on other targets provides practical benefits that extend past EBV research.

※

The neutralising and non-neutralising antibodies that were isolated against gB bind a range of epitopes on the post-fusion structure. Based on competition data with mAbs whose epitopes have been characterised structurally, it appears that a large proportion of the panel bind on or near to the post-fusion crown of gB, DIV. A rarer set of mAbs bind epitopes around the torso of the post-fusion ectodomain in DII, including 3A3, ECO12 and ECO48.

From the neutralisation data that was acquired, the latter population contain a higher frequency of mAbs capable of neutralising EBV infection *in vitro*. This could suggest that the post-fusion crown of gB may act as an immunological distraction by presenting non-neutralising epitopes, generalised here into 'antigenic sites' called Site 1, 2 and 3.

Whilst DII is clearly a site of vulnerability, newly described as containing antigenic Site 4, the mechanism(s) of neutralisation by mAbs recognising this region are unknown. A surprising finding of this work was that they do not appear to bind membrane-expressed gB as well as other mAbs in the panel that show comparable binding behaviour against the soluble ectodomain. This would suggest that either the epitopes of these mAbs are less accessible due to some kind of membrane effect, or that the antigen in its pre-fusion conformation is poorly recognised. Intuitively, one might expect neutralising antibodies to disproportionately target the pre-fusion form, thus blocking the fusion process. Instead, however, these preliminary results suggest that the most potent neutralisers in the mAb

panel show preference for post-fusion gB. This binding preference should be confirmed once a known pre-fusion stabilised version of gB is available.

7.1.3 Pre-fusion Stabilisation in the Context of Vaccination

The findings described here for RabG and EBV gB provide little evidence to support pre-fusion stabilisation for improving the quality or quantity of antibody induction by Class III fusion protein immunogens.

Regarding RabG, the unstabilised, full length WT form of the antigen is strongly immunogenic when delivered via an adenovirus vector or as an mRNA vaccine. It may well present largely in the pre-fusion conformation under physiological conditions, and it is possible that levels of expression of the WT protein are already sufficient to effectively 'saturate' the surface of transduced cells *in vivo*, such that further improvement in expression levels has no effect upon antigen availability to the immune system.

For EBV gB, the inability to directly test a pre-fusion stabilised gB antigen prevents the drawing of such concrete conclusions as for RabG. Failure to isolate pre-fusion specific antibodies, however, may suggest they play a minor role in the antibody response raised to it. Furthermore, these early attempts to map neutralising mAbs onto the structure of gB suggest one site recognised by neutralising antibodies may be better presented on the post-fusion structure than the pre-fusion. Clearly, however, understanding pre-fusion gB and its immunogenicity requires substantial further study, aspects of which are discussed in the next section.

It is important to consider the findings of this work in the context of pre-fusion stabilisation more broadly. Ultimately, this work supports the case that two conditions must be satisfied for pre-fusion stabilisation to convey an immunological benefit:

1) **The pre-fusion form of the antigen needs to be unstable enough that immunisation with the wild-type fusogen would not otherwise lead to its presentation to the immune system.**

The rabies virus glycoprotein may represent a good example of this principle's importance. Given that vectored immunogens of RabG probably adopt the pre-fusion conformation *in vivo* anyway, additional stabilisation is unlikely to provide much benefit.

An exception to this might be in the case where stabilising the pre-fusion conformation improves levels of antigen expression *in vivo* relative to the WT. This may be sufficient to improve immunogenicity even when the pre-fusion conformation is sufficiently stable simply by more efficiently exposing the immune system to properly folded antigen. In the case of RabG, such an effect was not observed, but in theory it remains possible for other antigens/vaccine platforms.

2) The pre-fusion conformation must provide some immunological gain over the post-fusion form.

This benefit is likely to manifest in the presentation of neutralising epitopes that are exposed in a conformationally specific manner. Perhaps the best example of this is RSV F, where there exists a clear distinction between the epitopes on, and antibodies to, the pre- and post-fusion forms, of which only the former is protective (Ruckwardt *et al*, 2019).

For RabG and EBV gB, the relevance of this pre-fusion specific immune response is unknown. On account of condition (1), the question may not be relevant for RabG given it likely adopts the pre-fusion conformation *in vivo* anyway. That is, discovering the pre-fusion-specific immune response is superior to that raised against the post-fusion is a moot point if the WT antigen expresses as pre-fusion already. Considering gB's instability, however, establishing this fact remains critical. Should such a pre-fusion response be protective against EBV infection, significant effort should be invested into characterising it.

The antibodies characterised here do not lend support to the importance of the pre-fusion response given that no conformationally specific mAb was identified. Despite there being several anti-gB antibodies characterised elsewhere, no other studies have identified such

mAbs either (Zhang *et al*, 2022; Hong *et al*, 2022; Snijder *et al*, 2018). For EBV at least, current understanding suggests condition (2) may not be met.

Mouse studies on a pre-fusion-like, stabilised form of HCMV gB appear to support this. The authors show that the stabilised antigen induces comparable antibody responses to the wild-type, post-fusion form (Sponholtz *et al*, 2024; Karthigeyan *et al*, 2024).

※

The suggestion that an antibody response targeting the pre-fusion form is not more protective than one against the post-fusion may be considered slightly surprising. A possible explanation, however, may be found in study of the murine γ-herpesvirus 68 (MHV-68). The MHV-68 gB trimer appears to undergo a conformational change between expression on the surface of extracellular virions, and in the late endosome, where it catalyses membrane fusion after endocytosis (Gillet *et al*, 2008). As part of this conformational change, neutralising epitopes on gB that were buried in the extracellular form are only presented after the primary structural transition, but immediately before membrane fusion (Gillet *et al*, 2008).

These findings therefore suggest that for MHV-68, the pre-fusion conformation of gB is itself a poor target for neutralising antibodies. Presumably to evade such an immune response, vulnerable epitopes are only expressed on a transitory form of gB that is presented immediately prior to the fusion step. Though similar behaviour has not been documented for any human herpesvirus, such a strategy may explain why pre-fusion gB is not a better immunogen than post-fusion gB. This raises the intriguing possibility that pre-fusion gB itself may be an immunological decoy.

※

At the time of writing, evidence for the successful implementation of pre-fusion stabilisation strategies for improved immunity could only be identified for Class I fusion proteins. These include RSV-F (Ngwuta *et al*, 2015; McLellan, 2015), parainfluenza virus F (Stewart-Jones *et al*, 2018), Nipah virus F (Loomis *et al*, 2020) and, possibly, the

coronaviruses (Pallesen *et al*, 2017; Bowen *et al*, 2022; Lu *et al*, 2022). Whilst this may simply be the result of Class I fusion proteins generally being better studied, the possibility that such efforts only provide benefits for this family of fusogen should be considered.

7.2 Future Directions

7.2.1 Rabies Virus

The findings presented here suggest that future efforts to develop next-generation rabies vaccines may be better spent focusing on the testing of different vaccine platforms to deliver RabG, rather than engineering it. The ultimate goal of these studies should be to develop vaccines that require minimal or ideally no boosting to induce protective, long-lasting anti-RabG responses.

In this study, an adenovirus-vectored vaccine platform was shown to induce neutralising responses in mice, as were LNP-encapsulated mRNA constructs encoding RabG. Though these and other similar studies suggest such vaccines are promising, clinical trials are required to assess the protectiveness and longevity of the responses they induce.

To this end, a ChAdOx2 vectored RabG vaccine was recently shown to have an acceptable safety profile in a Phase I study (Jenkin *et al*, 2022). Participants received a low (5×10^9 virus particles (v.p.)), medium (2.5×10^{10} v.p.) or high (5×10^{10} v.p.) dose of the vaccine intramuscularly. Immunology studies revealed that all 9 participants in the medium and high dose groups raised antibody titres greater than 0.5 IU/mL, the internationally recognised correlate of protection (Jenkin *et al*, 2022). After one-year post-vaccination, 6 of 7 returning participants in these dose groups maintained antibody titres above this threshold (Jenkin *et al*, 2022).

These findings suggest long-lasting protective antibody responses targeting RabG are inducible after single-dose vaccination. An ongoing Phase II trial (ClinicalTrials.gov ID: NCT04270838) seeks to investigate the vaccine's immunogenicity in adults and children over a 5.5-year follow-up period. This will determine how long such protection may last. Should lasting antibody responses be induced, this vaccine candidate, and

others that may follow it, could substantially alter the cost-benefit landscape of administering rabies PrEP in high-risk areas.

Further vaccine development work should therefore focus on comparison of different RabG-based vaccine platforms. Those that can be produced at low cost and induce long-lived neutralising responses are likely to play a major role in reducing the human disease burden over the next few decades.

7.2.2 Epstein-Barr Virus

The failure to isolate pre-fusion specific anti-gB antibodies suggests that in order to study this conformation, developing a stabilised version of this protein is a necessity. Concurrently with the preparation of this thesis, researchers at the University of Washington published a pre-print article in which they describe such a stabilised EBV gB variant (McCallum & Veesler, 2024).

Using an iterative, computationally driven approach, the pre-fusion conformation of gB was stabilised through multiple engineering strategies. These included the removal of a flexible loop between DII and DIII, introducing an inter-promoter disulphide bond to staple the trimer together, stabilising predicted hinge points in DI and adding a trimerisation domain to the C-terminus of the ectodomain (McCallum & Veesler, 2024).

Whilst the variant's sequence and its structure have not yet been made available, the authors cite structural similarities to pre-fusion HCMV gB (Liu *et al*, 2021a; McCallum & Veesler, 2024). Ultimately, once fully public, this construct will allow for the direct comparison of pre- and post-fusion gB immunogens. In the process, it will clarify the importance of a pre-fusion specific immune response.

The study of pre-fusion gB may prove beneficial for designing a subunit vaccine against EBV. It is, however, important to remember that other surface glycoproteins expressed by the virus may be promising vaccine candidates in their own right. Robust comparison of these antigens with respect to their immunogenicity is both lacking and likely to be critical for success. Determining which antigen, and/or what combinations, induce the most protective immune response remains challenging without such studies.

Animal-based comparisons may shed light on which antigen(s) might be most promising. The immunisation of rabbits with EBV gH/gL, gB and gp350 revealed that gH/gL and gB induce greater neutralising titres than gp350 and showed synergistic neutralisation behaviour (Cui *et al*, 2016). Furthermore, passive immunisation of a humanised mouse model with the gH/gL and gB-reactive sera protected against lethal EBV challenge (Cui *et al*, 2021). In this study, all 6 mice administered anti-gB serum showed protection against challenge, significantly higher than for the anti-gH/gL, in which 3 animals died within 100 days post-infection (Cui *et al*, 2021).

Though these findings give some credence to notion that gB is a promising vaccine candidate, they are only preliminary and would benefit from supporting human data. Similarly, combining antigens appears a promising approach to improving protectiveness. This strategy has been adopted in the development of Moderna's EBV vaccine, that combines gp220 (a gp350 splice variant), gp42 and gH/gL, but not gB (Phase I/II ongoing, ClinicalTrials.gov ID: NCT05164094).

※

Exactly what aspects of an anti-gB response are protective are still largely unknown. Functional characterisation of the antibodies isolated here was limited to *in vitro* neutralisation assays in which direct inhibition of viral entry is tested. Given that the *in vitro* neutralising capability of ECO100 was enhanced by the addition of exogenous complement, however, Fc-effector functions may also contribute to protection.

The focus on direct neutralisation – not just in this study but more widely in the field - has perhaps biased against characterising the contribution of Fc effector functions to protection. In the case of HCMV, however, non-neutralising anti-gB antibody contributes to protection via complement activity in both animal models and gB/MF59-immunised humans (Cui *et al*, 2018; Chiuppesi *et al*, 2018; Loomis *et al*, 2013; Li *et al*, 2017).

As well as complement-mediated activity, non-neutralising antibodies might also protect via antibody-dependent cell mediated mechanisms including ADCC and ADCP, as they are thought to for HSV-1/2 and HCMV (Nelson *et al*, 2018b; Eberhard *et al*, 2021;

Kuraoka *et al*, 2023; Kohl *et al*, 1990). Study of these functionalities will likely require significant assay development as well as new *in vivo* models.

※

Selecting promising antigen(s) for EBV vaccines is only the start of developing an effective therapeutic. EBV's ability to remain latent for decades makes vaccine-induced clearance of infection unfeasible. This leaves two possible intervention strategies for consideration:

1) A prophylactic vaccine administered prior to primary infection that induces sterilising immunity. Consensus is that achieving such protective immune responses through vaccination is a high bar (Rozman *et al*, 2022; Balfour *et al*, 2020). Given that primary infection may occur in young children (Jean-Pierre *et al*, 2021), such a strategy would likely be predicated on early (possibly infant) immunisation.

2) A therapeutic vaccine that is administered after primary infection but might prevent re-activation of the virus or symptomatic disease. Re-entry into the lytic lifecycle stage has been implicated in the development of multiple EBV-associated cancers (Murata *et al*, 2021) and post-transplant lymphoproliferative disorders (Chakravorty *et al*, 2022). This is perhaps more feasible than the former strategy. A gp350 vaccine candidate has already been shown to prevent infectious mononucleosis in human trials, despite having no effect on EBV infection rate (Sokal *et al*, 2007).

   A possible drawback of this approach, however, is that the role of lytic reactivation in MS development is still unknown (Soldan & Lieberman, 2022). Without such a mechanistic link between diseases and virus reactivation, targeting lytic antigen(s) may not be fully effective.

Long-term clinical trials are the only way of determining whether therapeutic vaccines are efficacious given the unpredictable nature of developing EBV-associated diseases (cancers, MS). How effective targeting the fusion protein and/or other surface

glycoproteins will be in preventing clinically relevant disease therefore depends on the willingness to pursue these targets in this fashion.

7.3 Final Remarks

The elegant example of pre-fusion stabilisation for the RSV F protein highlighted the potential such strategies may have for vaccine development. Given the findings presented here for the EBV and rabies fusogens, as well as those for HCMV (Karthigeyan *et al*, 2024; Sponholtz *et al*, 2024), the effectiveness of this approach may not be as widely applicable as had been hoped. It is therefore critical that this strategy does not become too great a part of the focus for the development of vaccines against enveloped viruses. The importance of fundamental vaccinology work including comparison of different antigens, vaccine platforms and regimens should not be overlooked.

8 Bibliography

Abramson J, Adler J, Dunger J, Evans R, Green T, Pritzel A, Ronneberger O, Willmore L, Ballard AJ, Bambrick J, *et al* (2024) Accurate structure prediction of biomolecular interactions with AlphaFold 3. *Nature 2024 630:8016* 630: 493–500

Albertini AA, Mérigoux C, Libersou S, Madiona K, Bressanelli S, Roche S, Lepault J, Melki R, Vachette P & Gaudin Y (2012a) Characterization of monomeric intermediates during VSV glycoprotein structural transition. *PLoS Pathog* 8

Albertini AAV, Baquero E, Ferlin A & Gaudin Y (2012b) Molecular and Cellular Aspects of Rhabdovirus Entry. *Viruses* 4: 117–139

Alfaleh MA, Alsaab HO, Mahmoud AB, Alkayyal AA, Jones ML, Mahler SM & Hashem AM (2020) Phage Display Derived Monoclonal Antibodies: From Bench to Bedside. *Front Immunol* 11

Andrei G & Snoeck R (2021) Advances and Perspectives in the Management of Varicella-Zoster Virus Infections. *Molecules* 26

Asthagiri Arunkumar G, Ioannou A, Wohlbold TJ, Meade P, Aslam S, Amanat F, Ayllon J, García-Sastre A & Krammer F (2019) Broadly Cross-Reactive, Nonneutralizing Antibodies against Influenza B Virus Hemagglutinin Demonstrate Effector Function-Dependent Protection against Lethal Viral Challenge in Mice. *J Virol* 93: 1696–1714

Astray RM, Jorge SAC & Pereira CA (2017) Rabies vaccine development by expression of recombinant viral glycoprotein. *Arch Virol* 162: 323–332

Atanasiu D, Whitbeck JC, Cairns TM, Reilly B, Cohen GH & Eisenberg RJ (2007) Bimolecular complementation reveals that glycoproteins gB and gH/gL of herpes simplex virus interact with each other during cell fusion. *Proc Natl Acad Sci U S A* 104: 18718–18723

Auerswald H, Maestri A, Touch S, In S, Ya N, Heng B, Bosch-Castells V, Augard C, Petit C, Dussart P, *et al* (2023) Side-by-side Comparative Study of the Immunogenicity of the Intramuscular and Intradermal Rabies Post-exposure Prophylaxis Regimens in a Cohort of Suspected Rabies Virus Exposed Individuals. *Clin Infect Dis* 77: 910

Backovic M & Jardetzky TS (2011) Class III viral membrane fusion proteins. *Adv Exp Med Biol* 950: 91–101

Backovic M, Jardetzky TS & Longnecker R (2007) Hydrophobic Residues That Form Putative Fusion Loops of Epstein-Barr Virus Glycoprotein B Are Critical for Fusion Activity. *J Virol* 81: 9596–9600

Backovic M, Longnecker R & Jardetzky TS (2009) Structure of a trimeric variant of the Epstein-Barr virus glycoprotein B. *Proc Natl Acad Sci U S A* 106: 2880–2885

Bagdonaite I, Nordén R, Joshi HJ, King SL, Vakhrushev SY, Olofsson S & Wandall HH (2016) Global mapping of o-glycosylation of varicella zoster virus, human cytomegalovirus, and Epstein-Barr virus. *Journal of Biological Chemistry* 291: 12014–12028

Bagdonaite I & Wandall HH (2018) Global aspects of viral glycosylation. *Glycobiology* 28: 443–467

Bailey-Serres J (1999) Selective translation of cytoplasmic mRNAs in plants. *Trends Plant Sci* 4: 142–148

Balfour HH, Schmeling DO & Grimm-Geris JM (2020) The promise of a prophylactic Epstein-Barr virus vaccine. *Pediatr Res* 87: 345–352

Baquero E, Albertini AA, Vachette P, Lepault J, Bressanelli S & Gaudin Y (2013) Intermediate conformations during viral fusion glycoprotein structural transition. *Curr Opin Virol* 3: 143–150

Baquero E, Albertini AAV & Gaudin Y (2015) Recent mechanistic and structural insights on class III viral fusion glycoproteins. *Curr Opin Struct Biol* 33: 52–60

Baraniak I, Gomes AC, Sodi I, Langstone T, Rothwell E, Atkinson C, Pichon S, Piras-Douce F, Griffiths PD & Reeves MB (2019) Seronegative patients vaccinated with cytomegalovirus gB-MF59 vaccine have evidence of neutralising antibody responses against gB early post-transplantation. *EBioMedicine* 50: 45–54

Baraniak I, Kropff B, Ambrose L, McIntosh M, McLean GR, Pichon S, Atkinson C, Milne RSB, Mach M, Griffiths PD, *et al* (2018a) Protection from cytomegalovirus viremia following glycoprotein B vaccination is not dependent on neutralizing antibodies. *Proc Natl Acad Sci U S A* 115: 6273–6278

Baraniak I, Kropff B, McLean GR, Pichon S, Piras-Douce F, Milne RSB, Smith C, Mach M, Griffiths PD & Reeves MB (2018b) Epitope-Specific Humoral Responses to Human Cytomegalovirus Glycoprotein-B Vaccine With MF59: Anti-AD2 Levels Correlate With Protection From Viremia. *J Infect Dis* 217: 1907–1917

Barrett JR, Pipini D, Wright ND, Cooper AJR, Gorini G, Quinkert D, Lias AM, Davies H, Rigby CA, Aleshnick M, *et al* (2024) Analysis of the diverse antigenic landscape of the malaria protein RH5 identifies a potent vaccine-induced human public antibody clonotype. *Cell* 187: 4964-4980.e21

Bedi P & Sharma C (2016) Community detection in social networks. *Wiley Interdiscip Rev Data Min Knowl Discov* 6: 115–135

Behrens AJ, Vasiljevic S, Pritchard LK, Harvey DJ, Andev RS, Krumm SA, Struwe WB, Cupo A, Kumar A, Zitzmann N, *et al* (2016) Composition and Antigenic Effects of Individual Glycan Sites of a Trimeric HIV-1 Envelope Glycoprotein. *Cell Rep* 14: 2695

Bender FC, Samanta M, Heldwein EE, Leon MP de, Bilman E, Lou H, Whitbeck JC, Eisenberg RJ & Cohen GH (2007) Antigenic and Mutational Analyses of Herpes Simplex Virus Glycoprotein B Reveal Four Functional Regions. *J Virol* 81: 3827

Benhaim M & Lee KK (2018) Single-Molecule Analysis of a Viral Fusion Protein Illuminates a Fusion-Active Intermediate State. *Cell* 174: 775–777

Bernstein DI, Munoz FM, Callahan ST, Rupp R, Wootton SH, Edwards KM, Turley CB, Stanberry LR, Patel SM, Mcneal MM, *et al* (2016) Safety and efficacy of a cytomegalovirus glycoprotein B (gB) vaccine in adolescent girls: A randomized clinical trial. *Vaccine* 34: 313–319

Bernstein DI, Reap EA, Katen K, Watson A, Smith K, Norberg P, Olmsted RA, Hoeper A, Morris J, Negri S, *et al* (2009) Randomized, double-blind, Phase 1 trial of an alphavirus replicon vaccine for cytomegalovirus in CMV seronegative adult volunteers. *Vaccine* 28: 484–493

Birkenbach M, Tong X, Bradbury LE, Tedder TF & Kieff E (1992) Characterization of an Epstein-Barr virus receptor on human epithelial cells. *Journal of Experimental Medicine* 176: 1405–1414

Bjornevik K, Cortese M, Healy BC, Kuhle J, Mina MJ, Leng Y, Elledge SJ, Niebuhr DW, Scher AI, Munger KL, *et al* (2022) Longitudinal analysis reveals high prevalence of Epstein-Barr virus associated with multiple sclerosis. *Science (1979)* 375: 296–301

Bjornevik K, Münz C, Cohen JI & Ascherio A (2023) Epstein–Barr virus as a leading cause of multiple sclerosis: mechanisms and implications. *Nature Reviews Neurology 2023 19:3* 19: 160–171

Von Boehmer L, Liu C, Ackerman S, Gitlin AD, Wang Q, Gazumyan A & Nussenzweig MC (2016) Sequencing and cloning of antigen-specific antibodies from mouse memory B cells. *Nature Protocols 2016 11:10* 11: 1908–1923

Bootz A, Karbach A, Spindler J, Kropff B, Reuter N, Sticht H, Winkler TH, Britt WJ & Mach M (2017) Protective capacity of neutralizing and non-neutralizing antibodies against glycoprotein B of cytomegalovirus. *PLoS Pathog* 13: e1006601

Borza CM & Hutt-Fletcher LM (2002) Alternate replication in B cells and epithelial cells switches tropism of Epstein-Barr virus. *Nat Med* 8: 594–599

Bos AB, Luan P, Duque JN, Reilly D, Harms PD & Wong AW (2015) Optimization and automation of an end-to-end high throughput microscale transient protein production process. *Biotechnol Bioeng* 112: 1832–1842

Bos R, Rutten L, van der Lubbe JEM, Bakkers MJG, Hardenberg G, Wegmann F, Zuijdgeest D, de Wilde AH, Koornneef A, Verwilligen A, *et al* (2020) Ad26 vector-based COVID-19 vaccine encoding a prefusion-stabilized SARS-CoV-2 Spike immunogen induces potent humoral and cellular immune responses. *npj Vaccines 2020 5:1* 5: 1–11

Bowen JE, Park Y-J, Stewart C, Brown JT, Sharkey WK, Walls AC, Joshi A, Sprouse KR, McCallum M, Tortorici MA, *et al* (2022) SARS-CoV-2 spike conformation determines plasma neutralizing activity elicited by a wide panel of human vaccines. *Sci Immunol*

Brüggemann M, Osborn MJ, Ma B, Hayre J, Avis S, Lundstrom B & Buelow R (2015) Human Antibody Production in Transgenic Animals. *Arch Immunol Ther Exp (Warsz)* 63: 101–108

Brunker K & Mollentze N (2018) Rabies Virus. *Trends Microbiol* 26: 886–887

Bu W, Joyce MG, Nguyen H, Banh D V., Aguilar F, Tariq Z, Yap ML, Tsujimura Y, Gillespie RA, Tsybovsky Y, *et al* (2019) Immunization with Components of the Viral Fusion Apparatus Elicits Antibodies That Neutralize Epstein-Barr Virus in B Cells and Epithelial Cells. *Immunity* 50: 1305-1316.e6

Bullough PA, Hughson FM, Skehel JJ & Wiley DC (1994) Structure of influenza haemagglutinin at the pH of membrane fusion. *Nature 1994 371:6492* 371: 37–43

Burke HG & Heldwein EE (2015) Crystal Structure of the Human Cytomegalovirus Glycoprotein B. *PLoS Pathog* 11: e1005227

Burman L, Chong YE, Duncan S, Klaus A, Rauch K, Hamel K, Hervé K, Pfaffen S, Collins DW, Heyries K, *et al* (2020) Isolation of monoclonal antibodies from anti-synthetase syndrome patients and affinity maturation by recombination of independent somatic variants. *MAbs* 12

Buus S, Rockberg J, Forsström B, Nilsson P, Uhlen M & Schafer-Nielsen C (2012) High-resolution Mapping of Linear Antibody Epitopes Using Ultrahigh-density Peptide Microarrays. *Mol Cell Proteomics* 11: 1790

Cairns TM, Fontana J, Huang Z-Y, Whitbeck JC, Atanasiu D, Rao S, Shelly SS, Lou H, Ponce de Leon M, Steven AC, *et al* (2014a) Mechanism of Neutralization of Herpes Simplex Virus by Antibodies Directed at the Fusion Domain of Glycoprotein B. *J Virol* 88: 2677–2689

Cairns TM, Huang Z-Y, Whitbeck JC, Ponce De Leon M, Lou H, Wald A, Krummenacher C, Eisenberg RJ & Cohen GH (2014b) Dissection of the Antibody Response against Herpes Simplex Virus Glycoproteins in Naturally Infected Humans Downloaded from. *J Virol* 88: 12612–12622

Callaway HM, Zyla D, Larrous F, de Melo GD, Hastie KM, Avalos RD, Agarwal A, Corti D, Bourhy H & Saphire EO (2022) Structure of the rabies virus glycoprotein trimer bound to a prefusion-specific neutralizing antibody. *Sci Adv* 8

Cao H, Li H, Luan N, Zhang H, Lin K, Hu J, Song J & Liu C (2024) A rabies mRNA vaccine with H270P mutation in its glycoprotein induces strong cellular and humoral immunity. *Vaccine* 42: 1116–1121

Cesarman E (2014) Gammaherpesviruses and lymphoproliferative disorders. *Annu Rev Pathol* 9: 349–372

Chakravorty S, Afzali B & Kazemian M (2022) EBV-associated diseases: Current therapeutics and emerging technologies. *Front Immunol* 13: 1059133

Chandler TL, Yang A, Otero CE, Permar SR & Caddy SL (2023) Protective mechanisms of nonneutralizing antiviral antibodies. *PLoS Pathog* 19: e1011670

Chandramouli S, Ciferri C, Nikitin PA, Caló S, Gerrein R, Balabanis K, Monroe J, Hebner C, Lilja AE, Settembre EC, *et al* (2015) Structure of HCMV glycoprotein B in the postfusion conformation bound to a neutralizing human antibody. *Nat Commun* 6: 1–12

Changalucha J, Steenson R, Grieve E, Cleaveland S, Lembo T, Lushasi K, Mchau G, Mtema Z, Sambo M, Nanai A, *et al* (2019) The need to improve access to rabies post-exposure vaccines: Lessons from Tanzania. *Vaccine* 37: A45

Chao LH, Klein DE, Schmidt AG, Peña JM & Harrison SC (2014) Sequential conformational rearrangements in flavivirus membrane fusion. *Elife* 3: e04389

Charles A Janeway J, Travers P, Walport M & Shlomchik MJ (2001) The structure of a typical antibody molecule.

Chen WC & Murawsky CM (2018) Strategies for generating diverse antibody repertoires using transgenic animals expressing human antibodies. *Front Immunol* 9: 333158

Chesnokova LS & Hutt-Fletcher LM (2011) Fusion of Epstein-Barr Virus with Epithelial Cells Can Be Triggered by αvβ5 in Addition to αvβ6 and αvβ8, and Integrin Binding Triggers a Conformational Change in Glycoproteins gHgL. *J Virol* 85: 13214–13223

Chiuppesi F, Nguyen J, Park S, Contreras H, Kha M, Meng Z, Kaltcheva T, Iniguez A, Martinez J, La Rosa C, *et al* (2018) Multiantigenic Modified Vaccinia Virus Ankara Vaccine Vectors To Elicit Potent Humoral and Cellular Immune Reponses against Human Cytomegalovirus in Mice. *J Virol* 92

Cliquet F, Aubert M & Sagné L (1998) Development of a fluorescent antibody virus neutralisation test (FAVN test) for the quantitation of rabies-neutralising antibody. *J Immunol Methods* 212: 79–87

Cohen JI (2020) Herpesvirus latency. *J Clin Invest* 130: 3361–3369

Connolly SA, Jardetzky TS & Longnecker R (2020) The structural basis of herpesvirus entry. *Nat Rev Microbiol*

Cooper RS & Heldwein EE (2015) Herpesvirus gB: A Finely Tuned Fusion Machine. *Viruses* 7: 6552–6569

Corey L, Langenberg AGM, Ashley R, Sekulovich RE, Izu AE, Douglas JM, Hunter Handsfield H, Warren T, Marr L, Tyring S, *et al* (1999) Recombinant glycoprotein vaccine for the prevention of genital HSV-2 infection: Two randomized controlled trials. *J Am Med Assoc* 282: 331–340

Craig DB & Dombkowski AA (2013) Disulfide by Design 2.0: A web-based tool for disulfide engineering in proteins. *BMC Bioinformatics* 14: 1–7

Cui X, Cao Z, Chen Q, Arjunaraja S, Snow AL & Snapper CM (2016) Rabbits immunized with Epstein-Barr virus gH/gL or gB recombinant proteins elicit higher serum virus neutralizing activity than gp350. *Vaccine* 34: 4050–4055

Cui X, Cao Z, Ishikawa Y, Cui S, Imadome K-I, Snapper CM, Tripp RA & Holst PJ (2021) Immunization with Epstein-Barr Virus Core Fusion Machinery Envelope Proteins Elicit High Titers of Neutralizing Activities and Protect Humanized Mice from Lethal Dose EBV Challenge. *Vaccines (Basel)* 9

Cui X, Cao Z, Wang S, Lee RB, Wang X, Murata H, Adler SP, McVoy MA & Snapper CM (2018) Novel trimeric human cytomegalovirus glycoprotein B elicits a high-titer neutralizing antibody response. *Vaccine* 36: 5580–5590

Cui X, Vervaeke P, Gao Y, Opsomer L, Sun Q, Snoeck J, Devriendt B, Zhong Z & Sanders NN (2024) Immunogenicity and biodistribution of lipid nanoparticle formulated self-amplifying mRNA vaccines against H5 avian influenza. *npj Vaccines 2024 9:1* 9: 1–13

Cunningham AL, Lal H, Kovac M, Chlibek R, Hwang S-J, Díez-Domingo J, Godeaux O, Levin MJ, McElhaney JE, Puig-Barberà J, *et al* (2016) Efficacy of the Herpes Zoster Subunit Vaccine in Adults 70 Years of Age or Older. *New England Journal of Medicine* 375: 1019–1032

Daibata M, Humphreys RE, Takada K & Sairenji T (1990) Activation of latent EBV via anti-IgG-triggered, second messenger pathways in the Burkitt's lymphoma cell line Akata. *The Journal of Immunology* 144: 4788–4793

Damania B, Kenney SC & Raab-Traub N (2022) Epstein-Barr virus: Biology and clinical disease. *Cell* 185: 3652–3670

Delecluse HJ, Hilsendegen T, Pich D, Zeidler R & Hammerschmidt W (1998) Propagation and recovery of intact, infectious Epstein-Barr virus from prokaryotic to human cells. *Proc Natl Acad Sci U S A* 95: 8245–8250

Delecluse H-J, Pich D, Hilsendegen T, Baum C & Hammerschmidt W (1999) A first-generation packaging cell line for Epstein–Barr virus-derived vectors. *Proceedings of the National Academy of Sciences* 96: 5188–5193

Desai DV & Kulkarni SS (2015) Herpes Simplex Virus: The Interplay Between HSV, Host, and HIV-1. *Viral Immunol* 28: 546–555

Dicks MDJ, Spencer AJ, Edwards NJ, Wadell G, Bojang K, Gilbert SC, Hill AVS & Cottingham MG (2012) A Novel Chimpanzee Adenovirus Vector with Low Human Seroprevalence: Improved Systems for Vector Derivation and Comparative Immunogenicity. *PLoS One* 7: e40385

Dollery SJ, Delboy MG & Nicola A V. (2010) Low pH-Induced Conformational Change in Herpes Simplex Virus Glycoprotein B. *J Virol* 84: 3759

Draper SJ, Moore AC, Goodman AL, Long CA, Holder AA, Gilbert SC, Hill F & Hill AVS (2008) Effective induction of high-titer antibodies by viral vector vaccines. *Nature Medicine 2008 14:8* 14: 819–821

Durocher Y, Perret S & Kamen A (2002) High-level and high-throughput recombinant protein production by transient transfection of suspension-growing human 293-EBNA1 cells. *Nucleic Acids Res* 30: e9

Ebel H, Benecke T & Vollmer B (2022) Stabilisation of Viral Membrane Fusion Proteins in Prefusion Conformation by Structure-Based Design for Structure Determination and Vaccine Development. *Viruses* 14: 1816

Eberhard S, Vietzen H, Görzer I, Jaksch P & Puchhammer-Stöckl E (2021) Analysis and fine specificity of the HCMV-specific cell-free and cell-associated antibody-dependent cellular phagocytosis (ADCP) responses in lung transplant recipients. *Int J Mol Sci* 22: 8206

Edwards KR, Schmidt K, Homad LJ, Kher GM, Xu G, Rodrigues KA, Ben-Akiva E, Abbott J, Prlic M, Newell EW, *et al* (2024) Vaccination with nanoparticles displaying gH/gL from Epstein-Barr virus elicits limited cross-protection against rhesus lymphocryptovirus. *Cell Rep Med* 0: 101587

Egan K, Hook LM, LaTourette P, Desmond A, Awasthi S & Friedman HM (2020) Vaccines to prevent genital herpes. *Translational Research* 220: 138–152

Egri SB, Wang X, Díaz-Salinas MA, Luban J, Dudkina N V., Munro JB & Shen K (2023) Detergent modulates the conformational equilibrium of SARS-CoV-2 Spike during cryo-EM structural determination. *Nature Communications 2023 14:1* 14: 1–10

Van Erp EA, Luytjes W, Ferwerda G & Van Kasteren PB (2019) Fc-mediated antibody effector functions during respiratory syncytial virus infection and disease. *Front Immunol* 10: 432851

Ertl HCJ (2019) New Rabies Vaccines for Use in Humans. *Vaccines 2019, Vol 7, Page 54* 7: 54

Escalante GM, Foley J, Mutsvunguma LZ, Rodriguez E, Mulama DH, Muniraju M, Ye P, Barasa AK & Ogembo JG (2020) A pentavalent epstein-barr virus-like particle vaccine elicits high titers of neutralizing antibodies against epstein-barr virus infection in immunized rabbits. *Vaccines (Basel)* 8: 169

Escalante GM, Mutsvunguma LZ, Muniraju M, Rodriguez E & Ogembo JG (2022) Four Decades of Prophylactic EBV Vaccine Research: A Systematic Review and Historical Perspective. *Front Immunol* 0: 1431

Escalante GM, Reidel IG, Mutsvunguma LZ, Cua S, Tello BA, Rodriguez E, Farelo MA, Zimmerman C, Muniraju M, Li H, *et al* (2024) Multivalent MVA-vectored vaccine elicits EBV neutralizing antibodies in rhesus macaques that reduce EBV infection in humanized mice. *Front Immunol* 15: 1445209

Falloon J, Yu J, Esser MT, Villafana T, Yu L, Dubovsky F, Takas T, Levin MJ & Falsey AR (2017) An Adjuvanted, Postfusion F Protein–Based Vaccine Did Not Prevent Respiratory Syncytial Virus Illness in Older Adults. *J Infect Dis* 216: 1362–1370

Fierro C, Brune D, Shaw M, Schwartz H, Knightly C, Lin J, Carfi A, Natenshon A, Kalidindi S, Reuter C, *et al* (2024) Safety and Immunogenicity of a Messenger RNA-Based Cytomegalovirus Vaccine in Healthy Adults: Results From a Phase 1 Randomized Clinical Trial. *J Infect Dis* 230

Fingeroth JD, Diamond ME, Sage DR, Hayman J & Yates JL (1999) CD21-Dependent Infection of an Epithelial Cell Line, 293, by Epstein-Barr Virus. *J Virol* 73: 2115–2125

Fisher CR & Schnell MJ (2018) New developments in rabies vaccination. *Rev Sci Tech* 37(2): 657–672

Fisher CR, Streicker DG & Schnell MJ (2018) The spread and evolution of rabies virus: conquering new frontiers. *Nature Reviews Microbiology 2018 16:4* 16: 241–255

Fooks AR, Cliquet F, Finke S, Freuling C, Hemachudha T, Mani RS, Müller T, Nadin-Davis S, Picard-Meyer E, Wilde H, *et al* (2017) Rabies. *Nature Reviews Disease Primers 2017 3:1* 3: 1–19

Gaa R, Menang-Ndi E, Pratapa S, Nguyen C, Kumar S & Doerner A (2021) Versatile and rapid microfluidics-assisted antibody discovery. *MAbs* 13

Gabutti G, Bolognesi N, Sandri F, Florescu C & Stefanati A (2019) Varicella zoster virus vaccines: an update. *Immunotargets Ther* Volume 8: 15–28

Gao Y, Zhu S, Li H, Hao X, Chen W, Pan D & Qian Z (2024) AntigenBoost: enhanced mRNA-based antigen expression through rational amino acid substitution. *Brief Bioinform* 25: bbae468

Garcia NJ, Chen J & Longnecker R (2013) Modulation of Epstein-Barr Virus Glycoprotein B (gB) Fusion Activity by the gB Cytoplasmic Tail Domain. *mBio* 4

Gaudin Y, Raux H, Flamand A & Ruigrok RW (1996) Identification of amino acids controlling the low-pH-induced conformational change of rabies virus glycoprotein. *J Virol* 70: 7371

Gaudin Y, Ruigrok RW, Knossow M & Flamand A (1993) Low-pH conformational changes of rabies virus glycoprotein and their role in membrane fusion. *J Virol* 67: 1365–1372

Gérard A, Woolfe A, Mottet G, Reichen M, Castrillon C, Menrath V, Ellouze S, Poitou A, Doineau R, Briseno-Roa L, *et al* (2020) High-throughput single-cell activity-based screening and sequencing of antibodies using droplet microfluidics. *Nature Biotechnology 2020 38:6* 38: 715–721

Gershoni JM, Roitburd-Berman A, Siman-Tov DD, Freund NT & Weiss Y (2007) Epitope mapping: The first step in developing epitope-based vaccines. *BioDrugs* 21: 145–156

Gillet L, Colaco S & Stevenson PG (2008) Glycoprotein B switches conformation during murid herpesvirus 4 entry. *Journal of General Virology* 89: 1352–1363

Glauser DL, Kratz AS & Stevenson PG (2012) Herpesvirus Glycoproteins Undergo Multiple Antigenic Changes before Membrane Fusion. *PLoS One* 7: e30152

Glowacka I, Bertram S, Müller MA, Allen P, Soilleux E, Pfefferle S, Steffen I, Tsegaye TS, He Y, Gnirss K, *et al* (2011) Evidence that TMPRSS2 Activates the Severe Acute Respiratory Syndrome Coronavirus Spike Protein for Membrane Fusion and Reduces Viral Control by the Humoral Immune Response. *J Virol* 85: 4122–4134

Goddard TD, Huang CC, Meng EC, Pettersen EF, Couch GS, Morris JH & Ferrin TE (2018) UCSF ChimeraX: Meeting modern challenges in visualization and analysis. *Protein Sci* 27: 14–25

Gomes AC, Baraniak IA, Lankina A, Moulder Z, Holenya P, Atkinson C, Tang G, Mahungu T, Kern F, Griffiths PD, *et al* (2023) The cytomegalovirus gB/MF59 vaccine candidate induces antibodies against an antigenic domain controlling cell-to-cell spread. *Nat Commun* 14: 1041

Gómez Román VR, Murray JC & Weiner LM (2014) Antibody-Dependent Cellular Cytotoxicity (ADCC). *Antibody Fc: Linking Adaptive and Innate Immunity*: 1–27

Goodwin ML, Webster HS, Wang HY, Jenks JA, Nelson CS, Tu JJ, Mangold JF, Valencia S, Pollara J, Edwards W, *et al* (2020) Specificity and effector functions of non-neutralizing gB-specific monoclonal antibodies isolated from healthy individuals with human cytomegalovirus infection. *Virology* 548: 182–191

Griffiths PD, Stanton A, McCarrell E, Smith C, Osman M, Harber M, Davenport A, Jones G, Wheeler DC, OBeirne J, *et al* (2011) Cytomegalovirus glycoprotein-B vaccine with MF59 adjuvant in transplant recipients: A phase 2 randomised placebo-controlled trial. *The Lancet* 377: 1256–1263

Gugliesi F, Coscia A, Griffante G, Galitska G, Pasquero S, Albano C & Biolatti M (2020) Where do we Stand after Decades of Studying Human Cytomegalovirus? *Microorganisms* 8

Guo S, Gao S, Liu R, Shen J, Shi X, Bai S, Wang H, Zheng K, Shao Z, Liang C, *et al* (2019a) Oncological and genetic factors impacting PDX model construction with NSG mice in pancreatic cancer. *FASEB Journal* 33: 873–884

Guo Y, Duan M, Wang X, Gao J, Guan Z & Zhang M (2019b) Early events in rabies virus infection—Attachment, entry, and intracellular trafficking. *Virus Res* 263: 217–225

Hamed SM, Sakr MM, El-Housseiny GS, Wasfi R & Aboshanab KM (2023) State of the art in epitope mapping and opportunities in COVID-19. *Future Sci OA* 9: 832

Hampson K, Coudeville L, Lembo T, Sambo M, Kieffer A, Attlan M, Barrat J, Blanton JD, Briggs DJ, Cleaveland S, *et al* (2015) Estimating the Global Burden of Endemic Canine Rabies. *PLoS Negl Trop Dis* 9: e0003709-

Haradanhalli RS, D Hanumanthaiah AN & Varadappa ST (2019) Cost of rabies post exposure prophylaxis in different healthcare settings in six states of India. *Indian J Public Health* 63: S44–S47

Harrison SC (2008) Viral membrane fusion. *Nature Structural & Molecular Biology 2008 15:7* 15: 690–698

Harrison SC (2015) Viral membrane fusion. *Virology* 479–480: 498–507

Hassett KJ, Rajlic IL, Bahl K, White R, Cowens K, Jacquinet E & Burke KE (2024) mRNA vaccine trafficking and resulting protein expression after intramuscular administration. *Mol Ther Nucleic Acids* 35

Heldwein EE, Lou H, Bender FC, Cohen GH, Eisenberg RJ & Harrison SC (2006) Crystal structure of glycoprotein B from herpes simplex virus 1. *Science* 313: 217–220

Hellert J, Buchrieser J, Larrous F, Minola A, de Melo GD, Soriaga L, England P, Haouz A, Telenti A, Schwartz O, *et al* (2020) Structure of the prefusion-locking broadly neutralizing antibody RVC20 bound to the rabies virus glycoprotein. *Nat Commun* 11: 1–8

Hong J, Wei D, Zhong L, Wu Q, Chen K, Zhang W, Yang Y, Chen J, Xia N, Zhang X, *et al* (2022) Glycoprotein B Antibodies Completely Neutralize EBV Infection of B Cells. *Front Immunol* 0: 2557

Hu D & Irving AT (2023) Massively-multiplexed epitope mapping techniques for viral antigen discovery. *Front Immunol* 14: 1192385

Hu G, Du H, Liu Y, Wu G & Han J (2022) Herpes B virus: History, zoonotic potential, and public health implications. *Biosaf Health* 4: 213–219

Hu X, Karthigeyan KP, Herbek S, Valencia SM, Jenks JA, Webster H, Miller IG, Connors M, Pollara J, Andy C, *et al* (2024) Human Cytomegalovirus mRNA-1647 Vaccine Candidate Elicits Potent and Broad Neutralization and Higher Antibody-Dependent Cellular Cytotoxicity Responses Than the gB/MF59 Vaccine. *J Infect Dis* 230: 455–466

Huang Y, Song Y, Li J, Lv C, Chen ZS & Liu Z (2022) Receptors and ligands for herpes simplex viruses: Novel insights for drug targeting. *Drug Discov Today* 27: 185–195

Hutt-Fletcher LM (2007) Epstein-Barr Virus Entry. *J Virol* 81: 7825–7832

Ike AC, Onu CJ, Ononugbo CM, Reward EE & Muo SO (2020) Immune Response to Herpes Simplex Virus Infection and Vaccine Development. *Vaccines (Basel)* 8: 302

Indari O, Ghosh S, Bal AS, James A, Garg M, Mishra A, Karmodiya K & Jha HC (2024) Awakening the sleeping giant: Epstein–Barr virus reactivation by biological agents. *Pathog Dis* 82

Irie T, Kankanamge PJ & Kawai A (2006) Two different conformations of rabies virus glycoprotein taken under neutral pH conditions. *Microbiol Immunol* 50: 435–446

Ivanovic T, Choi JL, Whelan SP, van Oijen AM & Harrison SC (2013) Influenza-virus membrane fusion by cooperative fold-back of stochastically induced hemagglutinin intermediates. *Elife* 2013

Jean-Pierre V, Lupo J, Buisson M, Morand P & Germi R (2021) Main Targets of Interest for the Development of a Prophylactic or Therapeutic Epstein-Barr Virus Vaccine. *Front Microbiol* 12: 701611

Jenkin D, Ritchie AJ, Aboagye J, Fedosyuk S, Thorley L, Provstgaad-Morys S, Sanders H, Bellamy D, Makinson R, Xiang ZQ, *et al* (2022) Safety and immunogenicity of a simian-adenovirus-vectored rabies vaccine: an open-label, non-randomised, dose-escalation, first-in-human, single-centre, phase 1 clinical trial. *Lancet Microbe* 3: e663–e671

Jenks JA, Nelson CS, Roark HK, Goodwin ML, Pass RF, Bernstein DI, Walter EB, Edwards KM, Wang D, Fu TM, *et al* (2020) Antibody binding to native

cytomegalovirus glycoprotein B predicts efficacy of the gB/MF59 vaccine in humans. *Sci Transl Med* 12: 3611

Johnston C, Gottlieb SL & Wald A (2016) Status of vaccine research and development of vaccines for herpes simplex virus. *Vaccine* 34: 2948–2952

Johnston C, Scheele S, Bachmann L, Boily MC, Chaiyakunapruk N, Deal C, Delany-Moretlwe S, Lee S, Looker K, Marshall C, *et al* (2024) Vaccine value profile for herpes simplex virus. *Vaccine* 42: S82–S100

Jumper J, Evans R, Pritzel A, Green T, Figurnov M, Ronneberger O, Tunyasuvunakool K, Bates R, Žídek A, Potapenko A, *et al* (2021) Highly accurate protein structure prediction with AlphaFold. *Nature 2021 596:7873* 596: 583–589

Kanda T, Yajima M, Ahsan N, Tanaka M & Takada K (2004) Production of high-titer Epstein-Barr virus recombinants derived from Akata cells by using a bacterial artificial chromosome system. *J Virol* 78: 7004–7015

Karthigeyan KP, Connors M, Binuya CR, Gross M, Fuller AS, Crooks CM, Wang H-Y, Sponholtz MR, Byrne PO, Herbek S, *et al* (2024) A human cytomegalovirus prefusion-like glycoprotein B subunit vaccine elicits similar humoral immunity to that of postfusion gB in mice. *bioRxiv*: 2024.11.18.624140

Kennedy PGE & Gershon AA (2018) Clinical Features of Varicella-Zoster Virus Infection. *Viruses* 10

Kerr JR (2019) Epstein-Barr virus (EBV) reactivation and therapeutic inhibitors. *J Clin Pathol* 72: 651–658

Kharfan-Dabaja MA, Boeckh M, Wilck MB, Langston AA, Chu AH, Wloch MK, Guterwill DF, Smith LR, Rolland AP & Kenney RT (2012) A novel therapeutic cytomegalovirus DNA vaccine in allogeneic haemopoietic stem-cell transplantation: A randomised, double-blind, placebo-controlled, phase 2 trial. *Lancet Infect Dis* 12: 290–299

Kim EJ, Jacobs MW, Ito-Cole T & Callaway EM (2016) Improved Monosynaptic Neural Circuit Tracing Using Engineered Rabies Virus Glycoproteins. *Cell Rep* 15: 692–699

Kim HW, Canchola JG, Brandt CD, Pyles G, Chanock RM, Jensen K & Parrott RH (1969) Respiratory syncytial virus disease in infants despite prior administration of antigenic inactivated vaccine. *Am J Epidemiol* 89: 422–434

Kima IS, Jenni S, Stanifer ML, Roth E, Whelan SPJ, Van Oijen AM & Harrison SC (2017) Mechanism of membrane fusion induced by vesicular stomatitis virus G protein. *Proc Natl Acad Sci U S A* 114: E28–E36

Knoll MD & Wonodi C (2021) Oxford–AstraZeneca COVID-19 vaccine efficacy. *The Lancet* 397: 72–74

Ko YA, Yu YH, Wu YF, Tseng YC, Chen CL, Goh KS, Liao HY, Chen TH, Cheng TJR, Yang AS, *et al* (2021) A non-neutralizing antibody broadly protects against influenza virus infection by engaging effector cells. *PLoS Pathog* 17: e1009724

Koch J, Uckeley ZM, Doldan P, Stanifer M, Boulant S & Lozach P (2021) TMPRSS2 expression dictates the entry route used by SARS-CoV-2 to infect host cells. *EMBO J* 40

Kohl S, Charlebois ED, Sigouroudinia M, Goldbeck C, Hartog K, Sekulovich RE, Langenberg AGM & Burke RL (2000) Limited Antibody-Dependent Cellular Cytotoxicity Antibody Response Induced by a Herpes Simplex Virus Type 2 Subunit Vaccine. *J Infect Dis* 181: 335–339

Kohl S, Strynadka NCJ, Hodges RS & Pereira L (1990) Analysis of the role of antibody-dependent cellular cytotoxic antibody activity in murine neonatal herpes simplex virus infection with antibodies to synthetic peptides of glycoprotein D and monoclonal antibodies to glycoprotein B. *J Clin Invest* 86: 273–278

Kotton CN, Schwendinge M, Thiry G, DeVos B, Boever F De, Leroux-Roels G & Lilja A (2018) 1531. A CMV Vaccine Based on Non-Replicating Lymphocytic Choriomeningitis Virus Vectors Expressing gB and pp65 Is Safe and Immunogenic in Healthy Volunteers, Allowing for Development of a Phase II Clinical Trial in Living Donor Kidney Transplant Recipients. *Open Forum Infect Dis* 5: S475

Krissinel E & Henrick K (2007) Inference of macromolecular assemblies from crystalline state. *J Mol Biol* 372: 774–797

Kumar A, Bhatt S, Kumar A & Rana T (2023) Canine rabies: An epidemiological significance, pathogenesis, diagnosis, prevention, and public health issues. *Comp Immunol Microbiol Infect Dis* 97: 101992

Kuraoka M, Aschner CB, Windsor IW, Mahant AM, Garforth SJ, Kong SL, Achkar JM, Almo SC, Kelsoe G & Herold BC (2023) A non-neutralizing glycoprotein B monoclonal antibody protects against herpes simplex virus disease in mice. *J Clin Invest* 133

Lal H, Cunningham AL, Godeaux O, Chlibek R, Diez-Domingo J, Hwang S-J, Levin MJ, McElhaney JE, Poder A, Puig-Barberà J, *et al* (2015) Efficacy of an Adjuvanted Herpes Zoster Subunit Vaccine in Older Adults. *New England Journal of Medicine* 372: 2087–2096

Lanz T V., Brewer RC, Ho PP, Moon JS, Jude KM, Fernandez D, Fernandes RA, Gomez AM, Nadj GS, Bartley CM, *et al* (2022) Clonally expanded B cells in multiple sclerosis bind EBV EBNA1 and GlialCAM. *Nature 2022 603:7900* 603: 321–327

Le K, Tan C, Gupta S, Guhan T, Barkhordarian H, Lull J, Stevens J & Munro T (2018) A novel mammalian cell line development platform utilizing nanofluidics and optoelectro positioning technology. *Biotechnol Prog* 34: 1438–1446

Ledsgaard L, Kilstrup M, Karatt-Vellatt A, McCafferty J & Laustsen AH (2018) Basics of Antibody Phage Display Technology. *Toxins (Basel)* 10

Leman JK, Weitzner BD, Lewis SM, Adolf-Bryfogle J, Alam N, Alford RF, Aprahamian M, Baker D, Barlow KA, Barth P, *et al* (2020) Macromolecular modeling and design in Rosetta: recent methods and frameworks. *Nature Methods 2020 17:7* 17: 665–680

Leppek K, Byeon GW, Kladwang W, Wayment-Steele HK, Kerr CH, Xu AF, Kim DS, Topkar V V., Choe C, Rothschild D, *et al* (2022) Combinatorial optimization of mRNA structure, stability, and translation for RNA-based therapeutics. *Nature Communications 2022 13:1* 13: 1–22

Leung AKC, Sauve RS & Davies HD (2003) Congenital cytomegalovirus infection. *J Natl Med Assoc* 95: 213

Li F, Freed D, Heidecker G, Galli J, Durr E & Wang D (2022) A novel high throughput assay to quantify Epstein-Barr virus neutralizing antibody activity against B-cell and epithelial cell infections for vaccine and therapeutic developments. *Vaccine* 40: 3638–3646

Li F, Freed DC, Tang A, Rustandi RR, Troutman MC, Espeseth AS, Zhang N, An Z, McVoy M, Zhu H, *et al* (2017) Complement enhances in vitro neutralizing potency of antibodies to human cytomegalovirus glycoprotein B (gB) and immune sera induced by gB/MF59 vaccination. *NPJ Vaccines* 2: 36

Li Q, Ali MA & Cohen JI (2006) Insulin Degrading Enzyme Is a Cellular Receptor Mediating Varicella-Zoster Virus Infection and Cell-to-Cell Spread. *Cell* 127: 305–316

Li Q, Yan R, Bai N, Tan Z, Yu Q, Su H, Wei X, Li A, Chen X, Li Z, *et al* (2023) Immunogenicity and Antigenicity of the Ectodomain of Rabies Virus Glycoprotein Stably Expressed in HEK293T Cells. *Int J Med Sci* 20: 1282–1292

Li QX, Young LS, Niedobitek G, Dawson CW, Birkenbach M, Wang F & Rickinson AB (1992) Epstein–Barr virus infection and replication in a human epithelial cell system. *Nature 1992 356:6367* 356: 347–350

Li S (2022) Detergents and alternatives in cryo-EM studies of membrane proteins: Detergents and alternatives in cryo-EM studies of membrane proteins. *Acta Biochim Biophys Sin (Shanghai)* 54: 1049

Liu Y, Heim KP, Che Y, Chi X, Qiu X, Han S, Dormitzer PR & Yang X (2021a) Prefusion structure of human cytomegalovirus glycoprotein B and structural basis for membrane fusion. *Sci Adv* 7: eabf3178

Liu Y, Yang Q & Zhao F (2021b) Synonymous but not Silent: The Codon Usage Code for Gene Expression and Protein Folding. *Annu Rev Biochem* 90: 375

Ljungman P, Bermudez A, Logan AC, Kharfan-Dabaja MA, Chevallier P, Martino R, Wulf G, Selleslag D, Kakihana K, Langston A, *et al* (2021) A randomised, placebo-controlled phase 3 study to evaluate the efficacy and safety of ASP0113, a DNA-based CMV vaccine, in seropositive allogeneic haematopoietic cell transplant recipients. *EClinicalMedicine* 33

Lonberg N (2008) Human Monoclonal Antibodies from Transgenic Mice. *Therapeutic Antibodies* 181: 69

Loomis RJ, Lilja AE, Monroe J, Balabanis KA, Brito LA, Palladino G, Franti M, Mandl CW, Barnett SW & Mason PW (2013) Vectored co-delivery of human cytomegalovirus gH and gL proteins elicits potent complement-independent neutralizing antibodies. *Vaccine* 31: 919–926

Loomis RJ, Stewart-Jones GBE, Tsybovsky Y, Caringal RT, Morabito KM, McLellan JS, Chamberlain AL, Nugent ST, Hutchinson GB, Kueltzo LA, *et al* (2020) Structure-Based Design of Nipah Virus Vaccines: A Generalizable Approach to Paramyxovirus Immunogen Development. *Front Immunol* 11: 518772

Lu M, Chamblee M, Zhang Y, Ye C, Dravid P, Park JG, Mahesh KC, Trivedi S, Murthy S, Sharma H, *et al* (2022) SARS-CoV-2 prefusion spike protein stabilized by six rather than two prolines is more potent for inducing antibodies that neutralize viral variants of concern. *Proc Natl Acad Sci U S A* 119: e2110105119

Mair CM, Meyer T, Schneider K, Huang Q, Veit M & Herrmann A (2014) A histidine residue of the influenza virus hemagglutinin controls the pH dependence of the conformational change mediating membrane fusion. *J Virol* 88: 13189–13200

Martinez OM & Krams SM (2017) The Immune Response to Epstein Barr Virus and Implications for Posttransplant Lymphoproliferative Disorder. *Transplantation* 101: 2009–2016

Matochko WL, Nelep C, Chen WC, Grauer S, McFadden K, Wilson V & Oxenoid K (2022) CellCelector^{TM} as a platform in isolating primary B cells for antibody discovery. *Antib Ther* 5: 11

Mayr LM, Su B & Moog C (2017) Non-neutralizing antibodies directed against HIV and their functions. *Front Immunol* 8: 307637

McCallum M & Veesler D (2024) Computational design of prefusion-stabilized Herpesvirus gB trimers. *bioRxiv*: 2024.10.23.619923

McLellan JS (2015) Neutralizing epitopes on the respiratory syncytial virus fusion glycoprotein. *Curr Opin Virol* 11: 70–75

Mertz GJ, Ashley R, Burke RL, Benedetti J, Critchlow C, Jones CC & Corey L (1990) Double-Blind, Placebo-Controlled Trial of a Herpes Simplex Virus Type 2 Glycoprotein Vaccine in Persons at High Risk for Genital Herpes Infection. *Journal of Infectious Diseases* 161: 653–660

Mestas J & Hughes CCW (2004) Of Mice and Not Men: Differences between Mouse and Human Immunology. *The Journal of Immunology* 172: 2731–2738

Meyer H, Sundqvist VA, Pereira L & Mach M (1992) Glycoprotein gp116 of human cytomegalovirus contains epitopes for strain-common and strain-specific antibodies. *Journal of General Virology* 73: 2375–2383

Miura K, Orcutt AC, Muratova O V., Miller LH, Saul A & Long CA (2008) Development and characterization of a standardized ELISA including a reference serum on each plate to detect antibodies induced by experimental malaria vaccines. *Vaccine* 26: 193–200

Morris SJ, Sebastian S, Spencer AJ & Gilbert SC (2016) Simian Adenoviruses As Vaccine Vectors. *Future Virol* 11: 649–659

Motta JM, Hassan H & Ibrahim SA (2023) Revisiting the Syndecans: Master Signaling Regulators with Prognostic and Targetable Therapeutic Values in Breast Carcinoma. *Cancers (Basel)* 15

Münz C (2019) Latency and lytic replication in Epstein–Barr virus-associated oncogenesis. *Nature Reviews Microbiology 2019 17:11* 17: 691–700

Murata T, Sugimoto A, Inagaki T, Yanagi Y, Watanabe T, Sato Y & Kimura H (2021) Molecular Basis of Epstein–Barr Virus Latency Establishment and Lytic Reactivation. *Viruses 2021, Vol 13, Page 2344* 13: 2344

Mustafa MI & Mohammed A (2024) Developing recombinant antibodies by phage display technology to neutralize viral infectious diseases. *SLAS Discovery* 29: 100140

Nanbo A, Kachi K, Yoshiyama H & Ohba Y (2016) Epstein–Barr virus exploits host endocytic machinery for cell-to-cell viral transmission rather than a virological synapse. *Journal of General Virology* 97: 2989–3006

Napolitano F, Merone R, Abbate A, Ammendola V, Horncastle E, Lanzaro F, Esposito M, Contino AM, Sbrocchi R, Sommella A, *et al* (2020) A next generation vaccine against human rabies based on a single dose of a chimpanzee adenovirus vector serotype C. *PLoS Negl Trop Dis* 14: e0008459

Naughton P, Healy M, Enright F & Lucey B (2021) Infectious Mononucleosis: diagnosis and clinical interpretation. *Br J Biomed Sci* 78: 107–116

Nelson CS, Herold BC & Permar SR (2018a) A new era in cytomegalovirus vaccinology: considerations for rational design of next-generation vaccines to prevent congenital cytomegalovirus infection. *NPJ Vaccines* 3

Nelson CS, Huffman T, Jenks JA, De La Rosa EC, Xie G, Vandergrift N, Pass RF, Pollara J & Permar SR (2018b) HCMV glycoprotein B subunit vaccine efficacy mediated by nonneutralizing antibody effector functions. *Proc Natl Acad Sci U S A* 115: 6267–6272

Ng WM, Fedosyuk S, English S, Augusto G, Berg A, Thorley L, Haselon A-S, Segireddy RR, Bowden TA & Douglas AD (2022) Structure of trimeric pre-fusion rabies virus glycoprotein in complex with two protective antibodies. *Cell Host Microbe* 30: 1219-1230.e7

Ngwuta JO, Chen M, Modjarrad K, Joyce MG, Kanekiyo M, Kumar A, Yassine HM, Moin SM, Killikelly AM, Chuang GY, *et al* (2015) Prefusion F-specific antibodies determine the magnitude of RSV neutralizing activity in human sera. *Sci Transl Med* 7

Nicola A V. (2016) Herpesvirus Entry into Host Cells Mediated by Endosomal Low pH. *Traffic* 17: 965–975

Nieuwkoop T, Terlouw BR, Stevens KG, Scheltema RA, De Ridder D, Van Der Oost J & Claassens NJ (2023) Revealing determinants of translation efficiency via whole-gene codon randomization and machine learning. *Nucleic Acids Res* 51: 2363–2376

Nutt SL, Hodgkin PD, Tarlinton DM & Corcoran LM (2015) The generation of antibody-secreting plasma cells. *Nature Reviews Immunology 2015 15:3* 15: 160–171

Oliver SL, Xing Y, Chen DH, Roh SH, Pintilie GD, Bushnell DA, Sommer MH, Yang E, Carfi A, Chiu W, *et al* (2020) A glycoprotein B-neutralizing antibody structure at 2.8 Å uncovers a critical domain for herpesvirus fusion initiation. *Nat Commun* 11: 1–15

Oliver SL, Yang E & Arvin AM (2016) Varicella-Zoster Virus Glycoproteins: Entry, Replication, and Pathogenesis. *Curr Clin Microbiol Rep* 3: 204–215

Orlandini von Niessen AG, Poleganov MA, Rechner C, Plaschke A, Kranz LM, Fesser S, Diken M, Löwer M, Vallazza B, Beissert T, *et al* (2019) Improving mRNA-Based Therapeutic Gene Delivery by Expression-Augmenting 3' UTRs Identified by Cellular Library Screening. *Mol Ther* 27: 824–836

Osborn MJ, Ma B, Avis S, Binnie A, Dilley J, Yang X, Lindquist K, Ménoret S, Iscache A-L, Ouisse L-H, *et al* (2013) High-Affinity IgG Antibodies Develop Naturally in Ig-Knockout Rats Carrying Germline Human IgH/Igκ/Igλ Loci Bearing the Rat CH Region. *The Journal of Immunology Author Choice* 190: 1481

Pallesen J, Wang N, Corbett KS, Wrapp D, Kirchdoerfer RN, Turner HL, Cottrell CA, Becker MM, Wang L, Shi W, *et al* (2017) Immunogenicity and structures of a rationally designed prefusion MERS-CoV spike antigen. *Proc Natl Acad Sci U S A* 114: E7348–E7357

Panther L, Basnet S, Fierro C, Brune D, Leggett R, Peterson J, Pickrell P, Lin J, Wu K, Lee H, *et al* (2023) 2892. Safety and Immunogenicity of mRNA-1647, an mRNA-Based Cytomegalovirus Vaccine in Healthy Adults: Results of a Phase 2, Randomized, Observer-Blind, Placebo-Controlled, Dose-Finding Trial. *Open Forum Infect Dis* 10

Papi A, Ison MG, Langley JM, Lee D-G, Leroux-Roels I, Martinon-Torres F, Schwarz TF, van Zyl-Smit RN, Campora L, Dezutter N, *et al* (2023) Respiratory Syncytial Virus Prefusion F Protein Vaccine in Older Adults. *New England Journal of Medicine* 388: 595–608

Pass RF, Zhang C, Evans A, Simpson T, Andrews W, Huang M-L, Corey L, Hill J, Davis E, Flanigan C, *et al* (2009) Vaccine Prevention of Maternal Cytomegalovirus Infection. *New England Journal of Medicine* 360: 1191–1199

Pateev I, Seregina K, Ivanov R & Reshetnikov V (2023) Biodistribution of RNA Vaccines and of Their Products: Evidence from Human and Animal Studies. *Biomedicines 2024, Vol 12, Page 59* 12: 59

Patel R, Kaki M, Potluri VS, Kahar P & Khanna D (2022) A comprehensive review of SARS-CoV-2 vaccines: Pfizer, Moderna & Johnson & Johnson. *Hum Vaccin Immunother* 18

Pedrioli A & Oxenius A (2021) Single B cell technologies for monoclonal antibody discovery. *Trends Immunol* 42: 1143–1158

Perotti M, Marcandalli J, Demurtas D, Sallusto F & Perez L (2020) Rationally designed Human Cytomegalovirus gB nanoparticle vaccine with improved immunogenicity. *PLoS Pathog* 16: e1009169

De Pijper CA, Langedijk AC, Terryn S, Van Gucht S, Grobusch MP, Goorhuis A & Stijnis C (2021) Long-term Memory Response After a Single Intramuscular Rabies Booster Vaccination 10–24 Years After Primary Immunization. *J Infect Dis* 226: 1052

Plate AE, Reimer JJ, Jardetzky TS & Longnecker R (2011) Mapping regions of Epstein-Barr virus (EBV) glycoprotein B (gB) important for fusion function with gH/gL. *Virology* 413: 26–38

Plotkin SA, Wang D, Oualim A, Diamond DJ, Kotton CN, Mossman S, Carfi A, Anderson D & Dormitzer PR (2020) The Status of Vaccine Development Against the Human Cytomegalovirus. *J Infect Dis* 221: S113–S122

Pollard AJ & Bijker EM (2020) A guide to vaccinology: from basic principles to new developments. *Nature Reviews Immunology 2020 21:2* 21: 83–100

Pötzsch S, Spindler N, Wiegers AK, Fisch T, Rücker P, Sticht H, Grieb N, Baroti T, Weisel F, Stamminger T, *et al* (2011) B cell repertoire analysis identifies new antigenic domains on glycoprotein b of human cytomegalovirus which are target of neutralizing antibodies. *PLoS Pathog* 7: e1002172

Puthanakit T, Prompetchara E, Gatechompol S, Ketloy C, Thitithanyanont A, Jongkaewwattana A, Buranapraditkun S, Ubolyam S, Kerr SJ, Sophonphan J, *et al* (2024) Phase II prefusion non-stabilised Covid-19 mRNA vaccine randomised study. *Scienti/c Reports 2024 14:1* 14: 1–10

Quiambao B, Varghese L, Demarteau N, Sengson RF, Javier J, Mukherjee P, Manio LC & Preiss S (2020) Health economic assessment of a rabies pre-exposure prophylaxis

program compared with post-exposure prophylaxis alone in high-risk age groups in the Philippines. *International Journal of Infectious Diseases* 97: 38–46

RABIES VACCINES: WHO POSITION PAPER (2018)

RABIES VACCINES: WHO POSITION PAPER WEEKLY EPIDEMIOLOGICAL RECORD (2010)

Reimer JJ, Backovic M, Deshpande CG, Jardetzky T & Longnecker R (2009) Analysis of Epstein-Barr Virus Glycoprotein B Functional Domains via Linker Insertion Mutagenesis. *J Virol* 83: 734–747

Richardson E, Binter, Kosmac M, Ghraichy M, von Niederhausern V, Kovaltsuk A, Galson J, Trück J, Kelly DF, Deane CM, *et al* (2023) Characterisation of the immune repertoire of a humanised transgenic mouse through immunophenotyping and high-throughput sequencing. *Elife* 12

Ritchie AJ, Meeyai A, Trotter C & Douglas AD (2025) Routine childhood rabies pre-exposure prophylaxis can be cost effective in low- and middle-income countries. *Vaccine* 47: 126703

Royal A, John D, Bharti O, Tanwar R, Bhagat DK, Padmawati RS, Chaudhary V, Umapathi R, Bhadola P & Utarini A (2022) A Cost-Effectiveness Analysis of Pre-Exposure Prophylaxis to Avert Rabies Deaths in School-Aged Children in India. *Vaccines 2023, Vol 11, Page 88* 11: 88

Rozman M, Korać P, Jambrosic K & Lepej SŽ (2022) Progress in Prophylactic and Therapeutic EBV Vaccine Development Based on Molecular Characteristics of EBV Target Antigens. *Pathogens 2022, Vol 11, Page 864* 11: 864

Ruckwardt TJ, Morabito KM & Graham BS (2019) Immunological Lessons from Respiratory Syncytial Virus Vaccine Development. *Immunity* 51: 429–442

Rühl J, Leung CS & Münz C (2020) Vaccination against the Epstein-Barr virus. *Cell Mol Life Sci* 77: 4315–4324

Säfsten P (2009) Epitope mapping by surface plasmon resonance. *Methods Mol Biol* 524: 67–76

Šali A & Blundell TL (1993) Comparative protein modelling by satisfaction of spatial restraints. *J Mol Biol* 234: 779–815

Sashihara J, Burbelo PD, Savoldo B, Pierson TC & Cohen JI (2009) Human antibody titers to Epstein-Barr Virus (EBV) gp350 correlate with neutralization of infectivity better than antibody titers to EBV gp42 using a rapid flow cytometry-based EBV neutralization assay. *Virology* 391: 249–256

Sathiyamoorthy K, Jiang J, Hu YX, Rowe CL, Möhl BS, Chen J, Jiang W, Mellins ED, Longnecker R, Zhou ZH, *et al* (2014) Assembly and Architecture of the EBV B Cell Entry Triggering Complex. *PLoS Pathog* 10: e1004309

Schardt JS, Sivaneri NS & Tessier PM (2024) Monoclonal Antibody Generation Using Single B Cell Screening for Treating Infectious Diseases. *Biodrugs* 38: 477

Schiffer JT & Gottlieb SL (2019) Biologic interactions between HSV-2 and HIV-1 and possible implications for HSV vaccine development. *Vaccine* 37: 7363–7371

Schnee M, Vogel AB, Voss D, Petsch B, Baumhof P, Kramps T & Stitz L (2016) An mRNA Vaccine Encoding Rabies Virus Glycoprotein Induces Protection against Lethal Infection in Mice and Correlates of Protection in Adult and Newborn Pigs. *PLoS Negl Trop Dis* 10: e0004746

Schoppel K, Haßfurther E, Britt W, Ohlin M, Borrebaeck CAK & Mach M (1996) Antibodies Specific for the Antigenic Domain 1 of Glycoprotein B (gpUL55) of Human Cytomegalovirus Bind to Different Substructures. *Virology* 216: 133–145

Schowalter RM, Chang A, Robach JG, Buchholz UJ & Dutch RE (2008) Low-pH Triggering of Human Metapneumovirus Fusion: Essential Residues and Importance in Entry. *J Virol* 83: 1511

Schwendinger M, Thiry G, De Vos B, Leroux-Roels G, Bruhwyler J, Huygens A, Ganeff C, Buchinger H, Orlinger KK, Pinschewer DD, *et al* (2020) A Randomized Dose-Escalating Phase I Trial of a Replication-Deficient Lymphocytic Choriomeningitis Virus Vector-Based Vaccine Against Human Cytomegalovirus. *J Infect Dis* XX: 1–12

Semmes EC, Miller IG, Rodgers N, Phan CT, Hurst JH, Walsh KM, Stanton RJ, Pollara J & Permar SR (2023) ADCC-activating antibodies correlate with decreased risk of congenital human cytomegalovirus transmission. *JCI Insight* 8

Semmes EC, Miller IG, Wimberly CE, Phan CT, Jenks JA, Harnois MJ, Berendam SJ, Webster H, Hurst JH, Kurtzberg J, *et al* (2022) Maternal Fc-mediated non-neutralizing antibody responses correlate with protection against congenital human cytomegalovirus infection. *J Clin Invest* 132

Shafaati M, Akbarpour S, Priyanka, Saied AA & Choudhary OP (2023) Tackling rabies by one health approach: Pitfalls on the road to global eradication. *New Microbes New Infect* 52: 101098

Shelly SS, Cairns TM, Whitbeck JC, Lou H, Krummenacher C, Cohen GH & Eisenberg RJ (2012) The Membrane-Proximal Region (MPR) of Herpes Simplex Virus gB Regulates Association of the Fusion Loops with Lipid Membranes. *mBio* 3: e00429-12

Shi C, Sun P, Yang P, Liu L, Tian L, Liu W, Wang M, Zheng X & Zheng W (2022) Research progress on neutralizing epitopes and antibodies for the Rabies virus. *Infectious Medicine* 1: 262–271

Sloan SE, Hanlon C, Weldon W, Niezgoda M, Blanton J, Self J, Rowley KJ, Mandell RB, Babcock GJ, Thomas WD, *et al* (2007) Identification and characterization of a human monoclonal antibody that potently neutralizes a broad panel of rabies virus isolates. *Vaccine* 25: 2800–2810

Smith L, Wloch M, Chaplin J, Gerber M & Rolland A (2013) Clinical Development of a Cytomegalovirus DNA Vaccine: From Product Concept to Pivotal Phase 3 Trial. *Vaccines (Basel)* 1: 398–414

Smith SA & Crowe, Jr. JE (2015) Use of Human Hybridoma Technology To Isolate Human Monoclonal Antibodies. *Microbiol Spectr* 3: AID

Snijder J, Ortego MS, Weidle C, Stuart AB, Gray MD, McElrath MJ, Pancera M, Veesler D & McGuire AT (2018) An Antibody Targeting the Fusion Machinery Neutralizes Dual-Tropic Infection and Defines a Site of Vulnerability on Epstein-Barr Virus. *Immunity* 48: 799-811.e9

Sokal EM, Hoppenbrouwers K, Vandermeulen C, Moutschen M, Léonard P, Moreels A, Haumont M, Bollen A, Smets F & Denis M (2007) Recombinant gp350 vaccine for infectious mononucleosis: A phase 2, randomized, double-blind, placebo-controlled trial to evaluate the safety, immunogenicity, and efficacy of an Epstein-Barr virus vaccine in healthy young adults. *Journal of Infectious Diseases* 196: 1749–1753

Soldan SS & Lieberman PM (2022) Epstein–Barr virus and multiple sclerosis. *Nature Reviews Microbiology 2022 21:1* 21: 51–64

Sorem J & Longnecker R (2009) Cleavage of Epstein-Barr virus glycoprotein B is required for full function in cell-cell fusion with both epithelial and B cells. *J Gen Virol* 90: 591–595

Spencer AJ, Morris S, Ulaszewska M, Powers C, Kailath R, Bissett C, Truby A, Thakur N, Newman J, Allen ER, *et al* (2022) The ChAdOx1 vectored vaccine, AZD2816, induces strong immunogenicity against SARS-CoV-2 beta (B.1.351) and other variants of concern in preclinical studies. *EBioMedicine* 77

Spindler N, Diestel U, Stump JD, Wiegers AK, Winkler TH, Sticht H, Mach M & Muller YA (2014) Structural Basis for the Recognition of Human Cytomegalovirus Glycoprotein B by a Neutralizing Human Antibody. *PLoS Pathog* 10

Sponholtz MR, Byrne PO, Lee AG, Ramamohan AR, Goldsmith JA, Mccool RS, Zhou L, Johnson N V, Hsieh C-L, Connors M, *et al* (2024) Structure-based design of a soluble human cytomegalovirus glycoprotein B antigen stabilized in a prefusion-like conformation. *Proceedings of the National Academy of Sciences* 121: e2404250121

Sridhar S, Reyes-Sandoval A, Draper SJ, Moore AC, Gilbert SC, Gao GP, Wilson JM & Hill AVS (2008) Single-dose protection against Plasmodium berghei by a simian adenovirus vector using a human cytomegalovirus promoter containing intron A. *J Virol* 82: 3822–3833

Ständer S, R. Grauslund L, Scarselli M, Norais N & Rand K (2021) Epitope Mapping of Polyclonal Antibodies by Hydrogen-Deuterium Exchange Mass Spectrometry (HDX-MS). *Anal Chem* 93: 11669–11678

Stewart-Jones GBE, Chuang GY, Xu K, Zhou T, Acharya P, Tsybovsky Y, Ou L, Zhang B, Fernandez-Rodriguez B, Gilardi V, *et al* (2018) Structure-based design of a quadrivalent fusion glycoprotein vaccine for human parainfluenza virus types 1–4. *Proc Natl Acad Sci U S A* 115: 12265–12270

Stoermer KA & Morrison TE (2011) Complement and viral pathogenesis. *Virology* 411: 362

Straus SE, Wald A, Kost RG, McKenzie R, Langenberg AGM, Hohman P, Lekstrom J, Cox E, Nakamura M, Sekulovich R, *et al* (1997) Immunotherapy of recurrent genital herpes with recombinant herpes simplex virus type 2 glycoproteins D and B: Results of a placebo-controlled vaccine trial. *Journal of Infectious Diseases* 176: 1129–1134

Takada K (1984) Cross-linking of cell surface immunoglobulins induces epstein-barr virus in burkitt lymphoma lines. *Int J Cancer* 33: 27–32

Tay MZ, Wiehe K & Pollara J (2019) Antibody dependent cellular phagocytosis in antiviral immune responses. *Front Immunol* 10: 443715

Thurman AR & Doncel GF (2012) Herpes simplex virus and HIV: genital infection synergy and novel approaches to dual prevention. *Int J STD AIDS* 23: 613–619

Vennard LM, Atanasiu D, Saw WT, Eisenberg RJ, Cohen GH & Fontana J (2018) Recent Insights Into the Structural Characterization of Herpes Simplex Virus Fusion protein, gB. *Future Virol* 13: 5–7

Vincenti F, Budde K, Merville P, Shihab F, Ram Peddi V, Shah M, Wyburn K, Cassuto-Viguier E, Weidemann A, Lee M, *et al* (2018) A randomized, phase 2 study of ASP0113, a DNA-based vaccine, for the prevention of CMV in CMV-seronegative kidney transplant recipients receiving a kidney from a CMV-seropositive donor. *American Journal of Transplantation* 18: 2945–2954

Vollmer B & Grünewald K (2020) Herpesvirus membrane fusion - a team effort. *Curr Opin Struct Biol* 62: 112–120

Vollmer B, Pražák V, Vasishtan D, Jefferys EE, Hernandez-Duran A, Vallbracht M, Klupp BG, Mettenleiter TC, Backovic M, Rey FA, *et al* (2020) The prefusion structure of herpes simplex virus glycoprotein B. *Sci Adv* 6: eabc1726

Wagner B, Kropff B, Kalbacher H, Britt W, Sundqvist VA, Ostberg L & Mach M (1992) A continuous sequence of more than 70 amino acids is essential for antibody binding to the dominant antigenic site of glycoprotein gp58 of human cytomegalovirus. *J Virol* 66

Wang C, Dulal P, Zhou X, Xiang Z, Goharriz H, Banyard A, Green N, Brunner L, Ventura R, Collin N, *et al* (2018) A simian-adenovirus-vectored rabies vaccine suitable for thermostabilisation and clinical development for low-cost single-dose pre-exposure prophylaxis. *PLoS Negl Trop Dis* 12: e0006870

Wang C, Hart M, Chui C, Ajuogu A, Brian IJ, de Cassan SC, Borrow P, Draper SJ & Douglas AD (2016) Germinal Center B Cell and T Follicular Helper Cell Responses to Viral Vector and Protein-in-Adjuvant Vaccines. *The Journal of Immunology* 197: 1242–1251

Wang HB, Zhang H, Zhang JP, Li Y, Zhao B, Feng GK, Du Y, Xiong D, Zhong Q, Liu WL, *et al* (2015) Neuropilin 1 is an entry factor that promotes EBV infection of nasopharyngeal epithelial cells. *Nature Communications 2015 6:1* 6: 1–13

Watanabe Y, Mendonça L, Allen ER, Howe A, Lee M, Allen JD, Chawla H, Pulido D, Donnellan F, Davies H, *et al* (2021) Native-like SARS-CoV-2 Spike Glycoprotein Expressed by ChAdOx1 nCoV-19/AZD1222 Vaccine. *ACS Cent Sci* 7: 594–602

Waterhouse A, Bertoni M, Bienert S, Studer G, Tauriello G, Gumienny R, Heer FT, De Beer TAP, Rempfer C, Bordoli L, *et al* (2018) SWISS-MODEL: homology modelling of protein structures and complexes. *Nucleic Acids Res* 46: W296–W303

Weed DJ, Pritchard SM, Gonzalez F, Aguilar HC & Nicola A V. (2017) Mildly Acidic pH Triggers an Irreversible Conformational Change in the Fusion Domain of Herpes Simplex Virus 1 Glycoprotein B and Inactivation of Viral Entry. *J Virol* 91

White JM, Delos SE, Brecher M & Schornberg K (2008) Structures and Mechanisms of Viral Membrane Fusion Proteins: Multiple Variations on a Common Theme. *Crit Rev Biochem Mol Biol* 43: 189–219

White JM, Ward AE, Odongo L & Tamm LK (2023) Viral Membrane Fusion: A Dance Between Proteins and Lipids. *Annu Rev Virol* 10: 139–161

Whitehouse ER, Mandra A, Bonwitt J, Beasley EA, Taliano J & Rao AK (2023) Human rabies despite post-exposure prophylaxis: a systematic review of fatal breakthrough infections after zoonotic exposures. *Lancet Infect Dis* 23: e167–e174

WHO EXPERT CONSULTATION ON RABIES: THIRD REPORT (2018)

Wiegers A-K, Sticht H, Winkler TH, Britt WJ & Mach M (2015) Identification of a Neutralizing Epitope within Antigenic Domain 5 of Glycoprotein B of Human Cytomegalovirus. *J Virol* 89: 361–372

Williams LTD, Ofek G, Schätzle S, McDaniel JR, Lu X, Nicely NI, Wu L, Lougheed CS, Bradley T, Louder MK, *et al* (2017) Potent and broad HIV-neutralizing antibodies in memory B cells and plasma. *Sci Immunol* 2

Wilmore JR, Jones DD & Allman D (2017) Protocol for improved resolution of plasma cell subpopulations by flow cytometry. *Eur J Immunol* 47: 1386–1388

Wloch MK, Smith LR, Boutsaboualoy S, Reyes L, Han C, Kehler J, Smith HD, Selk L, Nakamura R, Brown JM, *et al* (2008) Safety and immunogenicity of a bivalent cytomegalovirus DNA vaccine in healthy adult subjects. *Journal of Infectious Diseases* 197: 1634–1642

Wu L, Borza CM & Hutt-Fletcher LM (2005) Mutations of Epstein-Barr virus gH that are differentially able to support fusion with B cells or epithelial cells. *J Virol* 79: 10923–10930

Wüthrich K (1990) Protein structure determination in solution by NMR spectroscopy. *Journal of Biological Chemistry* 265: 22059–22062

Xiao X, Tang A, Cox KS, Wen Z, Callahan C, Sullivan NL, Nahas DD, Cosmi S, Galli JD, Minnier M, *et al* (2019) Characterization of potent RSV neutralizing antibodies isolated from human memory B cells and identification of diverse RSV/hMPV cross-neutralizing epitopes. *MAbs* 11: 1415–1427

Yager ML & Moore SM (2015) The Rapid Fluorescent Focus Inhibition Test. *Current Laboratory Techniques in Rabies Diagnosis, Research and Prevention* 2: 199–215

Yang F, Lin S, Ye F, Yang J, Qi J, Chen Z, Lin X, Wang J, Yue D, Cheng Y, *et al* (2020) Structural Analysis of Rabies Virus Glycoprotein Reveals pH-Dependent Conformational Changes and Interactions with a Neutralizing Antibody. *Cell Host Microbe* 27: 441-453.e7

Yang J, Yan R, Roy A, Xu D, Poisson J & Zhang Y (2014) The I-TASSER Suite: protein structure and function prediction. *Nature Methods 2015 12:1* 12: 7–8

Yao Y, Ghosh K, Epand RF, Epand RM & Ghosh HP (2003) Membrane fusion activity of vesicular stomatitis virus glycoprotein G is induced by low pH but not by heat or denaturant. *Virology* 310: 319–332

Young LS, Yap LF & Murray PG (2016) Epstein–Barr virus: more than 50 years old and still providing surprises. *Nature Reviews Cancer 2016 16:12* 16: 789–802

Zakeri B, Fierer JO, Celik E, Chittock EC, Schwarz-Linek U, Moy VT & Howarth M (2012) Peptide tag forming a rapid covalent bond to a protein, through engineering a bacterial adhesin. *Proc Natl Acad Sci U S A* 109: E690–E697

Zborowski M, Ostera GR, Moore LR, Milliron S, Chalmers JJ & Schechter AN (2003) Red Blood Cell Magnetophoresis. *Biophys J* 84: 2638

Zeev-Ben-Mordehai T, Vasishtan D, Durán AH, Vollmer B, White P, Pandurangan AP, Siebert CA, Topf M & Grünewald K (2016) Two distinct trimeric conformations of natively membrane-anchored full-length herpes simplex virus 1 glycoprotein B. *Proc Natl Acad Sci U S A* 113: 4176–4181

Zhang C (2012) Hybridoma technology for the generation of monoclonal antibodies. *Methods in Molecular Biology* 901: 117–135

Zhang H, Pelech S, Ruijtenbeek R, Felgenhauer T, Bischoff R, Breitling F & Stadler V (2012) Peptide arrays. *Microarrays in Diagnostics and Biomarker Development: Current and Future Applications*: 81–112

Zhang HJ, Tian J, Qi XK, Xiang T, He GP, Zhang H, Yu X, Zhang X, Zhao B, Feng QS, *et al* (2018) Epstein-Barr virus activates F-box protein FBXO2 to limit viral infectivity by targeting glycoprotein B for degradation. *PLoS Pathog* 14

Zhang X, Hong J, Zhong L, Wu Q, Zhang S, Zhu Q, Chen H, Wei D, Li R, Zhang W, *et al* (2022) Protective anti-gB neutralizing antibodies targeting two vulnerable sites for EBV-cell membrane fusion. *Proceedings of the National Academy of Sciences* 119

Zhang Y, Fang L, Wang Z, Zhang C, Zhao J, Daemi HB, Zhang M, Yuan L, Han X, Li L, *et al* (2024) A modified recombinant adenovirus vector containing dual rabies virus G expression cassettes confers robust and long-lasting humoral immunity in mice, cats, and dogs. *Emerg Microbes Infect* 13

Zhao GX, Fang XY, Bu GL, Chen SJ Bin, Sun C, Li T, Xie C, Wang Y, Li SX, Meng N, *et al* (2024) Potent human monoclonal antibodies targeting Epstein-Barr virus gp42 reveal vulnerable sites for virus infection. *Cell Rep Med* 5: 101573

Zhou YH, Chen Z, Purcell RH & Emerson SU (2007) Positive reactions on Western blots do not necessarily indicate the epitopes on antigens are continuous. *Immunol Cell Biol* 85: 73–78

Zhu QY, Shan S, Yu J, Peng SY, Sun C, Zuo Y, Zhong LY, Yan SM, Zhang X, Yang Z, *et al* (2021) A potent and protective human neutralizing antibody targeting a novel vulnerable site of Epstein-Barr virus. *Nature Communications 2021 12:1* 12: 1–13

Zucha D, Kubista M & Valihrach L (2021) Tutorial: Guidelines for single-cell rt-qpcr. *Cells* 10

Van Zyl DG, Mautner J & Delecluse HJ (2019) Progress in EBV Vaccines. *Front Oncol* 9